Spatial Patterns in Dryland Vegetation and the Significance of Dispersal, Infiltration and Complex Topography

by

Sally E. Thompson

Department of Environment
Duke University

Date: _____

Approved:

_____
Gabriel G. Katul, Advisor

_____
James S. Clark

_____
Karen E. Daniels

_____
Amilcare Porporato

Dissertation submitted in partial fulfillment of the requirements for the degree of
Doctor of Philosophy in the Department of Environment
in the Graduate School of Duke University
2010

Abstract
(Hydrology)

Spatial Patterns in Dryland Vegetation and the Significance of Dispersal, Infiltration and Complex Topography

by

Sally E. Thompson

Department of Environment
Duke University

Date: _____

Approved:

_____
Gabriel G. Katul, Advisor

_____
James S. Clark

_____
Karen E. Daniels

_____
Amilcare Porporato

An abstract of a dissertation submitted in partial fulfillment of the requirements for the degree of Doctor of Philosophy in the Department of Environment in the Graduate School of Duke University
2010

Abstract

Drylands, comprising arid and semi-arid areas and the dry subtropics, cover some 40% of the world's land area and support approximately 2 billion people, including at least 1 billion who depend on dryland agriculture and grazing. 10-20% of drylands are estimated to have already undergone degradation or desertification, and lack of monitoring and assessment remains a key impediment to preventing further desertification. Change in vegetation cover, specifically in the spatial organization of vegetation may occur prior to irreversible land degradation, and can be used to assess desertification risk. Coherent spatial structures arise in the distribution of dryland vegetation where plant growth is localized in regular spatial patterns. Such "patterned vegetation" occurs across a variety of vegetation and soil types, extends over at least 18 million hectares, occurs in 5 continents and is economically and environmentally valuable in its own right.

Vegetation patterning in drylands arises due to positive feedbacks between hydrological forcing and plant growth so that the patterns change in response to trends in mean annual rainfall. Mathematical models indicate that vegetation patterns collapse to a desertified state after undergoing a characteristic set of transformations, so that the condition of a pattern at any point in time can be explicitly linked to ecosystem health. This dissertation focuses on the mathematical description of vegetation patterns with a view to improving such predictions. It evaluates the validity of current mathematical descriptions of patterning for the specific case of small-

scale vegetation patterns and proposes alternative hypotheses for their formation. It assesses the significance of seed dispersal in determining pattern form and dynamics for two cases: vegetation growing on flat ground with isotropic patterning, and vegetation growing on slopes and having anisotropic (i.e. directional) patterning. Thirdly, the feedbacks between local biomass density and infiltration capacity, one of the positive feedbacks believed to contribute to patterning, are quantified across a wide range of soil and climatic conditions, and new mathematical descriptions of the biomass-infiltration relationship are proposed. Finally the influence of land surface microtopography on the partitioning of rainfall into infiltration and runoff is assessed.

Contents

List of Tables

List of Figures

Acknowledgements

My dissertation was generously supported by the General Sir John Monash Foundation. The Monash Foundation assists young leaders in extending their experiences and educational opportunities through a period of international study. I have appreciated the opportunities provided by the Monash Foundation's support enormously.

In addition to the Monash Foundation I have been financially supported by NSF grants EAR-0628342 and EAR-0635787.

The research contained in this thesis was conducted under the supervision of Prof. Gabriel Katul, an overwhelmingly generous and supportive mentor. Thanks also to my committee members and co-authors, Jim Clark, Karen Daniels, Ciaran Harman, Paul Heine, Sean McMahon and Amilcare Porporato; and to the fellow members of the Katul Lab, Alex Konings, Annalisa Molini, Kim Novick, and Mario Siqueira.

My cohort of PhD students at the Nicholas School have been a superlative peer group. Their diversity, talent and experience are exceptional, and their friendship has been a highlight of my tenure at Duke.

Finally, thanks to my husband, Nic George. In agreeing to move to Durham Nic gave me the freedom to pursue this PhD. From his practical assistance with field work, to his talent for spotting vegetation patterns (leading to the observations discussed in Chapter 2), and his unfailing support and enthusiasm, he has been an ideal partner and has my heartfelt thanks.

1

Introduction

Semi-arid landscapes are characterized by sparse and patchy vegetation cover, interspersed by areas of essentially bare ground. Vegetation cover in these landscapes correlates strongly with areas in which resources such as nutrients, soil organic carbon, and soil moisture are concentrated, in so-called: 'islands of fertility' [Schlesinger et al., 1996]. The spatial arrangement of vegetation in semi-arid landscapes varies from random to fractal (i.e. a power-law distribution of vegetation patch sizes) to highly organized [Caylor et al., 2004, Scanlon et al., 2007, Valentin and d'Herbes, 1999]. The explanation of this variation in spatial structure, and determining whether such structures offer meaningful insight into the condition and management of drylands, has drawn increasing attention [Kefi et al., 2007a]. Indeed, as the management of the global drylands comes under increasing scrutiny, efforts to monitor and diagnose the ecological, social and economic status of semi-arid ecosystems are being highlighted as critical scientific needs [Dryland Science for Development Consortium Working Group 1, 2009]. Remote sensing is an attractive tool for assessing the health of drylands, but simple measures of greeness such as NDVI are increasingly viewed as "blunt instruments", so that additional diagnostics of dryland status are desir-

able [Herrmann et al., 2005]. The broad objective of the research in this thesis is to progress towards a detailed understanding of highly organized vegetation patterns, and to develop components of the framework that will be needed to allow the interpretation of these patterns in terms of underlying ecosystem dynamics. If this aim can be achieved, then vegetation patterns may be used as indicators of regional ecosystem condition, adding a new diagnostic and potentially prognostic tool for improved monitoring and prediction in semi-arid environments.

A review of periodic vegetation patterning and the variety of theory proposed to describe it was published recently providing an excellent outline of the state of the field [Borgogno et al., 2009]. Given the recent publication of this review, this introduction focuses on providing a broad overview and motivation for the work undertaken in this dissertation, rather than repeating another detailed literature review. Thus, this introductory section will firstly introduce what is meant by vegetation patterns and outline their appearance, characteristics and global distribution. The potential value of monitoring vegetation patterns as a means of forecasting change in dryland ecosystems will be discussed with reference to modeling frameworks that are currently being employed. The value of numerical models of patterned vegetation will be highlighted, along with the rationale for focusing on model development in this thesis. Finally, a conceptual model for the use of vegetation patterns as indicators of ecosystem health in drylands will be presented, and the individual chapters of this thesis outlined with reference to this ultimate conceptual goal.

1.1 What are vegetation patterns?

Vegetation patterns, most broadly, refer to the spatial organization of vegetation in a landscape. This organization may be determined by species type, as observed in changing dominant species down a watershed catena [Hwang et al., 2009]; by bulk presence or absence of vegetation, as observed in the case of abrupt switches from

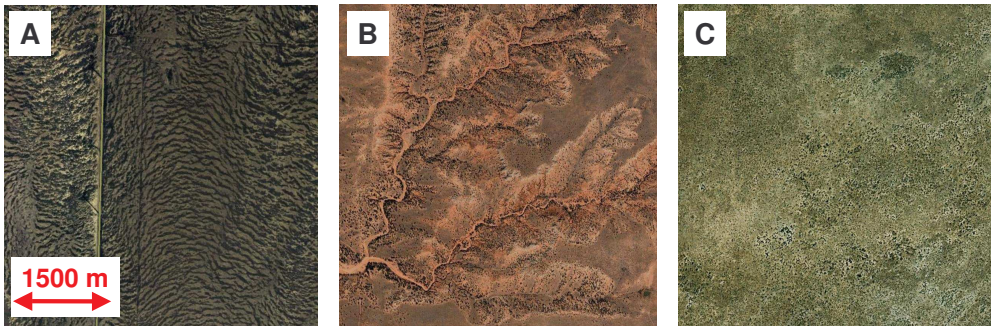

FIGURE 1.1: Examples of the different forms taken by vegetation spatial patterns. A) Coherent, regular patterns with a dominant wavelength. This example is from near Fort Stockon, Texas. B) Random patterns overlain on an optimal distribution of vegetation type determined by the river network (see Caylor et al. for details [Caylor et al., 2004]) in the Rio Salada River Basin, New Mexico. C) The size of vegetation patches in the Kalahari Desert has been shown to conform to a power law distribution. All examples taken from Google Earth.

trees to shrubs associated with changes in aspect in dryland catchments [Gutierrez-Jurado et al., 2006]; or by the spatial pattern of the matrix of perennial vegetation across otherwise bare, or annual dominated landscapes [Caylor et al., 2004, Puigdefabregas, 2005] (See Figure 1.1).

Vegetation patterns are of interest to a diverse community of ecologists, hydrologists, geomorphologists and micrometeorologists, because the structure imposed by the pattern feeds back on landscape-scale biological and physical processes [Puigdefabregas, 2005, Aguiar and Sala, 1999, Bergkamp, 1998, Bracken and Kirkby, 2005, Bracken and Croke, 2007, Dekker et al., 2007]. Here the focus will be upon a specific subset of vegetation patterns: those which have a *well-defined wavelength and are organized into coherent, periodic structures*. From this point onwards, when the term 'vegetation pattern' or 'pattern' is used it will refer specifically to such organized periodic structures.

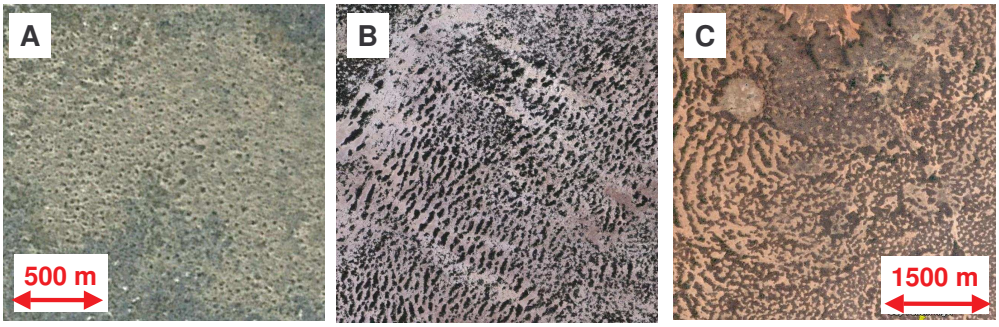

FIGURE 1.2: Examples of some of the morphologies adopated by patterned vegetation. A) Spotted patterns in southern Niger. B) Broken striped patterns in eastern Mali (same scale as A). C) A complex patterned landscape in which gapped patterns, labyrinthine patterns and striped patterns are all shown to locally coexist. The large circular feature at the top left of the image is a village, highlighting that these landscapes are anthropogenically influenced. The landscape is found in southern Niger. All examples taken from Google Earth.

1.1.1 Coherent periodic vegetation patterns

Coherent periodic vegetation patterns are characterized by having one, or several, dominant wave-vectors (wavenumbers) when viewed in the frequency domain. The vegetation pattern is typically formed by perennial trees, shrubs, chenopods or grasses overlying a matrix composed of bare soil, annually-colonized areas, or a contrasting vegetation type [D'Herbes et al., 2001]. Vegetation patterns may consist of largely linear features (stripes, also known as *Tiger Bush, Mulga* or *Mogote*), typically arrayed along slope contours, or they may have an imperfect three-fold symmetry and consist of spots, bare gaps within a vegetated matrix, or labyrinthine patterns [Lefever and Lejeune, 1997, Dunkerley, 2002b] (See Figure 1.2).

1.1.2 Distribution and typical characteristics of vegetation patterns

Vegetation patterns have a global distribution in semi-arid ecosystems, suggesting that rather than being a species- or area-specific trait, the phenomenon of vegetation patterning arises as a response to environmental conditions in these regions

[Deblauwe et al., 2008]. Vegetation patterns have been studied in the field in Eastern Africa (Somalia, Ethiopia, Sudan) [Boaler and Hodge, 1964, Wickens and Collier, 1971, Worrall, 1959, Deblauwe et al., 2008], in the Sahel (Niger, Mali, Mauritania and Senegal), Australia (Western Australia, the Northern Territory, western New South Wales and south-western Queensland), Mexico (Chihuahuan desert) and Texas (northern Chihuahuan desert) [Valentin and d'Herbes, 1999, Barbier et al., 2006, Leprun, 1999, Deblauwe et al., 2008, Dunkerley, 2002b, Dunkerley and Brown, 1999, Tongway and Ludwig, 1990, McDonald et al., 2009, Cornet et al., 1992, Anderson and Hodgkinson, 1997, Mabbutt and Fanning, 1987].

A recent biogeographic study by Deblauwe et al. [2008] verified that vegetation patterning arises on at least 0.4% of the global drylands, although this figure is almost certainly an underestimate since the study excluded patterns with wavelengths of less than 60m. This study was also able to identify several major determinants of the biogeography of vegetation patterns, namely the degree of aridity (as quantified with a humidity index), and high seasonality in either temperature or precipitation (although not both) [Deblauwe et al., 2008].

Beyond the climatic factors identified above, a number of consistent trends have been noted in sites containing periodic vegetation patterns. Patterned sites all experience periods of water stress generated by either highly seasonal rainfall or uniformly low rainfall rates. Patterns tend to occur on areas of low slope ($< 2\%$), with relatively fine textured soils (patterns have been observed to fail when sandy soils, deposited by wind erosion, were introduced to a previously patterned landscape), and are often associated with biological soil crusts [Rietkerk et al., 2002, Valentin and d'Herbes, 1999, Gilad, 2004]. A less commonly reported feature of patterned sites is the presence of a shallow confining layer, identified broadly in Niger [Barbier et al., 2006] and recently shown to occur in banded sites in Texas [McDonald et al., 2009].

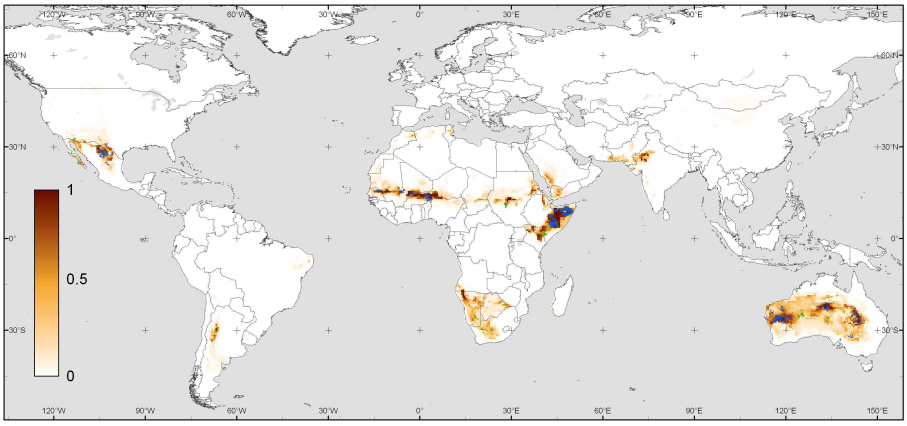

FIGURE 1.3: Deblauwe et al. predictions for the global distribution of coherent vegetation patterns based on a biogeographic analysis. The darker the shading the higher the predicted confidence (tending to a maximum of 1) that periodic patterns would occur in this region. Green areas indicate local verification of periodic patterning via remote sensing studies [Deblauwe et al., 2008].

1.1.3 Why do dryland vegetation patterns arise?

Arid vegetation patterns represent an example of a Turing instability [Turing, 1952], also known as a reaction-diffusion or activator-inhibitor instability [Murray, 2003b]. Such instabilities arise in the presence of at least two components which can move through space, and which have opposing effects on the generation of a pattern, with one component tending to cause growth in the pattern-forming medium (the *activator*), and the other tending to oppose growth (the *inhibitor*). If the rate at which these components moves through space differs, with the inhibitor moving faster than the activator, then conditions for pattern formation are established: the local growth of a pattern will be damped at its margins by the presence of the more rapidly moving inhibiting component. In a traditional framework, "movement" takes the form of diffusion, as appropriate to the chemical systems where Turing instabilities were initially studied [Borgogno et al., 2009].

Translating the Turing framework to the case of vegetation patterns is not en-

tirely straightforward, because rather than a particular state variable acting as an activator or inhibitor, the pattern formation arises from activating and inhibiting interactions between state variables [Borgogno et al., 2009]. If water is presumed to be a limiting resource, then mechanisms that increase water availability to plants are activating processes, and mechanisms that decrease its availability are inhibiting. Activation is associated with a number of mechanisms including increased infiltration rates in the proximity of plants compared to bare soil areas [Dunkerley, 2002b, Valentin and d'Herbes, 1999] and increased shading of the soil surface [Zeng et al., 2005, 2004, Scholes and Archer, 1997]. Inhibition is associated with plant competition for water, both locally (within individual vegetated patches) and globally, in terms of the ability for vegetated areas to intercept surface moisture resources that might otherwise infiltrate elsewhere. The relative importance of above- and below-ground competition for water is stressed differently in different models, with some explicitly accounting for extensive lateral root distributions [Gilad, 2004]. Recent field experiments have confirmed that the lateral extent of root systems in Niger exceeds 8m, largely confined to the surface soils by a shallow impervious layer [Barbier et al., 2006, 2008]. Thus, vegetation patterns are associated with a global constraint on water availability that is spatially modified by extensive rooting systems and/or significant runoff, leading to concentration of the soil moisture resource at vegetated sites.

1.2 Why are vegetation patterns important?

Other than their beauty and intriguing self organization, vegetation patterns are viewed as important for three reasons:

- The information contained in a spatial pattern may allow inference of important features of a system's ecology and hydrology;

- Models suggest that the existence of vegetation patterning is an indicator of a bistable system. Such systems may exhibit thresholds in their dynamical behaviour and encode the possibility of hysteresis; and

- Models further suggest that a predictable sequence of change in vegetation pattern morphology is encountered as the ecosystem transitions towards a nonlinear threshold (often referred to as a 'catastrophic ecosystem shift' i.e. desertification).

1.2.1 Observations of change in vegetation patterns

The best observational evidence of change in vegetation patterns associated with stressors including drought and grazing is presented in a study by Barbier et al. [2006]. These authors compared aerial photographs of vegetation in the vicinity of the Parc W Biosphere Reserve in southern Niger over a 45 year period. During this period, all vegetation experienced a drought; vegetation outside the Reserve was also subject to increased grazing. At all sites, the formerly homogeneous vegetation cover showed evidence of fragmentation over the 45 year period, including the formation of bare gaps. The most dramatic change was at a site that experienced heavy grazing in addition to the drought, where vegetation fragmented into a labyrinthine pattern (c.f. Figure 1.2, C) of interconnected bare and vegetated patches.

1.2.2 Simple models of vegetation patterns

The sequence of vegetation change observed in the study by Barbier et al. [2006] corresponds well to that predicted by several models of the dynamics of macroscopic vegetation patterns [Rietkerk et al., 2002, von Hardenberg et al., 2001]. These models firstly predict the existence of a bistability where ecosystems may exist in a patterned state or a desertified state essentially void of vegetation. Bifurcations between the steady states arise under very different climatic and land use conditions.

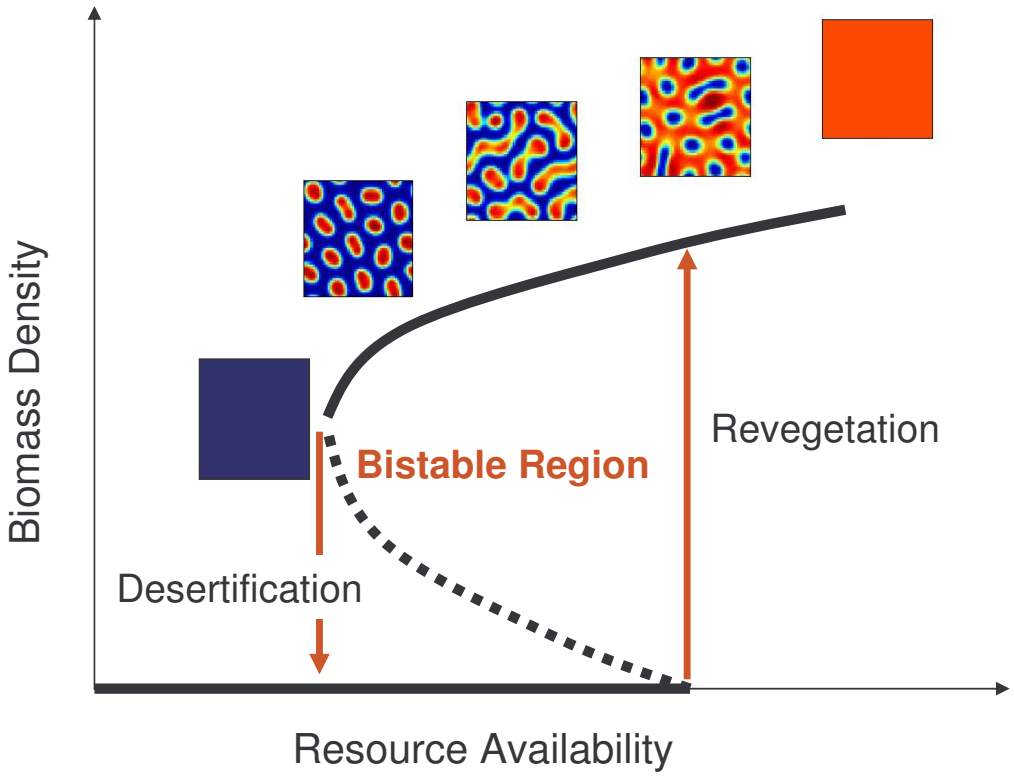

FIGURE 1.4: Schematic of the bistability in the desert ecosystem and the potential for abrupt transitions to and from desertified and vegetated states. The typical sequence of vegetation pattern change (for an isotropic case) is shown. The figure is adapted from Rietkerk et al. [2002].

The implication of this separation is that ecosystem change is strongly hysteretic, so that desertification is difficult to reverse. Finally, models predict that as a vegetated state is driven towards the desertification threshold, the morphology of the vegetation pattern will undergo a series of predictable changes. As the system desertifies, homogeneous states decay into gapped patterns, then labyrinths, then spots and finally bare soil. Similarly, under increased water stress the wavelength of banded patterns tends to increase, while the width of the vegetated bands decreases.

1.3 A conceptual approach for interpreting vegetation patterning

Given this background regarding vegetation patterns, it is possible to clearly articulate a process that capitalizes on the "important" properties of vegetation patterns outlined above to use vegetation patterns to learn about and forecast the behaviour of dryland ecosystems. This goal is schematically represented in Figure 1.5 below. Firstly, one or multiple observations of a vegetation pattern are combined with a process model to obtain estimates of the parameters that govern the pattern evolution. Physical and biological constraints on these parameters, as well as information regarding sensitivity of the model to these parameters can be used to simplify the parameter estimation problem. Having obtained parameter estimates, a working model of the ecosystem of interest can be constructed, and subjected to projections about future changes in land use, rainfall, temperature, CO_2 concentrations or other forcing variables. By running the model across multiple realizations of these projections, changes in resilience of the ecosystem (for instance as measured by the width of the bistable region) and the probability of desertification can be computed. This information can then be used to prioritize land use or management interventions.

A robust and reliable model of the pattern-forming ecohydrological interactions is a critical component of this conceptual approach. The model must be parameterized by "measurable" quantities (e.g. water use efficiency) for which reasonable projections can be made. Progressing towards such a model is the ultimate aim of the work presented in this dissertation. Although the contributions detailed here do not provide "closure" on the issue, they are necessary first steps towards improved understanding and prediction of vegetation patterning. The final section of this introduction will introduce an existing state-of-the-art model for vegetation patterning, highlight areas where progress is needed, and explain how the chapters of this thesis extend our understanding and the utility of the modeling approach.

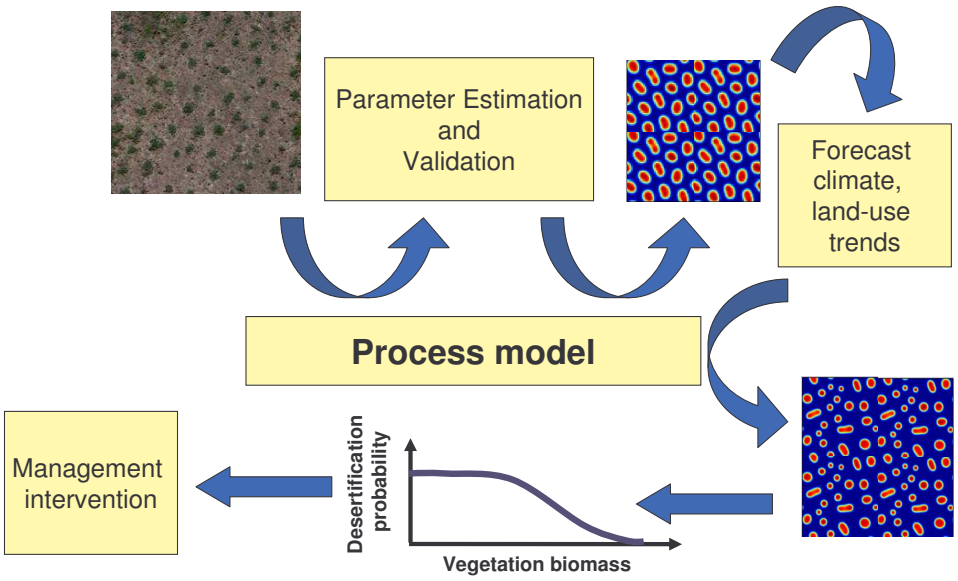

FIGURE 1.5: A conceptual model for assimilating information obtained from observations of vegetation patterns into a framework that can be used to project ecosystem resilience and desertification probabilties as a guide for land managers and decision makers.

1.3.1 Definition of the problem

The starting point for much of this work is the numerical model first proposed by HilleRisLambers et al. [2001] and refined by Rietkerk et al. [2002]. This model consists of three coupled differential equations linking surface water, soil moisture and biomass dynamics. The equations are:

$$\frac{\partial P}{\partial t} = cg_{max}\frac{W}{W+k_1}P - dP + D_p\nabla^2 P, \tag{1.1}$$

where P is the plant biomass in gm^{-2}.

$$\frac{\partial W}{\partial t} = \alpha O\frac{P+k_2W_o}{P+k_2} - g_{max}\frac{W}{W+k_1}P - r_wW + D_w\nabla^2 W, \tag{1.2}$$

Parameter	Definition
c	water uptake to plant growth relation, g $mm^{-1}m^{-2}$
g_{max}	maximum specific water uptake, mm m^2 g^{-1} day^{-1}
k_1	half saturation constant of water uptake, mm
d	death rate, day^{-1}
D_p	biomass diffusion coefficient, m^2 day^{-1}
D_w	soil moisture diffusion coefficient, m^2 day^{-1}
D_o	surface water diffusion coefficient m^2 day^{-1}
D_p	mean surface water velocity m day^{-1}
α	maximum infiltration rate day^{-1}
W_o	the rate of infiltration in the absence of plants, [ ]
r_w	timescale of water loss due to evaporation and drainage, day^{-1}
R	precipitation, mm day^{-1}
∇^2	The Laplacian, $\partial^2/\partial x^2 + \partial^2/\partial y^2$
x and y	Cartesian spatial coordinates

Table 1.1: Parameters of the HilleRisLambers / Rietkerk model

where W is the soil water depth in mm; and

$$\frac{\partial O}{\partial t} = R - \alpha O \frac{P + k_2 W_o}{P + k_2} + \left(D_o \nabla^2 O\right) or \left(V_o \frac{\partial O}{\partial x}\right), \tag{1.3}$$

where O is the surface water depth in mm. The parameters are defined in Table 1.1. This is the model that was used to generate the pattern sequence in Figure 1.4.

1.3.2 Refining the models

Examination of the model output (as shown in the examples in Figure 1.4) reveals a curious feature, in that by simply rescaling the process parameters, identical pattern morphologies could be produced spanning a range of cm to many 100s of meters. Indeed, von Hardenberg et al. [2001] have proposed a strongly analogous model intended to reproduce observed patterns at the scale of cm, in contrast to the much larger scale patterns discussed to date. This rescaling was largely achieved through consideration of systems with very high subsurface redistribution of soil moisture. Thus, the range of spatial scales over which these models can be meaningfully applied,

and verification of whether the mechanisms of pattern formation are truly scale invariant over many orders of magnitude must be clarified. Assessing the mechanism of pattern formation at very small scales (where the Turing model approach has not been verified by field measurements to date) forms the subject of Chapter 2 of this dissertation.

Examining the mathematical form of the model in Equations 1.1, 1.2, 1.3 reveals the largely phenomenological nature of its construction. Indeed, there are several features of the model construction that could be refined to improve the realism of the process representation. This dissertation focuses on three key areas:

- The representation of biomass transport processes;
- The form of the infiltration feedback; and
- The implications of micro-topography on overland flow.

Biomass transport

In the existing model biomass transport is represented as diffusive (the 'green slime' approach [Borgogno et al., 2009]). As such, biomass transport is isotropic (or at least based on an isotropic kernel) and driven strongly by local gradients of vegetation biomass. There are several issues associated with this representation. First, diffusion coefficients are difficult to estimate or measure based on field data, making parameterization of this term problematic [Okubo and Kareiva, 1980]. Second, the biomass gradients that drive diffusion exist only at the boundary of vegetated sites. However, vegetation reproduces at all locations, generating seed which may be transported nonlocally [Borgogno et al., 2009]. Finally, the assumption of isotropic biomass transport encoded in a diffusive representation is questionable, in light of measured seed bank distributions and preliminary modeling by Saco et al. [2007] that

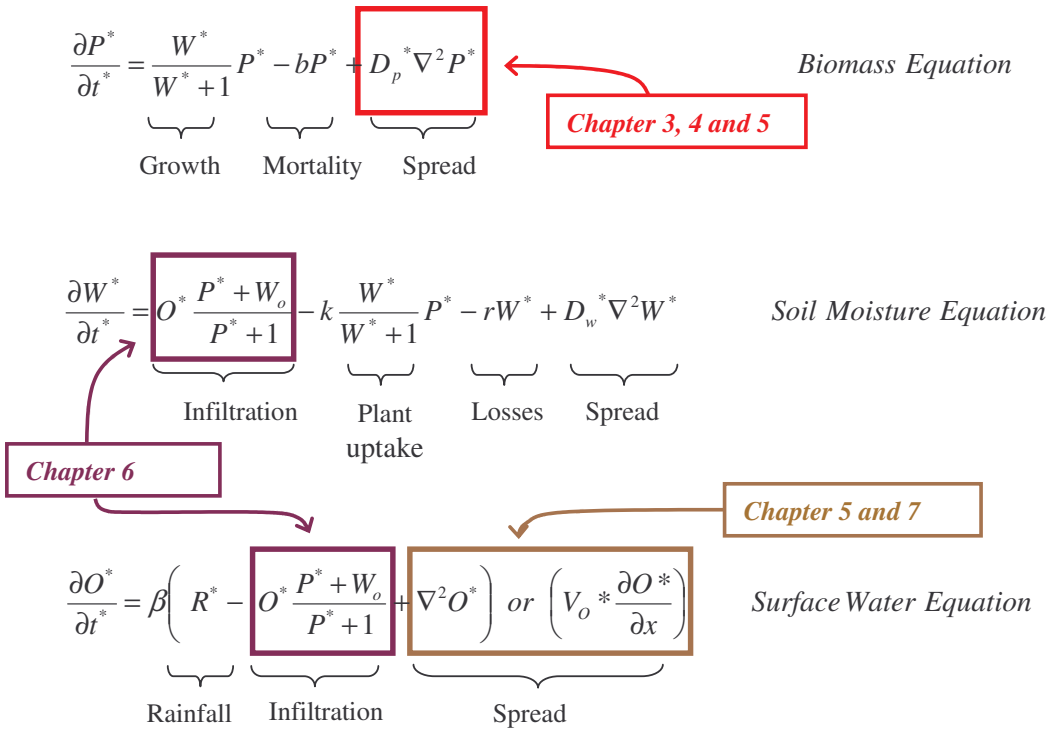

FIGURE 1.6: The chapters of this dissertation can be explicitly related to process issues associated with various components of the HilleRisLambers/ Rietkerk model.

suggest that a net downslope transport of seeds might be associated with overland flow, at least on sloping sites. Thus, three separate issues associated with biomass transport have been addressed: how to estimate a diffusion coefficient appropriately in the diffusive representation (Chapter 3); the effects of adopting a more realistic depiction of seed dispersal in the models (Chapter 4) and finally, the implications of anisotropy in seed dispersal behaviour (Chapter 5).

Feedback processes

The key feedback considered in Equations 1.1, 1.2, 1.3 is the feedback between infiltration rate and local biomass density, which is represented as a saturating Michaelis-Menten-type function. Despite numerous site-specific studies that demonstrate the

existence of biomass-infiltration relationships, the mathematical form of such relationships have not been confirmed. Nor has the sensitivity of a biomass-infiltration relationship to soil type or climate been elucidated. These issues are addressed in Chapter 6.

Challenges for hydrology

The final issue explored in this thesis is the potential for micro-topographic variations on the land surface to alter the behaviour of overland flow and infiltration in arid landscapes. Naturally, overland flow and micro-topography are not the only topic that frame these hydrologic challenges. However, in line with the main theme of this thesis, this Chapter was motivated by the observation that on the gently sloping landscapes where vegetation patterns arise, local micro-topography may provide a greater driver for surface water flow than does the mean slope. As a precursor to developing a process representation that specifically relates micro-topography to vegetation patterning, Chapter 7 develops an extension to existing hydrological theory that can account for the influence of micro-topography on rainfall-runoff partitioning under idealized circumstances.

Future Directions

While the number of eco-hydrologic processes to be explored in the context of patterned vegetation can be extended indefinitely, the final chapter of this thesis focuses on the next steps building on this work. They include a combination of proposed field experiments and novel facilities, a data assimilation framework to move towards forecasting ecosystem health using available remote sensing products, and further assessment of the coupling between the ecological, hydrological, and geomorphic attributes of patterned landscapes.

2

A porous convection model for small-scale grass patterns

2.1 Introduction

Ecological pattern formation occurs in a wide array of contexts [Rietkerk and van de Koppel, 2008], but the hypothesized mechanisms have focused on scale dependent feedback or reaction-diffusion processes. Mechanisms of this sort, where growth of the pattern is enhanced at small scales but suppressed at large scales, produce what are known as Turing patterns [Turing, 1952]. An alternative class of hydrodynamic pattern-forming mechanisms, arising from instabilities in the motion of fluids [Cross and Hohenberg, 1993], has been largely omitted from discussions of ecological patterns. Patterns arising due to Turing or hydrodynamic processes are not generally distinguishable on the basis of morphology alone.

Short wavelength (λ) vegetation patterns comprised of brown and green bands with $\lambda \approx 10$ cm have been observed in short-canopy warm season grasses [von Hardenberg et al., 2001, Meron et al., 2004, Miller, G. L. pers. com.] and were previously hypothesized to arise due to Turing-type effects based on water scarcity (as per

Valentin et al., 1999). Thus, they would form part of a scale-invariant spectrum of vegetation patterning along with patterns of $\lambda \approx 50$ to 100 m commonly occurring in deserts [Deblauwe et al., 2008, Rietkerk et al., 2004]. The small-scale grass patterns are morphologically similar to both Turing patterns and those produced by thermal convection of a fluid [Cross and Hohenberg, 1993, Shattuck et al., 1995].

We present a new hypothesis to explain these patterns: that a thermal gradient between warm ground and cool air is unstable to thermal convection, generating a pattern of rising warm air and falling cold air. Chilling injuries associated with the falling cold air then produce characteristic brown bands of 'dead' vegetation. This hypothesis is consistent with several features of small-scale vegetation patterns, including their length scale, rapid onset and transient nature. In contrast, for a Turing process driven by soil moisture availability to generate coherent, small-scale patterns would require a remarkable degree of organization within the soil, opposing the tendency of redistribution and root activity to homogenize soil moisture on short length scales [Katul et al., 1997]. In this paper we draw on established models of thermal convection to predict the conditions under which convection rolls might lead to patterning in a vegetation canopy. These quantitative predictions are then tested against field observations of a naturally occurring instance of grass patterning.

2.2 Thermal convection hypothesis

When a fluid-saturated porous medium is heated from below, heat is transported by thermal conduction. Although this heating results in the base layer of fluid being more buoyant than the overlying fluid, viscous drag and thermal diffusivity both oppose its upward motion. As the temperature at the base of the fluid column increases, the buoyancy overcomes these stabilizing effects and the conducting regime gives way to convection. The convective state is characterized by regions of rising warm fluid, adjacent to regions of falling, cold fluid [Ball, 2001, e.g.]. The resulting

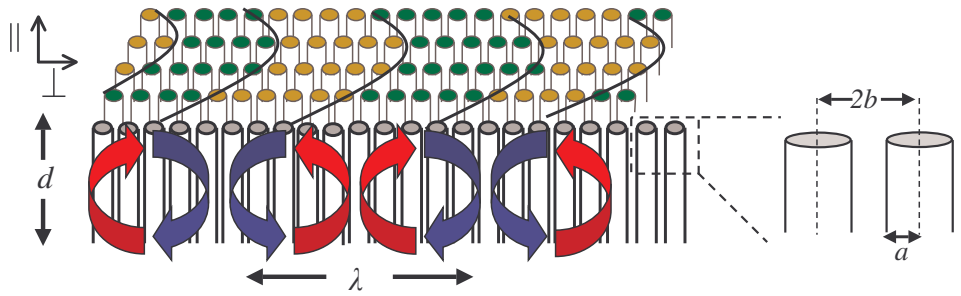

FIGURE 2.1: Schematic of parameters used in porous convection model (not to scale).

convection rolls are shown schematically in Figure 2.1, along with a definition of key parameters. Typically, convection rolls form locally-parallel stripes (which can bend to form labyrinthine patterns) or spots; in the case of convection within a porous medium [Howle et al., 1993, Shattuck et al., 1995], the patterns are morphologically similar to those observed in vegetation.

We hypothesize that small-scale grass patterns can be formed by this hydrodynamic process: the observed pattern of green and brown grasses could arise from the combination of convection and chill damage if falling air was cold enough to damage grass, and rising air warm enough to protect it. The rapid formation and transient nature of grass patterns is suggestive of chill-damage as a possible cause: such damage occurs when ambient temperatures drop too rapidly for plants to acclimate, and results in usually non-fatal tissue damage such as browning and death of leaves [Taiz and Zeiger, 2005]. Warm-season grasses can be damaged by less than an hour of exposure to near-freezing temperatures [Atwell et al., 1999].

The onset of porous medium convection occurs when buoyancy overcomes the stabilizing forces of viscosity and heat conduction. This balance is quantified by a ratio known as the Rayleigh number, where the buoyancy terms are in the numerator and the stabilizing terms in the denominator:

$$Ra = \frac{K\alpha g \Delta T d}{\kappa \nu}, \tag{2.1}$$

Here, α is the thermal expansion coefficient of the fluid, g is the acceleration due to gravity, ΔT is the difference in temperature between the solid bottom and the fluid at the upper boundary, d is the thickness of the porous medium, and ν is the kinematic viscosity of the fluid. Two parameters, the permeability K and the thermal conductivity κ, depend on the details of the porous medium, including the porosity ϕ and the geometry of the pores. When Ra exceeds a critical threshold Ra_c, convection begins [Lapwood, 1948]. In an isotropic medium, the critical Rayleigh number is given by $Ra_c = 4\pi^2$. However, the permeability of the voids in a vegetation canopy depends on whether the fluid is moving vertically (parallel to the grass blades) or horizontally (intercepting multiple grass blades). Thus, the canopy is anisotropic and the Rayleigh number must be redefined to account for directional effects:

$$Ra_c = \pi^2 \left[\left(\frac{\kappa_\perp / \kappa_\parallel}{K_\perp / K_\parallel} \right)^{1/2} + 1 \right]^2 . \tag{2.2}$$

The subscripted parameters (see Figure 2.1) indicate the material properties parallel and perpendicular to the temperature gradient and $K_\parallel$ and $\kappa_\parallel$ are used in Eq. 1. in place of the average values [Straus, 1974, Straus and Schubert, 1978, Kvernvold and Tyvand, 1979].

A grass canopy may be modeled as a series of upright cylindrical rods (grass blades) of radius a spaced a distance $2b$ apart, as shown in Figure 2.1. Using this approximation, we can estimate the permeabilities $K_\parallel$ and $K_\perp$ using the approach of Happel [1959]. The permeability in the lateral direction $K_\perp$ can be computed directly from the geometry:

$$K_\perp = \frac{b^2}{4} \left[\ln \frac{b}{a} - \frac{1}{2} \frac{b^4 - a^4}{b^4 + a^4} \right] . \tag{2.3}$$

To estimate the vertical permeability $K_\parallel$, the Carmen-Kozeny equation for K is equated to the solution for viscous flow about a cylinder to give $K_\parallel = \phi m^2 / k_\parallel$.

The geometric parameter m is analogous to the hydraulic radius and is given by $m = (b^2 - a^2)/2a$. The Kozeny constant $k_\parallel$ parametrizes the morphology of the porous medium and is estimated [Happel, 1959] as:

$$k_\parallel = \frac{2\phi^3}{(1-\phi)\left[2\ln(\frac{1}{1-\phi}) - 3 + 4(1-\phi) - (1-\phi)^2\right]}. \tag{2.4}$$

The porosity ϕ is determined from the grass blade radius a and blade density ρ via the relation $\phi = 1 - \rho(\pi a^2)$. To estimate the thermal diffusivity of the grass canopy, we average the component materials (water, grass) in proportion to their volumetric presence (ϕ and $(1-\phi)$, respectively), taking grass to be composed of 85% water and 15% cellulose. Given the high porosity of the canopy, we assume that $\kappa_\parallel \approx \kappa_\perp$. Thus, for known or measurable properties of a grass canopy, it is possible to calculate the value of ΔT_c required for the onset of convection ($Ra > Ra_c$).

For anisotropic media, the critical wavenumber of the convection pattern at onset is

$$q_c = \pi/d \left[\frac{K_\perp}{K_\parallel}\frac{\kappa_\perp}{\kappa_\parallel}\right]^{-1/4} \tag{2.5}$$

[Kvernvold and Tyvand, 1979]. Based on this analysis, we can determine the necessary conditions for the convection-chill hypothesis to hold, given measured values of a, d, ρ and ambient meteorological conditions. The requirements are a large enough temperature gradient ($\Delta T > \Delta T_c$), air temperature cold enough (e.g. $\lesssim 0$°C) to cause chill damage, and no wind or turbulence to disrupt convection. Secondly, we can predict the expected pattern wavelength given these conditions and compare with observations. Figure 2.2 (a,b) shows the dependence of ΔT_c and wavelength $\lambda_c = 2\pi/q_c$ (measured in units of d) on a and ρ. While ΔT_c is quite sensitive to the particular porosity (set by a and ρ), $\lambda_c \approx 1.8d$ over the full range of reasonable characteristics.

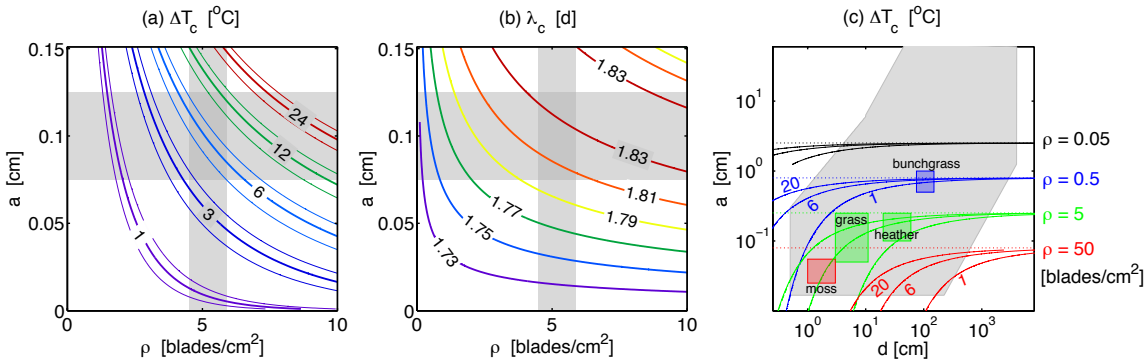

FIGURE 2.2: Contour plots of numerically computed values of ΔT_c and λ_c for a range of appropriate vegetation sizes (a, d) and densities (ρ). (a,b) Values computed for observed lawn grass parameter regime (see Figure 2.3). Gray bars indicate uncertainty in stem radius a and density ρ measurements, while the thin curves associated with each contour of ΔT_c indicate the uncertainty in the measurement of height d. (c) Critical temperature difference computed as function of a and d for a range of realistic vegetation densities: $\rho_{\text{moss}} \approx 50$ (red), $\rho_{\text{grass,heather}} \approx 5$ blades/cm^2 (green), $\rho_{\text{bunchgrass}} \approx 0.5$ blades/cm^2 (blue), very low $\rho = 0.05$ blades/cm^2 (black). For each ρ, contours show $\Delta T_c = 1, 6$ and 20°C, and shaded rectangles denote the approximate range of a and d values for the corresponding vegetation type (indicated by color). Gray shaded area indicates a realistic regime for terrestrial plants based on typical scaling laws for woody and non-woody species [Rich et al., 1986].

2.3 Field observations

Grass patterning with a labyrinthine morphology and wavelength $\lambda \approx 10 \pm 2$ cm was fortuitously observed on a lawn at Duke University (Durham, NC, USA) on 12 November 2008. The relevant geometric factors required to calculate the critical Rayleigh number Ra_c (Eq. 1) were measured in situ and confirmed using high resolution photographs of the patterns, allowing us to estimate ΔT_c and λ_c for the lawn. Meteorological data were obtained for the night of 10 November, the only recent, preceding night when a frost occurred. These data are presented in the Appendix A. The two day delay corresponds to the typical timeframe for symptoms of chill damage to appear [Atwell et al., 1999]. Meteorological data were obtained from the North Carolina State Climate Service [Office, 2008] for the six weather stations sur-

rounding Durham, NC that report both ground and air temperature (stations SILR, REED, OXFO, KTDF, KIGX and KRDU) and averaged to obtain an estimate of ΔT. Wind data were obtained from sonic anemometer instrumentation overlying a 50 cm tall grass field located at the Duke Forest, approximately 16 kilometers from the patterned site (see Novick et al. [2005] for site details). Immediately after the observation of the patterns we also measured volumetric soil moisture (θ) content in the root-zone (top 12 cm), taking a total of 52 measurements until rain commenced and further measurements were deemed unreliable.

2.4 Results

The measured geometric properties of the lawn were: grass blade radius $a = 0.1 \pm 0.025$ cm, canopy depth $d = 6 \pm 1$ cm, and lawn density $\rho = 5.2 \pm 0.7$ blades/cm^2; these values are typical for dense lawns [Brede, 1999, Hamilton and Waddington, 1999]. As shown in Figure 2.2(a,b), using these values in the thermal convection model predicted a value for $\Delta T_c = 6.3 \pm 3.6^\circ$ C and $\lambda_c = 10.9 \pm 1.8$ cm. The wavelength of the pattern was measured from photographs to be $\lambda = 10 \pm 2$ cm, in agreement with the model results for the measured lawn parameters. Figure 2.3 shows all measured field parameters.

The meteorological data showed that on 10 November 2008 ground temperatures dropped from 12.6°C to 11.3°C from midnight to 7am, while air temperatures dropped from 4.3°C to −0.4°C over the same period. Thus, ΔT ranged from 8.2°C to 12°C throughout the night, with the greatest ΔT coinciding with the coldest air temperatures close to dawn. An uncertainty of 2°C is associated with the measured ΔT due to variation across the six weather stations, however even when this is incorporated, the ambient ΔT exceeded the model estimate for ΔT_c. Wind conditions overnight were calm. The vertical momentum flux was 3×10^{-3} m^2/s^2 and the horizontal shear velocity was 0.06 m/s, indicating that the potential for production of

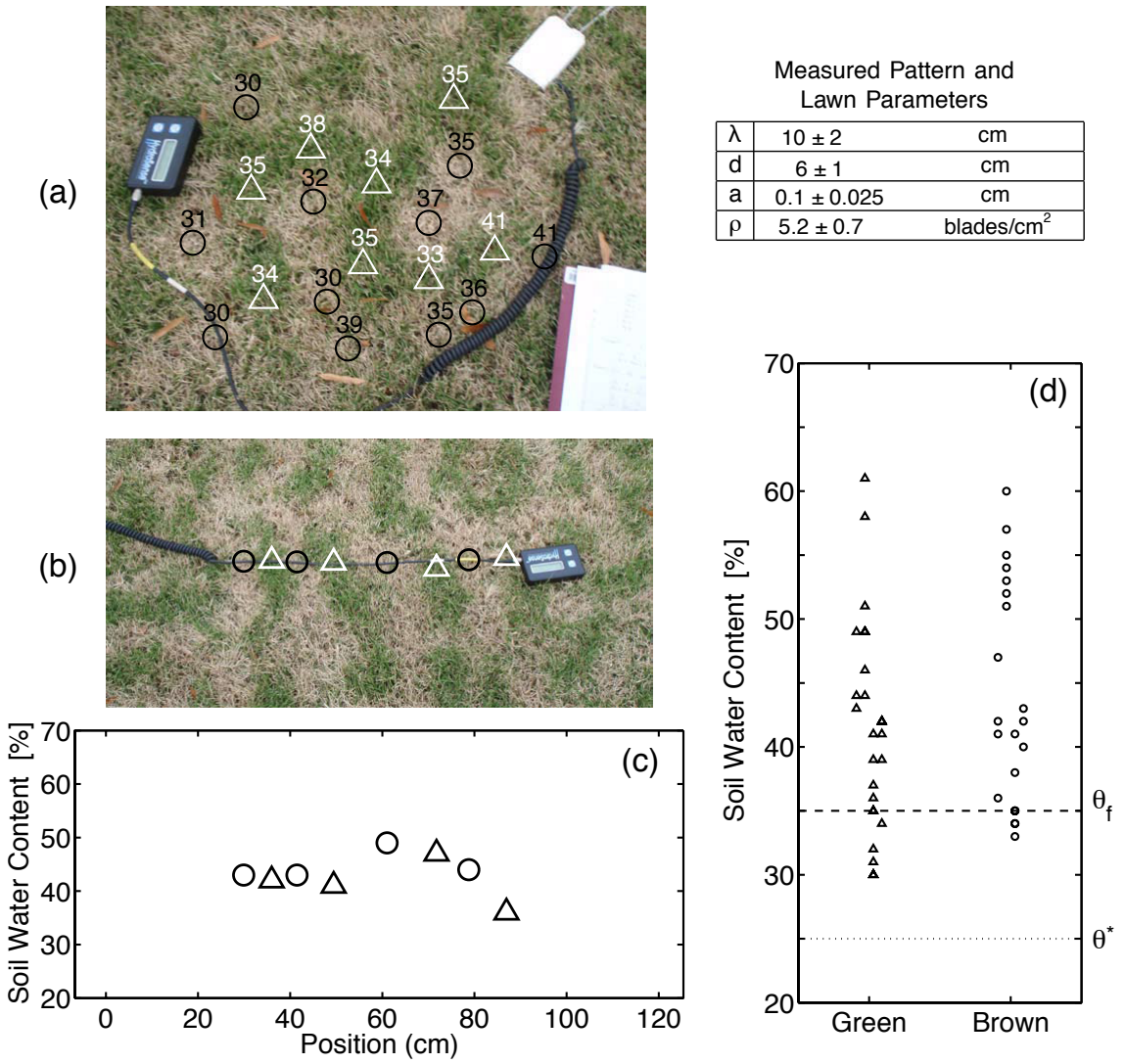

FIGURE 2.3: Sampling of soil water content θ at 52 points. (a) Measurements of θ within a labyrinthine pattern, printed within image. (b) Measurements of θ along a transect perpendicular to a striped pattern, plotted in (c). (d) All 52 θ measurements made on the site, sorted by brown/green location. Dashed line θ_f indicates the field capacity and dotted line θ^* indicates the wilting point [Rodriguez-Iturbe and Porporato, 2004]. Table: Parameters used to calculate ΔT_c and λ_c for grass canopy.

turbulence near ground level was negligible.

Two examples of the soil water content (θ) measurements as a function of brown/ green locations within the pattern are shown in Figure 2.3. No correlation between grass condition and θ could be discerned. All moisture readings exceeded the permanent wilting point θ^* at which plants begin to experience water stress. The mean θ for the brown patches was $\bar{\theta}_{brown} = 41.4\%$, slightly lower than $\bar{\theta}_{green} = 44.3\%$. This difference is comparable to the error in the instrument, and was not statistically significant ($p = 0.24$), nor, given that $\bar{\theta} > \theta^*$, was it large enough to be physiologically important [Rodriguez-Iturbe and Porporato, 2004].

2.5 Discussion and conclusions

Based on the observations of this occurrence of grass patterns, all data ($\Delta T > \Delta T_c$, $\lambda \approx \lambda_c$, still air conditions and $\bar{\theta}_{green} \approx \bar{\theta}_{brown} > \theta^*$) support the interpretation that convection and chill damage generated patterning. An unusually large ΔT two nights prior to the observation exceeded the predicted value of $\Delta T_c = 6.3 \pm 3.6$°C and coincided with air temperatures near freezing, which are low enough to cause chill damage to plants, but ground temperatures sufficiently warm to generate convective motion within the grass canopy and locally buffer grass from chill damage. Still atmospheric conditions suggest that thermal convection, not wind, was the major driving force for flow within the grass canopy.

The porous convection model is consistent with the observations of the grass patterning and provides an explanation for the transience of observed grass patterns, since chill damage is not fatal and plants recover rapidly. The infrequent observation of the phenomenon is explained by the specificity of the required non-biological and biological factors coinciding with the presence of plants susceptible to chill damage. The length scales of the observed patterning, along with length scales reported by other authors for similar grass patterns [von Hardenberg et al.,

2001], correspond well with predictions from the convection model. Thus, we find that the porous convection model explains multiple, independent aspects of the grass patterning phenomenon. Conversely, the lack of any discernible correlation between the grass pattern and water content is contrary to the predictions of a Turing model based on water availability. Unlike the Turing models [Rietkerk et al., 2002, von Hardenberg et al., 2001], the bifurcation to a patterned state is a simple, forward bifurcation with no bistability. Because chill damage does not change the porous properties of the vegetation there is no feedback between the pattern and the hydrodynamics, and thus no hysteresis.

The thermal convection mechanism could apply to a range of vegetation types, as shown in Figure 2.2(c), but in practice a realistic regime of terrestrial plants (gray shaded) coincides with reasonable temperature differences ($\Delta T_c \approx 6°\text{C}$) only in a limited regime with stem density $1 \lesssim \rho \lesssim 10$ blades/cm^2 and small stem diameter ($a \lesssim 1$ cm). For higher densities (e.g. mosses), ΔT_c becomes unrealistically large. Where densities are low and canopies tall, not only do wind-driven flows become more likely, but ΔT_c can be very small and thus unlikely to cause any chill-damage. A second consideration is that the vegetation must be of a type sensitive to chill-damage. Warm season grasses are ideal target species, but other ground-covering herbaceous species, or even small, low-growing woody species could sustain this mechanism. Because our model applies to canopy geometries which can be approximated by an array of cylinders, Figure 2.2(c) highlights mosses, lawn grasses, and bunch grasses. However, similar results would apply for other low and dense canopy geometries, such as heaths. More generally, we may conceive of other scenarios where hydrodynamic pattern formation structures ecological communities. Convection can occur whenever buoyant fluid underlies denser fluid, such as in shallow lakes, where bottom sediments heat faster than overlying water, lake or ocean floors subject to geothermal heating, or strong salinity clines. Because convection results in efficient and spatially

partitioned transport, it could establish microclimates relatively enriched or depleted in resources, with implications for the structure of organismal assemblages.

Hydrodynamic mechanisms for pattern formation are morphologically indistinguishable from Turing processes, yet they result from fundamentally different mechanisms and imply different dynamics. The thermal convection/chill damage hypothesis appears to explain multiple aspects of observed short wavelength vegetation patterns, and suggests that ecological patterns can arise from hydrodynamic processes. In addition, hydrodynamic instabilities should be more generally incorporated into thinking about ecological patterns to prevent similarity in pattern morphology from being equated with similarity in pattern formation mechanisms.

3

Plant propagation fronts and wind dispersal: An analytical model to upscale from seconds to decades using super-statistics

3.1 Introduction

Vegetation migration in response to environmental drivers is now receiving significant attention in studies of species invasion and climate change, and has been elevated to a fundamental discipline in spatial ecology [Neilson et al., 2005, Neuhauser, 2001, Okubo and Levin, 2001]. The basic challenge confronting models of vegetation movement is the large timescale separation between seed dispersal processes (seconds-hours) and vegetation growth (months-years). For wind-dispersed seeds, the scale separation is exacerbated by the importance of turbulence (which varies over fractions of seconds) governing seed uplifting and subsequent long distance seed dispersal [Horn et al., 2001, Nathan et al., 2002, Soons et al., 2004a,b, Tackenberg, 2003]. The contemporary approach to overcoming this "dimensionality curse" is to represent plant movement by wind as a diffusive process [HilleRisLambers et al., 2001, Klausmeier, 1999, Lejeune, 2002, Rietkerk et al., 2004]. An advantage to this

representation is that an explicit relationship between the diffusion coefficient (D), the intrinsic growth rate (r), and the speed of propagation of the biomass front (c) can be derived. For instance, for the prototypical case of the Fisher-Kolmogoroff equation with a constant D, the front speed is given by $c = 2\sqrt{rd}$ [Fisher, 1937, Kolmogoroff et al., 1937, Murray, 2003a]. However, the fact that D cannot be readily inferred from seed attributes (e.g. terminal velocity, release height, etc.) and wind conditions prevents prognostic use of such a result. Furthermore, representing plant migration via diffusion remains questionable, and dispersal data suggest a "super-diffusive" aspect to species migration and spread, which requires an alternative treatment. Comparisons between measured vegetation spread rates and those predicted by diffusion models show that diffusion underestimates the propagation speed of vegetation movement [Clark, 1998, Clark et al., 1998, 2001, 1999, Higgins et al., 2003, Nathan and Katul, 2005, Neilson et al., 2005]. To match the observed speeds of vegetation movement requires adopting a dispersion kernel with "fat tails" in comparison to the Gaussian kernel underpinning classical diffusion processes. To circumvent this limitation, several dispersion kernels have been proposed in models of c, based on empirical [Clark, 1998, Dauer et al., 2007, Robledo-Arnuncio and Gil, 2005], phenomenological [Kot et al., 1996, Lewis and Pacala, 2000, Neubert et al., 1995] and mechanistic grounds [Nathan and Katul, 2005, Neubert et al., 1995, Williams et al., 2006]. To date however, simultaneously preserving mathematical simplicity and prognostic capability remains elusive, and is the subject of this work. Recent studies have suggested that "up-scaling" the effects of turbulent transport processes on seed dispersal kernels from fractions of seconds to 1/2 hourly time scales can be achieved analytically via a mechanistic Wald Analytical Long-distance Dispersion (WALD) model [Katul et al., 2005], the kernel of which resembles an Inverse-Gaussian or a Wald distribution. The primary inputs to the WALD model are mean half hourly wind speeds ($\overline{U}$), basic seed attributes (e.g. terminal velocity),

and release heights. Furthermore, a number of studies have already shown that the distribution of $\overline{U}$, sampled over seasonal to annual time scales, can be approximated by a Weibull distribution, and wind atlases document these Weibull wind parameters spatially across continents for wind energy harvest [Troen and Peterson, 1989]. Building on these two findings for wind and its effect on seed dispersal, we propose to replace the diffusive term in the Fisher-Kolmogoroff equation by the scaled effect of the Wald and Weibull kernels and develop a novel analytical solution for the vegetation front speed. As a case study, order of magnitude predictions of c from the analytical solution are then compared to reported vegetation migration rates of the early Holocene period in the USA during the period of post-glacial expansion. Finally, the broader implications of the proposed modelling approach for assessing vegetation spread rates are presented in light of recent developments in the field of "super-statistics", which is now gaining attention in complex systems science [Beck and Cohen, 2003].

3.2 The model

3.2.1 The basic equations

The one-dimensional Fisher-Kolmogoroff equation, which describes the local increase and spread in space of a logistically growing population, is given by

$$\frac{\partial P\left(x,t\right)}{\partial t} = rP\left(x,t\right)\left(1-\frac{P\left(x,t\right)}{K}\right) + D\frac{\partial^2 P\left(x,t\right)}{\partial x^2},$$

where the total biomass of the species per unit area ($P\left(x,t\right)$, $[ML^{-2}]$) grows logistically at rate r $[ML^{-2}T^{-1}]$ before growth saturates at a carrying capacity $K, [ML^{-2}]$; x is distance $[L]$, and t is time. To consider the spread of a plant species due to seed dispersal, the equation can be generalized to

$$\frac{\partial P\left(x,t\right)}{\partial t} = rP\left(x,t\right)\left(1-\frac{P\left(x,t\right)}{K}\right)\left(P\left(x,t\right)+\alpha\int_{\Omega}W\left(x'\right)P\left(x',t\right)dx'\right), \quad (3.1)$$

Here x' is a dummy variable denoting distance $[L]$. At each time step (dt), a proportion (a, $[\mathrm{T}^{-1}]$) of the biomass is spatially distributed according to a dispersal kernel $W(x)$, applied over a spatial domain, Ω. All parameters (r, K, a) are assumed to be constant in space and time. The r and K parameters follow their standard interpretations from logistic growth models. The "spread and survival" parameter, α , is related to fecundity. For each timestep, and each point in space, it defines the biomass that is spread as seed from that point, and subsequently germinates and grows: i.e. the spreading and surviving biomass. In this formulation, α is defined as a proportion of $P(x,t)$, and it is assumed that $a << 1$. This treatment of movement contrasts to the original Fisher-Kolmogoroff equation in which biomass spread rates depend on the local spatial variation in biomass $\partial^2 P/\partial x^2$ and a diffusion coefficient D $[\mathrm{L}^2\mathrm{T}^{-1}]$. Equation 3.1 recovers the steady state solution of the traditional Fisher-Kolmogoroff equation if $W(x)$ is a Gaussian kernel (see Appendix B). In the case of wind dispersed biomass, fast turbulent processes must be resolved. For integrating across these processes to arrive at hourly time scales, the WALD model kernel is used and is given by

$$W\left(x\right) = \sqrt{\frac{\lambda}{2\pi x^3}}e^{-\frac{\lambda(x-\mu)^2}{2\mu^2 x}}, \quad (3.2)$$

where

$$\lambda^{1/2} \approx \frac{z_r}{\sqrt{\kappa h\left(2\theta\right)}},$$

and

$$\mu = \frac{z_r \overline{U}}{V_t}.$$

The parameters relate to the characteristics of the applied half hourly mean wind speed field ($\overline{U}$) and θ, (defined below), the seed release height of the plants (z_r) and the height of the surrounding canopy (h), and other than $\overline{U}$ are assumed to be constant in space and time. θ is defined as $\sigma_w/\overline{U}$, where σ_w is the standard deviation of the wind velocity in the vertical direction. The θ represents the importance of turbulence in lifting seed from the canopy versus the action of the mean wind speed in moving the seed horizontally; V_t, is the terminal velocity of the seeds, that is the steady velocity at which they fall; and κ is a proportionality constant relating the size of turbulent eddies within the canopy to the canopy height [Katul et al., 2005], where is of order 1, taken as 0.6 for the purposes of this study. In a standard boundary layer, where eddies scale with the height from the ground, $\kappa = 0.4$ and is Von Karman's constant; for within canopy flow conditions, however, κ is expected to be > 0.4 due to wake generation, and the fact that the seed-carrying eddies no longer scale with height from the ground. σ_w and $\overline{U}$ are strongly correlated, and θ can be approximated as a constant at near neutral atmospheric conditions just above the canopy (when heating or cooling of the air does not impact turbulent generation). The μ parameter defines the mean dispersal distance, while λ defines a scaling parameter. As evidenced from Equation 3.2, the WALD kernel yields a multiplicative combination of a power law term describing the dispersal kernel tails, "censored" by an exponential distribution that accounts for gravity. For high terminal velocities, the WALD kernel approaches a simple ballistic model. If seed terminal velocities are much less than the mean wind speed, then the kernel tails decay according to a power law ($\approx x^{-3/2}$) and at a slower rate than in many comparable dispersal kernels such as the bivariate student t-distribution [Clark et al., 1999]. For finite terminal velocities and mean

wind speeds, the WALD kernel is bounded, ensuring that asymptotic approaches to constant propagation speeds exist [Kot et al., 1996, Mollison, 1991].

3.2.2 The wave speed

The motion described by the generalised Fisher-Kolmogoroff equation generates a travelling wave front of expanding biomass. To recover the velocity of plant movement, the velocity of the nonlinear wave front is needed. To derive this velocity, the approach outlined in Kot et al. [1996] is used, beginning with the "linear conjecture" that the velocity of the nonlinear wave front is equivalent to that of its linearisation. This conjecture is valid for populations that do not exhibit an Allee effect, i.e. the net growth rate is independent of population density [Mollison, 1991]. The differential equation is linearised by assuming that at the leading edge of the wave, $P/K << 1$ (i.e. the population is very much less than the carrying capacity), resulting in

$$\frac{\partial P}{\partial t} = r\left(P + \alpha \int_{-\infty}^{\infty} P\left(x'\right) W\left(x - x'\right) dx'\right), \tag{3.3}$$

and in discrete form, this equation becomes

$$P_{t+1} = rdt\left(P_t + \alpha \int_{-\infty}^{\infty} P\left(x'\right) W\left(x - x'\right) dx'\right) + P_t, \tag{3.4}$$

where dt is the time step. By appropriately rescaling the rate terms r and a, dt can be set to unity and cancelled. If a steady travelling wave solution exists, then:

$$P_{t+1}\left(x\right) = P_t\left(x - c\right), \tag{3.5}$$

where c is the front speed to be determined next.

Assuming a solution of the form $P \propto e^{-sx}$ for the linearised equation, and substituting Equation 3.4 into Equation 3.5 gives:

$$e^{-s(c-x)} = r\left(e^{-sx} + \alpha \int_{-\infty}^{\infty} e^{-sx} W\left(x - x'\right) dx'\right) + e^{-sx}, \tag{3.6}$$

$$e^{sc} = r\left(1 + \alpha \int_{-\infty}^{\infty} e^{-s(x-x')} W\left(x - x'\right) dx'\right) + 1. \tag{3.7}$$

Let $u = x - x'$.

$$e^{sc} = r\left(1 + \alpha \int_{-\infty}^{\infty} e^{-su} W\left(u\right) du\right) + 1. \tag{3.8}$$

This expression gives the characteristic equation for the wave front speed c. The component $\int e^{-su} W\left(u\right) du$ is the moment generating function of the WALD distribution, hereafter referred to as $MG(s)$, which, for a finitely bounded WALD kernel, is differentiable and defined as:

$$MG\left(s\right) = \exp\left[\frac{\lambda}{\mu}\left[1 - \left(1 - \frac{2\mu^2 s}{\lambda}\right)^{\frac{1}{2}}\right]\right] \tag{3.9}$$

$$\frac{\partial MG\left(s\right)}{\partial s} = \frac{\mu \exp\left[\frac{\lambda}{\mu}\left[1 - \left(1 - \frac{2\mu^2 s}{\lambda}\right)^{\frac{1}{2}}\right]\right]}{\left(1 - \frac{2\mu^2 s}{\lambda}\right)^{\frac{1}{2}}} = \frac{\mu MG\left(s\right)}{\left(1 - \frac{2\mu^2 s}{\lambda}\right)^{\frac{1}{2}}} \tag{3.10}$$

The solution for the wave front must be real and positive, and therefore exists at the double root of the characteristic equation, given by its derivative:

$$ce^{sc} = r\alpha MG'\left(s\right) \tag{3.11}$$

.

Equation 3.11 combined with Equation 3.8 provides a parametric description of c and r:

$$c = \frac{r\alpha MG'(s)}{r(1+\alpha MG(s))+1}, \tag{3.12}$$

$$r = \frac{\exp\left[s\left(\frac{r\alpha MG'(s)}{r(\alpha MG(s))+1}\right)\right]-1}{(1+\alpha MG(s))}. \tag{3.13}$$

Using a known value of r to solve Equation 3.13 for s allows the direct determination of c. The solution is primarily dictated by the values of r, α, λ, and μ. Due to the implicit nature of the equation, a numerical root finding method is required. The linear conjecture implies that a number of more complicated models also have an asymptotic wave speed represented by equations 3.12 and 3.13. For instance, incorporating a time delay to maturity in the plants does not necessarily impact the asymptotic wave speed although the time to reach the asymptote increases. The results in equations 3.12 and 3.13 were derived by including the most basic processes of growth and dispersion, but neglecting retarding factors such as predation, inter-specific competition and landscape heterogeneity. Thus, the propagation rate predicted by such analysis can be taken as an upper bound on realistic values.

3.2.3 Up-scaling using super-statistics

Up to this point the model has assumed that all parameters are fixed in space and time. However, there are many sources of variability that impact these parameters over time scales commensurate with biomass growth and the spatial scales of migration. In the time domain, the most pervasive is the variation in mean half hourly ambient wind speed, which changes on hourly timescales, over a typical range of 0-12 ms^{-1}, i.e. several orders of magnitude, in the Eastern USA [Van der Hoven, 1957]. This exceeds variability in mean growth rate, or spread and survival rate, which vary by at most a single order of magnitude on seasonal to inter-annual scales. Resolving the effect of the rapid variation in half hourly mean wind speed is necessary before

attempting to understand variability in the slower processes, and is the focus of the analytical upscaling attempts in this paper. Despite the focus on the mean wind speed temporal variability, variability in other parameters can be considered via numerical simulations. The detailed consideration of variation in multiple parameters, however, confounds analytic tractability. Instead, a sensitivity analysis is presented to show the impact of variability in ecological and forcing parameters on c.

The distribution of hourly (or half hourly) mean wind speeds, $\overline{U}$, has been well studied, and is often represented as a Weibull distribution with scale parameter b and shape parameter k, i.e.

$$p\left(\overline{U}=y\right)=\frac{ky^{k-1}}{b^{k}}e^{\left(\frac{y}{b}\right)^{k}}, \tag{3.14}$$

typically expressed as $p\left(\overline{U}\right) = Weib\left(b,k\right)$ [Conradsen et al., 1984, Garcia et al., 1998, Takle and Brown, 1978]. Hence, variations in mean half hourly wind speed over long timescales (seasonal to inter-annual) are accounted for by drawing $\overline{U}$ from a Weibull distribution. This approach is known as "super-statistics", and is currently gaining considerable interest in complex systems science, whereby the statistics governing variability in distributional parameters are used to evaluate variation that is extensively spread in space or time. The resulting distributions are analogous to using "mixture models", analytical composites of the distributions describing long and short timescale processes [Beck and Cohen, 2003, Porporato et al., 2006]. The significance of turbulent transport is clearly seen in the super-statistical framework by constructing the dispersal kernels, at an annual timescale, for a purely ballistic scenario (i.e. in the absence of turbulence, using the Weibull distribution but not the Wald) and for a turbulent transport scenario, using the Weibull as a super-statistical input to the Wald kernel. Turbulence causes seed transport to be extended by up to two orders of magnitude over purely ballistic cases. The resulting dispersal kernels

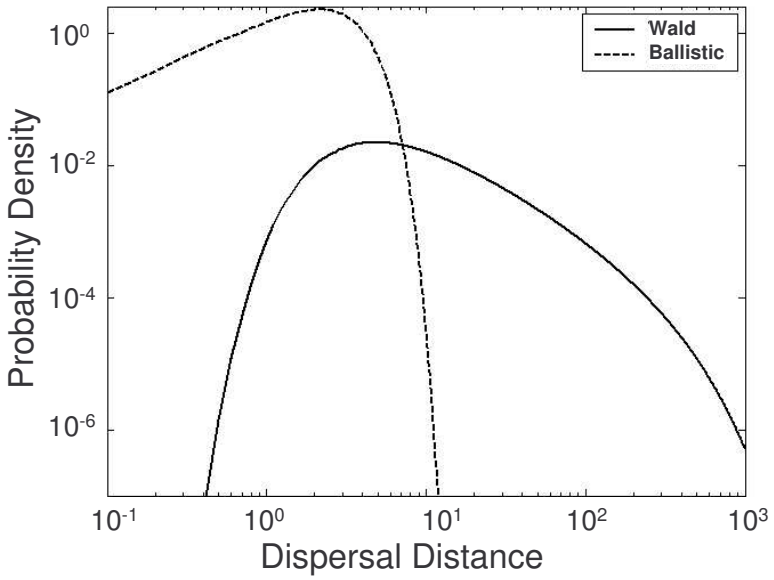

FIGURE 3.1: Comparison of Wald and Ballistic kernels on log-log plot. Kernels are shown for annual time scales and *Fraxinus pennsylvanica* parameters. The Ballistic kernel considers only advection of a seed falling with terminal velocity V_t and being advected by the mean wind speed, whose distribution is taken from the Weibull parameters. The Wald kernel accounts for turbulence in addition to advection, and results in finite probabilities of dispersion at length scales two orders of magnitude greater than those of the Ballistic kernel.

are shown in Figure 3.1.

The construction of the dispersal kernel as a mixture of the Weibull distribution and the Wald distribution also bears close analogy to existing phenomenological treatments of vegetation dispersion. For instance, the widely used 2Dt kernel is a mixture of a normal and exponential distribution [Clark et al., 1999], although in the current case the mixture is based upon the statistics of mechanistically derived processes. In summary, the model achieves an up-scaling from turbulent timescales to half hourly timescales via the WALD kernel, from half hourly timescales to annual timescales via the Weibull distribution of wind speeds, and can be further up-scaled

by consideration of inter-annual variability of Weibull parameters (Figure 3.2).

To use the analytical result in equations 3.12 and 3.13, a parameterisation that accounts for the Weibull variations in $\overline{U}$ and their interaction with the turbulent transport described by the Wald kernel is needed. What we seek is the appropriate (or effective) wind speed with which to parameterise a Wald dispersal kernel for wind-transported seeds over annual time-scales. Numerical simulations indicate that simple moments of the Weibull distribution (mean, mode etc.) grossly underestimate this wind speed. This is because the interaction of the Wald and the Weibull amplifies the effect of the tails of the distribution. There is no simple way to parameterise this effect, because that the marginal distribution arising from a Wald forced by the Weibull distribution cannot be obtained analytically. Given a realisation of the plant front velocity c, however, it is possible to work backwards (by using equations 3.12 and 3.13 in an inverse sense) to infer a single value for which would reproduce this c value from the numerical simulation. Determining this value for an ensemble of realisations of c, as generated by Monte Carlo analysis, a distribution of such "effective wind speeds" (U_{eff}) can be generated. The mean of U_{eff} $\left(\overline{U_{eff}}\right)$ reproduces the mean of the plant front velocities when applied to the numerical model. To proceed by defining $\overline{U_{eff}}$ preserves the flexibility of the model, which can be parameterised with $\overline{U_{eff}}$ (the determination of which is addressed in the following section) and appropriate WALD parameters for any combination of forest type and wind climate. A realisation of U_{eff} can be obtained from an empirically measured seed dispersal kernel over annual timescales by fitting the WALD parameterisation to this kernel. The difficulties associated with measuring the tails of the dispersal kernel, however, would likely cause this sample of U_{eff} to be underestimated, while reconstructing the distribution of U_{eff} would be highly labour intensive [Bullock et al., 2006]. The disparity between the applied Weibull distribution and the distribution of resulting from its application to the logistic-Wald model is shown in Figure 3.3.

Having defined U_{eff}, we proceed by constructing a relationship between the Weibull parameters and the effective velocity to allow prognostic usage. A wide range of wind distributions and their effect on c were explored by varying the parameters of the Weibull distribution in a range of $b \in [1, 3], k \in [1, 4]$ (covering the range of plausible values for winds). Distributions of c were obtained from a Monte Carlo simulation with 500 realisations for each combination of Weibull parameters (see Appendix B for details of numerical simulations), and distributions of computed from these using equations 3.12 and 3.13 in an inverse sense. Weibull, gamma and normal distributions were fitted to the resulting U_{eff} distribution, and goodness of fit assessed using the Akaike Information Criterion (AIC) [Akaike, 1974]. A relation between the distribution of U_{eff} and the distribution of mean applied wind speeds was empirically derived, using a curve fitting algorithm that tested multiple functional forms of the fitting functions and returned those with the least square error [Phillips, 2007]. Tenth and 90^{th} bounds on the parameters were derived numerically from the fitted distribution and used to provide bounds on the estimate of U_{eff}. The combination of the analytical results and these regression equations provided a closed-form semi-analytical model combining information about the wind climate and the vegetation properties to predict a likely range of wave speeds for vegetation dispersal.

3.2.4 Case study: North American post glacial expansion

The palynological record from the early Holocene epoch provides an ideal case study of vegetation migration as trees expanded their range in the wake of retreating glaciers [Delcourt and Delcourt, 1987, McDonald, 1993]. This record is useful because it extends over a sufficient temporal and spatial area to allow spread rates to be clearly determined, and, unlike contemporary records, is not confounded by anthropically enhanced dispersion. We used the analytical version of the logistic-

WALD model to examine the migration of eight wind-dispersed species (four *Acer* (maple) sp., two *Fraxinus* (ash) sp., one *Pinus* (pine) sp., and one *Betula* (birch) sp.). Our intent was not to obtain a one-to-one comparison but rather to demonstrate that the order of magnitude of spread rates could be independently derived from what is currently known about these species and assumed wind conditions. Seed terminal velocity data were obtained from the literature [Green, 1980, Matlack, 1992, 1987, Nathan et al., 2002, Williams et al., 2006], however biomass growth rates were not available. We estimated the biomass at maturity using allometric equations [Jenkins et al., 2003], in conjunction with diameter at breast height and stand age at maturity [United States Department of Agriculture, 1990] and used these as first order estimates of growth rate. For the smaller tree *Acer negundo* (Boxelder), which was outside the range of species considered by Jenkins et al., we adopted species specific allometric equations [Schlaegel, 1982]. The constants used are shown in Table 3.2. The vegetation expansion consisted of two phases: an initial replacement of low tundra by boreal forests, followed by replacement of boreal forest with deciduous forests [Delcourt and Delcourt, 1987]. Selection of wind data therefore needs to consider both the expansion into open tundra, most applicable to *Betula* and *Pinus* sp., and the later expansion into forested areas, applicable to *Acer* and *Fraxinus* sp. *Acer* sp. also expanded their range significantly into prairies in the Midwest, and thus the open conditions may apply to this genus as well. Accordingly, the mean, 10^{th} and 90^{th} percentile bounds on U_{eff} were estimated from a long-term 1/2 hourly mean wind speed records collected at the Duke Forest (near Durham, North Carolina) in a grass-covered forest clearing and above a hardwood canopy, and front propagation data are presented for both these conditions for all species (Appendix B). The θ was determined by assuming that the wind statistics should be derived from above the forest canopy. An estimate of $\theta = 0.36$ was obtained from typical wind statistics above a dense canopy. These estimates were then used in the semi-analytical

model to calculate the vegetation wave front propagation speed. Calculated wave speeds were divided by 2π to convert between the 1D analytical result and the 2D spread rates given by the pollen data, assuming random wind direction. A sensitivity analysis on the endogenous variables in the logistic-WALD model was undertaken (Appendix B). The major findings of this sensitivity analysis, (discussed further in the results section), were that the front speed is linear in $\overline{U_{eff}}$, and that for small values of the spread and survival parameter $a\,(< 0.01)$ the choice of a does not significantly alter c, but only the time taken to reach the asymptote. Accordingly, a was set to 5×10^{-6}, an order of magnitude estimate at half hourly timescales. To assess the suitability of using the Duke Forest wind data as a surrogate for data across the range of the post-glacial expansion, a further sensitivity analysis was undertaken on the Weibull parameters. This analysis indicated that the likely variability in across a sample of forested sites in North Carolina, Indiana, Massachusetts and Maine was of the order of 8%, and that this was directly comparable to the likely variation associated with changes in land cover type (9%). Given the linearity of the front speed in $\overline{U_{eff}}$, the geographic variability in the Weibull statistics is expressed as uncertainty of less than 10% in the biomass front speed.

3.3 Results

3.3.1 Generation of effective wind velocity from Weibull wind parameters

Based on the AIC, a gamma distribution was the best fit to the U_{eff} distribution arising from the Monte Carlo simulations. Hence, in a first-order estimate of U_{eff}, a gamma distribution was used, with the distribution gamma(ω, ν) described as:

$$p\left(x|\omega,\nu\right) = \frac{1}{\nu^{\omega}\Gamma\left(\omega\right)} x^{\omega-1} e^{-x/\nu}, \tag{3.15}$$

where Γ is the gamma function. The non-linear regression between the Weibull (b, k)

Parameter	Regression Equation	Regression Coefficients	r^2
$\overline{U_{eff}}$	$\overline{U_{eff}} = \varsigma_0 \tanh(k) + \varsigma_1 \left(\frac{b}{k^{1.5}}\right) + \varsigma_2$	$\varsigma_0 = 0.8187$ $\varsigma_1 = 3.4233$ $\varsigma_2 = 0.0963$	0.99
ω_{gamma}	$\omega = \gamma_0 (arctan(b)\, k^2) + \gamma_1 \left(\frac{k^2}{b}\right) + \gamma_2$	$\gamma_0 = 8.3426$ $\gamma_1 = 6.3476$ $\gamma_2 = 10.900$	0.99
ν_{gamma}	$\nu = \varphi_0 \frac{tan(b)}{k^2} + \frac{\varphi_1 \tanh(b)}{k^2} + \varphi_2$	$\varphi_0 = -0.0086$ $\varphi_1 = 0.4172$ $\varphi_2 = -0.0184$	0.88

Table 3.1: Regression equations and r^2 (coefficient of determination) values for $\overline{U_{eff}}$, ω and ν as a function of the Weibull parameters b and k.

parameters for $\overline{U}$ and the effective wind speed U_{eff} generated functions to predict the mean of U_{eff} (denoted $\overline{U_{eff}}$) given the wind statistics. The gamma parameters ω and ν, which are required to specify the distribution of U_{eff} were also determined. High coefficients of determination (r^2), were achieved for all regressions (Table 3.1, Figure 3.4).

3.3.2 Applications to the case study

The mean speed of vegetation movement predicted in the case study was within a factor of five or better of that in the palynological record, for all species considered (Table 3.2). The sensitivity analysis of the wind statistics indicated that there is a linear correlation between the Weibull parameters when compared across multiple sites, and that this correlation damps the effect of changes in the wind statistics. Over the area of interest, this resulted in a near-linear sensitivity of $\overline{U_{eff}}$ to the Weibull parameters, and constrained the error associated with geographic variation to the order of 10% (see Appendix B). This uncertainty did not greatly alter the quality of the predictions by comparison to the mean cases. The sensitivity analysis of endogenous parameters indicated that the dependence of the predicted wave speeds

was approximately linear in the growth rate (r) and the wind speed applied ($\overline{U_{eff}}$), near linear in the canopy height (h) and the vertical velocity standard deviation (σ_w), and nonlinear in terminal velocity (V_t), release height (z_r), and the spread and survival parameter (α). In particular, for values of α of less than 0.01, the propagation speed was almost insensitive to further decreases in α over several orders of magnitude (Appendix B).

3.4 Discussion

By linking the Weibull mean wind statistics to the description of the WALD parameters through $\overline{U_{eff}}$, the half hourly timescale of wind variability is scaled up to the timescales of biomass growth. In analysing the numerical results to achieve this scaling, our goal was to ensure that direct analytical implementation was achievable. This motivated the approximation of the distribution of U_{eff} as gamma(ω, ν). In reality, the distribution of U_{eff} is a transformation of the Weibull via the WALD kernel and the logistic equation with no known analytical representation and cannot be fully represented via a two-parameter approximation such as the gamma distribution. As such, the quality of the gamma distribution in describing U_{eff} varies with the parameters of the Weibull function, resulting in some inevitable error. However, the linear dependence of the wave speed on U_{eff} ensures that the impact of these errors is first order only, meaning that the achieved fit is acceptable given the aims of the model to provide a tractable approach to estimating spread rates. If greater accuracy is needed, U_{eff} should be calculated more precisely via numerical simulations.

The logistic-WALD model reproduced vegetation propagation speeds to a good approximation without invoking isolated extreme events (e.g. hurricanes) as the mechanism promoting long distance dispersal. Rather than relying on such phenomena the logistic-WALD model implies that long distance dispersal is an expected

outcome of the interaction between seed movement and the complex wind statistics across a range of timescales. Mathematically, this is the result of the interaction between the tails of the Weibull (whose genesis is meso-scale and weather related variation about $\overline{U}$) and WALD (whose genesis is turbulent dispersion) distributions, as outlined in Figure 3.2.

Several limitations to the data used in the post-glacial expansion case study prevented a one-on-one comparison between predicted and recorded biomass propagation speeds. While terminal velocity data were measured for all species, other parameters, particularly the growth rate, were estimated based on generic allometric equations and basic assumptions such as a constant growth rate throughout the plant's lifespan. Results presented for wind data collected both from a forest clearing, most applicable to early colonising species, and from a forest canopy, as applicable to later succession species, were both within the order of magnitude limits sought. The linear impact on c of changing land cover type or geographic location was small, at $\approx 10\%$, and by comparison to the uncertainties associated with approximating the paleoclimatological record with contemporary wind statistics this variation can be considered negligible. For contemporary applications of the model, results could be improved through appropriate spatial averaging of wind statistics. However, it should be noted that errors remain in approximating the post-glacial expansion wind statistics by current wind distributional properties of the Weibull.

The logistic-WALD model is a simplified representation of some of the complex processes that govern species migration and which currently constitute an active topic of research [Lewis and Pacala, 2000, Moorcroft et al., 2006]. Despite the simplicity of the model, it contains an appropriate treatment of the multi-scale processes involved, and its results hold clear analogies to more complex representations. As outlined in the introduction, the omission of retarding processes, such as competition, from the process description allows us to consider the derived speed to be a

maximum, obtained under ideal conditions for invasion. As such it is analogous to the concept of "invasion by extremes", in which the most rapidly transported seeds become responsible for invasion and population establishment [Clark et al., 2001]. Using fat-tailed dispersal kernels, Clark et al. were unable to reproduce the Holocene invasion speeds for a range of species without artificially increasing seed survival rates (the α parameter in our formulation). Our finding that c loses sensitivity to α as α becomes arbitrarily small allows the logistic-WALD model to recover the appropriate order of magnitude of the spread rates without such artificial increases in survival. Provided dispersal occurs over a sufficiently long period to allow the asymptotic speed to be reached, low seed viability does not necessarily restrict the vegetation front movement, just the timing at which the maximum front speed occurs. Note that the α parameter addresses the distribution and establishment of seed biomass only; increasing seedling mortality effectively reduces the growth rate parameter r in the logistic-WALD model, with resulting linear reductions in the wave speed.

Stochastic studies of plant movement via long range dispersal events have highlighted the importance of the "outlier - expansion" effect, in which outlier populations establish remotely from the main population, remain effectively stationary for some period of time, and then expand to close the gaps between the populations, often with remarkable speed [Clark, 1998, Clark et al., 1998, 2001, 1999, Kawasaki et al., 2006, Neilson et al., 2005, Shigesada et al., 1995]. In continuous terms, the logistic-WALD model accomplishes this expansion by a very similar mechanism. Small quantities of biomass are distributed at long distances from the established population, and the biomass associated with these populations remains small (in comparison to the carrying capacity) for a considerable period of time. These small quantities can be conceptualised as representing a distribution of potential outlier populations away from the starting point. As the wave front passes these points, a large and rapid increase in biomass occurs, analogous to the expansion phase of the outlier-expansion

model.

Within the many diffusion models of biomass movement, parameterisation of the diffusion coefficient remains a challenge and source of uncertainty [Murray, 2003a, Okubo and Kareiva, 1980]. Exemplified by "Reid's paradox" [Clark et al., 1998], the effective diffusion coefficients needed to reproduce typical biomass migration rates exceed those derived from experimental observations relying on spread distance and time scale arguments (i.e. approximations of diffusion coefficients D as L^2/T) by orders of magnitude. For wind-dispersed plants, the logistic-WALD model offers a way to improve the parameterisation of such "effective" diffusion coefficients. The WALD kernel can be parameterised using local wind statistics and the characteristics of the dominant plant species under consideration. The semi-analytical solution can then be used to give the asymptotic wave speed, c. An effective diffusion coefficient, should it be needed, can then be determined using the relationship $D = c^2/4r$. The use of the logistic-WALD model to derive an effective diffusion coefficient in these cases provides a new, and defensible approach to parameterisation of existing diffusion based models.

3.5 Conclusion

Our aim in formulating a biomass dispersal model based upon the WALD kernel was to mimic the simplicity of diffusion as a description of biomass movement, that is an expression approaching the simplicity of $c = 2\sqrt{rD}$, while avoiding the anomalous results produced by diffusion, and improving spread rate parameterisation. This approach required that, with the exception of the mean wind speed, parameters be treated as constant in space and time. The logistic-WALD model achieves the improvements for wind-dispersed biomass in three ways. Firstly, the up-scaling from turbulent transport timescales to biomass growth timescales is now explicit and mechanistic, rather than assumed or empirically fitted to one particu-

lar site. Secondly, the logistic-WALD model can be completely parameterised from independent data: knowing sufficient information about the species' growth rate, the wind climate in which it grows, and the seed attributes provides sufficient information to estimate upper bounds on the speed of the biomass front. Thirdly, the logistic-WALD model is shown to provide reasonable estimates of known biomass dispersal rates for the early Holocene expansion - circumstances in which diffusion-based estimates are known to grossly underestimate such data. The super statistical approach adopted here, in which processes are related across scales through deriving relationships between their statistical descriptors, is now showing promise in many applications including the prediction of rainfall on inter-annual timescales [Porporato et al., 2006] or improved descriptions of turbulent motion [Beck and Cohen, 2003]. Future application of such approaches could allow a similarly simple model to account for variability at the inter-annual scale. Long time series data of wind measurements are starting to become available which capture several decades of variability at multiple spatial scales [Kalnay et al., 1996], providing appropriate datasets for examination of inter-annual variability in a "normal" setting, and thus baselines against which to evaluate future trends in the wind climate. Studies of potential changes to the wind climate show an emerging trend of change in the extremes of wind climate ranging from fewer extreme events associated with weakening of the Asian monsoon, to expectation of increasing severity of hurricane activity associated with warmer sea surface temperatures [Emanuel, 1987, Knutson and Tuleya, 1999, Lun and Lam, 2000, Pryor et al., 2006, Walsh, 2004, Webster et al., 2005, Xu et al., 2006, Yan et al., 2006]. The sensitivity of wind dispersal to extremes of the wind regime means that these changes have important implications for plant migration, which can now be accounted for within a proposed framework of "hierarchical superstatistics". Here the superstatistics of the Weibull distribution would be evaluated from time series data and scaling relationships developed to predict $\overline{U_{eff}}$ over longer

timescales, as depicted conceptually in Figure 3.2. Such hierarchical superstatistical models are expected to find broad applicability in a wide range of ecological modelling problems in which the "dimensionality curse" impairs predictive capacity and important processes span a range of timescales from fractions of seconds to multiple years.

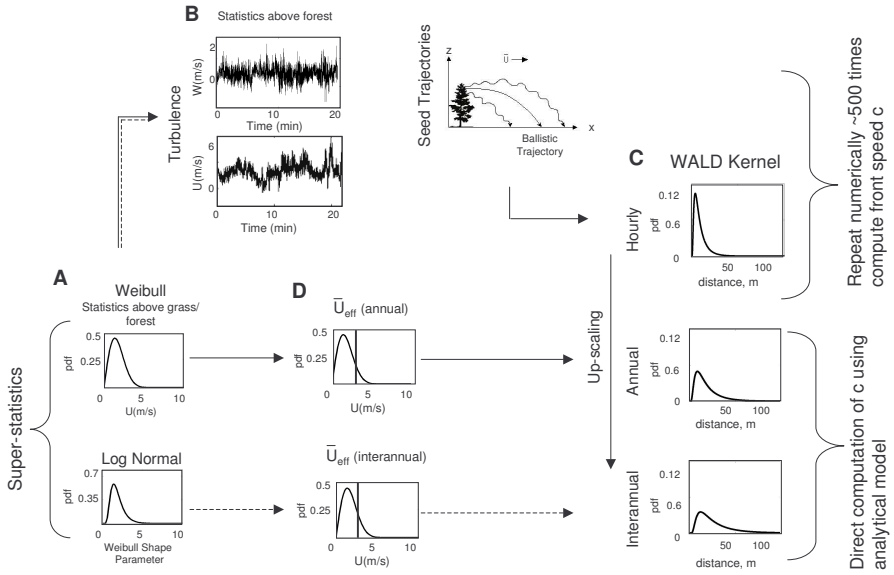

FIGURE 3.2: Conceptual model for scaling of biomass growth and dispersal. The Weibull and (conceptually) a lognormal distribution generate U values that force the WALD kernels at different time scales (A). The WALD kernel (showing the pdf of seed dispersal distances) results from a distribution of seed trajectories and provides the scaling between turbulent and half hourly timescales (B). At longer time scales the increasing variability results in "fatter" tails in the WALD kernel (C). Computation of the vegetation front speed may proceed numerically via Monte Carlo simulation, where a mean wind speed is repeatedly sampled from the Weibull distribution, the hourly WALD kernel computed and the process repeated until the asymptotic front speed is reached. This is repeated $\approx$ 500 times to predict the front speed. More expediently, the U_{eff} parameter can be computed (D) and used to directly describe the annual (or, conceptually, the interannual) WALD kernels, which are then solved analytically for the vegetation front speed.

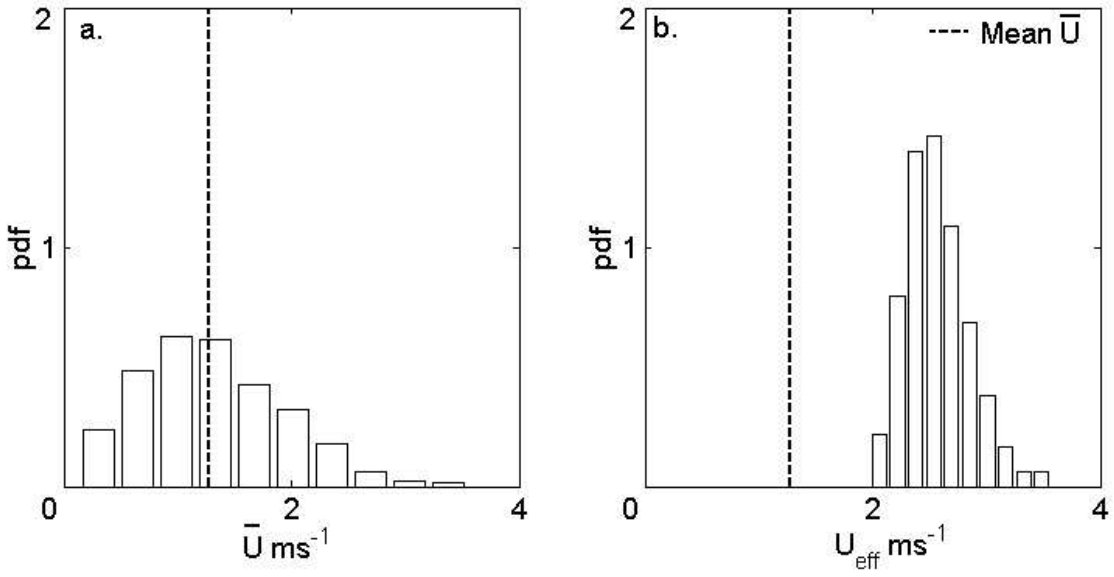

FIGURE 3.3: Distribution of mean half-hourly wind speeds ($\overline{U}$), with the mean of the distribution shown. b. Distribution of effective wind speeds (U_{eff}), derived from numerical simulations of the Logistic-Wald model, for the forcing shown in a. Note that the mean of the forcing wind speed (dashed line) under-predicts the distribution of effective wind speeds.

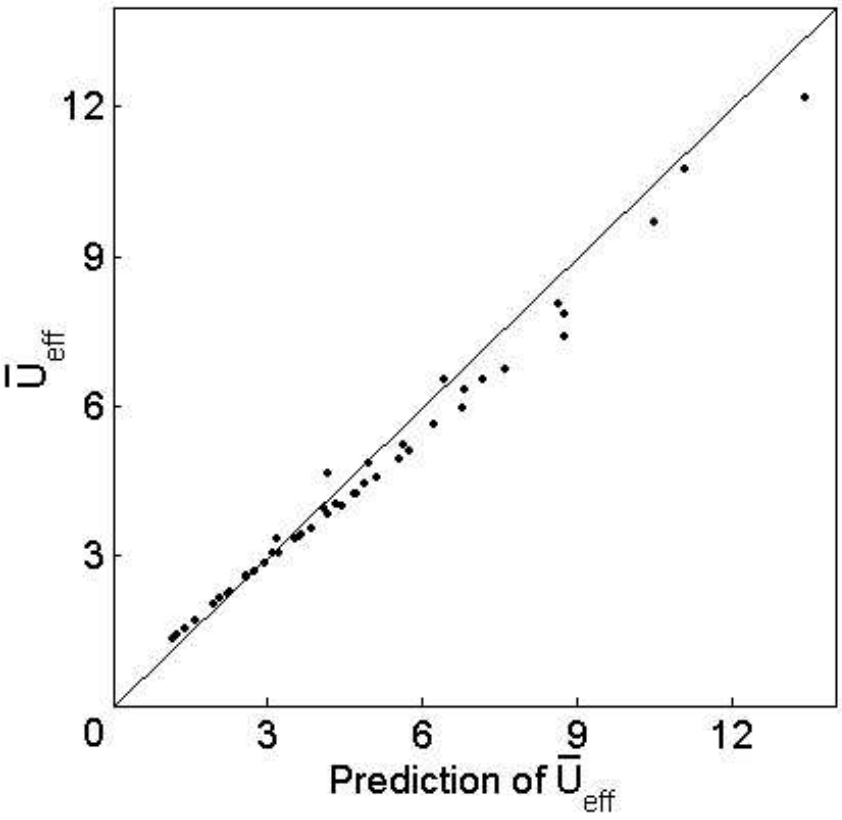

FIGURE 3.4: Pairwise plot of $\overline{U_{eff}}$ predicted via regression and $\overline{U_{eff}}$

Species name	Diameter at Breast Height (cm)	Mature Biomass (kg)	Estimated Growth Rate (kg/yr)	Terminal Velocity (m/s)	Seed release height (m)	Canopy height (m)	Pollen Record Wave Speed (m/yr)	Mean Predicted Wave Speed (m/yr) Forest - Open	Error bounds due to Geographic Variation: Forest-Open	Mean Predicted Wave Speed (m/yr) Forest - Forest	Error bounds due to Geographic Variation: Forest-Forest
ACRU	8.9	21	2.6	0.67	10	17.2	126-200	218	134-334	262	238-384
ACSA	19	143	3.6	1.0	10	17.2	126-200	131	81-201	158	143-231
ACNE	60	114	1.9	0.92	9.5	19	126-200	94	58-144	113	102-165
ACSC	29.7	341	7.9	0.87	12.5	25	126-200	581	359-888	696	634-1021
BELE	20.1	137	3.4	1.6	15	20	212	59	37-90	71	65-105
FRAM	15.8	91	2.5	1.4	13.1	18.7	123	52	31-78	62	56-91
FRPE	20	162	7.7	1.6	11.9	17	123	111	69-170	133	121-195
PITA	23	164	8.2	0.7	11.7	14.6	81-400	542	335-829	650	591-953
Mean							169	224		268	

Table 3.2: Data used to parameterise the logistic-WALD model, front speed results from the pollen record and the predicted speeds from the logistic-WALD model. The error bounds shown incorporate the 10^{th} and 90^{th} percentile estimates of U_{eff} and an 8% error associated with geographic variation in wind properties. κ was set to 0.6 for the simulations. ACRU - *Acer rubrum*, ACSA - *Acer saccharum*, ACNE - *Acer negundo*, ACSC - *Acer saccharinum*, BELE - *Betula lenta*, FRMA - *Fraxinus americana*, FRPR - *Fraxinus pennsylvanica*, PITA - *Pinus taeda*

4

Role of biomass spread in vegetation pattern formation within arid ecosystems

4.1 Introduction

Self-organization of vegetation into regular patterns has been observed in arid and semiarid ecosystems worldwide, across a wide variety of plant species and forms, and on a range of soil types [Tongway and Ludwig, 2001, Rietkerk and van de Koppel, 2008]. Patterned vegetation was first noticed by air in the 1950s [Clos-Arcedue, 1956], and the intriguing landforms generated extensive field studies that identified many of the important commonalities of patterned landscapes: an arid to semiarid climate, high-intensity rainfall, minimal soil type differences between vegetated and bare zones beyond those immediately attributable to the presence of vegetation, noticeable crusting in the bare zones, and a dependence on a topographic gradient that resulted in a transition from anisotropic banding patterns to isotropic labyrinth, gap, and spotted patterns as the slope declined to less than 0.2% [D'Herbes et al., 2001, Tongway and Ludwig, 2001, Rietkerk et al., 2002, Galle et al., 2001]. These features suggest that patterns arise as an emergent feature of nonlinear plant-water

interactions, where water availability increases beneath vegetation, as a result of the suppression of growth of biological soil crusts [Belnap and Lange, 2001], the presence of roots and macropores increasing infiltration rates and potentially plant canopies shading the soil surface, reducing soil evaporation [Scholes and Archer, 1997]. The net result is a locally elevated soil moisture resource in the proximity of vegetation [Bromley et al., 1997, Valentin et al., 1999]. An extensive literature has examined the importance of patterned landscapes as resource harvesting structures [Greene and Valentin, 2001, Mauchamp et al., 2001, Thiery et al., 1995, Rietkerk and van de Koppel, 2008], but only in the last decade has theoretical attention been given to these landscapes as dynamic nonlinear systems in which the self organization of vegetation can be generically studied despite large differences in ecosystem types [Thiery et al., 1995, Klausmeier, 1999, HilleRisLambers et al., 2001, von Hardenberg et al., 2001, Lejeune, 2002, Rietkerk et al., 2002, Gilad, 2004, Rietkerk et al., 2004]. Initially this approach was driven by phenomenological models of facilitation and competition between vegetation structures [Lefever and Lejeune, 1997] then through coupling biomass and soil moisture budgets explicitly [Klausmeier, 1999, von Hardenberg et al., 2001]. However, it has largely been the inclusion of surface water transport in these models that reproduced realistic patterning length scales, and these three-component models represent the current state of the art with respect to process simulation of patterned landscapes [Rietkerk et al., 2002, Gilad, 2004, Yizhaq et al., 2005]. The existing model frameworks have been refined with respect to the importance of stochasticity in rainfall [D'Odorico et al., 2006a, Ursino and Contarini, 2006] and aspects of plant physiology [Ursino, 2007] pertinent to photosynthesis, respiration, and stomatal response to mean vapor pressure deficit [Kefi et al., 2008]; as well as soil properties [Ursino, 2005]. A critical finding from this effort has been that patterned landscapes are bistable states that may undergo "catastrophic ecosystem shifts" to a desertified state from which the previous patterned condition cannot be

recovered [Rietkerk et al., 2004, Kefi et al., 2007a,b]. Research into patterned landscapes has therefore shifted perspective from the original questions concerning the maintenance and function of these intriguing systems to research that aims to use the condition of the emergent patterns as an indicator of ecosystem health. A critical component of research into these patterns involves developing the capacity to infer the state of the ecosystem given "observable" patterns of vegetation. Such inference is of necessity based upon models that contain the appropriate representation of the key processes occurring within the ecosystem.

In evaluating the state of the science in this manner, two observations can be made about key knowledge gaps. The first is that despite extensive refinement of the models used, an evident difference remains between modeled and real vegetation patterns, in that the former are smooth, while the latter display a conspicuous degree of disorder (Figures 4.1a and 4.1e). The second is that the representation of plant movement, critical to the formation of a pattern, has not been considered in detail, but instead has been represented via diffusion in almost all models formulated, or accounted for phenomenologically by representation of long-range interactions [D'Odorico et al., 2006a]. Diffusion results in a representation of biomass movement that is localized and depends upon biomass gradients to determine the relative rate of transport. In contrast, real plant population movement, assuming sexual reproduction, is driven by the production and transport of seeds. These observations lead to an initial question, namely, is the disorder observed in real patterns representative of underlying randomness at small scales as is known to exist in soil properties, or might it arise because biomass movement is less diffusive than its representation in current models?

To answer this question, we couple a "dispersal kernel", defined as the probability distribution of seed distances from their parent source [Clark, 1998, Clark et al., 1998, 1999] to existing pattern formation models as an alternative to diffusion. Dispersal

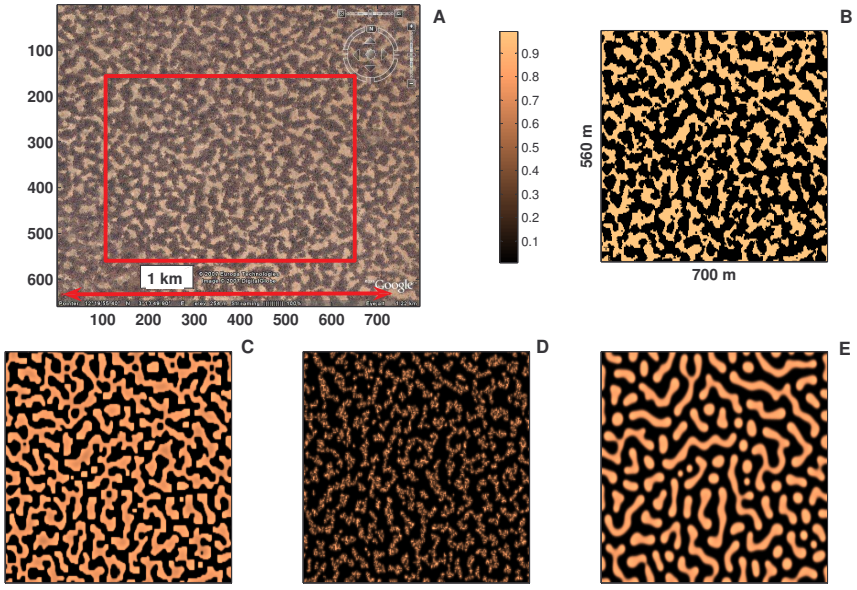

FIGURE 4.1: (a) An image taken from Google Earth at $12°19'55.40''N$ and $3°10'49.90''E$ in Niger on 28 January 2006. (b) A subsampling and smoothing of the image, which was then used as the initial condition for the simulation results (Figures 1c1e). (c) The results from the dispersion model, (d) the diffusion model with stochastic soil properties, and (e) the original diffusion model. The parameter values used were $c = 10$, $g_{max} = 0.05$, $k_1 = 5$, $D_p = 0.1$, $\alpha = 0.2$, $k_2 = 5$, $W_o = 0.2$, $r_w = 0.2$, $D_w = 0.1$,$D_o = 100$, $R = 1$, $d = 0.23$.

kernels describe both local and nonlocal movement and are independent of biomass gradients. The use of a dispersal kernel differs somewhat from previous kernel-based models [Lefever and Lejeune, 1997, D'Odorico et al., 2006a] in which the kernel encodes the interactions responsible for local facilitation and long-range inhibition of vegetation growth, i.e., the genesis of pattern formation [Murray, 2003b]. Instead, the dispersal kernel approach solely dictates the rates and spatial scales of biomass transport, while the facilitative and inhibitory processes are determined by the interactions of biomass and water, just as in the diffusion-based model. The coupling of seed dispersal kernels with pattern-forming models can address several questions

fundamental to understanding vegetation patterns in arid and semiarid systems: Can patterns be maintained in the absence of a diffusive representation of biomass? What is the "direction" of pattern evolution, toward or away from more continuous cover? Finally, could feedbacks exist between dispersal ecology, soil moisture redistribution, and pattern formation in these highly organized ecosystems? The paper proceeds by outlining the basic features of dispersal ecology in arid ecosystems first, then addressing the incorporation of a seed dispersal kernel into a model of pattern formation, which is used to address the questions outlined above.

4.2 Seed dispersal

The dispersal of seed determines ecological characteristics of plants and their communities, such as gene flow and the genetic structure of populations [Cain et al., 2000, van der Pijl, 1972], the survival and success of subsequent generations of plants, rates of expansion into new terrain and the spatial distribution of plants at multiple spatial scales in terms of habitat, range, and spatial organization within the landscape [Clark, 1998, Clark et al., 1998, 2001]. Dispersal is broadly characterized by a canonical length scale over which seeds move and by a dispersal vector that transports them. The length scales of dispersal vary from highly localized (< 1 m) to long distance (LDD, 10^0-10^2 m). Transporting vectors change the statistical properties of kernels, with exponential kernels induced by simple ballistics, longer range and often leptokurtic kernels associated with wind or water dispersal, and with the stochastic, anisotropic and potentially nonrandom transport by insects, birds, or animals often difficult to represent via kernel approaches [van der Pijl, 1972, Ellner and Shmida, 1981, Fragoso, 1997, Russo et al., 2006], and see Chapter 3. Dispersal in desert plants typically occurs over short length scales [Davidson and Morton, 1984, Chambers and MacMahon, 1994] with many species seeds lacking adaptations to promote dispersal (atelechory) or exhibiting adaptations that limit dispersal (antitelechory) [van der

Pijl, 1972, Ellner and Shmida, 1981]. Many desert perennial species rarely propagate from seed, and asexual reproduction is common [Abrams, 1988, Thiombiano et al., 2003] . The dispersal ecology of species comprising patterned vegetation is variable, and has not been comprehensively studied [Montana et al., 2001]. Some species, such as *Combretum micranthum* (West Africa), appear to have adaptations for secondary wind dispersal, with roundwinged seeds that "tumble" along the ground [Midgley, 1998]. Other species, such as Acacia aneura (Australia), are dispersed primarily by ants [Davidson and Morton, 1984]. Several of the species involved in pattern formation have the capacity to reproduce asexually (e.g., *Combretum micranthum, Guiera senegalensis, Pleuraphis* (formerly *Hilaria*) *murtica*) [Couteron and Lejeune, 2001, Thiombiano et al., 2003, Uchytil, 1988]. However, seedling recruitment is often described within patterned sites suggesting that seed dispersal is an important process in these landscapes. Where soil crusts are well formed, they may pose an obstruction to seedling recruitment [Prasse and Bornkamm, 2000] and indeed Montana et al. [2001] show that where the slope of the ground is significant($> 0.2\%$) the seed bank tends to lie within vegetated areas, as a result of secondary transport by runoff from the interband. This study, however, considers only cases where there is no significant slope, so the velocities of surface water and seed transport by water are relatively low and oriented toward local vegetated sites. Secondary transport thus effectively shortens dispersal length in this scenario and is not considered explicitly here. For the case of a slope grade large enough to impose a preferential direction of flow, alternative and anisotropic descriptions of seed transport are needed.

4.3 Methods

4.3.1 Ecohydrological model

The study is based on an adaptation of a simple spatial model of arid ecosystem vegetation-water relations developed by HilleRisLambers et al. [2001] and Rietkerk

et al. [2002]. The original model equations are:

$$\frac{\partial P}{\partial t} = cg_{max}\frac{W}{W+k_1}P - dP + D_p\nabla^2 P, \tag{4.1}$$

where P is the plant biomass in gm^{-2}.

$$\frac{\partial W}{\partial t} = \alpha O\frac{P+k_2W_o}{P+k_2} - r_wW - g_{max}\frac{W}{W+k_1} + D_w\nabla^2 W, \tag{4.2}$$

where W is the soil water depth in mm; and

$$\frac{\partial O}{\partial t} = R - \alpha O\frac{P+k_2W_o}{P+k_2} + D_o\nabla^2 O, \tag{4.3}$$

where O is the surface water depth in mm. The model parameters are c (water uptake to plant growth relation, g mm^{-1} m^{-2}, g_{max} (maximum specific water uptake mm m^2 g^{-1} day^{-1}), k_1 (half saturation constant of water uptake, mm), d (death rate, day^{-1}), D_p (biomass diffusion coefficient m^2 day^{-1}), α (maximum infiltration rate day^{-1}), W_o (the rate of infiltration in the absence of plants, [ ]), r_w (timescale of water loss due to evaporation and drainage, day^{-1}), R (precipitation, mm day^{-1}), and $\nabla^2 = \partial^2/\partial x^2 + \partial^2/\partial y^2$, where x and y are the Cartesian coordinates.

The model represents a positive feedback between water and carbon where infiltration relates to biomass density in a Michaelis-Menten sense [Briggs and Haldane, 1925]. Soil water uptake increases with vegetation biomass, resulting in a negative feedback due to competition for the limited available water. Spatial movement of water and biomass is represented as diffusion. The model produces spatial patterns with a characteristic wavelength following the typical spot-labyrinth-gap sequence as water availability increases. This pattern sequence is shown in Figure 4.2c for the original model equations.

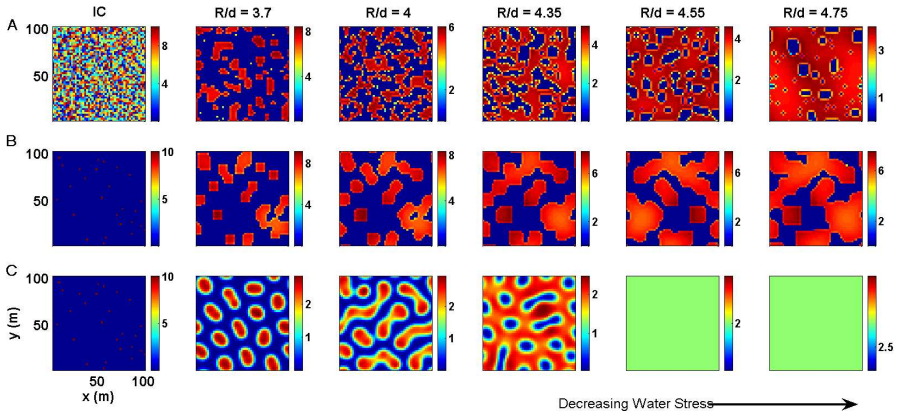

FIGURE 4.2: Simulation results of dimensionless biomass along a gradient of decreasing water stress for (a) the dispersion model with random initial conditions, (b) the dispersion model with random point initial conditions, and (c) the original diffusion model. The initial condition (IC) for each set of models is given. Length scales are shown on the left and the colors indicate the dimensionless biomass density (nondimensionalized by the biomass saturation constant for water infiltration). Increasing R/d (rainfall to death rate) decreases soil moisture stress on growth. Note that the color scale differs between plots. The parameter values used were $c = 10$, $g_{max} = 0.05$, $k_1 = 5$, $D_p = 0.1$, $\alpha = 0.2$, $k_2 = 5$, $W_o = 0.2$, $r_w = 0.2$, $D_w = 0.1$, $D_o = 100$, $R = 1$.

To refine the representation of biomass transport, the diffusion term in the P equation is replaced by a convolution of a dispersion kernel and standing biomass, defining the seed rain about a parent plant (see Chapter 3). This adjustment to the biomass equation removes the dependence of the spatial movement on biomass gradients and allows for a variable length scale for dispersal, giving:

$$\frac{\partial P}{\partial t} = \left(c g_{max} \frac{W}{W + k_1} P - dP \right) (1 - \phi) + \phi \int \int \nu \left(x - x', y - y' \right) P \left(x', y' \right) dx' dy', \tag{4.4}$$

where ν is the dispersal kernel (that can account for secondary dispersal mechanisms

if known), ϕ represents the proportion of standing biomass dispersed per unit time, and x' and y' define the distance seeds move from the parent, integrated over the domain.

Determining ϕ is problematic, as fecundity values vary strikingly between individuals and species, may change with environmental conditions, and are not typically reported as a percentage of biomass. The proportion of biomass that is allocated to reproduction can be as much as 50% for annuals, but is far less for many species [Aronson et al., 1993]. Determining the duration over which dispersal occurs complicates the conversion of this allocation to a rate. Assuming that the period during which a plant disperses seed ranges from 1 month to 1 year, and that 1-50% of the standing biomass is allocated to seed, then f can be considered to range from $10^{-4} - 10^{-2}$ day^{-1}. A plausible value in this range, 2.5×10^{-3}, was used for numerical simulations.

A number of process- and timescale-related limitations apply to the model. Many of these have been addressed explicitly in other studies (see, e.g., Ursino [2005, 2007], Ursino and Contarini [2006]) and are also discussed in Appendix C. The most significant concern is that representing the dynamics of a highly stochastic system using a deterministic model may misrepresent the systems drivers. This concern was addressed by linearizing the model equations at steady state and showing that the mean rainfall predicts the temporally averaged biomass response under stochastic rainfall conditions. This result is subject to limitations, as sporadic rainfall can annihilate the vegetation patterns and render further predictions or inference moot, but justifies the use of mean rainfall as a driver for this simple model at the timescales on which biomass changes. Details of the linearization are presented in Appendix C.

Other studies addressing the question of stochasticity and its relationship to patterning have concluded that stochastic rainfall may be a driver of pattern formation [D'Odorico et al., 2006a, 2007] and that while stochasticity changes the type of pat-

tern formed for a given mean rainfall, it does not influence the overall shape of the patterns [Ursino and Contarini, 2006]. Finally, the hydrological processes represented in the model are also simplistic and based upon diffusion. Improvement of process representation in the hydrology and their integrated effects to timescales commensurate with biomass changes is an outstanding problem in this research field.

4.3.2 Dispersal kernels

A Wald kernel, defined by a Wald or Inverse Gaussian distribution was used for the simulations here. The kernel is given in radial coordinates by:

$$\nu_{Wald} = \frac{1}{4\pi dr}\sqrt{\frac{\lambda}{2\pi\left(r-r'\right)^3}}\exp\left[\frac{-\lambda\left(\left(r-r'\right)-\mu\right)^2}{2\mu^2\left(r-r'\right)}\right] \tag{4.5}$$

where $\mu > 0$ is the mean of the distribution, $\lambda > 0$ is a scale parameter, $r = \sqrt{x^2+y^2}$, $dr = \sqrt{dx^2+dy^2}$ and $r' = \sqrt{x'^2y'^2}$. The variance of the this distribution is given by $\sigma = \mu^3/\lambda$. The Wald kernel can be used to represent any dispersion length scale. In the local limit, it approximates a ballistic spread of seed about the parent and replicates the scale and spatial pattern of a Laplacian (i.e., the spatial term responsible for diffusion). In the nonlocal limit, the kernel allows for wind-dispersed seeds to travel long distances [Katul et al., 2005].

4.3.3 Numerical simulations and methods of analysis

The numerical simulations performed are summarized in Table 1. All simulations were run on a 100×100 m grid with 2×2 m cells and periodic boundary conditions with a timestep of 0.008 days. Simulations initialized with a remote sensing image were run on a 550×700 m grid with 2.8×2.8 m cells. Numerical calculations were performed using an Euler forward difference scheme, and the convolution between the biomass and the dispersal kernel was performed in the Fourier domain using

Research Question	Kernel	Initial Conditions	Parameter Notes[1]
Where does small-scale disorder come from (Qu. 1)?	diffusion and square wave	binary filter of remotely sensed image	$R/d = 4.4$ mm; D_p= 0.01; one run with k_2 randomized, 5 ± 0.5
Can patterns be maintained without diffusion (Qu. 2a)?	square wave	point and randomized	death rate $d = 0.17 - 0.27$ day^{-1}
What is the influence of initial conditions (Qu. 2b)?	square wave	point and randomized	death rate $d = 0.17 - 0.27$ day^{-1}
Does a kernel model admit bifurcations (Qu. 3)?	square wave	point and randomized	dispersal allocation ($\phi = 10^{-4} - 0.3$ day^{-1} $d = 0.17 - 0.27$ day^{-1}
What is the impact of dispersal length scale on patterns (Qu. 4)?	Wald	randomized	Wald variance $\sigma^2 = 0.5 = 0.32$ death rate $d = 0.17 - 0.27$ day^{-1}

Table 4.1: Details of numerical simulations and the scientific questions addressed. 1. The parameter values used for all simulations were $c = 10$, $g_{max} = 0.05$, $k_1 = 5$, $D_p = 0.1$,$a = 0.2$, $k_2 = 5$,$W_o = 0.2$,$r_w = 0.2$,$D_w = 0.1$,$D_o = 100$, $R = 1$.

a fast Fourier transform algorithm for two-dimensional convolutions [Rosa, 2004]. Simulations were run until the steady state biomass was reached, typically 2000 days (determined as the point where the rate of change in biomass, normalized by the standing biomass, was less than 1×10^{-4}). Unless shown otherwise in Table 4.1, all model parameters are those used by Rietkerk et al. [2002]. Table 4.1 shows five different model runs, addressing the 4 key research questions outlined in the introduction (and elaborated upon next), as well as important tests of model validity, specifically with respect to identifying bifurcations in model behavior. The methodological details are below.

4.3.4 Question 1: Does small-scale disorder in vegetation patterns arise from extrinsic randomness or intrinsic processes?

To address this question, three cases were considered: a basic diffusion model, the kernel model using a square wave kernel, and the diffusion model running on a grid where the soil parameter k_2 (the half saturation constant for the infiltration rate) was treated as an uncorrelated Gaussian random field varying by 10% around its mean. Extensive studies into the nature and scaling of soil heterogeneity support the notion that variability in soil properties is uncorrelated on scales of 1–100 m, those relevant to this model, and thus support the treatment of small-scale randomness as uncorrelated in space [Buchter et al., 1991]. To remove uncertainty regarding the initial conditions, the models were initialized with an image taken from remote sensing and passed through a binary filter. Runs were initialized by holding the biomass constant in time until the water terms reached steady state. Biomass was then allowed to adjust to this new soil moisture spatial distribution. This approach avoided creating transient artifacts that might disrupt the initial biomass conditions while the water terms equilibrated. The model was run with different rainfall values until an optimal approximation of the original biomass pattern was reached (tested by the absolute difference and RMS difference between steady state results and the initial condition). A water availability measure of $R/d = 4.4$ mm was adopted for all simulations. Power spectra of the steady state solutions were calculated using a twodimensional Fourier transform. For clarity, the most energetic modes, normalized by the area under the spectrum, were plotted against wavelength.

4.3.5 Question 2: Can vegetation patterns be generated withour treating vegetation transport as diffusion? What are the influences of the initial conditions?

These questions were addressed in concert by running comparisons of the original diffusion model and the square wave kernel based model across a gradient of water

stress for different initial conditions and comparing the results. The initial conditions used consisted first of a perturbation about continuous biomass cover in the range of 0 – 50 g m^{-2} ("random" initial conditions), broadly analogous to a drying climate fragmenting initially continuous vegetation cover. Other ranges of variability in the random initial condition were also tested. The second initial condition used was a random seeding of an otherwise unvegetated landscape (5% of cells initiated at a biomass density of 50 g m^{-2}, other cells at 0 g m^{-2}, "point" initial conditions), broadly analogous to the revegetation of a desertified region via random germination from a seedbank or randomly dispersed individual seeds. The initial conditions are shown as the leftmost column in Figure 4.2.

4.3.6 Question 3: Does the kernel-based model admit bifurcations?

The possibility of bifurcations existing in the new model was explored by changing the dispersion allocation parameter ϕ over the biologically realistic range for varying values of plant stress.

4.3.7 Question 4: What is the impact of the dispersion length scale on the biomass steady state?

The dependence of the steady state biomass characteristics on the length scale of dispersal was evaluated by varying the plant stress term and the dispersal length scales concurrently. Dispersal length scales were varied from 0.5 to 32 m, encompassing scales both smaller and greater than the typical length scales of vegetation patterns. The characteristics of the biomass were evaluated in terms of the total standing biomass at steady state (nondimensionalized by k_2) and the site occupancy, expressed as a percentage of the domain size. A site was defined as occupied if the scaled biomass density $(P/k_2) > 1$. This threshold was set to exceed the biomass density within "bare patches" and to encapsulate all biomass within occupied patches over all simulations. Trends in the characteristic length scales of the patterns as eval-

uated from power spectra, and in the amplitude of the patterning were also recorded.

4.4 Results and discussion

From the simulations in Table 4.1, the results are presented thematically following the questions outlined previously. It should be emphasized here that the simulation results are generic and are not intended to represent a particular ecosystem.

4.4.1 Question 1: Does small-scale disorder in vegetation patterns arise from extrinsic randomness or Intrinsic Processes?

Initiating the model with a vegetation pattern taken from a remote sensing image allows an evaluation of the models capability to preserve real features of patterned vegetation, and permits a direct comparison of the fine-scale features of different model results in terms of two dimensional power spectra. Encouragingly, for appropriate choices of the rainfall/mortality forcing, the models used preserved many of the spatial features of the initial condition. A comparison of the patterns generated by the diffusion model, a diffusion model with random soil properties, and a dispersion model showed that the dispersion model best preserved the energetic length scales found in field data (Figure 4.3b and 4.3c). A comparison of the power spectra of these cases showed good correspondence between the remotely sensed image and the dispersion model. The addition of random soil properties through randomization of the k_2 term generated new energetic length scales and spread the energy out over this range, reducing the distinctiveness of the pattern (Figure 4.3c), while the diffusion model alone constrained the range of energetic length scales (Figure 4.3d). Preservation of the energetic length scales of real data is a necessary but not sufficient condition upon which to evaluate the models performance; these results provide encouraging but not conclusive support for the use of the kernel-based model.

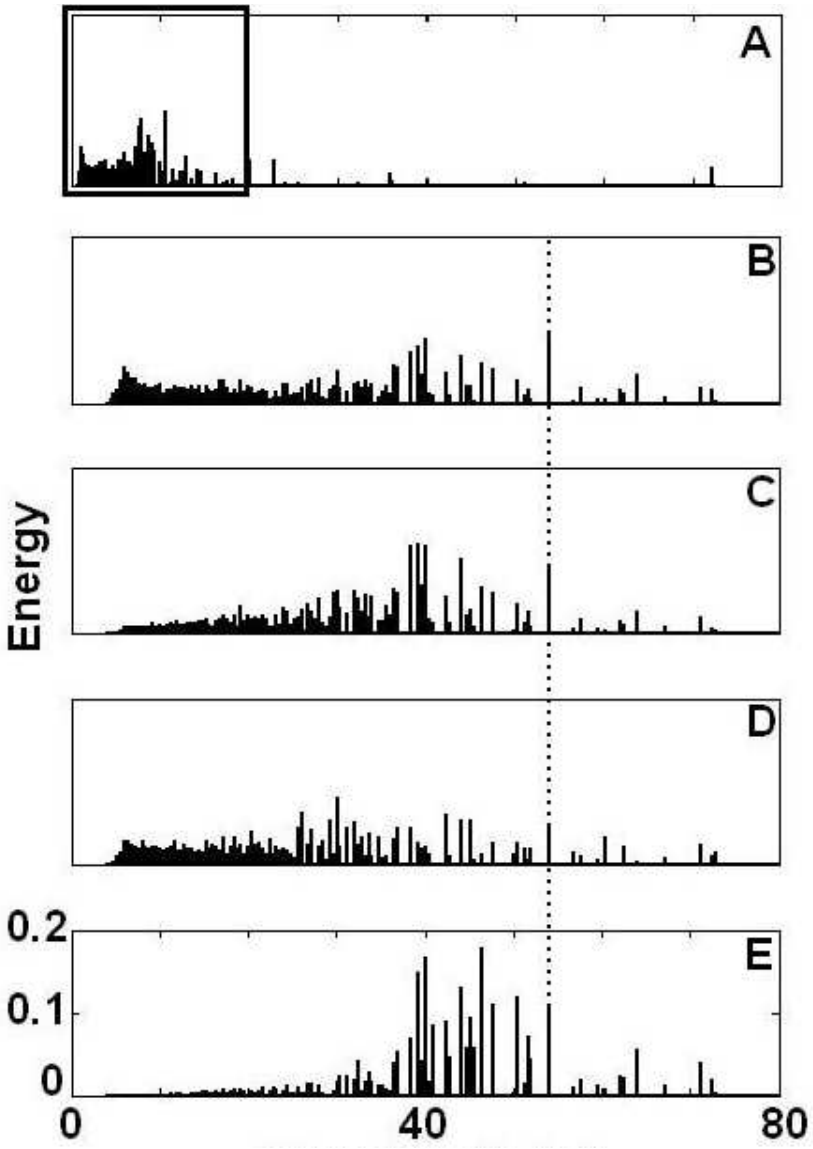

FIGURE 4.3: Comparison of measured and modeled power spectra, represented here by a scalar wavelength. The spectra are normalized by their respective areas. (a) The full spectrum obtained from the remote sensing image (Figure 1a). (b) Magnification of area indicated by insert in Figure 3a. (c) The spectrum from the dispersion model for the same range in wavelengths. (d) The analogous spectrum arising from the diffusion model runs with stochastic soil properties. (e) The spectrum from a diffusion model assuming homogeneous soil/vegetation parameters in space. The dotted vertical line indicates the most energetic length scale observed from the Google Earth image.

4.4.2 Question 2a: Can patterns be maintained in the absence of diffusion?

The model results indicate that pattern formation can persist without requiring biomass to diffuse. This is an important confirmation that the proposed mechanisms for pattern formation, which until now have been demonstrated only with idealized descriptions of vegetation transport, are compatible with realistic vegetation movement processes. The results obtained via a dispersal kernel contrast to those obtained from previous kernel and diffusion based models by increasing the steady state biomass density and decreasing the regularity of the steady state biomass patterns. Despite differences in pattern appearance, the disordered patterns generated by the dispersion model recapitulated the trends with water stress seen in the diffusion model. Linear stability analysis supported the interpretation that dispersion destabilized the pattern formation properties of the model, as the range of unstable wavelengths increased markedly [Murray, 2003b] (see also Appendix C). The outcomes from using kernels in pattern-forming models depend on the shape and purpose of the kernel. Lefever and Lejeune [1997] use a kernel to encode the feedbacks that result in pattern formation to generate smooth, regular patterns. By contrast, our kernel purely results in transport of biomass and has the effect of removing sensitivity of that transport to biomass gradients, a sensitivity that was maintained in the Lejeune and Lefever model. The kernel in this model is independent of biomass gradients. It is thus less diffusive and admits disordered solutions that diffusion would tend to smooth out. In fact, some of the patterns generated by the dispersion model appear less regular than those observed in nature, raising the possibility that biomass movement might preserve some diffusive features. A potential source of such behavior might lie in vegetative reproduction (through clonal growth), which is known to occur in several of the species that form patterned vegetation (e.g., *Combretum micranthum, Guiera senegalensis, Pleuraphis* (formerly

Hilaria) *murtica*) [Couteron and Lejeune, 2001]. The prevalence of vegetative versus sexual reproduction, however, is not clear [Thiombiano et al., 2003, Uchytil, 1988]. Another possible explanation for the models less regular patterns is that the coupling in time between rainfall and seed production or dispersal, as is common in arid ecosystem [Ellner and Shmida, 1981], may act to smooth patterns by subsuming smaller scales during periods of vegetation expansion or consuming them during periods of water stress. These two effects do "smooth out" biomass fronts.

4.4.3 Question 2b: What is the influence of initial conditions on pattern formation?

The dependence on ICs between the diffusion model and the kernel-based model was quite different. The final pattern form was largely independent of the ICs in the diffusion model, but was highly sensitive to ICs in the dispersion case, shifting from a frozen state generated by point ICs where biomass expanded about the initial points until the expansion was halted by water depletion at the boundary of the vegetation patches, as in Figure 4.2b, to the "disordered" patterns generated from random ICs, as in Figure 4.2a. The sensitivity of the final pattern to the degree of randomness imposed in the random initial condition was also tested. The patterns displayed less disorder as the magnitude of the initial disturbance declined, but remained highly disordered in comparison to a diffusion model. This dramatic change in spatial organization and sensitivity to initial conditions in contrast to diffusion-based models can be understood as a combination of two factors: the stabilization of sharp biomass fronts, and the importance of connectivity between vegetation patches in moderating the plant-water spatial dynamics. While diffusion acts to erode sharp biomass fronts, these fronts remain stable in the kernel-based model, and are susceptible to being "pinned" by equally abrupt water limitation at the expanding edge, preventing the growth and establishment of dispersed seed ahead of the front. Under such circumstances, isolated patches expand outward symmetrically until the growth is halted

by water limitation. These patches do not fragment but remain cohesive within the pinned boundary, generating the "frozen state". When the model is initiated with continuous vegetation cover, the vegetation patterning is not driven by the expansion and pinning of patches but by the disintegration of the initial vegetation cover due to the surface water dynamics. The point initiation case can be viewed as being driven by the expansion of the biomass, and the random initial conditions case by the reallocation of soil moisture, with different results for the ultimate spatial organization. The unrealistic form of the patterns generated by the point diffusion case suggests that vegetation patterns are unlikely to have resulted from colonization of sites by dispersed seed, and lends support to the possibility that patterns originate from the fragmentation of homogeneous vegetation cover under increasing water stress.

4.4.4 Question 3: Does the dispersion kernel model admit bifurcations?

Bifurcations between disordered patterns, ordered patterns, and homogeneous vegetation occurred with changes in ϕ, however these were located at values of $\phi > 1 \times 10^{-2}$ day^{-1}, outside the biologically realistic range of $\phi \in (1 \times 10^{-4} - 1 \times 10^{-2}$ day$^{-1})$. Realistic ϕ values generated disordered patterns or homogeneous biomass. These results provide confidence that the variations observed in the dispersion model output were independent of the choice of ϕ.

4.4.5 Question 4: What is the impact of dispersal length scale on observed patterns?

Trends in spatial organization, biomass, occupancy ($P/k_2 > 1$), pattern amplitude and pattern length scale were evident with changing dispersion length scales and water stress. Trends in pattern length scale and amplitude appeared to be specific to the pattern type. Length scales of gaps (i.e., bare sites) and spots (i.e., vegetated sites) declined as the dispersion length increased, while the length scales of labyrinthine patterns were largely unchanged. The trends in amplitude reflected the

trends in length scale, with biomass generally increasing as vegetation cover declined. Overall the magnitude of these changes was on the order of 10-15% while dispersal length changed over 2 orders of magnitude. Despite the trends, it was difficult to identify any signal of changing dispersion length in power spectra of the patterns. This is rather encouraging from the perspective of inverse modeling, as it suggests that the dispersal length parameter, which is difficult to estimate a priori, will have only a minimal influence on the remainder of the pattern form.

The impact of the trends in total biomass and site occupancy was evaluated using an index that combined the total biomass and the degree of site occupancy by multiplying the standing biomass (normalized by the maximum standing biomass achieved under the environmental conditions) by the percentage of occupied cells, and normalizing again by the highest value of this index for each set of environmental conditions tested. Trends in the index (Figure 4.4a), as well as for the amplitude (Figure 4.4b) and pattern length scale (Figure 4.4c), are shown in Figure 4.4 for the random initial conditions case. The index decreased with increased dispersion distance, with the greatest decreases associated with the highest water stress and approaching zero as the water stress was reduced. The use of a simple multiplicative index to capture the variations in standing biomass and its distribution was based upon a simplified assumption that plants in general should seek to maximize both their standing biomass and their extent. This assumption neglects the subtleties of real ecological responses and should be treated with caution: nonetheless the trends found are intriguing and suggest that there may indeed be a feedback between the pattern formation in these systems and dispersal strategy selection. The trends furthermore agree with empirical evidence of a preponderance of anti telechory and atelechory (localized dispersal) in desert ecosystems, and suggest that there may be a link between water availability and seed dispersal length scales. Within the model framework, the decline in the index with dispersal length can be attributed to the

increased probability of seeds being dispersed to regions with an impoverished soil moisture resource as the dispersal length increases. At short dispersal distances a greater proportion of seeds germinate in a region of relatively high water availability near the parent. We note that although we did not explicitly incorporate the inhibition of seedling germination over crusted soils into this model, that this would be a further feedback enhancing plant success when seed dispersal preferentially routed seeds to vegetated sites. This might also lead to more regular vegetation patterns (see above). This simple description is intriguing, and while obviously limited by lack of explicit consideration of genetics, intergenerational competition and other factors needed to evaluate optimal reproductive strategies for plants, it indicates that the links between plant dispersal strategies, organizing features in the environment, and other edaphic drivers deserves more detailed theoretical treatment.

4.5 Conclusions

While extensive effort has been invested in understanding the nonlinear interactions between plants and water in pattern-forming vegetation within the last decade or so, the role of vegetation transport has been less studied. It appears, however, that the description of spatial movement of the plant population has the capacity to significantly alter the steady state spatial patterns in these systems, through changing sensitivity to initial conditions and destabilizing the patterns formed over a wider range of length scales. Indeed, the increased range of length scales may result in improved representations of steady state biomass, on the basis of a comparison with measured spatial power spectra of vegetation density. These results suggest that spatial heterogeneity, for example in soil properties, need not be the source of disorder in vegetation patterns, but that the decoupling between biomass gradients and dispersion terms may also act to introduce a broader spectrum of length scales of variability. To further evaluate this hypothesis, studies of the dispersal ecology of

pattern forming species are needed, to quantify modes of reproduction (sexual versus asexual), length scales of dispersal and the relationship between soil moisture availability and seedling success and survival. In an environment limited by the soil water resource, such studies may allow the separation of the roles of biomass movement and water supply as the processes determining patterns of spatial organization.

4.6 Further implications

The apparent interaction of water availability and dispersal length scales in determining steady state biomass parameters remains intriguing and warrants further investigation. In particular, it raises the question of whether environmental controls upon dispersal behavior can be identified more generally across ecosystem types. Studies of the interaction between dispersal strategy and environment at the ecosystem level suggest that factors such as climate and disturbance play important roles in selecting dispersal mechanisms [Ellner and Shmida, 1981, Fragoso, 1997, Fragoso et al., 2003, Reichman, 1984, Abrams, 1988, Clauss and Venable, 2000], while broad trends can be identified between ecosystems. To view such trends through an ecohydrological lens, the classical Budyko Curve [Budyko, 1974] provides a tantalizing starting point toward a conceptual framework (Figure 4.5). A survey of typical modes of dispersal across biomes suggests that there is a predominance of short-range dispersal in arid ecosystems, longer-range wind- and animal-driven dispersal in grasslands and temperate ecosystems, and long-range animal dispersal (with little wind dispersal) in tropical ecosystems [Chambers and MacMahon, 1994, Howe and Smallwood, 1982]. The findings in this study suggest that it may be possible to quantify the linkage between an edaphic forcing term (such as precipitation) and dispersal optimization in arid ecosystems. We speculate that, given the control of hydraulics on plant height, resource availability on canopy densities, and energy inputs on disturbance, it may be possible to establish a general framework relating

optimal ecosystem dispersion strategies to the processes, patterns, and organizing principles that drive their physical environments.

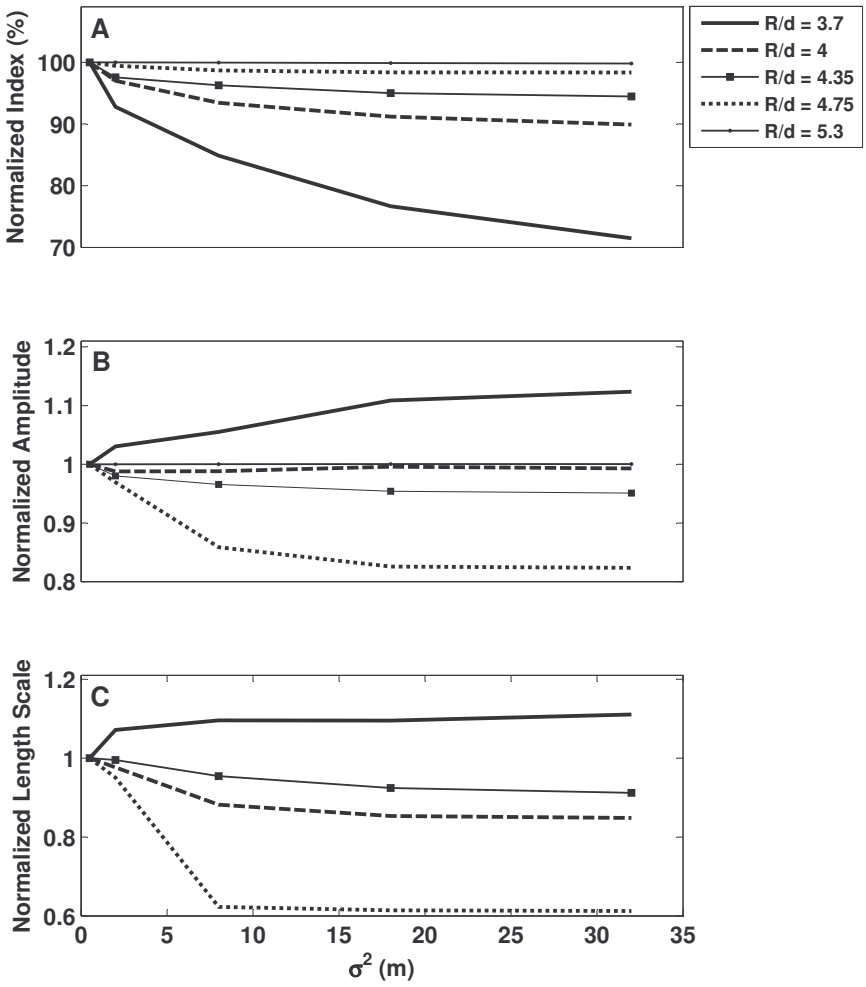

FIGURE 4.4: Variations in pattern properties with changing length scales of seed dispersal. (a) Changes in the combined biomass/occupancy index for random initial conditions. (b) Trends in the amplitude of the patterns, with the amplitude shown normalized against the $\sigma^2 = 0.5$ case. (c) Changes in the characteristic length scale (as interpreted from power spectra) of the patterns, with the length scale shown normalized against the $\sigma^2 = 0.5$ case. Increasing R/d indicates decreasing water stress.

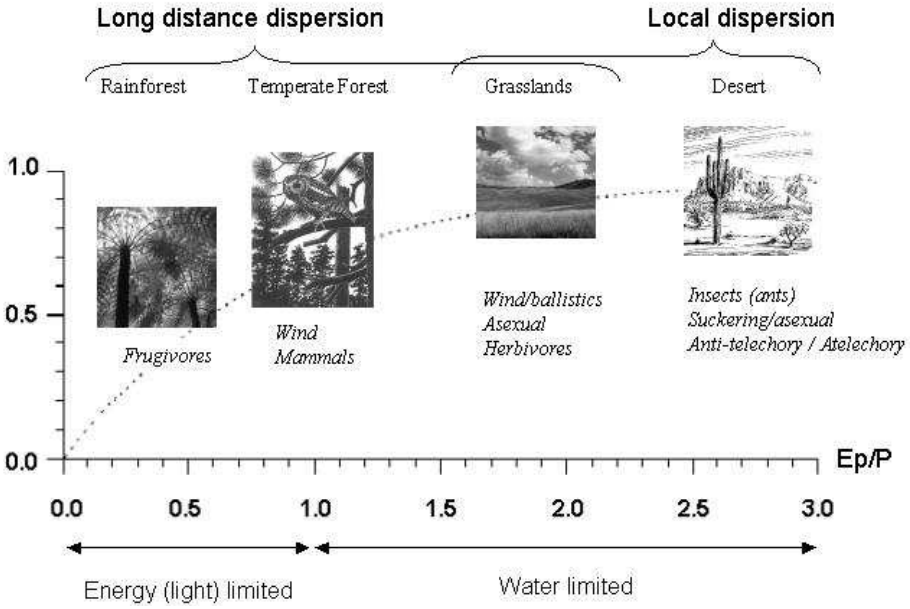

FIGURE 4.5: Trends in dispersal length and strategy broadly vary along the Budyko Curve. The abscissa value, Budykos "radiative index of dryness" represents the ratio of potential evapotranspiration to precipitation, and as such is a measure of water limitation ($E_p/P > 1$, i.e., more water can be removed from the landscape via evapotranspiration than is delivered to it) or energy limitation ($E_p/P < 1$, i.e., more water is delivered to the landscape than evapotranspiration can remove). The ordinate value is the ratio of actual evaporation to precipitation.

5

Secondary seed dispersal and its role in landscape organization

5.1 Introduction

Banded vegetation, consisting of interspersed bands of vegetation and bare soil, occurs in arid ecosystems worldwide in association with biological soil crusts, intense, infrequent rainfall, and slopes of 0.2-2% [Valentin et al., 1999]. Vegetation patterns are thought to arise from a positive feedback between soil moisture availability and biomass density, emergent properties of coupled hydrological and ecological processes [D'Herbes et al., 2001]. The dynamics of these systems have attracted interest due to their occurrence in areas prone to desertification [Goutorbe et al., 1997], their importance as a source of forage [Safriel and Adeel, 2003], and numerical predictions suggesting the patterns are indicators of desertification [Rietkerk et al., 2002, 2004]. Numerical models repeatedly predict upslope migration of vegetated patches due to increased facilitation at the upslope edges of the bands, encouraging expansion at rates of 10-100 m/year in many models [Klausmeier, 1999, Rietkerk et al., 2002, Thiery et al., 1995, von Hardenberg et al., 2001]. This prediction remains one

of the most debated questions regarding band dynamics [Seghieri and Dunkerley, 2001, Worrall, 1959]. Measures of upslope vegetation movement at rates of 0.10 to 0.15m/year have been reported [Leprun, 1999], but other studies found no evidence of migration over 5-8 years [Cornet et al., 1992, Montana, 1992]. Over short observation windows, systematic upslope migration is difficult to distinguish from temporary expansion/contraction of bands [Tongway and Ludwig, 2001]. Increasingly, field studies are concluding that spatial variation of band vegetation reflects niche partitioning and not upslope migration [Couteron et al., 2000]. Mathematical models of banded systems predict an unequivocal and rapid (10 - 100 m/year) migration of the vegetation bands, 2-3 orders of magnitude faster than observations [Klausmeier, 1999, Rietkerk et al., 2002, Thiery et al., 1995, von Hardenberg et al., 2001]. This is a key point of disagreement between theory and observation. It is argued here that this disagreement can be resolved by consideration of seed transport, or more precisely, its representation in the modelling framework used in previous studies. Although seed dispersal is critical for migration of vegetation communities, these processes are only now being incorporated into models of patterned vegetation [Pueyo et al., 2008] (and see Chapter 4). We hypothesise that the rapid band migration generated by contemporary models arises from the failure of diffusion-based representations of biomass migration to capture important features of seed dispersal in these systems. Seed banks in banded systems are concentrated within vegetated bands, where the seed density can be 180 times greater than in the bare interband [Mauchamp et al., 1993, Seghieri et al., 1997]. Seeds are transported down slope from bare sites by runoff [Aerts et al., 2006]. This advection can be the dominant dispersal mechanism for some species, even in dry environments [Friedman and Stein, 1980]. Recruitment of seedlings on the biological crusts in the interband is minimal [Montana et al., 2001, Prasse and Bornkamm, 2000], and this exaggerates tendency for recruitment to occur within the bands rather than at their edges. Two different

approaches are taken to incorporate secondary dispersal of seed. The first approach adds advection of seeds to a process-based model that couples water and biomass dynamics to predict upslope migration of vegetation bands [Rietkerk et al., 2002]. Promisingly, previous qualitative examination of secondary seed dispersal by similar mechanisms suggests that it may alter band migration dynamics [Saco et al., 2007]. The second uses a kernel-based approach (see Chapter 4) to improve the realism of dispersal modelling. In this kernel based model framework, an anisotropic seed dispersal kernel parameterises the combined effect of isotropic primary dispersal and directional (downslope) secondary seed dispersal. The use of the two different models of seed transport allows conclusions about secondary dispersal to be decoupled from the exact treatment of seed movement. It should be understood that the underlying ecological and hydrological representation of banded vegetation dynamics is equivalent between the two models, which differ only in their precise depiction of seed transport.

5.2 Model

The starting point is Rietkerk et al. [2002] reaction-diffusion model on a slope:

$$\frac{\partial P}{\partial t} = cg_{max}\frac{W}{W+k_1}P - dP + D_p\nabla^2 P, \tag{5.1}$$

where P is the plant biomass in gm^{-2}.

$$\frac{\partial W}{\partial t} = \alpha O\frac{P+k_2W_o}{P+k_2} - g_{max}\frac{W}{W+k_1} - r_wW + D_w\nabla^2 W, \tag{5.2}$$

where W is the soil water depth in mm; and

$$\frac{\partial O}{\partial t} = R - \alpha O\frac{P+k_2W_o}{P+k_2} + V_o\frac{\partial O}{\partial x}, \tag{5.3}$$

where O is the surface water depth in mm. The remaining terms in this model are given in Table 1. The modification consists of the addition of a term representing down slope advection of seeds to the biomass equation. This term is the spatial derivative of the advective biomass flux, a product of the mobile biomass (κP) and its advection velocity V_p. To first order, it is assumed that the proportionality constant κ and the biomass velocity are spatially uniform, so that $\frac{\partial V_p \kappa P}{\partial x} = V_p \kappa \frac{\partial P}{\partial x}$. Advection in surface runoff is assumed to be primarily responsible for seed transport down-slope, so $V_p \leq V_o$. In this refined model seed dispersal is a two-stage process. The first stage of isotropic primary dispersal of seed from the plant to the ground is parameterized by D'_p, and subsequent, directional secondary dispersal in overland flow occurs with rate V'_p. Selection of an appropriate value of κ is problematic given that the continuous model allows biomass movement to occur continuously rather than seasonally. Plants commit a wide range of biomass to reproduction, up to 50% for some annuals [Aronson et al., 1993]. An intermediate value of $\kappa = 0.2$ was used for all simulations. The revisions can be incorporated in other models of banded vegetation and the Rietkerk model is used here primarily as a case study.

The model was nondimensionalized to facilitate numerical investigations. The nondimensional equations are (see Table 1 for definition of parameters):

$$\frac{\partial P'}{\partial t'} = \frac{W'}{W'+1} P' - bP' + D'_p \nabla^2 P' + V'_p \kappa \frac{\partial P'}{\partial x'}, \tag{5.4}$$

$$\frac{\partial W'}{\partial t'} = O' \frac{P' + W_o}{P'+1} - k' \frac{W'}{W'+1} - rW' + D'_w \nabla^2 W', \tag{5.5}$$

$$\gamma \frac{\partial O'}{\partial t'} = R' - O' \frac{P' + W_o}{P'+1} + \frac{\partial O'}{\partial x'}, \tag{5.6}$$

The properties of the original model are examined in several other papers [Hil-

leRisLambers et al., 2001, Rietkerk et al., 2002] and are not repeated here. Instead the focus is on band migration and the related control parameters V_p' and D_p'. The impact of varying V_p' and D_p' on band migration, while holding all other parameters constant (Table 1), was investigated in a 1D model, following the observation that patterns tended towards a 1D steady state. V_p' was varied with $D_p' = 8 \times 10^{-4}$, while D_p' was varied while holding $V_p' = 0.1$, corresponding to realistic dimensional parameters [Rietkerk et al., 2002]. Initial conditions consisted of equally spaced bands of varying wavelength k. The premise that biomass movement is diffusive remains questionable given the non-Gaussian nature of many dispersal kernels. The kernel-based model outlined in Chapter 4 was used as a reference to test if the retardation of upslope band movement is linked with biomass diffusion. This model represents biomass movement processes in a seed dispersal kernel that captures the statistics of seed transport from an individual plant. This model modifies the biomass equation as follows:

$$\frac{\partial P}{\partial t} = \left(c g_{max} \frac{W}{W + k_1} P - dP \right) (1 - \phi) + \phi \left(\iint \nu \left(x - x', y - y' \right) P \left(x', y' \right) dx' dy' \right), \tag{5.7}$$

Here ν is the dispersal kernel (that can account for secondary dispersal processes if known), ϕ represents the proportion of standing biomass dispersed per unit time (on the order of 4×10^{-4} g/m^{2}day, see Chapter 4) and x' and y' define the distance seeds move from the parent, integrated over the domain. integrated over the domain. No measured dispersal kernels J accounting for both primary and secondary transport in banded systems were available. A qualitative approach was adopted by taking an isotropic Wald or Inverse Gaussian kernel, often used to represent wind dispersal of seed (see Chapter 4). The anisotropy associated with secondary dispersal was incorporated by weighting the upslope half of the kernel to one fiftieth of the value

of the downslope half (a conservative value compared to the 180-fold discrepancy observed in seed bank density) and normalized. The precise treatment of all eco-hydrological processes in both modelling approaches can be criticized ad infinitum. However, to address the study objective here, it suffices to demonstrate that banded vegetation migration rates can be significantly retarded when a primitive treatment of secondary dispersal is included. The model results here should not be viewed as providing finality to the migration of banded vegetation problem but are logical first steps highlighting processes that require further consideration.

5.3 Results

Band migration velocities produced by the unmodified Rietkerk model [Rietkerk et al., 2002] were on the order of 20 - 200 m/year, depending on the band wavenumber, with the parameter values in Table A.1. The isotropic kernel-based model generated velocities of approximately 10 m/year. Both models in their unmodified form therefore generated band migration at rates at least an order of magnitude greater than field observations could support, although we emphasise that the models have not been calibrated to a specific ecosystem, and that these results are included solely to provide a frame of reference for typical model output. The hypothesis that band migration is inhibited by the inclusion of anisotropy in seed dispersal was explored through the advection-diffusion and a kernel-based model. The band velocities for varying degrees of secondary dispersal are presented as a ratio of the band velocity when dispersal was purely isotropic in Figure 5.1. Snapshots of the band evolution for the two models in isotropic and anisotropic modes are provided in Figure 5.2. In the case of the advection diffusion model, systematic variation of the parameters V_p' and D_p' slowed and eventually reversed the band migration velocity (Figure 5.1a). The band velocity was also found to depend upon the wavenumber of the pattern, with upslope movement favoured at low wavenumbers. Downslope movement of the

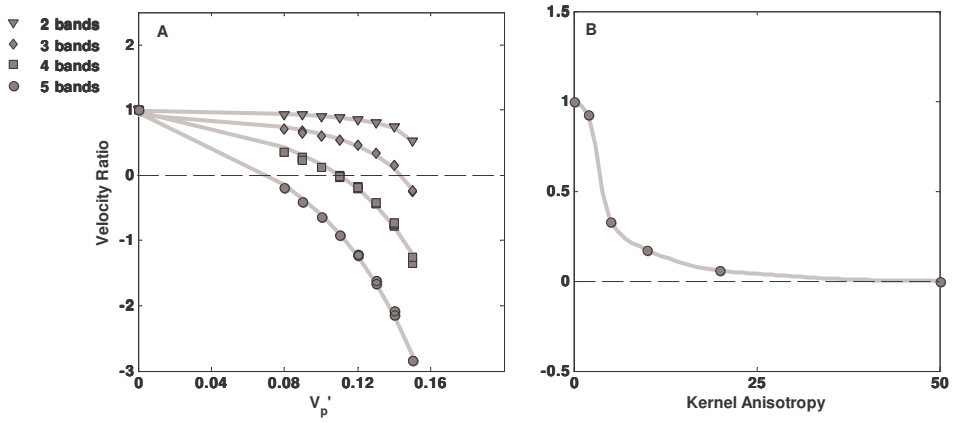

FIGURE 5.1: Band velocities shown as ratios between the anisotropic test cases and the equivalent isotropic model. The same initial conditions are used for each set of data points on a given line. (a) Decline and eventual reversal of the velocity ratio with increasing downslope advection. (b) Decline of the velocity ratio as the degree of anisotropy in the kernel is increased from a factor to 2 to a factor of 50.

bands occurred at large values of the dimensionless seed advection velocity V_p', and small values of the dimensionless seed diffusion coefficient D_p'. As will be elaborated on in the discussion, the prediction of bands downslope band migration should be treated with caution. These results should be interpreted as indicating the regime in which upslope migration is precluded. For the kernel-based model, an increasing degree of anisotropy in the kernel slowed and eventually halted band evolution in the direction of the slope gradient, so that band migration dynamics occurred primary across the slope. In the absence of information to constrain the possible forms of the anisotropic kernel, only the effects of upslope-downslope anisotropy were tested, generating the velocity ratio data shown in Figure 5.1 b.

5.4 Discussion and conclusions

The model results indicate that a down-slope flux of biomass associated with secondary dispersal of seeds in overland flow is sufficient to freeze or even reverse the upslope migration of vegetation bands. This result can be physically understood

by relating the model parameters V_p' and D_p' to more commonly used measures of seed and dispersal properties. Seed transport in overland flow can be described as saltation [Bagnold, 1973], in which V_p equals V_o minus a thrust term accounting for particle re-suspension. This thrust approximately equals the seed terminal velocity V_g, that may be estimated from gravity (g), the seed drag coefficient C_d, diameter d, and specific gravity γ_g of a seed. So:

$$V_p' = \frac{1}{\gamma}\frac{V_p}{V_o} = \frac{1}{\gamma}\frac{V_o - V_g}{V_o} = \frac{1}{\gamma}\left(1 - \frac{1}{V_o}\sqrt{\frac{4gd}{3C_d}\gamma_g}\right). \tag{5.8}$$

Dimensional analysis offers an interpretation of D_p'. Firstly a definition of $D_p = C_p^2/4r$, where r is the average growth rate of the population is used. C_p, the migration velocity of the vegetation population, can be derived from the properties of most seed dispersal kernels using the procedure described in Chapter 3. Substituting for D_p and γ,

$$D_p' = \frac{C_p^2\alpha}{4rV_o^2}\frac{\alpha}{cg_{max}}. \tag{5.9}$$

When water is plentiful $r \Rightarrow cg_{max}$, and so $D_p' = \left(C_p/2\gamma V_o\right)^2$. The control parameters thus give the ratio of biomass transport induced by primary seed dispersal to the rate of water transport (D_p') and of seed to flow velocity (V_p'). Upslope band migration ceases when $C_p < V_o$ or as $V_p \to V_o$. The effect of wavenumber on band migration can be understood in terms of resource delivery to the upslope edge of the band, which is maximised for low wavenumbers and declines as wavenumbers increase. At low wavenumbers the increased availability of resources upslope of the band results in high survival and rapid growth of the relatively few seeds dispersed there. As resource availability and upslope survival declines (higher wavenumbers), the higher density of the downslope seed bank becomes the dominant driver of band migra-

tion. Although the model results predict downslope migration of the bands, this is probably a consequence of the simple representation of dispersal. Vegetation bands are effective in trapping particles and slowing the velocity of water. The difference in the seed bank density within and outside bands [Seghieri et al., 1997] suggests that bands are effective at trapping seeds. Advection of seeds in runoff is likely to transport seed to, but not through, the bands. Down-slope migration should be interpreted as indicative of a regime where upslope migration is prevented. Models of banded vegetation have consisted of primarily hydrological models focused upon surface water dynamics with minimal representation of vegetation [Ludwig et al., 1994, 1999, Mauchamp et al., 1994], or reaction-diffusion models coupling simplified vegetation and hydrological dynamics (as used in this study) [Barbier et al., 2008, Klausmeier, 1999, Rietkerk et al., 2002]. This distinction is not surprising given the timescale separation between the fast hydrologic and slow biomass movement dynamics. The results here suggest that a reconciliation of these approaches is needed to formally scale up over the fast timescales determining water and seed redistribution, to the slower timescales determining vegetation growth. This averaging approach will require stochastic treatment of input parameters, particularly rainfall distributions, to evaluate infiltration and biomass responses. It may be facilitated by tracer studies in the vadose zone [Allison et al., 1994, Allison and Hughes, 1978, Scanlon, 2000], offering insight into soil moisture residence time, transport paths, and the water sources used by plants. New approaches should also extend the use of kernel-based descriptions of seed dispersal dynamics. This work suggests that the heretofore little studied process of secondary seed dispersal in overland flow may alter the macroscopic spatial dynamics of vegetation communities. This process is physically mediated and readily amenable to physical analysis. Detailed studies of such processes, in combination with relevant field measurements of primary and secondary dispersal (e.g., through release of buoyant tracers [Boedeltje et al., 2004, Merritt and

Wohl, 2002]) would allow the elucidation of the full anisotropic seed dispersal kernel, and the quantitative use of kernel based models.

Dimensional Parameters	Value	Nondimensional Parameter	Value
c(g mm^{-1} m^{-2}) Water uptake: plant growth ratio	10	$b = \dfrac{d}{c\, g_{max}}$	0.8
g_{max} (mm m^{2}g^{-1} day^{-1}) Maximum specific water uptake	0.05	$r = \dfrac{r_w}{c\, g_m ax}$	0.2
R (mm day^{-1}) Precipitation	0.75	$R' = \dfrac{R}{k_1\, c\, g_{max}}$	0.5
k_1 (mm) Half saturation constant of water uptake	3	$k = \dfrac{k_2}{k_1\, c}$	0.167777
k_2 (g m^2) Half saturation constant of infiltration	5	$D'_p = \dfrac{D_p \alpha^2}{V_o^2 c\, g_{max}}$	0.00002 - 0.008
D_p (m^2 day^{-1}) Biomass diffusion coefficient	0.004-1.6	$D'_w = \dfrac{D_w \alpha^2}{V_o^2 c\, g_{max}}$	0.00008
α (day^{-1}) Maximum infiltration rate	0.1	$\dfrac{V_p}{V_o} \dfrac{\alpha}{c\, g_{max}}$	0.08-0.2
V_o (m day^{-1}) Surface water velocity	2	$\gamma = \dfrac{c\, g_{max}}{\alpha}$	5
D_w (m^2 day^{-1}) Soil-water diffusion coefficient	0.01	$x' = \dfrac{x\alpha}{V_o}\, y' = \dfrac{y\alpha}{V_o}$	0.2
V_p (m day^{-1}) Seed advection velocity	0.4-0.2	$t' = t\, c\, g_{max}$	0.5
dx, dy (m) Cartesian increments	1		
dt (day) Time increments	1		
d (day^{-1}) Mortality rate	0.1		
r_w (day^{-1}) Water loss to drainage / evaporation	0.1		

Table 5.1: Model parameters (dimensional and nondimensional) used in analysis

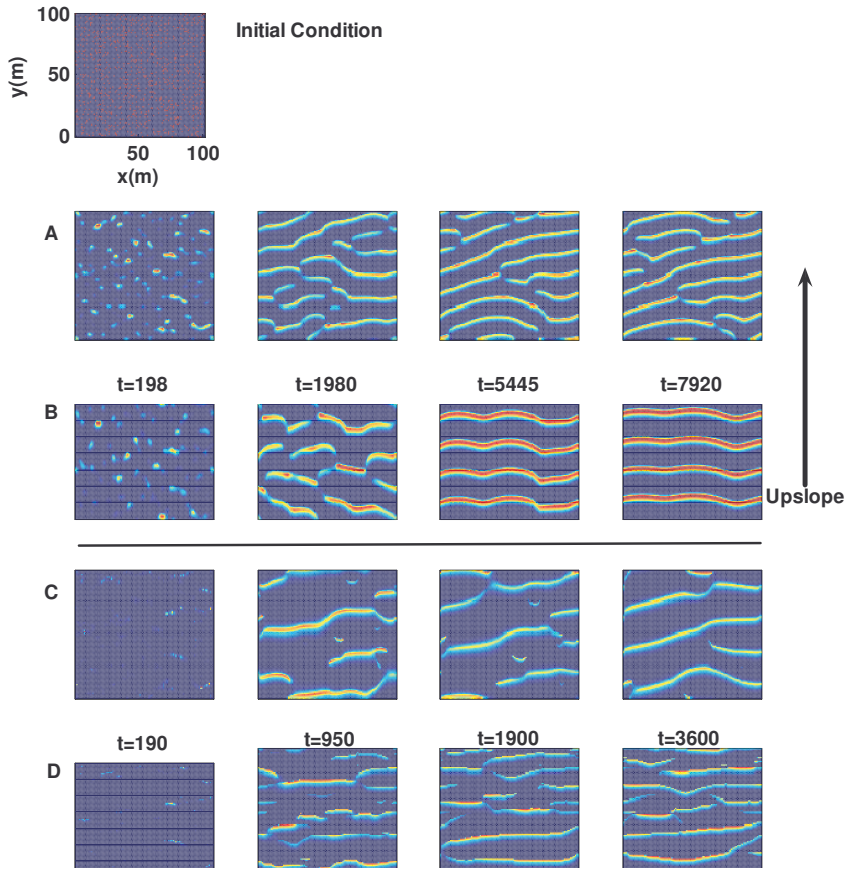

FIGURE 5.2: Snapshots in time of the modelled spatial biomass density. The same initial condition was used in each case. (a) Results from the reaction-diffusion model with diffusive biomass transport. The bands move rapidly upslope. (b) Model output when a downslope biomass velocity of 0.46 m/s was added. Band migration rates approach zero, and the bands evolve towards a 1D pattern. (c) Kernel model output with an isotropic kernel. Bands rapidly migrate upslope. (d) Same model in which the kernel is weighted by a factor of 50:1 downslope. Band migration is essentially confined to the crossslope direction.

6

Biomass-infiltration relationships across climate and soil type gradients

6.1 Introduction

Vegetation feedbacks to the water cycle have drawn increased interest in the past thirty years [Bosch and Hewlett, 1982, Jackson et al., 2000, Gerten et al., 2004]. Processes such as stomatal optimization with respect to water availability [Cowan, 1978, 1986, Makela et al., 1996]; hydraulic lift [Richards and Caldwell, 1987, Dawson, 1993, Caldwell et al., 1998]; and the constraints imposed by water stress on carbon allocation [Porporato et al., 2001, Schwinning and Ehleringer, 2001, Givnish, 1986] have become foci of research and theoretical development, and their consequences are now being up-scaled from the leaf, root and plant level to communities and catchments [Schymanski et al., 2009, Caylor et al., 2004]. There are, however, feedbacks between vegetation and the water cycle that do not directly result from plant activity. One such feedback is the alteration of the infiltration capacity of soils through biotic processes. This positive feedback (i.e. the presence of vegetation increases infiltration capacity) is well documented in arid ecosystems where it can lead to spa-

tial organization [Bromley et al., 1997, Couteron and Kokou, 1997, D'Herbes et al., 2001, HilleRisLambers et al., 2001, Rietkerk et al., 2002, D'Odorico et al., 2006b, Saco et al., 2007]. The processes that generate vegetation-infiltration capacity feedbacks have been widely explored in drylands [Lyford and Qashu, 1969, Schlesinger et al., 1996, Bergkamp, 1998, Dunkerley, 2000, 2002a, Wainwright et al., 2002]. They include physical factors, such as protection of the soil surface, and biological factors, such as the creation of habitat for soil macrofauna. Vegetation - infiltration relationships are starting to be incorporated into hydrological models of arid ecosystems to predict rainfall-runoff partitioning, soil moisture distribution, vegetation dynamics and geomorphology of drylands [Ludwig et al., 1999, Couteron and Lejeune, 2001, Mauchamp et al., 2001, Ursino, 2005, Zeng et al., 2005, Bracken and Croke, 2007, Mayor et al., 2008]. Unlike stomatal conductance, infiltration capacity is not under the direct control of plants on short timescales. However, water can be the limiting resource for plant growth and consequently reproduction, and infiltration into the soil is unquestionably a key process that replenishes the root-zone soil moisture. Regardless of climate or soil type, many plant systems have a marginal safety factor when the minimum observed leaf pressure is compared with pressures needed to induce cavitation in the plant hydraulic system [Sperry, 2000]. That is, the hydraulic apparatus of the soil-plant system appears to function near the 'edge'. On long timescales, it is therefore plausible that plants have evolved strategies that enhance infiltration of water. It is logical to ask whether vegetation-infiltration relationships represent the cumulative effects of plant strategies that affect water availability in the root zone. Before this question can be effectively explored, several key uncertainties regarding vegetation-infiltration feedbacks must be addressed, specifically:

- Does vegetation modify infiltration capacity at the soil surface in mesic and hydric climates, and if so, what processes contribute to this modification?

- Based on available data, is there a canonical relationship that describes the interaction between vegetation indices and infiltration rates (in arid and humid climates)?

- How does this relationship change across climates?

These questions are important in the predictive modelling of runoff-infiltration partitioning and water balance as well as in addressing the question of plant strategy. The first question explores the generality of the postulated vegetation-infiltration feedback, which has not been established either in humid climates, nor generalized between multiple arid sites. It is unclear if and how vegetation alters infiltration capacity in wetter climates. Given the relative scarcity of vegetation and infiltration studies in these climates, new field results are needed that can delineate the role of vegetation when water is not necessarily limiting.

The second question asks if it is reasonable to express infiltration rates as a function of vegetation biomass or cover. Such an expression, if identified, is not intended to negate the complexity of the feedbacks between vegetation and soil that result in a vegetation-infiltration relationship. Instead, it parameterizes the cumulative effect of these feedbacks, allowing general and large scale predictions to be made without requiring detailed site specific parameters. The nature of the nonlinearity of such a relationship is also important, and determines whether the relationship saturates or generates threshold-type responses with respect to vegetation cover. The third question relates to the strength of the relationship and its sensitivity to climatic drivers. Note that there is no expectation that infiltration capacity itself would respond to climate, but only the nature of the relationship between infiltration capacity and local vegetation.

This work addresses these questions in two different ways. Firstly, infiltration capacity was measured in a humid field site in Duke Forest, North Carolina, where a

pine plantation, a hardwood forest and a grass field are all co-located on the same soil series and experience the same climatic regime. Secondly the results from this field study were combined with a meta-analysis of studies measuring infiltration capacity and vegetation biomass. The meta-analysis gathered information from 21 studies spanning 32 different locations, 32 different soil types spanning the full range of texture classes, and 48 vegetation communities across North and South America, Europe, Africa, Asia and Australia and ranging from hyper-arid to tropical climates.

To allow meaningful comparison between sites, above-ground biomass density (i.e. mass biomass per area of ground) was adopted as the independent variable. Unlike other measures such as percentage vegetation cover, biomass density does not saturate as climates become wetter and canopies close. Above-ground biomass is also likely to be correlated to important latent variables such as below-ground biomass [Clark et al., 1986, Naidu et al., 1998] and leaf biomass [McCarthy and Enquist, 2007] that are expected to affect the vegetation-infiltration relationship but are not commonly measured in studies of infiltration.

The three questions guiding this research may have different answers depending on the scale at which they are considered. We distinguish between biomass-infiltration relationships that arise within a single vegetation/ecosystem type ('within site variation') and those arising between vegetation/ecosystem types ('between site variation'). The former affects hillslope-scale processes such as runoff generation [Bergkamp, 1998, Fiedler et al., 2002, Ludwig et al., 2005, Puigdefabregas, 2005], while the latter is important for large-scale hydrological modelling over different land uses [Kirkby et al., 2002, Singh and Woolhiser, 2002]. Accordingly, biomass-infiltration trends are assessed both within and between sites.

6.2 Methods and materials

The two components of the study, namely the field research and the meta-analysis are addressed separately.

6.2.1 Field study

Site description

The study ecosystems are co-located in the Blackwood Division of the Duke Forest near Durham, NC (351980N, 79180W, 163 m a.s.l.). The study sites consisted of plots in three vegetation types: a grass field, a pine plantation and an 80-100 years old hardwood site. Details of the soil series, climate and species found in the study sites are provided in Table 6.1. The soil profile of all ecosystems is dominated by a clay pan at a depth of ca. 30-50 cm, which largely confines root growth to the surface soils [Stoy et al., 2008]. Within each vegetation type three 20 x 20 m plots were subdivided into 2 x 2 m subplots. For each large plot, four subplots were selected at random to perform infiltration measurements, giving a total of 36 infiltration sites, 12 for each vegetation type. Each infiltration measurement required an undisturbed site 20 cm in diameter. An optimal site for infiltration measurements was selected within each subplot, avoiding steep slopes, impermeable surfaces (i.e. rocks) and large trees.

Infiltration measurements

At each site, an infiltration measurement was made using a 20 cm diameter tension disk infiltrometer (Soil Measurement Systems, Arizona). Tensions were manually set using a Mariotte bottle at -8, -4, -1 and 1 cm. The infiltration rate was measured by monitoring the water level changes in the infiltrometer reservoir. The sites were prepared by placing a 20 cm diameter ring on the ground and trimming all litter and standing vegetation within the ring. Trimmed litter was removed and stored

Table 6.1: Species, soil and meteorological properties of the Duke Forest infiltration locations. Data from: 1) Pataki and Oren [2003], Palmroth et al. [2005], Stoy et al. [2005], 2) Oren et al. [2001], Stoy et al. [2006], 3) Novick et al. [2005]

	Hardwood[1]	**Pine**[2]	**Grass**[3]
Mean annual rainfall	1145 mm		
Mean annual pan evap.	1076 mm		
Mean annual temperature	15.5° C		
Soil series	Iredell (sandy clay loams)		
Dominant species	*Quercus* (oak) and *Carya* (hickory) sp.	*Pinus taeda*	*Festuca arundinacea*
Other species	*P. taeda* and *Juniperus virginiana*	Diverse understorey	Forbs, other grasses
Canopy height	30 m	19 m	0-1.5m harvested annually

for determination of biomass. Care was taken to leave the soil surface intact during this removal. Where a thick O horizon was present (in the pine plantation), organic mulch was removed until the surface of the mineral soil was exposed. A thin layer of contact sand (Pavestone 'all purpose') was used to create a level soil surface, and dampened with water. The infiltrometer was levelled against the sand pad prior to commencing the infiltration measurements. These measurements were made starting from the highest tension (-8 cm). Infiltration ran for a minimum of 30 minutes. If a steady state rate had not been reached at this time, infiltration continued until a near-steady state was reached (typically 45 minutes).

Soil coring

Following the infiltration measurements, the contact sand was removed and four 5cm diameter, 30 cm deep soil cores were taken from within the 20 cm diameter infiltration ring. The cores were separated into three components by depth: 0-5 cm, 5-15 cm and 15-30 cm. Two of the four cores were bulked for estimating root

density, and two were bulked for laboratory analysis. Rocky subsoils prevented a complete sample set from being obtained at every site. Within each vegetation type one infiltration site was trenched, rather than cored, and intact soil samples taken for further analysis (reported elsewhere).

Saturated hydraulic conductivity estimation

Wooding's solution for three dimensional infiltration was used to infer the saturated hydraulic conductivity of the soil [Wooding, 1968, Smettem and Smith, 2002]. Firstly, a curve was fitted to the measurements of infiltration rate to estimate the steady state infiltration value. Wooding's solution was applied to a pair of steady state infiltration values measured at two different tensions, which allowed an estimate of Gardner's parameter α (arising from a simplified exponential model of the unsaturated conductivity given as $K = K_{sat}e^{\alpha h}$), where h is the tension. The saturated hydraulic conductivity we report is based on the estimates at the two lowest tensions, namely -1 and +1 cm. The formulation is given by:

$$K_{sat} = \frac{Q}{\pi r^2 e^{\alpha h}\left(1 + \frac{4}{\pi r \alpha}\right)}, \tag{6.1}$$

and

$$\alpha = \frac{\ln\left(Q\left(h_1\right)/Q\left(h_2\right)\right)}{h_2 - h_2}, \tag{6.2}$$

where Q is the measured steady-state flow rate into the soil, h is the tension and r is the radius of the infiltrometer plate. Theoretically, Gardner's parameter (α) should be constant across multiple tensions; however, we found that the estimates of α varied depending on which pairs of tensions were considered. Accordingly, we computed K_{sat} based on piecewise regression between successive data points [Smettem and Smith, 2002].

Macropore flux estimation

The capillary equation determines the radii (r_{min}) of conducting soil pores under a given tension based on the tension (h, cm), the contact angle θ (which may be estimated as 0), the density of water ρ (0.998 g/cm^2), the air-solid surface tension σ (0.0073 cm/s^2) and gravity g (0.0981 cm/s^2) [Batchelor, 1967] given as:

$$r_{min} = -\frac{2\sigma \cos\theta}{\rho g h} \approx \frac{-0.15}{h}, \tag{6.3}$$

for h in cm. The estimates of hydraulic conductivity obtained at different tensions increase as the tension applied approaches zero. If this increase in flow is attributed to the activation of macropores with radii too large to have been conducting under the previous (higher) tension, then the change in K_{sat} may be used as an estimate of the conductivity of macropores of a given radius 'activated' at each reduction in tension [Watson and Luxmoore, 1986, Buttle and McDonald, 2000, Holden, 2009]. The additional flow arising due to the activation of these macropores is referred to as the 'macropore flux', which is reported as a percentage of K_{sat} estimated at zero tension.

Hydrophobicity estimation

Infiltration measurements suggested that soils in the pine plantation were hydrophobic. To assess hydrophobicity, drop penetration tests were conducted in the field and on subsamples of oven dried soil. Drop penetration tests are conducted by placing a drop of de-ionized water on the soil surface and measuring the time interval in which it remains beaded on the soil surface. Penetration times of more than 1 s were taken as indicative of some degree of hydrophobicity (c.f. Dekker et al. [1998] who used a threshold of 5 s). Three drop penetration tests were conducted per soil sample in the lab. Field drop penetration tests were undertaken in the pines following removal

of the O horizon.

Root measurements

Root mass within the soil cores was estimated by washing each core in a 2 m water column through which compressed air was blown. Washed cores were decanted into 0.5 mm sieves and the roots removed with tweezers. Roots were picked out until at least 95% of the root mass was removed from the sample. Roots were washed clean of all soil particles, wrapped in absorbent paper and oven dried at 70^oC for 48 hours. Roots were weighed and the mass of all fragments greater than 2 mm diameter (coarse roots) recorded separately from the mass of smaller fractions (fine roots).

Laboratory measurements

Several standard soil analyses were performed in the laboratory. Bulk density measurements were made based on oven-dried weights of the bulked soil samples and the known volume of the soil cores. Sub samples of soil were tested for total carbon and nitrogen. The sub-samples were homogenized by pulverizing in a shatterbox (Spex Inc., Edison NJ) and analyzed by dry combustion on a Flash EA1112 elemental analyzer (ThermQuest, Rodano Italy). Sand, silt, and clay fractions of the sampled soils were determined gravimetrically by the pipette method [Gee and Or, 2002]. Replicate samples allowed quantification of the error at approximately 2%.

Biomass and litter measurements

The litter removed from each site prior to the infiltration measurements was bagged and dried at 70°C for 48 hours before being weighed. Aboveground biomass estimates in the forests were conducted by measuring the diameter at breast height (dbh) of all trees with $dbh > 1$ cm located within a 3 m radius of the infiltration site. Allometric equations (Naidu et al. [1998] for pines and Clark et al. [1986] for hardwoods) were

used to estimate the mass of these trees, allowing an estimate of the standing biomass within a 3 m radius of the infiltration site and thus an estimate of local above-ground biomass density. Within the grass sites, live and dead grasses were trimmed together and a single estimate of biomass made.

Data analysis

Within each vegetation type multiple step-wise regression was used to obtain the best fit between covariates and infiltration rates measured. Infiltration rates were log transformed prior to this analysis. When considering goodness of fit, we report the unbiased coefficient of determination (i.e. 'adjusted r^2' value), which allows meaningful comparisons between models with 1 or 2 predictive variables (unlike a raw r^2, this parameter may adopt negative values). The adjusted r^2 is computed using the residual degrees of freedom ($v = n - m$), where n is the number of data points and m is the number of total fitted coefficients. The adjusted r^2 is then computed as $1 - r^2 \times (n-1)/(v)$ where r^2 is the standard coefficient of determination. The adjusted r^2 only increases if additional parameters increase the predictive capacity of a model relative to a single parameter model, and as such compensates against spurious over-parameterization [Wooldridge, 2009].

Between sites, a non-parametric analysis of variance (one way Kruskal-Wallis test [Gibbons, 1985, Hollander and Wolfe, 1999]) was used to determine whether significant differences in infiltration and other explanatory covariates were in place.

6.2.2 Meta-analysis

The meta-analysis consisted of data gathering, standardization and analysis.

Data gathering

A literature survey was conducted to assemble a database of co-located measurements of infiltration capacity and biomass. Studies were chosen to meet the following

criteria:

- Reported direct measurements of biomass, or sufficient information to allow biomass estimates to be made (e.g. through allometry of the dominant species).
- Reported sufficient information to derive a robust estimate of infiltration capacity or saturated hydraulic conductivity. Studies that reported cumulative infiltration, sorptivity or a runoff coefficient, rather than steady state runoff or infiltration rates, were excluded.
- Studies where the effect of vegetation could not be separated from disturbance were excluded. The majority of infiltration studies in mesic climates have been undertaken in the context of agricultural and tillage research, and consequently were excluded from the meta-analysis. Due to the paucity of data in mesic sites, we included data from three tropical agroforesty sites.

After these criteria were applied, 21 studies were retained for analysis. Combined, these studies yielded 261 infiltration and biomass measurements. These data are summarized in Appendix E, which also details the specific references used to arrive at biomass estimates, and where applicable (see below) the sources used to obtain climatic and soil properties, if these were not explicitly reported in the original studies.

Data standardization

Unsurprisingly, there was considerable variety in data gathering methods, the nature of the data reported and the format of reporting across the 21 studies reviewed. Data were standardized with the aim of obtaining an estimate of infiltration capacity (or equivalently the saturated hydraulic conductivity of the undisturbed soil surface) in mm/hr; an estimate of above-ground biomass in g/m^2; average annual precipitation

and pan evaporation; and soil textural properties in terms of the sand, silt and clay fractions. Infiltration and biomass estimates were of primary importance, and some studies with incomplete soil or meteorological data were retained for analysis.

Biomass estimates

Standing biomass was the most problematic parameter to standardize, as it is not widely reported. Biomass estimates were available directly for 13 of the 21 studies [Branson et al., 1962, Johnston, 1962, Rhoades et al., 1964, Kelly and Walker, 1976, Blackburn et al., 1992, Hulugalle and Ndi, 1993, Nicolau et al., 1996, Spaeth et al., 1996, Hester et al., 1997, Mwendera and Saleem, 1997, Chirwa et al., 2003, Boone Kauffman et al., 2004, Bowen et al., 2005]. Aboveground biomass was computed allometrically for the Duke Forest sites as reported above. For the remaining studies, biomass was estimated by:

- regression between a subset of site biomass estimates reported in the study and the reported percentage vegetation cover (for example in shrubland in Burkina Faso [Rietkerk et al., 2000] and woodland in Australia [Loch, 2000]),
- estimates of biomass density in similar vegetation types at the same or similar locations (for example the estimates of forest biomass in Ecuador, the Southern Appalachians and Puerto Rico [Harden and Scruggs, 2003])
- application of allometric equations to site specific parameters such as tree density, age and height (for example in a teak plantation in Sri Lanka [Mapa, 1995], and the Khalenberg forest in Germany [Buczko et al., 2006])
- application of allometric equations to dominant species, combined with site-specific measures such as percentage canopy cover, vegetation volume or height. For example in the North American deserts allometry for *Larrea tridentata*,

Prosopsis glandulosa and *Bouteloua eriopoda* was used to estimate biomass based on percentage cover and other measures of the geometry of the vegetation distribution [Castellano and Valone, 2007, Bedford and Small, 2008], and in the degraded sites in the Andes, biomass density estimates for *Cynodon dactylon, Holcus latanus, Vulpia myuros, Trifolium* sp. and *Pennisetum clandestinum* were made based on available literature, averaged to obtain an estimate of biomass density for fully vegetated sites, and then the percentage vegetation cover at individual sites was used to estimate biomass as a proportion of the estimated biomass density [Molina et al., 2007].

Infiltration capacity estimates

There are many different methods to measure infiltration capacity, which agree with each other to differing extents. Unfortunately, there is no consensus position in the literature for normalizing these different measurement techniques. This is not surprising considering that tension infiltrometers, for example, have been found to underestimate infiltration by comparison to ring or rainfall simulators [Reynolds et al., 2000], to overestimate infiltration compared to ring infiltrometers while being comparable to rainfall simulators [Gomez et al., 2001], to provide a better estimate of infiltration capacity than (underestimating) ring or rainfall simulators [Pott and De Maria, 2003], or to provide comparable estimates [Bagarello et al., 2000]. Site-specific details are often the determinants of which method is most applicable [Smettem and Smith, 2002]. Given this uncertainty, no correction to measured infiltration rates has been applied on the basis of methodology. Where multiple estimates of the infiltration rate were made at a site, we report those estimates made by ring infiltrometers or rainfall simulators. This choice simply reflects that the preponderance of available data was gathered using these methods and is an attempt to limit variability in the data set arising from infiltrometer type.

Soil texture estimates

When no specific soil textural data were available, the average sand, silt and clay fractions were estimated based on reported site soil type or soil series. For four sites, soil data were not available.

Climatic data

Annual rainfall estimates were reported for almost all of the study sites. Pan evaporation, and where necessary, annual rainfall, were taken from the nearest weather station providing pan evaporation rates. In some cases, particularly for African, Asian and South American sites, estimates of pan evaporation were made on the basis of other studies at nearby sites. For two studies, pan evaporation data was not available. In one study, excellent biomass and infiltration data were available, but site locations were reported only to the level of the state (within the USA) in which the sites were located. For this study, meteorological data are omitted. These sites, located in US rangelands, were grouped with the dry sites.

Data analysis

Prior to analysis, the data were divided into mesic-hydric sites and arid sites, based on the ratio of annual evaporative demand (estimated as pan evaporation) to annual precipitation: E_p/P. The formulation E_p/P is comparable to the dryness index used in the Budyko Curve [Budyko, 1974], and other climatic classification schemes. Because of the somewhat arbitrary nature of the classification, we did not correct the pan evaporation estimates to estimates of potential evapotranspiration (PET). Sites where $E_p/P > 1$ were treated as arid, and were analysed separately from mesic-hydric sites where $E_p/P < 1$.

We used linear regression to assess the following relationships within and between sites: log biomass and log infiltration, log biomass and soil texture, and log

infiltration and soil texture. For several sites, only a single estimate of biomass or of soil texture fraction was available for multiple infiltration rates. To account for this, we took the geometric mean of the measured infiltration capacities to obtain a single representative data point for a given biomass or soil texture estimate, prior to log-transformation.

The choice of a power-law regression in this case is a reasonable approximation for characterising infiltration as a porous media flow problem. Vegetation-biomass relationships arise from flow through a fractal network of pore spaces, modified by the likewise-fractal root network. Given the suitability of power laws for describing flow through fractal media [Neuman, 1995], they represent a reasonable model to fit. Note, however, that the use of power laws is not intended to indicate a known mechanistic model for the observed biomass-infiltration relationships.

We re-evaluated the biomass-infiltration relationship after controlling for the effect of soil type. Two different controls were adopted: a statistical control in which the effect of soil type was accounted for via linear regression; and a mechanistic control in which the effect of soil type was accounted for by normalization against empirical hydraulic conductivity properties documented by Clapp and Hornberger [Clapp and Hornberger, 1978].

Within-site variability was assessed using all data points to determine statistical agreement between log biomass and log infiltration capacity within a given site. Finally, the strength of the within-site biomass infiltration relationship, as quantified by the slope of the log-log regression, was assessed for those sites where:

- There were at least three data points available (to avoid spurious regressions between two points),
- Regression relationships were significant at an 80% confidence level (this relatively low threshold for assessing significance was chosen to reflect the large

degree of variability associated with most of the data analyzed), and

- There was an estimate of E_p/P (i.e. reliable climatic data).

Variation in the slope of the biomass-infiltration regression was examined as a function of E_p/P as a surrogate for climate type.

6.3 Results

The results section will again present results separately for the field and meta-analytical components of this work. The links between the results and the three driving questions that motivated this study are addressed in the Discussion.

6.3.1 Field Study

The data gathered from the Duke Forest field study and subsequent laboratory analyses are presented in Appendix D.

Infiltration rates between sites

Mean infiltration capacity (f) was $\approx$ 20% greater in the hardwood forest, where the mean infiltration rate was 14.4 (15.15) mm/hr, standard deviation is shown in brackets; than in the grass field (11.77(11.6) mm/hr). The pine plantation had substantially lower infiltration rates of 5.3(4.9) mm/hr. These differences were not significant at the 95% confidence level as assessed by non-parametric Kruskal-Wallis analysis of variance (see Figure 6.1).

The low infiltration rates observed in the pine plantation were attributed to hydrophobicity in the soil there. Drop penetration tests conducted on samples of surface soils from the pine plantation found that 7 of 10 sampled soils had a drop penetration time exceeding 1 s and three of the samples had drop penetration times exceeding 1 minute. In one sample, drop penetration time repeatedly exceeded 5 minutes.

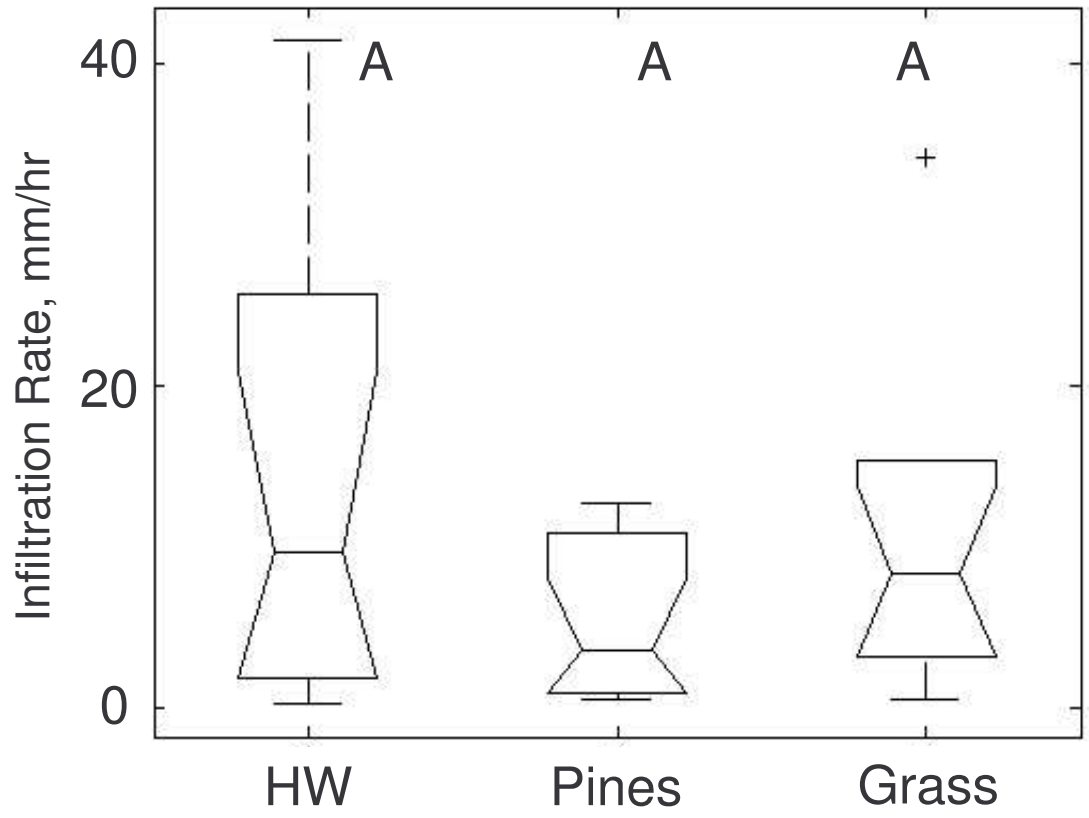

FIGURE 6.1: Box plot of infiltration values in the three vegetation types. Letters (A) indicate no significant difference (at 95% confidence level) between sites as evaluated with a non-parametric Kruskal-Wallis test. Note that HW indicates the hardwood site.

Field drop penetration tests indicated that the degree of hydrophobicity varied at the centimeter scale. Hydrophobicity is known to confound interpretation of tension infiltrometer readings [Clothier, 2001], so the pine infiltration data were excluded from the meta-analysis. No hydrophobicity was identified in the hardwood or grass sites. Hydrophobicity of soils is widely reported for evergreen species including pines. Water repellency in the soil is associated with the presence of hydrophobic organic compounds such as cuticular waxes in pine needles [Doerr et al., 2000]. The accumulation of these compounds in the soil is associated with relatively low rates of decomposition, leading to deep litter layers as observed in the Duke Forest pines, and

with low intensity fires, leading to the accumulation of hydrophobicity in the organic and mineral surface soils respectively. Although an ecological role for hydrophobicity as analogous to allelopathy has been proposed [Ens et al., 2009], it remains unclear whether hydrophobicity should be considered primarily as a byproduct of plant-soil-environment interactions, or whether it confers competitive advantage and may as such be considered to be a plant strategy. These complex interactions are beyond the scope of this study and will not be further addressed.

Infiltration capacity within sites

Infiltration trends in the hardwood site were explained by significant (p= 0.04) negative correlations to the soil clay content and the coarse root mass (CRM), which determined 60% of the variance in log transformed infiltration rates. The relevant regression equation was:

$$Log(f) = -47.4761(\%\text{clay}) - 1.4608(\text{CRM}) + 8.0333 \tag{6.4}$$

No significant relationships to the measured covariates were identified in the pine plantation, presumably due to the hydrophobicity. An infiltration-soil relationship was identified for the grass site, although it was weaker than the relationship for the hardwood site and not significant ($r^2 = 0.21$, p= 0.1787):

$$Log(f) = -43.3948(\%\text{clay}) + 7.7738. \tag{6.5}$$

Factors varying between sites

With the exception of the total root mass and the soil nitrogen content, significant differences were found between all covariates at all sites (Table 6.2). The pine site differed from the grass and hardwood sites in having higher carbon and sand content, more litter mass, and lower bulk densities. Lower macropore fluxes arose on the pine

Table 6.2: Average value of covariates between sites. Superscript letters indicate that there is no significant difference between measures.

Factor	**Hardwood Mean**	**Pines Mean**	**Grass Mean**
Biomass	56.8025 ^{a}	17.0808^{a}	0.2425
Litter	0.2330 ^{a}	0.4636	0.2416^{a}
Bulk Density	0.7997 ^{a}	0.6217	0.7548^{a}
Surface Nitrogen	0.21 %^{a}	0.19%^{a}	0.18%^{a}
Surface Carbon	3.24 %	4.88%	2.49%
Macropore Flux (%K_{sat})	10%^{a}	15%^{a,b}	15%^{b}
Fine Roots	0.8694 ^{a}	0.8137 ^{a}	1.8134
Coarse Roots	0.6188 ^{a}	0.4364 ^{a}	0.0185
Total Roots	1.4882 ^{a}	1.2501 ^{a}	1.8319^{a}
% Sand	0.4500 ^{a}	0.5356	0.4840^{a}
% Silt	0.4318	0.3356 ^{a}	0.3800^{a}
% Clay	0.1182 ^{a}	0.1300 ^{a,b}	0.1360^{b}

site than in the other vegetation types. The total macro-pore flux was similar between the grass and hardwood sites, but macro-pore flow represented a greater proportion of the total flux on the grass site than in the hardwoods. As expected, the grass and hardwood sites differed significantly in terms of biomass and root properties, with significantly more root biomass occurring in the form of coarse roots in the hardwood site than the grass site. The soil properties varied significantly between all sites, but all soils could be classified as loams.

6.3.2 Meta-analysis

Soil type-biomass relationship

The various soil fractions (% sand, silt and clay) were regressed against the log transformed biomass values. In the mesic-hydric sites (where $E_p/P < 1$), none of the soil fractions were related to biomass (for each fraction, adjusted $r^2 < 0$, $p > 0.05$). In the arid sites, there were no significant relationships between biomass and soil type ($p > 0.05$ for all fractions).

Soil type - infiltration relationship

Regression analysis was performed between the sand/silt/clay fractions and the log transformed infiltration values. In the hydric sites, a relationship was found between the clay fraction and the log of infiltration (adjusted $r^2 = 0.630$ and $p < 0.05$ respectively), but there were no significant relationships with the sand and silt fractions (adjusted $r^2 = 0.12, 0.02$, respectively, and $p > 0.05$). In the xeric sites, no significant relationship could be discerned between soil type and infiltration measurements ($p > 0.05$ for all soil fractions).

Biomass - infiltration relationship

Mesic-hydric sites: between site variation

Biomass was not related to infiltration capacity on hydric sites (adjusted $r^2 < 0$ for the log biomass - log infiltration regression). Nor did biomass explain the variance in infiltration capacity after controlling for soil type via a multiple regression. This result was verified using the empirical values of K_{sat} published by Clapp and Hornberger (hereafter C&H) to 'normalize' the measured values of Ksat based on soil type. Log biomass did not explain the variance in the transformed variable $log\left[K_{sat}\,(\text{measured})\,/K_{sat}\,(\text{C\&H})\right]$.

Mesic-hydric sites: within site variation

With the exception of a single agro-forestry study in Sri Lanka ('Map', see Figure 6.2), the within-site biomass-infiltration dependence was also weak. Controlling for the effects of soil improved the relationship between biomass and infiltration in some sites (Duke Forest sites and Kahlenberg Forest, Germany), but worsened it in others (Andes highland sites and the Sri Lankan agroforestry site). No clear trends in infiltration capacity with respect to variation in biomass could be ascertained within or between the mesic-hydric sites (see Figure 6.2 and Table 6.3).

Xeric sites: between site variation

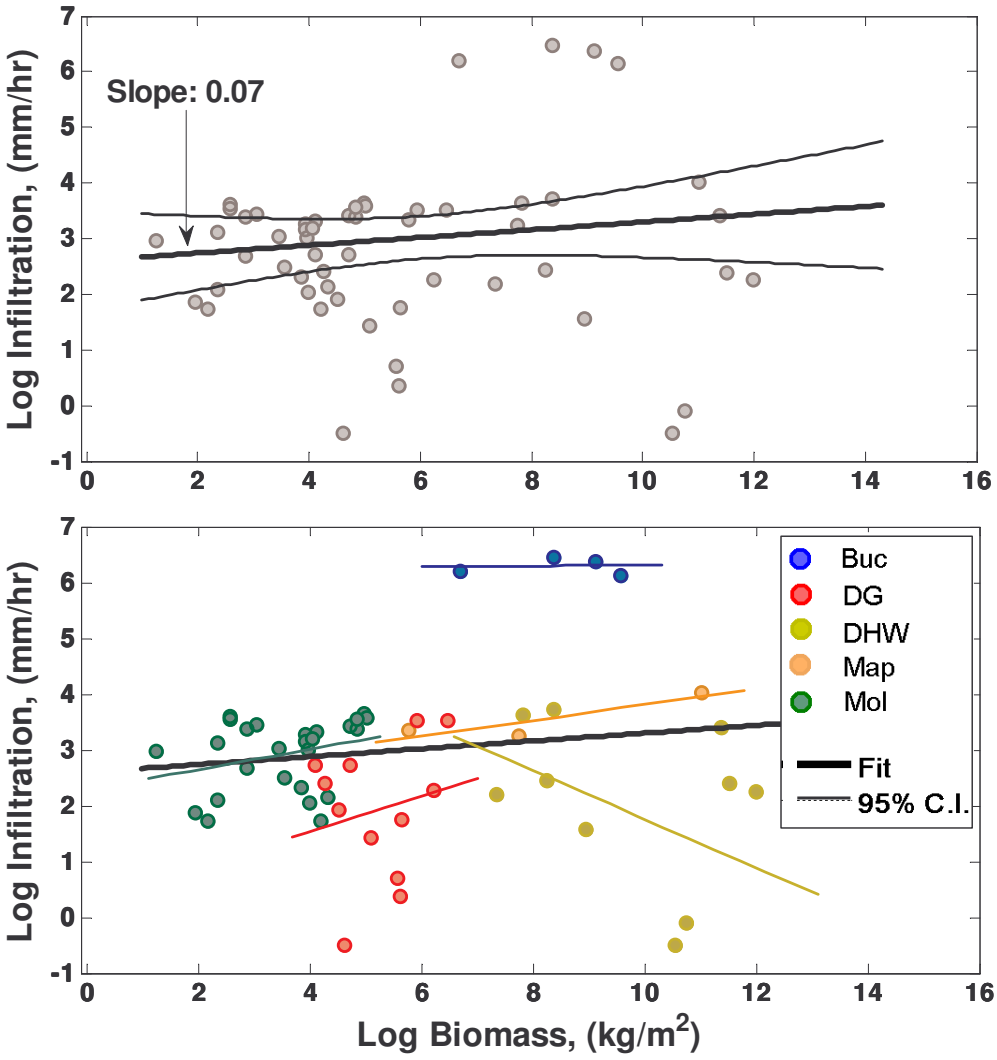

FIGURE 6.2: Biomass-Infiltration relationships between (upper panel) and within (lower panel) mesic-hydric sites (the slopes shown are those from a multiple regression between % sand, biomass and infiltration). Site names, slope values, correlation coefficients and p values are shown in Table 6.3

Table 6.3: Regression parameters for all sites with > 1 data point. Regression is for log (infiltration) against log biomass, excluding soil type in the xeric sites, and controlling for soil type in the mesic sites.

Site	**Label**	**Slope**	**r^2**	**p value**
Within Xeric Sites				
BS	Bedford and Small	-0.4753	0.0072	0.8730
Bla	Blackburn	0.2988	1 (only 2 sites)	NA
Bow	Bowen	1.3782	0.8180	0.0956
BK	Boone Kauffman	-3.5011	1 (only 2 sites)	NA
Bra	Branson	1.0094	1 (only 2 sites)	NA
Cas	Castellano	-0.0780	0.0125	0.8328
Chi	Chirwa	0.0054	0	0.9780
Hes	Hester	0.1156	0.8836	0.0600
KW	Kelly and Walker	-0.2551	0.0318	0.6463
Loc	Loch	0.5440	0.8697	0.0001
Mwe	Mwendera	-5.8608	1 (only 2 sites)	NA
Nic	Nicolau	0.5045	0.3467	0.0164
Rk	Rietkerk	0.1773	0.2017	0.0213
Spa	Spaeth	0.0712	0.0098	0.6526
Between Xeric Sites		0.4293	0.3552	0.00
Within Mesic-Hydric Sites				
Buc	Buczko	0.0099	0.0067	0.9179
DG	Duke Grass	0.2271	0.0249	0.6633
DHW	Duke Hardwood	-0.2530	0.0905	0.3982
Map	Mapa	0.1417	0.77	0.3176
Mol	Molina	0.1826	0.09	0.1418
Between Mesic-Hydric Sites		0.1315	0.65	0.0282

Biomass was significantly related to infiltration capacity without controlling for soil on arid sites with $r^2 = 0.35$ and p≈ 0.00 (see Figure 6.3 and Table 6.3). Including soil type caused a large increase in r^2, which appeared to be largely due to the averaging procedure, whereby single, averaged biomass and infiltration values were used for each soil type measurement. Other averaging procedures (including all biomass-infiltration measurements, or averaging on a site, rather than soil-type basis) while controlling for soil type resulted in r^2 values of ≈ 0.3. Controlling for soil type via the C&H values resulted in an r^2 of ≈ 0.3 for the transformed variable

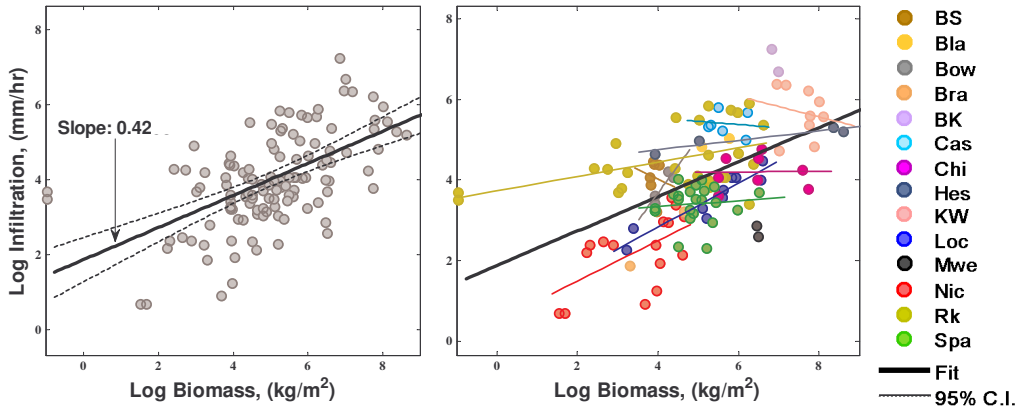

FIGURE 6.3: Biomass-Infiltration relationships between (left panel) and within (right panel) xeric sites (the slopes shown are those from a regression between biomass and infiltration). Site names, slope values and correlation coefficients given in Table 6.3

$log\left[K_{sat}\left(\text{measured}\right)/K_{sat}\left(\text{C\&H}\right)\right]$.

Xeric sites: within site variation

Within individual arid sites, the relationship between biomass and infiltration varied from strong (e.g. in the Australian woodland site measured by Loch, $r^2 = 0.86$, $p < 0.01$, ponderosa pine stands measured by Hester, $r^2 = 0.88$, $p < 0.1$, and Arizona desert plots measured by Bowen $r^2 = 0.81$, $p < 0.1$); to moderate (e.g. in Burkina Faso shrublands measured by Rietkerk, $r^2 = 0.2$, $p < 0.05$ in Spanish badlands measured by Nicolau $r^2 = 0.34$, $p < 0.05$), or very weak (see Figure 6.3 and Table 6.3). Several studies reporting only 1 or 2 data points were included in the overall between-site regressions but are not of value for understanding relationships within sites.

Trends with climate

There were six sites within which the regression relationship:

$$\log\left(f\right) = a\log\left(B\right) + b, \tag{6.6}$$

was significant at an 80% confidence level. Amongst these sites, there was an in-

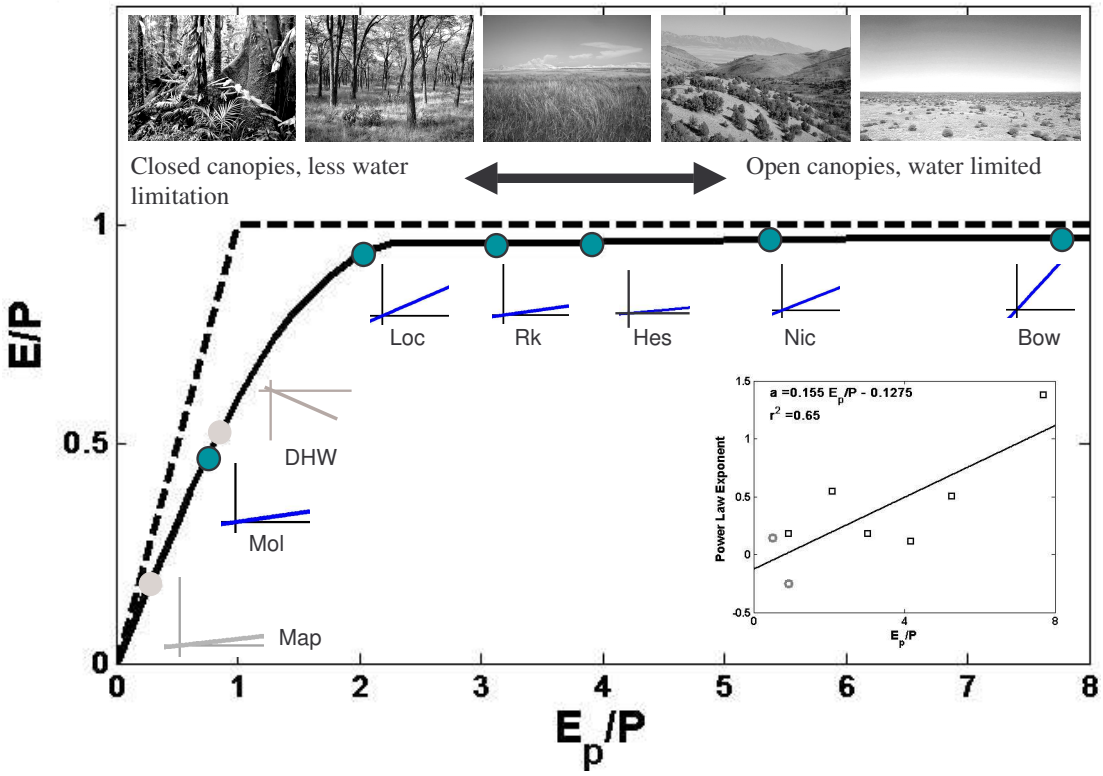

FIGURE 6.4: Hypothesized relationships between the power law exponent characterizing the biomass-infiltration relationship, and the dryness index. The relationship is suggestive of ordering on the Budyko Curve. The linear fit between the dryness index and the power law exponent for all sites is shown as an inset (within site biomass-infiltration relationship adjusted $r^2 > 0.05$, sites where $p > 0.2$ are shown in grey). Site name abbreviations are defined in Table 6.3. Images sourced from [Schoch, 2005, Kell, 2005, Hillewaert, 2005, Temsabuita, 2007, Bureau of Land Management, 2008]

creasing trend in the slope a (i.e. the exponent of the power-law with E_p/P). When a linear regression was taken between E_p/P and a, climate explained some 58% of the variance in the values, with the slope of the E_p/P - a relationship being 0.15. Because the significance criterion resulted in relatively few sites being included in this analysis, we broadened the analysis to include all sites where the regression explained more than 5% of the variance in the data set. This lead to eight sites being included, an r^2 value of 0.65, and again a slope of 0.15 (see Figure 6.4).

6.4 Discussion

Three goals motivated this study: to examine whether the known trends in vegetation biomass and infiltration extended outside of arid climates; to determine a mathematical relationship between infiltration and biomass, and to evaluate the climatic sensitivity of that relationship and the processes contributing to it.

6.4.1 Biomass-infiltration trends in mesic-hydric climates

Biomass-infiltration trends did not appear to occur within sites in mesic-hydric climates, in contrast to the existence of strong and significant within-site trends in arid climates (ref. Table 6.3). Nor did biomass values correlate to infiltration rates between sites. Instead, soil type was the dominant factor in determining infiltration rates in mesic-hydric sites. Thus, we conclude that the infiltration-biomass relationship does not generally persist in wetter climates. The processes contributing to the biomass-infiltration feedback are presumed to either saturate under humid conditions or the driver for plants to develop features that enhance infiltration rates is too weak to allow for the feedback to be observed. In well-watered sites it is likely that light and nutrient limitation are co-limiting with water and are thus additional drivers of allocation. Consequently, large shifts in the allocation ratio above and below-ground may be observed depending on relative nutrient status [Oren et al., 2001]. The use of the above-ground biomass as an independent variable in humid sites may be problematic if these allocation ratios are highly variable. Further measurements to relate infiltration capacity to root distributions and density in mesic-wet climates would provide insight not only into the relative effects of changing root biomass and distribution on infiltration properties, but also on how these links feed back to water or nutrient limitation and plant allocation strategy.

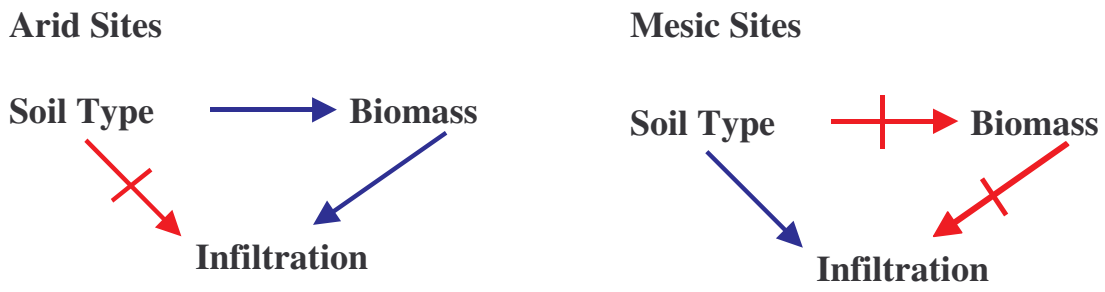

FIGURE 6.5: Hypothesized causal relationships between soil, biomass and infiltration in arid and mesic sites. The former is consistent with the effect of surface processes decoupling infiltration rates (to a large extent) from the underlying soil type. The latter is consistent soil type being the primary determinant of infiltration capacity.

6.4.2 Nature and strength of biomass-infiltration trends

The observed statistical relationships amongst soil, biomass and infiltration in this study support the interpretation that biomass constitutes a primary influence on infiltration capacity in water limited ecosystems. TThe data contradict a plausible hypothesis that improved soil texture increases infiltration capacity which leads to higher above-ground biomass.Instead, in mesic-hydric climates, biomass was decoupled from the trend in infiltration behavior, and in xeric sites infiltration and soil type were uncorrelated (ref Fig. 6.5).

Note that the potential links between below-ground biomass and infiltration capacity, however, cannot be assessed with the available data, and remain as an area where additional future work is required. In water limited climates power-law relationships were relatively successful in describing the biomass-infiltration relationship (ref Figs. 6.2 and 6.3). Power-law biomass-infiltration relationships between sites described approximately 35% of the variance in the infiltration values across an aridity gradient. Infiltration capacity is not under the direct physiological control of plants, and therefore the coupling between vegetation and infiltration is unlikely to be 'first order' in nature. Thus, finding that biomass explained such a large proportion of

variance in infiltration rate over such a broad range of sites is somewhat surprising. Throughout the study the use of aboveground biomass has been motivated in part by an expected order-of-magnitude relationship between aboveground biomass and root extent. While this may be suitable for discerning between-site variability, there is considerable scope for variation in the shoot:root ratio within individual species or sites [Pallida et al., 2009, Martre et al., 2002, Gerard et al., 1982]. Consequently, belowground biomass might be expected to exert important controls on infiltration behaviour, and further data are needed to constrain such relationships.

6.4.3 Climatic sensitivity of biomass-infiltration relationship

Two broad trends were observed with changes in climate as measured by the dryness index. The first was that the slope of the log biomass - log infiltration regression declined as climates became wetter. A linear trend emerged in the power exponent of individual sites where biomass-infiltration relationships existed (ref. Figure 6.4). The second trend was the influence of soil type on infiltration. Soil type increased in importance from being weakly related to infiltration in arid sites, to explaining some 60% of the variance in infiltration in wet sites. Furthermore, in examining the factors influencing infiltration in one particular location, where the climate and soil type were the same (e.g. the Duke Forest sites), it was evident that soil texture and coarse root mass, but not aboveground biomass, were correlated with infiltration capacity.

6.5 Conclusions and future work

The influence of vegetation on soil properties and soil formation (i.e. pedogenesis) has been studied since the late 1800's when V.D. Dokuchaev introduced the concept of dynamic soils that evolve under the influence of climate and vegetation. Exploring biomass-infiltration trends extends this conceptual framework to emergent

properties of the soil-climate-vegetation system. Future work is needed to discriminate the generality of processes that result in the large-scale biomass-infiltration relationships identified in this study. In particular, it remains to be determined whether the trend observed in arid sites is a passive response to increased soil cover, or whether it is strongly influenced by adaptive features and dynamics of vegetation. The strongest 'within site' biomass-infiltration trends occurred on sites with patchy vegetation cover, suggestive of a binary presence/absence relationship between infiltration and vegetation cover. Certainly physical and biological processes including the prevention of physical crusts or seals and the 'resource island' effect which concentrates ecological processes near vegetation [Schlesinger et al., 1996] are consistent with such a binary relationship. However, spatially explicit studies of infiltration in the proximity of Australian mulga (*Acacia aneura*) found that infiltration capacity increased with proximity to the mulga trunk, and declined smoothly with distance from the trunk over distances of up to 10m. The absence of a discontinuity in infiltration capacity at the canopy edge (2-3m from the trunk) suggests that the modification of infiltration capacity is associated with root properties and not simply surface cover [Dunkerley, 2002b]. Consequently, further research to elucidate the links between belowground biomass characteristics and infiltration response is needed. Similarly, a study by Spaeth (1996) concluded that plant species effects significantly improved prediction of infiltration capacity compared to purely physically based predictions. These observations are suggestive of a complex suite of processes affecting infiltration into the rooting zone. Manipulative experiments that can discriminate between presence/absence effects induced by natural or artificial soil protection, as well as further studies of infiltration processes at a species specific level are needed to resolve this question.

7

The role of microtopography in rainfall-runoff partitioning: an analysis using idealized geometry

7.1 Introduction

The small-scale profile of surfaces, or their microtopography, is of interest across many diverse disciplines including micro-fluidics, metallurgy, biophysics, and materials science. It is particularly important in determining the interactions of a surface with other substances and its immediate environment [Costa, 2004, Hale and Mitchell, 2002, Jager et al., 2007, Lloyd, 2003, Semler et al., 2006, Vananckevort, 1984]. Microtopography is also important in the geosciences, where it refers to topographic variation about a mean surface trend with amplitudes much smaller than hillslope or basin scales.

In arid and semi-arid environments, the partitioning of rainfall between infiltration and runoff at the soil surface is particularly important, since water lost to Hortonian runoff processes cannot contribute to sustaining vegetation at a site (although it may contribute to the growth of vegetation at sites downslope) [Descroix et al., 2007, Lehmann et al., 2007, Noy-Meir, 1979, Kirkby and Chorley, 1967]. Mi-

crotopography is anticipated to play an important role in ecohydrological processes of arid and semi-arid systems.

Hydrologically, microtopography may be characterized by two distinguishing features: (1) the vertical variations are on the same order of magnitude as the flow depth during runoff events (i.e. mm to cm), and (2) the horizontal variation of the microtopographic features are 2-3 orders of magnitude smaller than the hillslope length (i.e. 10 to 100 cm). The geometric attributes of these features can be variable as shown in Figure 7.1, and may be produced by biogenic or physical processes (e.g. Figure 7.1, case b). The statistical and scaling properties of microtopography on natural hillslopes have rarely been quantified. Data from tillage research suggests that much of the natural variation of the soil surface is fractal [Pardini and Gallart, 1998, Perfect and Kay, 1995, Vazquez et al., 2005, Burrough, 1983], while larger scales of topographic variation (i.e. 2-5 m scales associated with dunes and vegetation mounding) also display power law scaling [Pachepsky and Ritchie, 1998, Pachepsky et al., 1997].

Despite its ubiquity, microtopography is rarely incorporated into hydrological analyses except in the parameterization of roughness coefficients. The effects of microtopography have been investigated in tillage research and largely considered the consequences of tillage on slowing runoff and erosion [Allmaras et al., 1966, DeLima et al., 1989, Gayle and Skaggs, 1978, Hansen et al., 1999, Linden and Vandoren, 1986, Mitchell and Jones, 1976, Mohamoud et al., 1990, Onstad, 1984, Planchon et al., 2002, Van Oost et al., 2006, Zobeck and Onstad, 1987]. The results have been equivocal: many studies indicate a reduction in erosion and runoff in the presence of increased microtopographic variation [Johnson et al., 1979, Steichen, 1984], while other studies found that roughness increased erosion rates, presumably by concentrating the flow [Darboux and Huang, 2005, Helming et al., 1998]. Microtopography has been investigated in the context of 'interactive infiltration' studies, which ex-

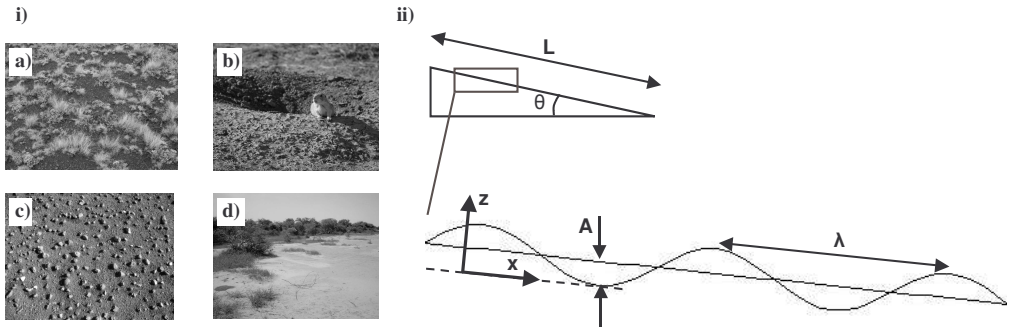

FIGURE 7.1: i) Examples of microtopographic variation - a) terracette formation on hillslopes in Idaho (formed by interaction of vegetation, erosion and flow), b) prairie dog mounds (formed by fauna), c) stony desert pavement (formed by aeolian erosion) and d) mounding associated with vegetation in semi-arid woodlands (formed by aeolian and rain-splash erosion). ii) Definition of geometric parameters describing the hillslope and microtopography. Images (a, b) are courtesy of Ciaran Harman, image c) [Deschodt, 2003] and image d) [Deschodt, 2003].

plicitly account for variability in infiltration and runoff behaviour when the two processes are coupled across a hillslope, resulting in: *"an areal hydrologic [runoff] response not typified by classical point-scale infiltration theory "* [Fiedler et al., 2002]. A few studies have shown significant perturbations in infiltration and runoff response when surface elevation variation is accounted for, compared to microtopographically smooth surfaces [Fiedler et al., 2002, Esteves et al., 2000].

The governing equations that may be used to describe hillslope hydrology are the shallow water equations for surface runoff flow and Richards' equation for infiltration and soil moisture redistribution. Accounting for microtopography requires that these equations be coupled across all spatially variable boundaries. This coupling problem was confronted via brute-force numerical simulations [Esteves et al., 2000, Fiedler and Ramirez, 2000, Tayfur et al., 1993], but such an approach has several drawbacks. First, the spatial scales that must be resolved span the finest micro-topographic detail to the entire hillslope length. Similar scale issues arise in

the temporal domain, with scales ranging from seconds-minutes for the activation of overland flow, to several months over which subsurface redistribution determines soil moisture conditions. This high dimensionality in space and time, coupled with the need for high-resolution characterization of the microtopography and soil properties as well as site specific calibration [Esteves et al., 2000, Fiedler and Ramirez, 2000, Tayfur et al., 1993], prohibits a general treatment of microtopography through direct simulations of the governing equations, and indeed the effects of microtopography on hydrological response have largely resisted a generalizable theoretical treatment. An exception is a study by Dunne et al. [1991], that considered the effects of tillage-like microtopography where flow occurred in channels between 'hills'. Dunne et al. showed how correlations between the height of these features and their infiltration capacity resulted in a nonlinear scaling of hillslope-scale infiltration capacity with the depth of flow. Here, 'first-order' effects of microtopography on runoff-infiltration partitioning for simplified cases are analyzed. Our goal is to provide a complementary approach to that adopted by Dunne et al. in complexity and ease of making generalizations. Given the focus on arid and semi-arid environments we target the storm event scale and treat storm events as essentially independent.

7.2 Conceptual view

Consider a sloping surface with microtopographic variability consisting of mounds and depressions of different sizes. If this surface is exposed to persistent rainfall, and rainfall intensity (I) exceeds the infiltration capacity ($f(t)$), then a number of different regimes can be defined (Figure 7.2) [Horton, 1945]. Prior to ponding, water infiltrates without surface redistribution. Following surface ponding, ponded water collects in depressions, delaying the onset of runoff from the immediate catchment of each depression (A). As the smallest depressions overtop, runoff establishes flow and hydrologic connectivity between upslope and downslope locations (B). Eventually,

this connectivity links runoff flow paths to the channel, allowing export of surface water from the hillslope. As the depth of flow on the surface increases, some of the microtopographic features are submerged, creating a complex 2-3 dimensional "mixed flow" regime around emergent microtopographic mounds (C). Further increases in water depth "drown" these features, leading to a sheet flow condition (D). Conceptualising these cases separately allows for different simplifications to be made to the governing equations. Replacing a "real" microtopographic surface with an idealized version permits further simplifications. For instance, on an idealized one-dimensional hillslope with uniform sinusoidal microtopography, cases B and C do not occur since depressions fill and over-top uniformly, immediately generating sheet flow (Case D). In such an ideal case, a "toy model" describing rainfall-runoff partitioning requires only three components: a model of the surface prior to ponding, the filling of the surface store as described in case A and sheet flow over the microtopography as described in case D. Although simple, this sinusoidal microtopography offers some key advantages. Firstly, any general theory for complex microtopography, must, in the limit, recover this idealized set up. Second, the orientation of microtopography here is at 90o to that utilized in the study by Dunne et al., allowing the two cases to be considered as 'end members' that constrain plausible flow behaviour on microtopographically varying landscapes. Finally, a large number of studies already consider the problem of how a wavy surface affects bulk flow properties [Poggi et al., 2007]. Hence this representation of microtopography allows us to draw from a rich literature in fluid mechanics when describing flow responses [Belcher and Hunt, 1998, 1993, Finnigan and Belcher, 2004, Patton and Katul, 2009, Poggi et al., 2008]. In short, a sinusoidal topography provides a parsimonious and tractable representation of the variable surface and its effects on infiltration and surface runoff.

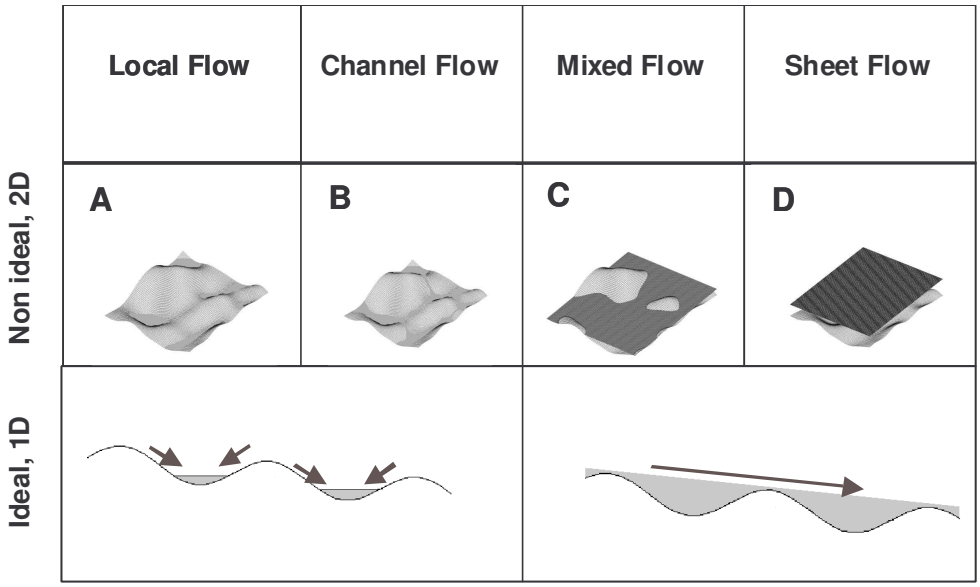

FIGURE 7.2: Separation of the storm event into multiple flow regimes depending on the degree of inundation of the microtopographic features. Our focus here is on the 'end-member' cases A and D.

7.3 Idealized model and assumptions

As outlined above, the idealized model consists of a 1-D hillslope on which microtopographic variation is represented as sinusoidal excursions with fixed amplitude A and fixed wavelength λ as shown in Figure 7.1(ii). Soil properties, specifically the hydraulic conductivity K_{sat} and sorptivity (χ_o, a measure of the soil's tendency to imbibe water due to matric effects) are initially assumed to be homogeneous across the entire hillslope length ($L >> \lambda$). We address the case where the soil is uniformly dry at the onset of a storm, and where rainfall can be treated as having a uniform

intensity (I) for the storm duration, and where overland flow mechanisms rather than water table responses dominate runoff production (i.e. arid rather than humid systems, c.f. Freeze [1972, 1974]). It is assumed that the microtopography is fixed and no erosion or accretion occurs. These assumptions are not generally met on real hillslopes. In the discussion, some of the implications of relaxing the assumption of homogeneity, specifically for the dynamically relevant cases where heterogeneities correlate with microtopographic features, are investigated. The range of plausible variability in soil hydraulic properties, roughness, macroporosity, vegetation growth and initial water content, however, means that addressing heterogeneity is an essentially unconstrained problem, lying beyond the scope of a single study, and its implications on upscaling the effects of microtopography are therefore discussed in general terms only.

Two research questions were selected to guide the investigation of this simplified surface:

- Does microtopography change the partitioning of rainfall into runoff and infiltration compared to a 'background' state without microtopography (i.e. having $A = 0$)? and,

- How do soil, slope, storm and microtopographic dimensions influence the degree of this change?

As outlined above, this one-dimensional surface focuses the analysis on the two "end-member" cases A and D. Extensions of this approach by allowing for two-dimensionality and for hydro-eco-geomorphological feedbacks are outlined in the Discussion. Subscripts of "$m.t.$" for microtopography, and "$b.g.$" for the background reference case will be used to distinguish between background ($A = 0$) and microtopographically variable surfaces ($A > 0$) in the following description of the model.

7.3.1 Infiltration prior to ponding

In dry soils, the water potential gradient imposed by the soil matrix dominates infiltration and gravitational effects may be neglected. As soils approaching saturation, matric potential effects are insignificant and infiltration is primarily driven by the gravitational potential or a unit gradient, resulting in essentially vertical flow [Philip, 1957]. Thus, the early stages of infiltration should respond to increases in infiltrating surface area (SA) regardless of its orientation, while the latter, vertical stages of infiltration would be dictated by the horizontal projection of SA. Thus, microtopography would increase the rate at which water is sorbed by the soil surface relative to a background state covering the same horizontal area. This behaviour can be captured in the magnitude of the soil sorptivity [Brutsaert, 2005]. Where microtopographic variation is significant, the sorptivity measured at a point χ_o should underestimate the sorptivity at the hillslope scale ($= \chi_{o\,m.t.}$), unless a scaling factor is included to adjust for the increased surface area. We refer to this scaled value as the "effective sorptivity". Using Philip's solution for infiltration from hemispherical depressions [Philip, 1955, 1969, 1991] and a numerical model of infiltration based on Richard's equation over a sinusoidal depression, we verified that the effective sorptivity scaled in an almost one to one fashion with the infiltrating surface area (SA) (Figure 7.3). Based on these results, it follows that

$$\chi_{o\,m.t.} = \frac{SA_{m.t.}}{SA_{b.g.}}\chi_o. \tag{7.1}$$

The major implication of the increased effective sorptivity is that the time to ponding (t_p), which is related to the square of the sorptivity, tends to increase. A Smith and Parlange estimate of the time to ponding was adopted [Parlange and Smith, 1976],

$$t_p = \frac{\chi_o^2}{2IK_{sat}log\left(I/\left(I-K_{sat}\right)\right)}, \tag{7.2}$$

where I is, as before, the rainfall intensity assumed to be uniform throughout the storm and across the hill slope, χ_o is the sorptivity and should be replaced by $\chi_{o\,m.t.}$ in the presence of microtopography ($A > 0$), and K_{sat} is the saturated hydraulic conductivity. Note that where the A is small enough to approximate the scale of a soil pore, the continuum assumption behind this description of infiltration breaks down. Consequently, the surface area scaling should be treated as a macroscopic property and applied only for sufficiently large values of A.

7.3.2 Surface storage (Case A)

Following ponding, runoff is locally initiated [Horton, 1945]. In the presence of microtopography, the initiation of non-local runoff until micro-topographic depressions are filled. The volume of water that can be "sequestered" by these depressions is known as the surface store [Allmaras et al., 1966, DeLima et al., 1989, Gayle and Skaggs, 1978, Hansen et al., 1999, Linden and Vandoren, 1986, Mitchell and Jones, 1976, Mohamoud et al., 1990, Onstad, 1984, Planchon et al., 2002, Van Oost et al., 2006, Zobeck and Onstad, 1987]. Some $40-70\%$ of the time lag between rainfall and runoff initiation in experiments has been related to the peak size of the surface store [Darboux and Huang, 2005]. Strong positive linear correlations between amplitude and storage [Darboux et al., 2001, Kamphorst et al., 2000, Onstad, 1984, Zobeck and Onstad, 1987], and strong negative linear correlations between slope angle and storage [Huang and Bradford, 1990, Kirkby, 2001] have been found, presumably as a direct geometric result. A toy model that accounts for the effects of the surface store can be constructed by computing a peak storage volume, given the microtopographic geometry, and delaying the initiation of runoff until a time t_r when this storage is

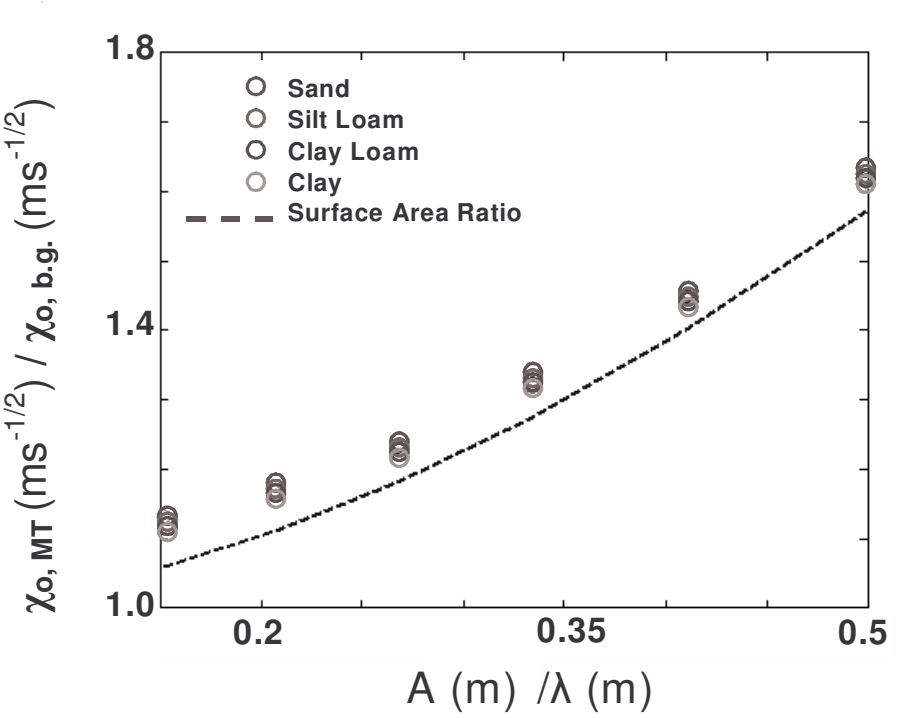

FIGURE 7.3: Effects of microtopography on infiltration dynamics based on a numerical solution to Richards Equation over a sinusoidal depression and for varying soil types. The effective sorptivity scales approximately 1:1 with the surface area ratio.

filled:

$$t_r = t_{p_{m.t.}} + \frac{V_s}{\int_{t_{p\,m.t.}}^{t_r} (I - f)\, dt} \tag{7.3}$$

where V_s is the storage volume, and f is the infiltration rate which, following ponding, is given by

$$f = K_{sat} + \frac{1}{2}\chi_o^2 \left(t - (t_p - t_{ca})\right), \tag{7.4}$$

where t_{ca} is the compression time introduced to account for the shift in boundary

condition from unsaturated to ponded infiltration [Sivapalan and Milly, 1989]. The choice of χ_o and t_p in equation 7.3 should reflect the surface condition (i.e. *b.g.* or *m.t.*).

7.3.3 Sheet flow (Case D)

The flow over a microtopographic surface is complex and its complete description requires solution of (at least) the shallow water equations. IA simple scale analysis of the shallow water mean momentum equation can provide insight into its behaviour. If time scales as the microtopographic length scale over the bulk velocity ($2A/V$), and as the microtopographic length-scale ($2A$), then:

$$\frac{\partial}{\partial t}\left(Vh\right) + \frac{\partial}{\partial x}\left(V^2 h\right) + hg\frac{\partial h}{\partial x} = gh\left(S_o - S_f\right), \tag{7.5}$$

and

$$\approx \left(\frac{V^2}{gh}\right)\left(\frac{h}{2A}\right) = S_o - S_f, \tag{7.6}$$

Here S_o and S_f are the bed and energy grade-line (or friction) slopes, V is the depth-averaged velocity, h is the water depth, g the gravitational acceleration, and x is the direction along the hill slope. This analysis suggests that the Froude Number $Fr = V^2/gh$ and the inundation ratio $h/2A$ are the two control parameters for the shallow-water system, and are directly related to the local slope and roughness imposed by microtopography. The emergence of the Froude number as a control variable is expected for free surface flows, while the inundation ratio is the logical geometric variable.

The most elementary treatment of roughness is via a Darcy-Weisbach friction factor given by $f_D = 8\tau/\rho V^2$, where τ is the surface shear stress (viscous, turbulent, or their sum), and ρ is the water density. The dominant contribution to the shear is

taken to be the pressure gradient term so that the friction factor may be decomposed as $\frac{8gh\sin\theta}{V^2} = \frac{8\sin\theta}{Fr^2}$, suggesting that a macroscopic parameterization of the roughness via a friction factor must implicitly depend upon Fr. Again, this is consistent with the importance of free surface effects (as parameterized by Fr) in contributing to the resistance to flow (parameterized by f_D) [Smith et al., 2007]. Experimentally, the friction factor that parameterises resistance to a particular microtopographic arrangement varies with the inundation ratio [Lawrence, 1997, 2000]. The nature of this variation appears to be sensitive to specific geometric arrangements, making generalization of existing semi-empirical models challenging. As an alternative, we adopt the simple and conservative assumption that the resistance to the flow can be parameterised by relating the microtopography to the momentum roughness height (z_o) [Katul et al., 2002, Chen, 1991], and assuming that z_o scales linearly with the depression height $2A$. We follow Katul et al. [2002] in linking the value of the friction factor to an estimate of Manning's friction factor (n) (or $f_D = 8n^2g/h^{1/3}$), such that $n \approx 0.06\, z_o^{1/6}$ (assuming turbulent flows). The n estimate is then used to parameterize a kinematic wave approximation to the overland flow. While this approach is undoubtedly an oversimplification, it provides a consistent and reproducible method to apply within the scope of the toy model. It offers a conservative estimate of the resistance in that this parameterization strictly applies to 'deep flows' over microtopography, and probably under-estimates the resistance where the inundation ratio is close to one [Katul et al., 2002]. We solved the flow equations following Giraldez and Woolhiser [1996] using the method of characteristics and accounting for the unsteady lateral inflow terms imposed by rainfall and infiltration:

$$\frac{dh}{dt} = I - f, \tag{7.7}$$

$$\frac{dx}{dt} = aK_r \left(h - 2A\right)^{a-1,} \tag{7.8}$$

where I is the rainfall intensity, f, as before, is the infiltration rate (enhanced by microtopography), K_r is a kinematic resistance parameter defined in terms of the slope S_o and the roughness coefficient n, and is given as $K_r = \sqrt{S_o}/n$, and the exponent $a = 5/3$ for a turbulent overland flow regime (assumed when linking n to z_o) though a can be as large as 3 for a laminar flow regime. The modification to the celerity (equation 7.8) by incorporating dependence on a reduced depth simply ensures that no flow occurs when the depth of ponding is less than the storage depth. The kinematic treatment assumes 1D flow and $K - r$ inversely proportional to n. A finer level of detail could be obtained by considering a 2D formulation where the vertical dimension is explicitly incorporated and the differences in dynamics across the various water levels above the undulating surface are retained. Such a refinement would consider the effects of the undulating surface in depth (z) and longitudinal distance (x) along the hill slope on the time-averaged longitudinal (U) and vertical (W) velocities via,

$$\frac{\partial U}{\partial x} + \frac{\partial W}{\partial z} = 0 \tag{7.9}$$

$$U\frac{\partial U}{\partial x} + W\frac{\partial W}{\partial z} \approx -\frac{1}{\rho}\frac{\partial P}{\partial x} - \frac{\partial \tau}{\partial z} - \frac{1}{2}C_d U^2, \tag{7.10}$$

where C_d is the effective drag coefficient imposed by the microtopography on the flow (due to pressure and viscous effects), and τ is the sum of the turbulent and viscous stresses. The analysis can be simplified by assuming that the undulating surface primarily perturbs the mean pressure gradient $\partial P/\partial x$ (which is approximately out of phase with microtopography), in a vertically uniform manner, and that the mean

longitudinal momentum balance responds by creating the advection terms. These advection terms modify the τ gradients given by $\tau = -(\nu + m + \nu_t)(\partial U/\partial z + \partial W/\partial x)$, where ν_t and ν_m are the turbulent and eddy-viscosities. Once the solution for $U(x,z)$ is derived using appropriate models for ν_t from this system (as originally proposed by Jackson and Hunt [1975] [Belcher and Hunt, 1998, Jackson and Hunt, 1975, Poggi et al., 2007]), formal spatial averaging across the entire hill length can be employed to arrive at a bulk roughness parameter:

$$f_D = \frac{1}{L}\int_0^L \frac{1}{h(x)}\int_0^{h(x)} \frac{8\tau(x,z)}{\rho U(x,z)^2} dz dx. \tag{7.11}$$

Since the first order analysis with 1D flow did not indicate a strong sensitivity to the parameterization of the overland flow (see below), this elaboration was not introduced for the numerical analysis presented here.

7.4 Numerical analysis of the idealized case

Even the simple toy model is dependent on a large number of parameters, precluding a comprehensive sensitivity analysis across the entire parameter space. As an alternative, a reasonable reference condition was defined using realistic but static (unless otherwise specified) parameter values (Table 1). The reference soil properties correspond to clays with saturated hydraulic conductivities on the order of $10^{-6}\ m/s$. The sorptivity of the soil χ_o was set to $3.7 \times 10^{-4}\ m/s^{1/2}$. Reference microtopography was set with an amplitude A of 2.5 cm and a wavelength λ of 40 cm, and reference rainfall was taken as an intense rainstorm with intensity 3.5×10^{-5} m/s and duration (t_d) of 30 minutes. For comparison, this approximates intensities associated with 2 year storms in several dryland areas (e.g. northwestern Australia or the northern Chihuahuan desert [Australian BoM, 2009, Texas Department of Transport, 2010]). From this baseline, the soil properties (K_{sat}, χ_o), geometry (A,

Parameter	Reference Value	Model Run	Range
A (m)	0.025	A	1mm - 10 cm
λ (m)	0.4	A	10cm - 2m
I (m/s)	3.5×10^{-6}	B	$10^{-6} - 10^{-2} m/s$
t_d (min)	30	B	30 min - 5 hr
K_{sat} (m/s)	1×10^{-6}	C	$10^{-10} - 10^{-2}$ m/s
χ_o (m/s$^{1/2}$	3.7×10^{-4}	C	$10^{-6} - 10^{-3}$ m/s$^{1/2}$
S_o ($^\circ$)	2	D (results not shown)	10°
n (m$^{-1/3}$/s)	0.06 (2A)$^{1/6}$ (mt) 0.02 (smooth)	E (results not shown)	0.02

Table 7.1: Parameter values for the reference case, identification of the model runs in which their effects were assessed, and the range of values employed in these model runs

λ), and storm properties (I, t_d) were varied. For each model run, the percentage of the rain that was partitioned into infiltration was calculated. To assess the sensitivity of this partitioning to microtopography, this proportion was normalized by the partitioning to infiltration on a hillslope with $A = 0$ under otherwise identical conditions (i.e. the background state), and it is this ratio that is reported. These model runs were repeated for slope angles of 2° and 10°; and for a test case where the flow resistance parameter was held constant between the microtopographic and the background cases. The relative significance of the microtopography in increasing the time to ponding, the time to runoff generation (ie $t_r - t_p$), and the runoff regime (hydrographs) were also evaluated. Microtopography induced large increases in the proportion of incident rainfall that infiltrated, approximately doubling the percentage of rainfall that infiltrates in the reference case. The existence and magnitude of an increase in infiltration were sensitive to the soil properties, storm characteristics and microtopographic geometry. Similarly, the degree to which increased infiltration could be attributed to changes in time to ponding, the existence of the surface store or the change in hydraulic resistance varied with these factors.

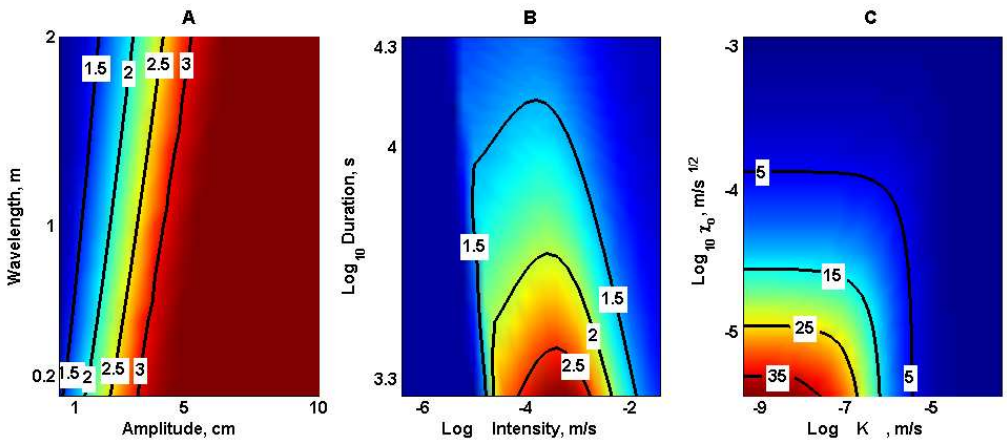

FIGURE 7.4: The proportional increase in infiltration per storm in the presence of microtopography ($A > 0$) relative to the background state ($A = 0$). Each plot represents variation in A) microtopographic properties, B) Storm properties, C) Soil properties about the background case (see Table 7.1).

7.4.1 Sensitivity to microtopographic dimensions

For specified micro-topographic amplitude, increasing the wavelength diminished the effects of microtopography. This decrease was subtle for low slope angles (Figure 7.4A), but became pronounced as the slope angles increased (not shown). Given a fixed microtopographic wavelength, we found that increasing the amplitude of the microtopography increased the proportion of rainfall infiltration markedly (as would be expected from surface area considerations alone).

The strong positive association of infiltration with increased microtopographic amplitude arose from the direct scaling between the amplitude and the time to ponding, the surface store and the resistance parameter (Figure 7.5, A and B). In contrast, the relative increase in time to ponding declined as the microtopographic wavelength increased, while the size of the surface store and the resistance parameter were nearly invariant with respect to wavelength (Figure 7.5, A and B). The significant changes in partitioning associated with changes in the surface storage alone suggest that increases in the relative proportion of infiltrated water may still occur even where

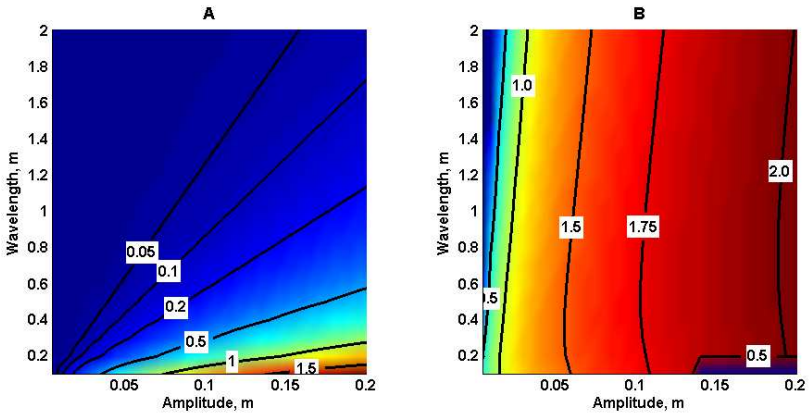

FIGURE 7.5: The increase in runoff initiation associated with the time to ponding and the storage time, both referenced against the time to ponding in the background case (see Table 7.1 for values). The proportional increases are rendered on a log scale to show their variation. A) Time to ponding in the presence of microtopography relative to the background state, B) Storage time associated with microtopography again relative to time to ponding. The runs were conducted with the usual reference properties and result in the change in total infiltration presented in Figure 7.4(A).

microtopographic variation is associated with the presence of impermeable obstacles (e.g. rocks, vegetation or debris).

7.4.2 Sensitivity to storm properties

The sensitivity of the partitioning to storm properties peaked at intermediate rainfall intensities, and was generally greatest for storms of short duration. Where rainfall intensities were low, the time to ponding was not reached, or was of very short duration, such that discrepancies between background and microtopographic cases were minimal. Where rainfall intensities were high, the proportion of infiltration was low relative to the total rainfall volume for both microtopographic and background cases. Thus, an intermediate regime where rainfall intensities were 2-3 orders of magnitude greater than Ksat generated the most sensitive response (Figure 7.4B). Provided storm duration (td) was long enough to induce ponding on the background

surface, the impact of microtopography was greatest for short storms.

7.4.3 Sensitivity to soil properties

Microtopography caused the greatest increase in proportional infiltration where both the saturated hydraulic conductivity and the sorptivity were low. The increases in infiltration observed in this model run were entirely due to increased time to ponding relative to the background case as sorptivity declined. At high sorptivities, time to ponding was not reached. At intermediate sorptivities, although time to ponding was reached, it occurred relatively late in the storm duration, and both surfaces, regardless of microtopography, infiltrated the majority of the rainfall. Thus at low sorptivities the background surface ponded rapidly and generated the most marked response.

7.4.4 Slope and roughness effects

Two additional cases were considered. In the first of these cases, the results for a 2o slope as presented in Figure 7.4 and Figure 7.5 were compared to the results for a 10° slope. Microtopography continued to exert an increase in infiltration relative to the background surfaces, but this increase declined (e.g. from a doubling of infiltration to a 50% increase for the background case), primarily due to decreased storage volumes. The overall trends presented in Figure 7.4 and Figure 7.5 remain representative, despite the change in magnitude. The second comparison utilized a consistent resistance parameter for the background and microtopographically varying cases. This induced a small decrease in the effects of microtopography on infiltration, and suggested that overall sensitivity to the resistance terms was not large in comparison to the infiltration effects.

7.5 Discussion

7.5.1 Toy model implications

Based on the model results, microtopography may induce increases in the proportion of rainfall that infiltrates of $20 - 200\%$ for short storms on shallow slopes. These increases are substantially larger for larger microtopographic amplitude, or where soils are very heavy, degraded, or exhibit surface crusting and sealing (lower K_{sat} and χ_o). The increases persist, albeit with smaller magnitudes, for less intense rainstorms, smaller microtopographic amplitudes and more permeable soils. The results suggest that a suite of dimensionless numbers can be defined that control the sensitivity of the partitioning to microtopography: $\frac{I}{K_{sat}}$, $\frac{I\sqrt{t_d}}{\chi_o}$, $\frac{A}{\lambda}$, $\frac{L}{\lambda}$ and $\frac{n_{m.t.}}{n_{b.g.}}$ are all positively correlated to an increase in infiltration relative to the background surface. S_o, $\frac{t_d}{t_{p\,m.t.}}$ and $\frac{t_d}{t}$ are negatively correlated to an increase in infiltration relative to a background surface. Microtopography increased infiltration and altered runoff thresholds. The relatively simple alteration of sorptivity and the large number of existing empirical models available for estimating the size of the surface store mean that it is not onerous to make first order amendments to existing hydrological models to account for these effects.

7.5.2 Theoretical extensions

As stated previously, the assumption of homogeneity and stationarity in the treatment above is not representative of 'real world' conditions, where heterogeneity in soil properties is legion. Rather than attempt to address all possible sources of heterogeneity and their implications, we make an immediate distinction between heterogeneity induced by microtopography, and heterogeneity that may be superimposed on microtopographic landscapes. In the former case, the literature offers several in-

teresting examples that provide opportunities to extend the simple treatment above, while the latter situation pertains primarily to upscaling results obtained to date.

Heterogeneity induced by microtopography

Several sources of heterogeneity and non-stationarity are expected to correlate with microtopography. Fox et al. [1998] showed that microtopography was progressively eroded during a simulated rainfall event. Infiltration rates in the depressions were shown to be significantly less than those associated with mounds. The low infiltration rates were associated with the wash-in of fines and surface sealing. Drier soils may be expected at the peaks of microtopographic geometries and wetter conditions in the troughs. To explore the possible effects of such variation, we consider two prototypical cases where the infiltration rate is a function of the inundation. In one case, infiltration rates are highest on the mounds [Fox et al., 1998, Dunne et al., 1991, Bochet et al., 2000]. We also present the alternative case, where infiltration rates are highest in the depressions, as might arise if clay soils result in increased cracking and macroporosity. Further extensions can be made where correlations develop during a storm e.g. due to surface sealing, or if A also becomes a function of time. Existing work developing infiltration theory in such cases provides an appropriate starting point [Assouline and Mualem, 1997, 2002]. For the temporally constant cases, a mathematical derivation is presented in the supplementary material and only the key results are discussed here. The results in the supplementary material suggest that if correlations between microtopography and K_{sat} alter the spatially averaged value of K_{sat} relative to the background case, then the correlations may significantly dampen or amplify the effects of the microtopography depending on their phase relationship with microtopography. However, where the correlations leave the spatially averaged K_{sat} unaltered, they have essentially no impact on the partitioning. This result appears surprising when compared to Dunne et al.'s results, which showed

strong sensitivity to correlations with K_{sat} and z. The distinction lies in the fact that in order to generate any runoff in this geometry, a depression must be fully inundated. For low slope conditions this results in essentially all the variability in K_{sat} being explored prior to runoff generation. Thus, the effective infiltration rate at the point of runoff generation is dictated by the spatial average of all values of K_{sat}, not a subset constrained by a comparative shallow depth of flow as per Dunne et al.'s study. Consequently, the nonlinear coupling between runoff and infiltration is more dynamically variable and significant in that geometric arrangement.

Large-scale heterogeneities and upscaling

Large-scale heterogeneities impose new length scales on hillslopes. If the effects of heterogeneity in isolation are anticipated to be on the same order of magnitude as the microtopographic effects, it may be necessary to move towards an explicit simulation approach [Fiedler and Ramirez, 2000, Fiedler et al., 2002]. If, however, the impacts of imposed heterogeneities are sufficiently severe, then their effects may be dealt with by spatially decomposing the hillslope. Below the characteristic length scale on which the heterogeneities act, the microtopographic effects described here would dominate, while at longer length scales, the effects of the heterogeneities would become more pronounced. In combination with non-linearities in the dynamics and length scales induced by the microtopographic variability itself (see below), this leads to the potential for highly scale-specific runoff and infiltration processes on hillslopes, as are known to arise in arid landscapes [Kirkby, 2001, Kirkby et al., 2002].

Challenges for generalization

When motivating this problem, two additional cases, B and C, were identified as posing challenges requiring new theoretical developments. The first development addresses the transition of the hillslope from a series of isolated depressions with

independent and localized hydrologic balance to a connected network of basins contributing flow to their downstream neighbours and ultimately the channel. These fill-spill processes determine the formation of a surface flow network and have been identified as important in generating scale dependence in runoff [Bergkamp, 1998, Joel et al., 2002, van de Giesen et al., 2000, Kirkby et al., 2002, Puigdefabregas et al., 1999, Wood et al., 1988], as well as introducing nonlinearity into runoff generation mechanisms [Darboux et al., 2001, Esteves and Lapetite, 2003, Kirkby, 2001, Lehmann et al., 2007, Planchon et al., 2002, Reaney et al., 2007, van de Giesen et al., 2000]. Similar nonlinear scaling is familiar in the physics literature in studies of percolation or systems displaying criticality [Bak et al., 1987, Berkowitz and Ewing, 1998, Hammersley, 1957, Isichenko, 1992], and often yielding universal scaling properties [Narayan and Fisher, 1994]. Extending such approaches to account for infiltrating surfaces and flow forced by rainfall may provide useful and generalizable insights into surface connectivity. The second theoretical challenge addresses the description of the bulk flow properties of a partially submerged surface. Such flow is inherently complex, consisting of flow over, and around submerged or emergent microtopographic features [Lawrence, 1997]. Macroscopically, microtopography segregates the flow into fast flowing "threads" moving at velocities 2-7 times greater than the mean velocity, and slow moving backwaters in which velocities approach zero [Dunkerley, 2003, 2004]. Up-scaling such variation, even empirically, is challenging [Abrahams and Parsons, 1990]. The development of theoretical approaches to study flows of this nature has been driven by approaches from the geomorphology, canopy flows, and gravel-bed river communities [Cooper et al., 2006, Ferguson, 2007, Ferro, 2003, Hardy et al., 2007, Katul et al., 2002, Lacey and Roy, 2007, Lawrence, 1997, 2000, MacVicar and Roy, 2007, Marquis and Roy, 2006]. All approaches highlight the importance of the relative degree of inundation of roughness elements. Similarity and scaling approaches based on the inundation ratio have proven at least as successful

at describing the bulk flow properties as existing semi-empirical models [Hey, 1979, Katul et al., 2002, Lawrence, 2000, Leopold and Wolman, 1960]. The description of the average properties of spatially variable flows remains challenging [Canovaro et al., 2007], although new techniques are becoming available, such as acoustic "grazing angle sound propagation", which allows measurement of bulk roughness properties from the acoustic profile of the water surface [Cooper et al., 2006]. The applicability of such techniques to overland flows is limited due to the shallow and variable depth of flow, meaning that drawing analogies from deeper, gravel lined channels, and scaled flume experiments remains the most promising way forward.

7.5.3 Feedbacks in dynamic landscapes

At long timescales, feedbacks between vegetation, hydrology and geomorphology suggest the possibility of co-evolution of hillslope features. A prototypical example of the feedbacks between vegetation, microtopography and hydrology is in the role of vegetation in generating soil mounds [Bochet et al., 2000, Nash et al., 2003] with infiltration rates up to 2-8 times greater than surrounding soil [Valentin et al., 1999]. Saco et al. [2007] demonstrated that feedbacks between biomass density, infiltration capacity and erodibility generated regular arrays of both vegetation and microtopographic mounds on arid hillslopes. Feedbacks between aeolian geomorphic features and vegetation are generate signatures of vegetation in landscape structures [Baas and Nield, 2007, Nield and Baas, 2008], while feedbacks between aeolian processes and hydrology have been shown to generate ring patterns in arid ecosystem vegetation [Ravi et al., 2007]. The generation of microtopographic terracettes was explicitly considered by Sanchez and Puigdefabregas [1994] using cellular automata. Extending the focus of these studies from the generation of microtopography to the evolution of hydrological partitioning and ecological functioning is an area ripe for further exploration.

7.6 Conclusion

Microtopographic variation was predicted to significantly alter hydrological partitioning where soils had low permeability and were subject to intense rainstorms. The net effect of microtopography was to enhance the retention of rainfall in hillslope soils, which may represent a significant improvement in habitat and growing conditions for plants in the semiarid systems under consideration. The results suggest that under certain circumstances, ignoring microtopographic variation may lead to significant biases in prediction of hydrological partitioning of rainfall into infiltration and runoff. Modifications to classical hydrological theory through the use of an "effective sorptivity" and accounting for the peak surface store can be immediately applied. However, a more comprehensive theory that accounts for connectivity and the bulk representation of flow properties over variable terrain is needed, along with upscaling approaches to factor in other sources of variability in infiltration properties through space and time. Characterizing the properties of microtopography in real landscapes to allow its effective simulation and parsimonious description is a priority. Linking theoretical developments to the co-evolution of landscapes, specifically with regard to hydrological, geomorphological and ecological feedbacks, presents an exciting set of challenges for understanding and managing arid landscapes.

8

Summary and conclusions

A brief summary of the main findings and key conclusions are presented. The conclusions here lay out a framework for progressing with future studies, also described here.

8.1 Summary of results

The research presented in this dissertation focused on four key areas: exploring alternative explanations for observed vegetation patterning; biomass transport by seed dispersal; the alteration of surface hydrology by the presence of vegetation and the implications of land surface micro-topography on infiltration and runoff generation. Taken together, the results from these studies present a rich and complex picture of the eco-hydrological dynamics of structural organization in vegetation communities.

Chapter 2 demonstrated the plausibility of alternative, non-Turing mechanisms being responsible for vegetation patterning. This work highlighted the difficulty of determining mechanisms of pattern formation solely from the morphology of the patterns formed. It provided one of the first known examples of fluid instabilities

being responsible for vegetation patterning in terrestrial ecosystems and opened up the possibilities of alternative ecological pattern forming mechanisms beyond those typically discussed in the literature.

Chapter 3 developed a methodology to estimate dispersal kernels and diffusion coefficients from the measured properties of seeds and wind. The focus of this work in developing scaling methods to account for the effects of variability in mean wind speeds on the rate of plant population movement remains suitable for continuous treatment adopted. The estimates of plant migration rate provided in the chapter, however, are susceptible to biases arising from the continuous representation. The minimum biomass density at a point within a continuous model should be equivalent to the biomass density of an individual seed. Applying such a minimum biomass threshold effectively truncates the propagation front. The predicted population migration rate turns out to be extremely sensitive to this truncation, and this sensitivity is exacerbated for the case of power-law seed dispersal kernels. Simulations indicate that in the case of an exponential kernel (c.f. diffusion), truncating the traveling wave at biomass values of $\approx 1\%$ of carrying capacity (an unrealistically high threshold) results in a 40% decline in the predicted wavespeed. Conversely, a decline of 40% of the wavespeed is achieved in the case of a Wald kernel for a truncation threshold of just $2 \times 10^{-9}\times$ the carrying capacity - a rather plausible threshold for typical seed masses (on the order of mg) versus typical carrying capacities (on the order of 100s of kg). The sensitivity of the propagation velocity to such truncation in the range $1 \times 10^{-10} \times K$ to $1 \times 10^{-8} \times K$ (recall that K is the carrying capacity) is shown in Figure 8.1. Consequently, predicted migration rates presented in Chapter 3 should be regarded as containing a bias due to the failure to account for the discrete nature of seed dispersal.

This bias alone would suggest that the migration rates obtained in the case study in Chapter 3 should be viewed with caution. There are, additionally, numerous other

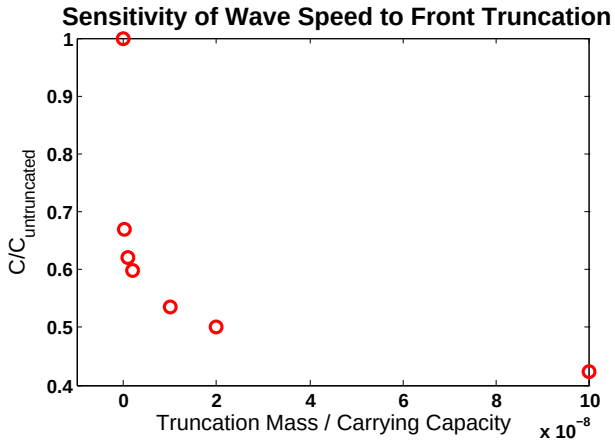

FIGURE 8.1: Proportional change in predicted wavespeed (c) when the traveling wave is truncated. The results shown were generated for a WALD kernel and show the strong sensitivity to truncation associated with the power law kernel.

reasons for viewing these as over-estimates of migration rate. Specifically, the pollen record must be viewed as incomplete. Utilising contemporary pollen and macrofossils extracted from surficial lake sediments, McLachlan and Clark [2004] were unable to reconstruct the current range of beech and birch species in the US. Sparse populations did not leave a detectable record, even over large areas within the contemporary range. This finding was backed by molecular data which suggested that the pattern of expanation of maple and beech species after the last glacial maximum cannot be spatiall reconciled with that predicted from the pollen record [McLachlan et al., 2005]. These data indicate that tree species' ranges during the last glacial maximum extended beyond those indicated by the pollen record, such that the rates of population expansion predicted solely from the pollen record are necessarily overestimated. In addition to the biases associated with continuous representations of a discrete population, the model employed in Chapter 3 ignored numerous other processes, known to be important in plant population migration, and likely to retard the front speed: these include finite fecundity [Clark et al., 2004], mortality of dispersed seed [Clark et al., 2001], and ignoring the time needed for trees to reach maturity and commence seed dispersal at the front [Clark et al., 2003]. Consequently, Chapter 3 needs to be viewed as identifying the importance of variability when upscaling wind speeds, but emphatically not as advocating a realistic model for plant population migration, nor as having predicted reasonable rates of biomass migration, given the limitations of the pollen record.

Chapters 4 through 5 developed a framework for examining the significance of seed dispersal in determining the structures of vegetation communities. The numerical treatment of seed dispersal developed in Chapter 3 was then applied to extend existing models of vegetation pattern formation by examining the influence of non-diffusive biomass movement on patterning, as well as the role of anisotropy in secondary seed dispersal. This work showed that patchy landscapes were formed

regardless of the characteristic length scale of seed dispersal, but that in the absence of diffusive seed movement the spatial pattern of vegetation distribution became disordered and sensitive to initial conditions. The results suggested that the formation of ordered patchy landscapes was more likely to result from fragmentation of coherent vegetation cover than expansion vegetation into bare sites. Secondary dispersal was shown, phenomenologically, to have a potentially significant role in explaining the evolution of vegetation patterns and moderating landscape dynamics in sloping patchy systems.

Chapters 6 and 7 outlined two key influences on the partitioning of water at the land surface: the presence of vegetation cover and the significance of local micro-topography. Local biomass density was shown to correlate to local infiltration capacity in drylands, such that higher local biomass resulted in high infiltration rates, independently of soil type. Secondly, micro-topographic features were shown to generally enhance the infiltration volume when compared to an idealized flat case. These two features suggest that the perturbations to the surface hydrological budget induced by vegetation on arid hillslopes are significant and potentially difficult to account for with standard surface hydrological approaches. The incorporation of a refined treatment of surface hydrology into pattern forming equations is the next outstanding challenge in this area.

8.2 Future work

The scope for further study of these issues is extensive, and can be subdivided into several areas, namely

- further exploration of pattern forming processes;
- further refinement of pattern forming models;
- further examination of secondary dispersal processes; and

- further study of the interaction of micro-topography and hydrology.

Finally, the potential links to land use and land and water resources management are discussed.

8.2.1 Further exploration of pattern forming processes

Elucidating the mechanisms of vegetation pattern formation in drylands remains an active subject of research. To date mechanistic pattern forming models have not been comprehensively tested with field, modelling and remote sensing studies. Their validity and suitability for reproducing the dynamics of patterned systems remains uncertain until such validation takes place. Recently the phenomenological models developed by Lefever and Lejeune have been refined and assessed in the field using gapped vegetation patterns as a case study. These studies have introduced new possibilities for the ecosystem dynamics of patterned systems, and highlighted the significance of plant allometry, specifically the ratio of the crown to rooting-zone diameters, in determining the dynamics of pattern formation and collapse [Lefever et al., 2009]. Such results suggest that further linking plant physiology (which controls the allocation of carbon above and below ground, and thus moderates plant allometry) to spatial patterning may offer valuable insights.

As a complementary problem, theories regarding the formation of spatially patchy systems where vegetation distributions do not display a dominant wavelength are largely undeveloped. However, in many of these systems, similar feedbacks to those observed in patterned systems are present and result in the concentration of nutrient and water resources under plant canopies. The determinents of spatial patchiness in these "disorganized" systems and the development of spatial models that can be used to examine their evolution remains a largely outstanding problem (but see Manor and Shnerb [2008] and Kefi et al. [2007b] for some approaches based on cellular automaton methods).

8.2.2 Refinement of pattern forming models

Several outstanding challenges remain in representing the pattern forming processes mechanistically in numerical models. Firstly, the role of stochasticity in time and space have not been comprehensively addressed. Existing models adopt mean field approaches that neglect the intermittency of rainfall, and which assume that soil properties are uniform over the domain of interest. Accounting for stochasticity in rainfall introduces a need to resolve water transport processes at the scale of individual storms, a significant refinement from existing models. This refinement can now, however, benefit from the empirical relationships between biomass and infiltration derived in this thesis, and can be readily modified to incorporate micro-topographic effects. Incorporating intermittency in rainfall in pattern forming models will also require refinements to the representation of plant physiology to incorporate the effect of drought survival strategies by vegetation (but see Guttal and Jayaprakash [2007] for a phenomenological approach to this issue). In the spatial domain, random variation in soil properties may act to obscure vegetation patterning to such a degree that interpretation of pattern features becomes impossible, or may even interact non-linearly with the pattern forming process in potentially complex ways (see Lowe et al. [1983], Coullet [1986] for examples in other pattern forming systems). There is scope to develop experimental treatments to further investigate the pattern forming process at the laboratory scale. Constructing a large "vegetated flume" where water input, soil properties, slope, drainage and vegetation type can be controlled offers the scope to experiment with the growth of model organisms. Similar experimental flumes have been installed within the hillslopes at the Coweeta Hydrological Facility and formed the basis for fundamental research into hillslope discharge processes [Hewlett and Hibbert, 1963]. Given recent calls to extend hydrological efforts in laboratory-scale experiments [Kleinhans et al., 2009], such a facility

would provide one of relatively few set-ups to investigate the coupling of hydrological, geomorphological and ecological roles at small scales.

Finally, development of appropriate parameter estimation techniques for spatially extended systems responding to stochastic forcing but existing largely near their equilibrium condition are also needed in order to progress from prognostic modeling of vegetation patterns to suitable inverse modeling schemes that can allow inference of ecosystem properties based on observations of pattern dynamics. Recent methods to allow parameter estimation from ensembles of chaotically evolving convection patterns have been developed, offering several models that could form the basis for such an extension [Sitz et al., 2003, Cornick et al., 2009].

8.2.3 Mechanistic treatment of secondary dispersal

In the context of patterned vegetation and elsewhere, secondary seed dispersal is largely under-studied, and has been most thoroughly explored in the context of animal mediated dispersion. Experimental and observational studies have demonstrated the importance of secondary dispersal for seed location, burial and germination success, but to date, only one study has mechanistically linked secondary dispersal to environmental conditions and thus developed a predictive framework [Schurr et al., 2005]. Given the importance of secondary dispersal in spatially structuring plant populations in dry-land ecosystems and the value of the need for mechanistic descriptions of secondary dispersal that can be used for predictive purposes, secondary dispersal is ripe for more detailed mechanistic treatments through a combination of modeling, experimental and field studies.

8.2.4 Microtopography and hydrology

As discussed in the conclusions of Chapter 7, several studies have begun to explore the links between hydrology, ecology and geomorphology, often with a bias towards

determining the processes that form micro-topographic features. Extending these approaches with field and experimental studies to assess the co-evolution of micro-topography with hydrological transport paths and ecological function is a question ripe for further exploration. Recent novel flume studies addressing similar questions in the context of fluvial geomorphology have developed illustrative and useful models with extremely simple plants (e.g. alfalfa) [Tal and Paola, 2007]. Potentially, similar approaches for understanding the coupled ecological-hydrological and geomorphological dynamics of hillslopes could be adopted at laboratory scales, using the experimental set up outlined previously.

8.2.5 Social and management applications

The research effort reported in this dissertation concentrated largely on questions regarding the structure and functioning of spatially patchy arid ecosystems. Many of these ecosystems, however, are also significant source of primary production (either for agricultural production, livestock grazing or firewood harvest) and act as dryland water catchments (indeed the Millennium Ecosystem Assessment outlines the primary ecosystem service of arid ecosystems as being water regulation [Safriel and Adeel, 2003]). Decision-making about land use and management in these environments may constitute a major regulating factor or perturbation to the natural ecosystem, and one which to date has been inadequately explored with the exception of site-specific case studies [Berg and Dunkerley, 2004]. While some socio-economic modelers are now developing approaches to model the human element of desertification (e.g. [Hellden, 2007]), such models have so far represented primarily linear responses in the environment and thus cannot reproduce threshold or bistable behaviour, even where it is widely acknowledge to drive dryland dynamics. Syntheses of socio-economic and ecohydrological approaches to the dynamics of drylands are likely to occur at fairly phenomenological levels, but this integration nontheless must ensure

that the critical dynamics from each approach are faithfully maintained. Integrating the ecology, hydrology, economics and social sciences into a unified complex-systems-science approach to drylands remains a key challenge for ongoing management and decision making.

Appendix A

Meteorological data

Station	0:00am	1:00am	2:00am	3:00am	4:00am	5:00am	6:00am	7:00am
Air Temperatures								
KTDF	1.1	1.1	0.0	-1.1	-1.1	-1.1	-2.2	-2.2
KRDU	5.0	4.4	3.3	2.8	1.1	1.1	0.6	0.0
KIGX	6.7	5.0	3.3	2.8	1.7	1.7	1.1	1.1
SILR	0.6	-1.1	-1.1	-1.7	-2.2	-2.2	-2.8	-3.3
REED	6.7	6.7	4.4	3.3	2.2	2.8	2.2	1.1
OXFO	5.6	3.9	3.9	3.3	2.2	1.7	1.1	1.1
Soil Temperatures								
SILR	12.2	11.7	11.7	11.1	11.1	11.1	10.6	10.6
REED	13.3	12.8	12.8	12.8	12.2	12.2	12.2	12.2
OXFO	12.2	12.2	12.2	11.7	11.7	11.1	11.1	11.1
$\bar{T_{air}}$	4.3	3.3	2.3	1.6	0.6	0.6	0.0	-0.4
$\bar{T_{soil}}$	12.6	12.2	12.2	11.9	11.7	11.5	11.3	11.3
$\bar{\Delta T}$	8.3	8.9	9.9	10.3	11.0	10.8	11.3	11.7

Table A.1: Meteorological data from weather stations surrounding Durham NC on 12th Nov 2008

Appendix B

Wind data, scaling and sensitivity analyses

This appendix is presented in five sections. The first illustrates the relationship between diffusion models and models in which $W(x)$ is replaced by a Gaussian dispersal kernel $G(x)$ for the case of the Fisher-Kolmogoroff Equation, utilising a novel approach for deriving this result from a differential, rather than a difference equation. The second section provides the details of the numerical simulations used to construct the relationship between Ueff and the Weibull parameters. The third section deals with the collection, derivation and use of wind statistics in determining the resulting biomass movement. It outlines the collection of data from the Ameriflux sites, outlines the scaling and analysis of this data, and the derivation of sensitivity results for the front speed relative to the Weibull wind statistics across different geographic areas and land cover types. The fourth section treats the data derived for the Duke Forest Grass Field and Hardwood canopies in greater detail, and shows the derivation of the data used in the case study. The final section addresses a sensitivity analysis performed on the estimates of biomass propagation speed for parameters relevant to tree species and discusses the linear and nonlinear responses observed with

a view towards understanding where parameterisation effort should be invested.

B.1 The classical Fisher Equation and Gaussian dispersal kernels

We assumed that the one dimensional Fisher Equation

$$\frac{\partial P}{\partial t} = rP\left(1 - \frac{P}{K}\right) + D\frac{\partial^2 P}{\partial x^2} \tag{B.1}$$

could be approximated by a logistic growth function coupled to a Gaussian dispersal kernel:

$$\frac{\partial P}{\partial t} = rP\left(1 - \frac{P}{K}\right) \times \int_{-\infty}^{\infty} G\left(x - x'\right) P\left(x'\right) dx' \tag{B.2}$$

Using a similar analysis to that performed on the logistic-WALD model, we can linearise, and discretise Equation B.2 and derive the characteristic equation:

$$e^x = r\left(1 + \int_{-\infty}^{\infty} e^{su} G\left(u\right) du\right) + 1. \tag{B.3}$$

We recognise the integral as the moment generating function of the Gaussian distribution, $MG_{Gauss}\left(s\right)$, given by:

$$MG_{Gauss}\left(s\right) = \exp\left(\frac{\sigma^2 s^2}{2}\right), \tag{B.4}$$

and its derivative is

$$\frac{\partial MG_{Gauss}\left(s\right)}{\partial s} = 2s\exp\left(\frac{\sigma^2 s^2}{2}\right). \tag{B.5}$$

We require the solution to hold at the double root given by the derivative of the characteristic equation. This yields the expression for the wave speed as:

$$c = \frac{r\sigma^2 s exp\left(\frac{\sigma^2 s^2}{2}\right)}{r exp\left(\frac{\sigma^2 s^2}{2}\right) + 1}. \tag{B.6}$$

When $r \exp(\sigma^2 s^2/2) >> 1$, this expression simplifies to

$$c = \sigma^2 s, \tag{B.7}$$

giving the expression for r as

$$r = \frac{\exp(\sigma^2 s^2) - 1}{\exp\left(\frac{\sigma^2 s^2}{2}\right)} \approx \exp\left(\frac{\sigma^2 s^2}{2}\right), \tag{B.8}$$

and upon eliminating s yields:

$$c = \sigma\sqrt{2 \ln r}. \tag{B.9}$$

For a fixed growth rate, if we identify an effective diffusion coefficient, $D = \ln r\sigma^2/2r$, we recover the speed of invasion derived for the Fisher equation:

$$c = 2\sqrt{Dr}. \tag{B.10}$$

Numerical simulations of the two models show close matching of wave profiles, convergence of wave speeds, and for low ratios of $D : r$, a close match in the predicted location of the wave front (Figure B.1).

A point of difference between dispersal kernel models and diffusion models is the asymptotic approach to the maximum speed in dispersion kernel models, while in diffusion models, given appropriate initial conditions, the maximum speed is attained immediately [Kot et al., 1996, Murray, 2003a]. Both approaches are appropriate for predicting the maximum speed of biomass movement, but they will predict the location of the biomass wave front differently. The time at which the dispersion

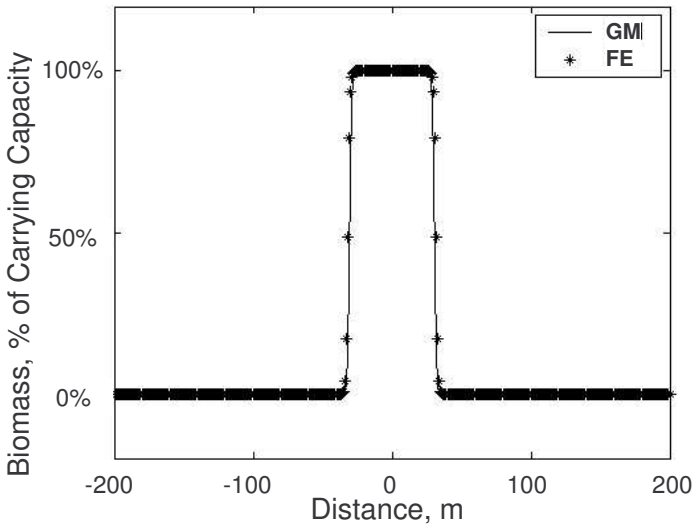

FIGURE B.1: Approximation of the solutions of the Fisher Equation (FE) with a Gaussian Kernel Model (GK). The growth rate r=1, and the ratio D:r is 0.042, resulting in a close match of both the speed and the location of the wave front.

speed approaches its asymptotic maximum varies with the biomass growth rate, but was always low with respect to the vegetation lifespan in numerical simulations.

B.2 Numerical simulations

Equation B.1 was integrated numerically using a finite difference scheme in 1D. At each timestep a random draw was made from a Weibull distribution and used to generate the Wald kernel. The convolution of the seed dispersal kernel (the WALD) and the standing biomass was performed in the Fourier domain using a fast Fourier transform algorithm for one-dimensional convolutions [Rosa, 2004]. Because of their efficiency, Fourier transforms are routinely used to simplify the computation of convolution integrals. The domain size was varied depending upon the Weibull parameters

used. As wind speeds increased, the domain size was increased from 3000m up to 12000m to ensure that the travelling wave was contained within the domain. Simulations were run at a half hourly timescale, with dt set to 0.025 hours. The spatial discretisation, dx was set to 1m. Logistic and tree parameters were set to values of: $r = 2$; $\alpha = 0.1$; $K = 500$; $V_t = 1.14$; $h = 2$; $z_r = 0.1$, $\theta = 0.36$, $\kappa = 0.4$. These values were selected to ensure that asymptotic speeds were reached rapidly and are not representative of any real system. The position of the front was evaluated at every timestep by determining the spatial location of the point where the biomass was equivalent to 50% of carrying capacity. The front speed was determined based upon the distance travelled during each timestep. Simulations were run for 200 timesteps, which provided sufficient time for the front speeds to reach steady state (this assumption was checked by comparison with longer simulations). Multiple fast Fourier transforms generated small instabilities ahead of the front. These instabilities remained small with respect to the front for the duration of the simulation, but became problematic if simulation length was greatly increased. Truncating the instabilities retarded the front speeds and changed the shape of the travelling wave, so they were left uncorrected. Simulations were manually checked prior to running the Monte Carlo simulations to optimise the domain size and simulation duration. Monte Carlo results were also manually checked for outliers, indicating that the wavefront had crossed the domain boundary. Monte Carlo simulations were conducted with 500 realisations for 47 combinations of Weibull parameters.

B.3 Wind data and wind statistics across multiple regions

This section addresses the collection and analysis of the mean wind velocity data. Data were collected from six locations across four experimental Ameriflux sites (`http://public.ornl.gov/ameriflux/data-get.cfm`), as detailed in Table B.1.

Wind speed data at the sites were collected via sonic anemometry at high fre-

Site name	Coords	Cover type	Canopy height	Sensor height	Date Range
Duke Forest, NC	35°58′16.33″ N 79°05′36.15″ W	Grass Clearing	1m	6m	2001-2005
Duke Forest, NC	35°58′24.90″ N 79°06′01.55″ W	Hardwood Forest	33m	42m	2001-2005
Duke Forest, NC	35°58′41.40″ N 79°05′39.10″ W	Pine Plantation	14m	15.5 m	2001-2005
Harvard Forest, Ma	42°32′15.92″ N 72°10′17.32″ W	Hardwood Forest	24m	30m	2001-2005
Morgan Monroe, In	39°19′23.34″ N 86°24′47.30″ W	Hardwood Forest	27m	48m	2001-2005
Howland Forest, Mn	45°12′14.65″ N 68°44′25.00″ W	Mixed Forest	19.5m	29m	2001-2004

Table B.1: Site details for wind data collection.

quency (e.g. 10Hz for Duke Forest sites) and averaged over half-hourly or hourly intervals [Novick et al., 2005]. Wind speed is a function of elevation, so that to allow an inter-comparison of the sites the data must be normalised to a common reference height with respect to the canopy surface. The wind speed profile can be approximated with a logarithmic function of the form:

$$\overline{U} = \frac{U^*}{\kappa_v} \ln\left(\frac{z-d}{z_o}\right) \tag{B.11}$$

Where U^* is the friction velocity, κ_v is von Karman's constant (0.4), z is the elevation above the ground surface; d is the zero plane displacement height which accounts for the fact that the flow regime within the canopy is independent of the flow above the canopy and which is typically estimated as $2h/3$ where h is the canopy height, and z_o is a reference elevation at which the velocity is zero, often referred to as the momentum roughness height. Using this logarithmic profile, all wind speeds were normalised to a reference height of 5 m above the canopy surface, commensurate with the values from the only forest edge site, the Duke Forest Grass Field. A Weibull

	Weibull Scale b	**Weibull Shape k**	$\overline{U_{eff}}$
Duke Grass Clearing	1.77	1.78	4.03
Duke Pine	1.98	1.82	4.40
Duke Hardwood	2.25	2.11	4.40
Maine	2.66	2.15	5.13
Harvard Forest	2.52	2.36	4.50
Indiana	3.09	2.64	5.07
Standard error (all surfaces)	20.15%	15.19%	9.30%
Stndard error (forests only)	16.83%	13.76%	7.81%
% difference Duke HW-Duke Grass	26.93%	18.79%	9.11%
% difference mean forests - Duke Grass	41.01%	24.45%	16.57%

Table B.2: Weibull Statistics and $\overline{U_{eff}}$ for the wind data scaled to 5m above the canopy across the six sites

Distribution was fit to the rescaled data for each year, and the average statistics and projected $\overline{U_{eff}}$ values computed. A comparison of the averaged Weibull parameters and $\overline{U_{eff}}$ across all sites (including all three Duke Forest sites) is shown in Table B.2. It can be inferred that the variability in the effective wind speed associated with geographical changes across the sites sampled is of the same order of magnitude as the variability in changing between different land cover types.

To assess whether the variation of the Weibull parameters exhibited any trends, the shape and scale parameters for each site were plotted against each other. A strong linear correlation was apparent, and a trend line could be fit (Figure B.2) as $k = 0.64 \times b + 0.62$, which fits the data with $r^2 = 0.89$.

The strong positive correlation between the Weibull statistics explains the relatively small changes in $\overline{U_{eff}}$ across the sites despite the large variability in b and k. While an increase in b tends to increase $\overline{U_{eff}}$, an increase in k tends to counteract this. Thus the correlation observed between the Weibull statistics tends to dampen the effect of variability on $\overline{U_{eff}}$. This can be formally assessed in a sensitivity analy-

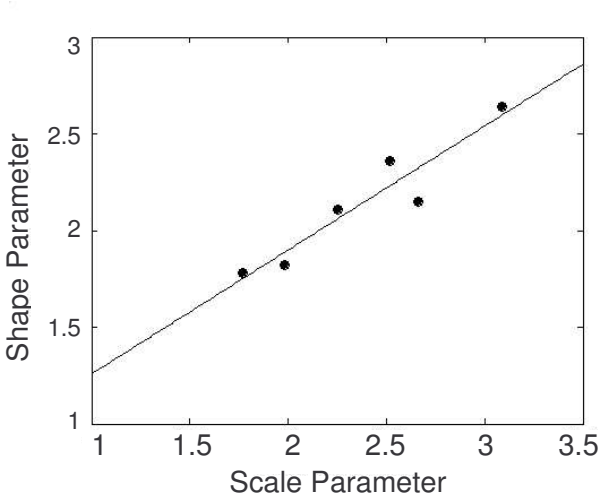

FIGURE B.2: Weibull scale and shape parameters plotted against each other across the six sites. The linear regression results in $k = 0.6409 \times b + 0.6167$.

sis in terms of the Weibull parameters' effect on $\overline{U_{eff}}$ (note that the effect of $\overline{U_{eff}}$ on the front speed c is treated separately in the next section). Expressing the variation in terms of the variability in b, we can predict the approximate impact on the shape parameter k using the linearly relationship, thus determine the resulting proportional change in $\overline{U_{eff}}$. This sensitivity analysis is shown in Table A3.

B.4 Wind data and wind statistics from Duke Forest

The data from the hardwood stand at Duke Forest were used to parameterise the case study for forest canopy conditions. The annual average of the half hourly Duke Forest hardwood stand wind speed data had a coefficient of variation of 3.34% across the years 2001 to 2005. Variability in the individual Weibull parameters was comparable at 3.31% in the scale parameter, and 3.99% in the shape parameter. The variability

		Proportional change in b applied				
		$\frac{1}{10}\times$	$\frac{1}{2}\times$	$1\times$	$2\times$	$3\times$
b	2	0.2	0.5	2	4	6
k	1.9	0.75	1.27	1.91	3.19	4.47
		Proportional change in $\overline{U_{eff}}$ resulting from change in b				
$\overline{U_{eff}}$	1.24	0.29×	0.75×	1×	1.35×	1.69×

Table B.3: Sensitivity of $\overline{U_{eff}}$ to variations in the Weibull scale parameter b. When b is changed, k changes in a near linear fashion. The resulting change in $\overline{U_{eff}}$ is strongly damped, limiting sensitivity to the Weibull parameters while the linear correlation between b and k applies.

Year	Weibull Parameters		Mean ann.	U_{eff}	$10\%ile$	$90\%ile$
	b	k	U (m/s)	(m/s)	U_{eff}	U_{eff}
2001	2.16	2.13	1.91	4.19	3.55	4.86
2002	2.23	2.20	1.98	4.22	3.59	4.87
2003	2.33	2.0	2.03	4.76	3.99	5.55
2004	2.29	2.12	2.02	4.44	3.76	5.15
2005	2.26	2.06	2.01	4.51	3.8	5.25
Mean	2.25	2.11	2.00	4.4	3.72	5.11
CoV	3.31%	3.99%	3.34%	5.96%	5.41%	6.41%
Max variation	4.19%	5.40%	4.21%	8.06%	7.21%	8.74%

Table B.4: Wind speed statistics and $\overline{U_{eff}}$ predictions from the Duke Forest Hardwood Stand, 2001-2005.

in the predicted values of $\overline{U_{eff}}$ exceeded that of the variability in the mean wind speeds at 5.96%, with similar levels of variability in the 10th percentile estimates of (5.41%) and the 90th percentile estimates (6.41%).

The data from the grass clearing at Duke Forest were used to parameterise the case study for forest edge conditions and to gain an initial understanding of inter-annual variability. The annual average of the half hourly Duke Forest grass clearing wind speed data had a coefficient of variation of 3.46% across the years 2001 to 2005. Variability in the individual Weibull parameters was comparable at 3.28% in the scale parameter, and 4.95% in the shape parameter. The variability in the predicted

Year	Weibull Parameters		Mean ann.	U_{eff}	$10\%ile$	$90\%ile$
	b	k	U (m/s)	(m/s)	U_{eff}	U_{eff}
2001	1.70	1.91	1.50	3.63	3.02	4.26
2002	1.82	1.74	1.62	4.21	3.45	5.00
2003	1.82	1.74	1.62	4.21	3.46	5.01
2004	1.76	1.76	1.57	4.04	3.32	4.79
2005	1.77	1.75	1.58	4.08	3.35	4.84
Mean	1.77	1.78	1.58	4.03	3.32	4.78
CoV	3.28%	4.59%	3.46%	6.82%	6.16%	7.33%
Max variation	8.32%	8.20%	8.32%	14.12%	13.06%	14.96%

Table B.5: Wind speed statistics and $\overline{U_{eff}}$ predictions from the Duke Forest Grass Clearing, 2001-2005.

values of exceeded that of the variability in the mean wind speeds at 6.82%, with similar levels of variability in the 10th percentile estimates of $\overline{U_{eff}}$ (6.16%) and the 90th percentile estimates (7.33%) (Table B.3).

Across both sites, the inter-annual variability in the annual mean wind speed was low compared to hourly variability at around 3.5%. The inter-annual variability in $\overline{U_{eff}}$ was greater than that of the mean wind speed, reflecting the sensitivity of the logistic-WALD model (and thus U_{eff}) to the shape of the distribution. Overall, however, variability in wind statistics observed at inter-annual timescales was low.

The Duke Forest wind data were also used to compute an estimate of the value of θ ($\sigma_w/\overline{U}$). Typically the ratio of σ_w/U^* (where U^* is the shear velocity) above a forested canopy is ≈ 1.2. The ratio of $\overline{U}$ to U^* is typically 3.3, giving a reasonable estimation of θ as 0.36 [Katul et al., 1998, Raupach et al., 1996].

B.5 Sensitivity analysis of semi-analytical model

A sensitivity analysis on the semi-analytical model was undertaken by considering a null case and then reducing and increasing individual parameters by appropriate factors while all other parameters were held constant. r, α and $\overline{U}$ (which can be

		Change in c when WALD parameters changed				
	Original value	$\frac{1}{100}\times$	$\frac{1}{10}\times$	$1\times$	$10\times$	$100\times$
r	7.78 kg/yr	0.2	0.5	2	4	6
α	0.01	0.75	1.27	1.91	3.19	4.47
$\overline{U}$	2.9 m/s	$0.01\times$	$0.1\times$	$1\times$	$10.00\times$	$100.00\times$
		$\frac{1}{10}\times$	$\frac{1}{2}\times$	$1\times$	$2\times$	$10\times$
V_t	1.6 m/s	$99.19\times$	$3.98\times$	$1\times$	$0.25\times$	$0.02\times$
x_{3r}	11.9 m	$0.99\times$	$0.99\times$	$1\times$	$1.02\times$	$1.63\times$
h	17 m	$0.16\times$	$0.51\times$	$1\times$	$1.99\times$	$9.92\times$
		$\frac{1}{100}\times$	$\frac{1}{10}\times$	$1\times$	$2\times$	$3\times$
$\sigma_w/\overline{U}$	0.4 m	$0.042\times$	$0.10\times$	$1\times$	$2.0\times$	$3.0\times$

Table B.6: Sensitivity analysis of the vegetation front speed to scaling of individual parameters.

considered as equivalent to $\overline{U}_{eff}$ for the analytical model, as this is the wind forcing used), which can conceivably range over large values, at least between species, were increased and decreased by factors of 10 and 100. Physiological parameters z_r, h and V_t which cannot realistically vary over such a large range were increased and decreased by factors of 2 and 10, and the ratio, $\sigma_w/\overline{U}$ which could not realistically take values significantly larger than 1 was reduced by factors of 100 and 10, and increased by factors of 2 and 3. For all cases, the resulting change in the predicted wave speed was computed. For instance a 100 fold decrease in the α parameter from the null case resulted in only a 2% decline in the wave speed. Note that nonlinear interactions between parameters have not been evaluated, and the results of this sensitivity analysis are expected to apply locally to the parameters listed above. These logistic-WALD parameters are those used to model the movement of *Fraxinus pennsylvanica*, which represented a 'mean' case for the species considered, and thus should be appropriate for considering the sensitivity of model for a range of tree species.

The results of the sensitivity analysis are largely intuitive. The linear implications of the growth rate, the wind speed, the canopy height or the variation in vertical wind

speed on the outcome of the biomass wave front speed follow from the linear nature of the processes they describe. Nonlinearities in Vt can be understood physically as the limiting behaviour as $V_t \rightarrow 0$ and as $Vt >> \overline{U}$. As $V_t \rightarrow 0$, the flight times of seeds approach an unrealistic "infinitely long" limit; resulting in huge increases in dispersion length and migration speed. As $V_t >> \overline{U}$ the seeds become insensitive to turbulent uplift and fall ballistically, confining dispersion to the immediate area of the parent and drastically slowing migration, as shown previously. The nonlinearities associated with the seed release height are similar to those associated with the terminal velocity - as the release height declines the kernel moves into a ballistic regime, although higher release heights do not change gravitational responses. In both cases the nonlinearity relates to a change in the dominant processes affecting the shape of the kernel. The most significant nonlinearity is in the α parameter. Intuitively we would expect that the fewer seeds survive, the slower the wave speed should be. The limited sensitivity to α was confirmed with numerical simulations but appears to confound intuition. The resolution lies in consideration of the asymptotic nature of the predicted wave speeds. In a continuous model, arbitrarily low survival values do not prevent biomass establishment at the periphery of the travelling wave, but rather reduce the amount of biomass that initially establishes. Once established, this biomass grows logistically, such that the difference in established biomass at a given outlying position between two models with different a values is eroded rapidly. Ultimately, decreasing α results in a slower approach to the asymptotic wave speed, but does not greatly impact the value of the wave speed itself. This is significant in that the a parameter is not straightforward to parameterise and that values of less than 1×10^{-6} tend to require the root finding algorithm to evaluate numbers smaller than the limit of precision for many computers. However at the half hourly timescale a will always be low, certainly lower than 1×10^{-4}. If a large decrease in α results in only a small decrease in the resulting wave speed, then there is less

need for robust parameterisation of α by comparison to the more significant determinants of the wave speed. In contrast to the results obtained by Clark et al. [2001], this allows us to recover the Holocene expansion speeds without having to assume an unrealistically high seed survival. Provided there is a sufficiently long lead time to allow the asymptotic wave speed to be reached, appropriate expansion rates are obtained even for arbitrarily small values of α.

Appendix C

Dispersal kernels and implications for linear stability analysis

This Appendix provides further detail regarding the model limitations, the shape of the dispersion kernels, interpretation of the linear stability analysis and derivation of the dispersion relation.

C.1 Model limitations - process and timescale considerations

The model used is a simplified description of the biology, ecology and hydrology of water-limited ecosystems. Given the essentially "infinite" complexity of a real system, a critique of such a simple model can be carried on indefinitely. We confine this critique to the most salient limitations of the Rietkerk model, which essentially amount to limitations in the process descriptions adopted, and the consequences of a deterministic representation of truly stochastic drivers, particularly rainfall. The plant physiology is simplified, treating growth as a function of water availability only (a reasonable but inexact approximation in arid ecosystems because of the instantaneous linkages between photosynthesis and water availability); and all parameters are

treated as constant in space and time, generating results representing mean responses over long timescales. The hydrology represented in the model is also primitive, relying upon a representation of both surface and soil water movement as diffusion. These representations are not strictly realistic, but given that infiltration and plant uptake are of interest rather than the precise routing of the flow to the plant, the simple representation is perhaps suitable at the biomass timescale. The model is continuous in space and time, and represents deterministic processes dependent upon the mean environmental conditions. As such it omits temporal variability, and cannot represent the stochastic nature of many important processes in arid ecosystem (e.g. rainfall). This approach, however, captures the trends at long timescales, and allows an evaluation of their effects in isolation from transient processes, which given the large separation of timescales between the surface water transport and the biomass response is reasonable. Furthermore, adopting a quasi-steady-state approximation and linearizing the equations, the time averaged biomass response can be shown predicted by the time averaged rainfall (see Linearisation of the surface water terms, below).

C.2 Linearization of the surface water term

The scale separation between the surface water response time and the biomass/soil water response time in the Rietkerk model can be evaluated in the diffusive framework by the ratio of $Do : Dp(1000)$, and in the dispersive framework by $D_o/\phi\sigma\left(\vartheta\right)$, where is the standard deviation of the dispersal kernel. Taking an upper limit of $\sigma\left(\vartheta\right) = 100$, the ratio can then be evaluated as: $100/0.25$ or ≈ 400. This large scale separation suggests that at steady state, changes in the surface water terms occur so rapidly in comparison to the biomass and soil moisture terms, as to allow the surface water to be approximated as stationary during biomass growth. The linearised equations are time averaged from the fast scales of overland flow (minutes) to the slower timescales of

biomass response (annual), with the aim of investigating how fluctuations in rainfall about the mean are propagated into the biomass evolution equation, and under what conditions it is reasonable to approximate the temporally variable rainfall by its long-term mean state for arriving at stationary patterns. Consider the model equations, reproduced here for convenience, at steady state. In this case, the rapid response of the surface water allows the approximation $\partial O/\partial t = 0$ to be made:

$$\begin{aligned}
\frac{\partial P}{\partial t} &= cg_{max}\frac{W}{W+k_1}P - dP + D_p\Delta P \\
\frac{\partial W}{\partial t} &= \alpha O\frac{P+k_2W_o}{P+k_2} - g_{max}\frac{W}{W+k_1}P - r_wW + D_w\Delta W \\
0 &= R - \alpha O\frac{P+k_2W_o}{P+k_2} + D_o\Delta O
\end{aligned} \tag{C.1}$$

That is:

$$O = \frac{1}{\alpha}\left(R + D_o\Delta O\right)\left(\frac{P+k_2}{P+k_2W_o}\right). \tag{C.2}$$

Note that P is plant biomass, gm^{-2}, W is the soil water depth, mm and O the surface water depth in mm. Hence, at steady state, changes in biomass occur much more slowly than changes in the surface water budget, and the multiplier can be considered to be constant, κ so that O is linearly forced by rainfall:

$$O = \frac{1}{\alpha}\left(R + D_o\Delta O\right)\kappa. \tag{C.3}$$

Substituting Equation C.2 into the steady state W equation allows the simplification:

$$\frac{\partial W}{\partial t} = (R + D_o \Delta O) - g_{max} \frac{W}{W + k_1} P - r_w W + D_w \Delta W \tag{C.4}$$

suggesting that the response of W to rainfall forcing is also linear. This approach removes one of the key nonlinearities but a further linearization step is necessary to treat the plant water uptake term $W/\left(W + k_1\right) P$. Performing Reynolds decomposition on this term yields

$$\frac{\overline{W} + W'}{\overline{W} + W' + k_1} \left(\overline{P} + P'\right), \tag{C.5}$$

where primed quantities are excursions from the temporal average indicated by an overbar. When the fluctuations in soil moisture are small by comparison to k_1 (a reasonable assumption as the maximum steady state soil moisture is typically on the order of k_1), and upon time averaging this term, we obtain:

$$\overline{\left(\frac{W}{W + k_1} P\right)} \approx \frac{\overline{WP}}{\overline{W} + k_1} \left(1 + \frac{\overline{W'P'}}{\overline{WP}}\right) = \frac{\overline{WP}}{\overline{W} + k_1} \left(1 + R_{W,P} \frac{\sigma_w}{\overline{W}} \frac{\sigma_P}{\overline{P}}\right), \tag{C.6}$$

where σ is the standard deviation, and $R_{W,P} \in [0, 1]$ is the correlation coefficient between rainfall and soil moisture variability (positive in this case). Hence, a necessary condition for using only mean annual rainfall in biomass models is that:

$$R_{W,P} \frac{\sigma_w}{\overline{W}} \frac{\sigma_P}{\overline{P}} << 1 \tag{C.7}$$

Given that $R_{W,P} \approx 1$ in arid ecosystems, the condition above is reasonable if the coefficients of variation in rainfall and soil moisture do not exceed 30% each.

C.3 Linear stability analysis and the dispersion relation

The analysis follows the methods used by HilleRisLambers et al. [2001] and is not reproduced in full here. The pertinent steps may be summarised as:

- Nondimensionalise the model equations
- Recognise that the timescales of surface water transport are 103 times greater than biomass or soil water response, thus at long timescales a pseudo-steady state approximation can be applied (i.e. $\partial 0/\partial t = 0$).
- Determine the steady state solution(s) and apply a periodic perturbation.
- By the pseudo-steady state approximation, the growth in the perturbation of the surface water can also be taken as zero
- Use this approach to contract the system of 3 equations to 2 ODES describing the growth of the perturbations in the soil and biomass terms.

Before proceeding two points must be noted: this procedure does not allow us to define the dispersion relation and so determines conditions for pattern formation, but it does not identify the most rapidly growing modes; secondly most of the pattern formation that is important in this model arises due to nonlinear instabilities, and these results should be treated as indicative only of the impact of replacing a diffusive term with a dispersion term. In this analysis, we examine the case of the bare soil steady state. Performing a similar analysis at the vegetated state fails to reveal significant differences between the dispersion and diffusion approaches, again suggesting that the nonlinear instabilities are principally responsible for the changes in pattern behaviour.

In one dimension, perturbations in the biomass and soil water terms are given by:

$$\epsilon(x,t) = \epsilon(t)\cos(qx), \quad \text{Biomass} \tag{C.8}$$
$$\psi(x,t) = \psi(t)\cos(qx), \quad \text{Soil Water}$$

Here q represents the wavenumber of the perturbations. Linearising around the steady states by taking $P = P + \epsilon(t)$ and $W = W + \psi(t)$ and using the pseudo-steady state approximation, an expression for the growth of the perturbations is obtained:

$$\frac{\partial \epsilon(t)}{\partial t} = -\left(D_p q^2\right)\epsilon(t) + \frac{P}{(W+1)^2}\psi(t) \tag{C.9}$$
$$\frac{\partial \psi(t)}{\partial t} = \left(\frac{P}{(W+1)^2} - \frac{P+W_o}{P+1} \times \frac{\left(-O\frac{1-W_o}{P+1}\right)}{\left(-\frac{P+W_o}{P+1} - q^2\right)}\right)\epsilon(t) + \left(-\left(\frac{kP}{(W+1)^2} + r\right) - D_w q^2\right)\psi(t)$$

The Jacobian for this system of equations can be found:

$$J = \begin{bmatrix} -D_p q^2 & \frac{P}{(W+1)^2} \\ -bk + O\frac{1-W_o}{1+P} + O\frac{1-W_o}{1+P^2}\frac{(P+W_o)}{\left(q^2+\frac{P+W_o}{1+P}\right)} & D_w q^2 - r - \frac{kP}{(1+W)^2} \end{bmatrix} \tag{C.10}$$

and conditions for the stability of the steady states in terms of the wavenumber q can be determined based on the typical conditions for stability:

$$Tr(J) < 0 \tag{C.11}$$
$$Det(J) > 0$$

where

$$Tr\left(J\right) = -D_p q^2 + D_w q^2 - r - \frac{kP}{\left(1+W^2\right)}, \tag{C.12}$$

and

$$\begin{aligned} Det\left(J\right) = & -\left(D_p q^2\right)\left(D_w q^2 - r - \tfrac{kP}{(1+W)^2}\right) \\ & -\left(-bk + O\tfrac{1-W_o}{(1+P)^2}\tfrac{P+W_o}{\left(q^2+\frac{P+W_o}{1+P}\right)}\right)\left(\tfrac{P}{(W+1)^2}\right). \end{aligned} \tag{C.13}$$

We are interested in cases where pattern formation occurs, which implies that one of the inequalities for stability must be compromised. Considering the case of bare soil as a starting point, and using the parameters that have been used throughout the modelling study with $d/R = 0.23$ (although note that for this steady state the stability analysis is essentially independent of R);

$$\begin{aligned} Tr\left(J\right) &= -0.4 \\ Det\left(J\right) &= -\frac{q^2 = \left(-0.4 + \frac{q^2}{2500}\right)}{2500} \end{aligned} \tag{C.14}$$

Thus the condition on the trace is always met, and modes grow when the determinant changes sign as q increases past 31.6. By contrast, if we replace the biomass diffusion term with a dispersion term, then the term $-D_p q^2$ is replaced by $\phi\left(FT\left(q\right)\right)$, where $FT\left(q\right)$ represents the one-dimensional Fourier transform of the dispersion kernel. For the case where the kernel can be approximated by a square wave, the Fourier transform is:

$$FT\left(q\right)=ie^{-i(c_1+c_2)q}\left(-e^{ic_1q}+e^{ic_2q}-e^{i(2c_1+c_2)q}+e^{i(c_1+2c_2)q}\right)\frac{H|c_1-c_2|}{2q|c_1-c_2|}. \quad \text{(C.15)}$$

where c_1 and c_2 can be taken as $dx/2$ and $3dx/2$, or 1 and 3 for the case modelled in this paper ($dx = 2$), and where H represents the Heaviside function. Thus we obtain:

$$Tr\left(J\right)=-\phi FT\left(q\right)+D_wq^2-r-\frac{kP}{\left(1+W\right)^2}, \quad \text{(C.16)}$$

and

$$\begin{aligned} Det\left(J\right)= & -\left(-\phi FT\left(q\right)\right)\left(D_wq^2-r-\tfrac{kP}{(1+W)^2}\right) \quad \text{(C.17)}\\ & -\left(-bk+O\tfrac{1-W_o}{1+P}+O\tfrac{1-W_o}{(1+P)^2}\tfrac{P+W_o}{q^2+\frac{P+W_o}{1+P}}\right)\left(\tfrac{P}{(W+1)^2}\right). \end{aligned}$$

Again taking the no-biomass steady state and the parameters used in this paper, we obtain:

$$Tr\left(J\right)=-0.4+\frac{q^2}{2500}-2.5\times10^{-3}FT\left(q\right) \quad \text{(C.18)}$$

$$Det\left(J\right)=0.01-2.5\times10^{-3}FT\left(q\right)\left(-0.42+\frac{q^2}{2500}\right). \quad \text{(C.19)}$$

Figure C.1 shows that all wave numbers greater than 31.6 are again unstable, now due to the sign change in Tr(J), while additional wavenumbers are introduced due to the oscillations of $Det(J)$. This broadening of the range of linearly unstable wavenumbers is indicative of a general destabilisation of the model to spatially variable perturbations.

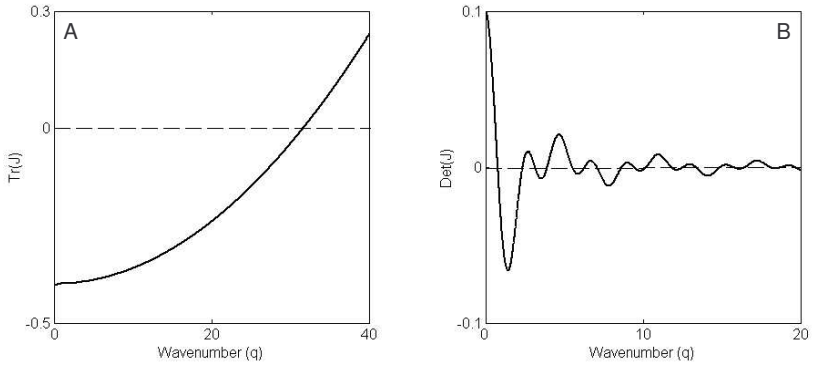

FIGURE C.1: Plot of the trace (A) and determinant (B) of the Jacobian matrix describing the growth of perturbations about the bare soil steady state. By comparison to a constant value of the trace and a single sign change in the determinant with positive wavenumbers obtained for the diffusion situation, the use of the dispersion equation introduces a sign change into the description of the trace, and "spreads" the instability over a wide range of wavenumbers due to the fluctuations in the determinant.

Appendix D

Duke Forest field experiment data

Table D.1: Measured infiltration rate, litter and biomass

	Site	K_{sat} (mm/hr)	**Litter** (g/m^2)	**Biomass** (kg/m^2)
Hardwood Sites	HW1A	4.83	189	7.60
	HW1B	0.91	118	46.1
	HW1C	9.69	301	158
	HW1D	0.30	188	153
	HW2A	Pressure transducer failed	342	82.6
	HW2B	0.61	421	37.1
	HW2C	30.48	299	86.1
	HW2D	11.64	251	3.77
	HW3A	41.50	147	4.3
	HW3B	38.27	178	2.48
	HW3C	9.07	146	1.52
	HW3D	11.05	215	98.2
Pine Sites	P4A	4.3	456	32.1
	P4B	10.0	593	4.4
	P4C	0.55	382	18.2
	P4D	2.98	613	19.2
	P51	8.35	276	8.84
	P5B	11.75	359	7.68
	P5C	12.72	276	30.3

Continued on Next Page...

Table D.1 – Continued

	Site	K_{sat} (mm/hr)	Litter (g/m^2)	Biomass (kg/m^2)
	P5D	1.08	639	19.7
	P61	5.96	281	17.5
	P6B	11.64	315	14.9
	P6C	0.69	465	20.0
	P6D	1.54	909	11.3
Grass Sites	G7A	15.28	56	5.61×10^{-2}
	G7B	9.74	496	0.496
	G7C	34.26	640	0.640
	G7D	5.89	280	0.280
	G8A	6.87	87	8.71×10^{-2}
	G8B	0.61	98	9.76×10^{-2}
	G8C	4.24	159	0.159
	G8D	11.20	65	6.51×10^{-2}
	G9A	15.42	109	0.109
	G9B	34.20	374	0.374
	G9C	1.46	271	0.271
	G9D	2.06	264	0.264

Table D.2: Soil carbon and nitrogen content and bulk density measurements at three depths.

	Site	$\%Carbon(g/g)$			$\%Nitrogen(g/g)$			Bulk Density (g/cm^3)		
		0-5 cm	5-15 cm	15-30 cm	0-5 cm	5-15 cm	15-30 cm	0-5 cm	5-15 cm	15-30 cm
Hardwood Sites	HW1A	3.79	1.86	0.635	0.262	0.117	0.46	0.453	0.756	1.10
	HW1B	2.78	0.80	0.449	0.172	0.498	0.296	0.787	1.20	1.02
	HW1C	3.00	1.00	0.551	0.177	0.665	0.338	0.715	0.993	1.12
	HW1D	Trench Dug								
	HW2A	3.27	1.56	–	0.220	0.115	–	1.32	1.18	–
	HW2B	2.52	1.20	0.607	0.166	0.968	0.440	1.03	1.19	1.23
	HW2C	3.92	1.75	0.686	0.265	0.127	0.466	0.555	0.982	1.09
	HW2D	2.75	1.08	0.567	0.205	0.870	0.397	1.06	1.73	1.23
	HW3A	2.73	0.98	0.474	0.199	0.751	0.318	0.789	1.04	1.18
	HW3B	4.45	1.69	–	0.270	0.115	–	0.574	0.649	–
	HW3C	3.42	1.71	0.904	0.231	0.114	0.604	0.744	0.433	0.812
	HW3D	2.98	0.92	0.524	0.176	0.588	0.41	0.769	0.927	0.924

Continued on Next Page...

Table D.2 – Continued

	Site	$\%Carbon(g/g)$			$\%Nitrogen(g/g)$			Bulk Density (g/cm^3)		
		0-5 cm	5-15 cm	15-30 cm	0-5 cm	5-15 cm	15-30 cm	0-5 cm	5-15 cm	15-30 cm
Pine Sites	P4A	3.05	0.96	–	0.126	0.483	–	0.490	1.13	0.987
	P4B	4.31	1.24	0.582	0.182	0.717	0.393	0.728	1.17	1.148
	P4C	4.03	1.58	0.709	0.194	0.887	0.458	0.589	0.765	1.04
	P4D	4.25	1.21	0.553	0.174	0.695	0.352	0.417	0.723	–
	P5A	3.67	–	–	0.162	–	–	0.550	–	–
	P5B	5.38	1.29	–	0.252	0.829	–	0.636	0.966	–
	P5C	13.6	1.89	0.729	0.300	0.861	0.414	0.330	0.850	1.03
	P5D	Trench Dug								
	P6A	–	1.19	0.544	–	0.677	0.348	–	0.954	0.274
	P6B	3.83	0.94	0.387	0.181	0.577	0.130	0.567	0.822	0.743
	P6C	1.71	2.22	0.434	0.120	0.103	0.295	1.30	0.471	0.824
	P6D	3.84	0.79	0.321	0.159	0.399	0.248	0.536	1.27	1.43
Grass Sites	G7A	2.23	1.32	–	0.170	0.96	–	0.720	1.01	–
	G7B	2.84	1.43	–	0.220	0.114	–	0.747	0.804	–
	G7C	2.31	1.30	–	0.179	0.998	–	0.823	0.841	–
	G7D	2.61	1.07	–	0.184	0.759	–	0.474	0.494	–
	G8A	2.44	1.00	–	0.184	0.759	–	0.795	1.06	–
	G8B	2.59	1.38	–	0.194	0.984	–	0.722	1.00	–
	G8C	2.59	1.38	–	0.194	0.984	–	0.722	1.00	–
	G8D	2.03	1.12	–	0.154	0.751	–	0.804	1.50	–
	G9A	2.34	1.25	–	0.174	0.874	–	0.912	1.10	–
	G9B	Trench Dug								
	G9C	2.72	1.01	0.428	0.202	0.762	0.26	0.958	0.947	1.54
	G9D	–	–	–	–	–	–	–	–	–

Table D.3: Root massses within 5cm cores taken at three different depths

	Site	0-5 cm roots (g)		5-15cm roots (g)		15-30cm roots (g)	
		Fine $< 2mm$	Coarse $> 2mm$	Fine $< 2mm$	Coarse $> 2mm$	Fine $< 2mm$	Coarse $> 2mm$
HW Sites	HW1A	0.414	0.0964	0.237	0.857	0.157	0.305
	HW1B	0.682	0.389	0.542	0.157	0.0976	0.0854
	HW1C	0.687	0.626	0.295	2.65	0.249	0.232
	HW1D	Trench Dug					

Continued on Next Page...

Table D.3 – Continued

	Site	0-5 cm roots (g)		5-15cm roots (g)		15-30cm roots (g)	
		Fine < 2mm	Coarse > 2mm	Fine < 2mm	Coarse > 2mm	Fine < 2mm	Coarse > 2mm
Hardwood Sites	HW2A	1.64	2.67	0.770	0.711	0.129	0
	HW2B	0.875	1.04	0.720	0	0.191	0.948
	HW2C	0.808	0.0837	0.764	1.03	0.194	0.499
	HW2D	1.06	0.142	0.394	1.99	0.109	0.0875
	HW3A	1.02	0	0.450	2.20	0.163	0.148
	HW3B	0.414	0.0940	0.562	6.02	0.111	0.0868
	HW3C	0.742	0.916	0.331	5.06	0.0437	0.404
	HW3D	1.22	0.754	0.466	1.84	0.177	0
Pine Sites	P4A	0.703	0	0.305	0	–	–
	P4B	0.410	1.18	0.480	1.26	0.357	0.440
	P4C	0.974	0.365	0.420	0.0611	0.131	0.0409
	P4D	0.753	1.20	0.449	1.68	–	–
	P5A	–	–	0.635	0.150	–	–
	P5B	0.631	0.0161	–	–	0.288	0.234
	P5C	1.13	0.667	0.548	2.01	0.328	1.12
	P5D	Trench Dug					
	P6A	1.89	0.251	1.11	1.29	0.836	0.272
	P6B	1.89	0.251	1.11	1.29	0.836	0.272
	P6C	0.627	0	0.450	0	0.127	0.0139
	P6D	1.23	0.466	0.812	2.16	0.161	0.0157
Grass Sites	G7A	1.47	0	0.558	0	–	–
	G7B	1.82	0	1.01	0	–	–
	G7C	1.32	0	0.811	0	–	–
	G7D	0.742	0	1.90	0	–	–
	G8A	0.656	0	0.340	0	0.0372	0
	G8B	2.57	0.118	0.950	0	–	–
	G8C	3.55	0	1.21	0	–	–
	G8D	3.01	0	2.44	0	–	–
	G9A	1.71	0.	0670	0.914	0 0.251	0
	G9B	Trench Dug					
	G9C	1.281	0	0.834	0	0.164	0.00310
	G9D	–	–	–	–	–	–

Table D.4: Macropore flux as a percentage of the total flux

	Site	Macropore Flux (as $\%K_{sat}$			Total Macropore Flux
		Small $< 4\mu m$	Medium 4-15 μm	Large $> 15\mu m$	
Hardwood Sites	HW1A	0	2%	5%	7%
	HW1B	10%	12%	13%	36%
	HW1C	3%	4%	6%	13%
	HW1D	0	0	13%	14%
	HW2A	Pressure Transducer Failed			
	HW2B	0	16%	18%	34%
	HW2C	2%	3%	4%	8%
	HW2D	2%	5%	6%	13%
	HW3A	4%	10%	31%	45%
	HW3B	1%	2%	3%	7%
	HW3C	2%	5%	7%	14%
	HW3D	4%	5%	7%	15%
Pine Sites	P4A	0	1%	1%	3%
	P4B	0	4%	7%	12%
	P4C	19%	19%	20%	58%
	P4D	0	0	22%	22%
	P5A	0	0	22%	22%
	P5B	0	16%	17%	33%
	P5C	0	6%	10%	16%
	P5D	0	0	22%	22%
	P6A	0	1%	2%	3%
	P6B	0	14%	17%	31%
	P6C	0	0	22%	22%
	P6D	0	19%	21%	40%
Grass Sites	G7A	7%	7%	9%	22%
	G7B	3%	3%	5%	11%
	G7C	1%	20%	16%	36%
	G7D	10%	16%	17%	43%
	G8A	0	9%	13%	22%
	G8B	0	17%	22%	38%
	G8C	0	11%	15%	26%
	G8D	0	10%	14%	24%
	G9A	0	5%	9%	14%
	G9B	15%	15%	17%	47%
	G9C	0	21%	22%	43%
	G9D	0	0	22%	22%

Table D.5: Soil textural analysis for cores taken at three depths

	Site	Surface			Middle			Depth		
		Sand	Clay	Silt	Sand	Clay	Silt	Sand	Clay	Silt
Hardwood Sites	HW1A	0.49	0.13	0.38	0.54	0.13	0.33	0.48	0.22	0.29
	HW1B	0.47	0.11	0.41	0.61	0.09	0.29	0.59	0.13	0.27
	HW1C	0.47	0.11	0.41	0.61	0.10	0.28	0.58	0.14	0.28
	HW1D	Trench Dug								
	HW2A	0.36	0.18	0.46	0.44	0.13	0.44	–	–	–
	HW2B	0.31	0.15	0.54	0.36	0.14	0.50	0.44	0.17	0.39
	HW2C	0.43	0.10	0.47	0.48	0.12	0.41	0.55	0.20	0.25
	HW2D	0.41	0.11	0.49	0.40	0.14	0.46	0.43	0.18	0.39
	HW3A	0.76	0.10	0.15	0.46	0.11	0.43	0.50	0.16	0.34
	HW3B	0.40	0.11	0.49	0.39	0.12	0.49	–	–	–
	HW3C	0.37	0.11	0.52	0.46	0.12	0.42	0.35	0.31	0.35
	HW3D	0.48	0.09	0.43	0.61	0.10	0.28	0.48	0.27	0.25
Pine Sites	P4A	0.58	0.12	0.30	0.60	0.12	0.29	0.45	0.21	0.34
	P4B	0.55	0.12	0.34	0.56	0.13	0.31	0.44	0.21	0.36
	P4C	0.51	0.11	0.39	0.57	0.12	0.31	0.60	0.14	0.26
	P4D	0.61	0.17	0.23	0.58	0.12	0.30	–	–	–
	P5A	0.59	0.10	0.31	–	–	–	–	–	–
	P5B	0.44	0.10	0.45	0.44	0.12	0.43	–	–	–
	P5C	0.56	0.18	0.25	0.54	0.13	0.33	0.52	0.18	0.30
	P5D	Trench Dug								
	P6A	–	–	–	0.54	0.12	0.33	0.55	0.15	0.29
	P6B	0.50	0.11	0.39	0.54	0.12	0.34	0.50	0.15	0.34
	P6C	0.55	0.12	0.33	0.55	0.13	0.32	0.48	0.16	0.36
	P6D	0.52	0.14	0.34	0.40	0.23	0.38	0.28	0.35	0.37
Grass Sites	G7A	0.50	0.14	0.35	0.58	0.14	0.28	–	–	–
	G7B	0.48	0.14	0.39	0.49	0.15	0.36	–	–	–
	G7C	0.49	0.13	0.38	0.60	0.11	0.30	–	–	–
	G7D	0.55	0.14	0.31	0.58	0.12	0.31	–	–	–
	G8A	0.47	0.13	0.40	0.59	0.12	0.30	–	–	–
	G8B	0.44	0.15	0.41	0.60	0.12	0.28	–	–	–
	G8C	0.44	0.16	0.40	0.53	0.14	0.33	–	–	–
	G8D	0.52	0.12	0.36	0.59	0.12	0.29	–	–	–
	G9A	0.49	0.12	0.39	0.55	0.10	0.35	–	–	–
	G9B	Trench Dug								
	G9C	0.46	0.13	0.41	0.50	0.11	0.39	0.47	0.18	0.36

Continued on Next Page...

Table D.5 – Continued

	Site	Surface			Middle			Depth		
		Sand	Clay	Silt	Sand	Clay	Silt	Sand	Clay	Silt
	G9D	–	–	–	–	–	–	–	–	–

Appendix E

Meta-analysis dataset

Ref #	Loc.	Plot	Precip. (mm)	Biomass (kg/m^2)	Evap. (mm/hr)	Type	Inf. Rate	% Sand	% Silt	% Clay	Source	Notes
1	Edwards Plateau, Tx	Bunchgrass	483	2353	0.32	RS	155	19.2	39.8	41	Blackburn et al. [1992]	Pan evaporation data over 3 years from 1986 - 1987, [Carlson et al., 1990]
2		Sodgrass	483	2353	0.16		126	18.7	41	40.3		
3	Wyoming	0	271	2048	0.05	DR	31	36.75	35.75	27.5	Bowen et al. [2005]	Pan evaporation for 2000-2007, [BoR, 2009]
4		20	271	2048	0.05		37	36.75	35.75	27.5		
5		40	271	2048	0.07		67	36.75	35.75	27.5		
6		60	271	2048	0.08		58	36.75	35.75	27.5		

Continued on Next Page...

Table E.1 – Continued

Ref #	Loc.	Plot	Precip. (mm)	Biomass (kg/m^2)	Evap. (mm/hr)	Type	Inf. Rate	% Sand	% Silt	% Clay	Source	Notes
7	Zimbabwe	1	500	2000	2.36	DR	271	65	10	25	Kelly and Walker [1976]	
8		2	500	2000	1.03		599	85	5	10		
9		3	500	2000	2.26		504	65	10	25		
10		4	500	2000	1.29		584	65	10	25		
11		5	500	2000	2.97		385	65	10	25		
12		6	500	2000	2.60		125	65	10	25		
13		7	500	2000	3.26		263	65	10	25		
14		8	500	2000	1.11		114	65	10	25		
15		9	500	2000	2.33		216	65	10	25		
16	Edwards Plateau, Tx	Oak	557	2353	4.19	RS	202	19	40	41	Hester et al. [1997]	Pan evaporation data over 3 years from 1986 - 1987, [Carlson et al., 1990]
17		Juniper	557	2353	5.45		183	19	40	41		
18		Bunchgrass	557	2353	0.15		146	19	40	41		
19		Shortgrass	557	2353	0.05		105	19	40	41		

Continued on Next Page...

Table E.1 – Continued

Ref #	Loc.	Plot	Precip. (mm)	Biomass (kg/m^2)	Evap. (mm/hr)	Type	Inf. Rate	% Sand	% Silt	% Clay	Source	Notes
20	Zambia	Sesbania	850	1600	0.29	DR	95	44	6	50	Chirwa et al. [2003]	Evaporation data from Wetlands Int. [2007]
21		Gliricidia	850	1600	2.26		44	44	6	50		
22		Leucaena	850	1600	0.24		37	44	6	50		
23		Acacia	850	1600	0.64		55	44	6	50		
24		Ac./Sesb.	850	1600	1.96		71	44	6	50		
25		Gli./Sesb.	850	1600	0.71		119	44	6	50		
26		Leuc./Sesb.	850	1600	0.65		94	44	6	50		
27		Fallow	850	1600	0.24		59	44	6	50		
28	Cameroon	Alley Cropping	1522	1200	0.69	DR	300	63	15	22	Hulugalle and Ndi [1993]	Evaporation data from FAO [2009]
29	Oklahoma	1	571	1800	1.41	RS	265	85	12	03	Rhoades et al. [1964]	Sand data from Lyles [1986]

Continued on Next Page...

Table E.1 – Continued

Ref #	Loc.	Plot	Precip. (mm)	Biomass (kg/m^2)	Evap. (mm/hr)	Type	Inf. Rate	% Sand	% Silt	% Clay	Source	Notes
30	Ethiopia Highlands	Ungrazed(1)	650	1456	0.63	RS	18	31	32	37	Mwendera and Saleem [1997]	Evap. data from Demlie et al. [2007]
31		Ungrazed(2)	650	1456	0.66		13	45	26	29		
32	Oregon, John Day River	Ungrazed(wet)	351	786	0.92	DR	1420	20	65	15	Boone Kauffman et al. [2004]	Evap. data from NOAA [2009b]
33		Ungrazed(dry)	351	786	1.08		810	20	65	15		

Continued on Next Page...

Table E.1 – Continued

Ref #	Loc.	Plot	Precip. (mm)	Biomass (kg/m^2)	Evap. (mm/hr)	Type	Inf. Rate	% Sand	% Silt	% Clay	Source	Notes
34	Alberta	Ungrazed	598	N.A.	1.13	RS	55	N.A.	N.A.	N.A.	Johnston [1962]	No reliable data located
35	Montana	Slick soil	333	1033	0.03	RS	7	N.A.	N.A.	N.A.	Branson et al. [1962]	No reliable soil data
36		Semi-slick soil	333	1033	0.1		25	N.A.	N.A.	N.A.		
37	Germany	84 yo p	620	791	13.97	DR	468	93.7	3.1	3.2	Buczko et al. [2006]	Evap. data from Weisse [2001] Tree density from Rumberger [2004] Wood density from Richter [2006]
38		76 yo p, 34 yo b	620	791	4.31		648	92.8	3.4	3.8		
39		114 yo p, 56 yo b	620	791	9.04		590	91.7	5.4	2.9		
40		91 yo b	620	791	0.80		493	89	6.2	4.8		

Continued on Next Page...

Table E.1 – Continued

Ref #	Loc.	Plot	Precip. (mm)	Biomass (kg/m^2)	Evap. (mm/hr)	Type	Inf. Rate	% Sand	% Silt	% Clay	Source	Notes
41	San Simon Valley, Az	1958, in	350	1903	0.5	DR	296	40	40	20	Castellano and Valone [2007]	Biomass estimated using volumetric allometry [Huenneke, 2001] Evaporation data from NOAA [2009a]
42		1958, out	350	1903	0.48		148	40	40	20		
43		1977, in	350	1903	0.24		330	40	40	20		
44		1977, out	350	1903	0.20		217	40	40	20		
45		1992, in	350	1903	0.19		206	40	40	20		
46		1992, out	350	1903	0.27		186	40	40	20		
47	Burkina Faso	Grass (per.)	850	2504	0.02	RS	138	32	29	40	Rietkerk et al. [2000]	Biomass data estimated based on measurements provided in paper. A linear regression through these measurements (n=3) and forced to intercept at zero was used to extrapolate ground cover to biomass
48		Grass (per.)	850	2540	0.08		258	32	29	40		
49		Grass (per.)	850	2540	0.15		245	32	29	40		
50		Grass (per.)	850	2540	0.19		349	32	29	40		
51		Grass (per.)	850	2540	0.33		312	32	29	40		
52		Grass (per.)	850	2540	0.39		292	32	29	40		
53		Grass (per.)	850	2540	0.52		368	32	29	40		
54		Grass (ann.)	850	2540	0.00		33	31	28	40		
55		Grass (ann.)	850	2540	0.00		40	31	28	40		
56		Grass (ann.)	850	2540	0.01		73	31	28	40		
57		Grass (ann.)	850	2540	0.02		71	31	28	40		
58		Grass (ann.)	850	2540	0.02		40	31	28	40		
59		Grass (ann.)	850	2540	0.02		45	31	28	40		
60		Grass (ann.)	850	2540	0.03		67	31	28	40		

Continued on Next Page...

Table E.1 – Continued

Ref #	Loc.	Plot	Precip. (mm)	Biomass (kg/m^2)	Evap. (mm/hr)	Type	Inf. Rate	% Sand	% Silt	% Clay	Source	Notes
61	Burkina Faso	Grass (ann.)	850	2540	0.08		74	31	28	40	Rietkerk et al. [2000]	
62		Grass (ann.)	850	2540	0.11		50	31	28	40		
63		Grass (ann.)	850	2540	0.15		61	31	28	40		
64		Grass (ann.)	850	2540	0.19		103	31	28	40		
65		Grass (ann.)	850	2540	0.19		54	31	28	40		
66		Grass (ann.)	850	2540	0.19	RS	45	31	28	40		
67		Grass (ann.)	850	2540	0.27		59	31	28	40		
68		Grass (ann.)	850	2540	0.29		59	31	28	40		
69		Grass (ann.)	850	2540	0.40		106	31	28	40		
70		Grass (ann.)	850	2540	0.52		30	31	28	40		
71		Grass (ann.)	850	2540	0.58		82	31	28	40		
72		Grass (ann.)	850	2540	0.74		217	31	28	40		
73	Ecuador, Jadan Catchment	Degraded	810	750	0.06		28	52	30	18	Molina et al. [2007]	Evaporation data from [Millán et al., 2008] Allometric data from [Guglielmini, 2002] [Mamolos, 2006] [Schippers, 2000] [Lush, 1990]
74		Degraded	810	750	0.14		39	53	33	14		
75		Degraded	810	750	0.02		32	9	41	50		
76		Degraded	810	750	0.02		30	7	41	52		
77		Degraded	810	750	0.01		23	60	30	10		
78		Degraded	810	750	0.01		7	60	33	7		
79		Degraded	810	750	0.00	RS	20	28	46	26		
80		Degraded	810	750	0.12		30	21	55	24		
81		Degraded	810	750	0.02		15	45	36	19		
82		Degraded	810	750	0.05		27	46	31	23		
83		Degraded	810	750	0.03		21	50	37	13		
84		Degraded	810	750	0.05		8	32	39	29		
85		Degraded	810	750	0.01		8	48	40	12		

Continued on Next Page...

Table E.1 – Continued

Ref #	Loc.	Plot	Precip. (mm)	Biomass (kg/m^2)	Evap. (mm/hr)	Type	Inf. Rate	% Sand	% Silt	% Clay	Source	Notes
86	Ecuador, Jadan Catchment	Degraded	810	750	0.15		36	44	28	28	Molina et al. [2007]	
87		Degraded	810	750	0.11		31	33	36	31		
88		Degraded	810	750	0.07		9	51	26	23		
89		Degraded	810	750	0.03		12	12	53	35		
90		Degraded	810	750	0.00		17	8	82	10		
91		Degraded	810	750	0.07		6	31	44	25		
92		Degraded	810	750	0.05		21	26	42	32		
93		Degraded	810	750	0.05		24	24	50	26		
94		Degraded	810	750	0.01		37	59	26	15		
95		Degraded	810	750	0.01		35	54	28	18		
96		Degraded	810	750	0.00		15	40	32	28		
97		Degraded	810	750	0.00		10	40	32	28		
98		Degraded	810	750	0.01	RS	6	39	28	33		
99		Degraded	810	750	0.12		36	25	32	43		
100		Degraded	810	750	0.00		10	33	38	29		
101		Degraded	810	750	0.05		10	37	38	25		
102		Degraded	810	750	0.00		10	36	34	30		
103		Degraded	810	750	0.00		14	36	32	32		
104		Degraded	810	750	0.00		22	36	32	32		
105		Degraded	810	750	0.00		18	36	32	32		
106		Degraded	810	750	0.00		14	15	34	51		
107		Degraded	810	750	0.00		14	56	22	22		
108		Degraded	810	750	0.06		25	21	34	45		
109		Degraded	810	750	0.00		20	36	26	38		
110		Degraded	810	750	0.00		13	36	26	38		

Continued on Next Page...

Table E.1 – Continued

Ref #	Loc.	Plot	Precip. (mm)	Biomass (kg/m^2)	Evap. (mm/hr)	Type	Inf. Rate	% Sand	% Silt	% Clay	Source	Notes
111		Degraded	810	750	0.00		23	36	26	38		
112	Tarong Mine Qld	1	776	1606	0.02	RS	10	61	12	27	Loch [2000]	Met data from [ABoM, 2009] Biomass estimates made from a total standing biomass estimate for the site and multiplied by the proportionof veg. cover in the plots
113		2	776	1606	0.03		17	61	12	27		
114		3	776	1606	0.16		27	61	12	27		
115		4	776	1606	0.18		21	61	12	27		
116		5	776	1606	0.27		35	61	12	27		
117		6	776	1606	0.28		43	61	12	27		
118		7	776	1606	0.34		58	61	12	27		
119		8	776	1606	0.37		58	61	12	27		
120		9	776	1606	0.70		54	61	12	27		
121		10	776	1606	0.73		89	61	12	27		
122	Andes (Ecuador)	1B	4100	750	26.85	DR	20	40	40	20	Harden and Scruggs [2003]	Evap. data from [Millán et al., 2008] allometry from Baker et al. [2004]
123		1B	4100	750	26.85		23	40	40	20		
124		1B	4100	750	26.85		36	40	40	20		
125		1B	4100	750	26.85		38	40	40	20		
126		1B	4100	750	26.85		41	40	40	20		
127		1B	4100	750	26.85		55	40	40	20		
128		1B	4100	750	26.85		79	40	40	20		
129		1B	4100	750	26.85		120	40	40	20		
130		2B	4100	750	26.85		27	40	40	20		
131		2B	4100	750	26.85		35	40	40	20		
132		2B	4100	750	26.85		47	40	40	20		
133		2B	4100	750	26.85		70	40	40	20		
134		2B	4100	750	26.85		127	40	40	20		
135		5B1	4100	750	26.85		8	40	40	20		

Continued on Next Page...

Table E.1 – Continued

Ref #	Loc.	Plot	Precip. (mm)	Biomass (kg/m^2)	Evap. (mm/hr)	Type	Inf. Rate	% Sand	% Silt	% Clay	Source	Notes
136	Andes (Ecuador)	5B2	4100	750	26.85	DR	88	40	40	20	Harden and Scruggs [2003]	
137		5B3	4100	750	26.85		98	40	40	20		
138		5B4	4100	750	26.85		59	40	40	20		
139		3B1	4100	750	26.85		82	40	40	20		
140		3B2	4100	750	26.85		125	40	40	20		
141		3B3	4100	750	26.85		136	40	40	20		
142		3B4	4100	750	26.85		156	40	40	20		
143		3B5	4100	750	26.85		156	40	40	20		
144		4B1	4100	750	26.85		77	40	40	20		
145		4B2	4100	750	26.85		86	40	40	20		
146		4B3	4100	750	26.85		175	40	40	20		
147		4B4	4100	750	26.85		206	40	40	20		
148	Southern Appalachians	C12.12 DF	1360	875	12.80	DR	98	20	60	20	Harden and Scruggs [2003]	Evap. data from [TVA, 2007] Biomass estimates from [Sollins, 1972] and [Johnson, 1987] references site specific to Oak Ridge
149		C12.13 DF	1360	875	12.8		66	20	60	20		
150		C12.22 DF	1360	875	12.8		73	20	60	20		
151		C12.23 DF	1360	875	12.8		74	20	60	20		
152		C12.14 DF	1360	875	12.8		76	20	60	20		
153		C12.15 DF	1360	875	12.8		109	20	60	20		
154		C12.24 DF	1360	875	12.8		93	20	60	20		
155		C12.25 DF	1360	875	12.8		59	20	60	20		
156		7.1.12 DF	1360	875	12.8		44	20	60	20		
157		7.1.13 DF	1360	875	12.8		84	20	60	20		
158		7.1.21 DF	1360	875	12.8		26	20	60	20		
159		7.1.23 DF	1360	875	12.8		61	20	60	20		
160		7.1.24 DF	1360	875	12.8		56	20	60	20		

Continued on Next Page...

Table E.1 – Continued

Ref #	Loc.	Plot	Precip. (mm)	Biomass (kg/m^2)	Evap. (mm/hr)	Type	Inf. Rate	% Sand	% Silt	% Clay	Source	Notes
161	Southern Appalachians	7.2.11 DF	1360	875	12.8	DR	84	20	60	20	Harden and Scruggs [2003]	
162		7.2.23 DF	1360	875	12.8		75	20	60	20		
163		7.3.1 G	1360	875	0.24		89	20	60	20		
164		7.3.12 G	1360	875	0.24		40	20	60	20		
165		7.3.13 G	1360	875	0.24		27	20	60	20		
166		7.3.22 G	1360	875	0.24		33	20	60	20		
167		7.4.11 DF	1360	875	12.8		107	20	60	20		
168		7.4.12 DF	1360	875	12.8		95	20	60	20		
169		7.4.21 DF	1360	875	12.8		71	20	60	20		
170		7.4.22 DF	1360	875	12.8		68	20	60	20		
171		wb2.11 DF	1360	875	12.8		94	20	60	20		
172		wb3.11 DF	1360	875	12.8		97	20	60	20		
173		wb3.12 DF	1360	875	12.8		75	20	60	20		
174		bc2.11 PF	1360	875	12.8		24	20	60	20		
175		bc2.12 PF	1360	875	12.8		23	20	60	20		
176		7.3.12 G	1360	875	12.8		31	20	60	20		
177		bc2.22 PF	1360	875	12.8		56	20	60	20		
178		bc3.21 PF	1360	875	12.8		72	20	60	20		
179		bc3.22 PF	1360	875	12.8		48	20	60	20		
180		bc5.11 G	1360	875	12.8		80	20	60	20		
181		bc5.21 G	1360	875	12.8		50	20	60	20		
182		pc1.12 DF	1360	875	12.8		113	20	60	20		
183		pc1.22 DF	1360	875	12.8		43	20	60	20		

Continued on Next Page...

Table E.1 – Continued

Ref #	Loc.	Plot	Precip. (mm)	Biomass (kg/m^2)	Evap. (mm/hr)	Type	Inf. Rate	% Sand	% Silt	% Clay	Source	Notes
184	Luquillo, PR	C.1.01 Col.	3100	2190	20	DR	83	N.A.	N.A.	N.A.	Harden and Scruggs [2003]	Evap. data from
185		C.2.01 Col.	3100	2190	20		1	N.A.	N.A.	N.A.		[Schellekens, 2000]
186		C.1.03 Col.	3100	2190	20		82	N.A.	N.A.	N.A.		Biomass data from
187		C.2.03 Col.	3100	2190	20		29	N.A.	N.A.	N.A.		[Scatena et al., 1993]
188		C.1.04 Col.	3100	2190	20		8	N.A.	N.A.	N.A.		[Weaver, 2000a]
189		C.2.04 Col.	3100	2190	20		51	N.A.	N.A.	N.A.		[Weaver, 2000b]
190		EP.1.01 CF.	3100	2190	8		6	N.A.	N.A.	N.A.		
191		EP.1.02 CF.	3100	2190	8		21	N.A.	N.A.	N.A.		
192		EP.1.03 CF.	3100	2190	8		7	N.A.	N.A.	N.A.		
193		EP.1.04 CF.	3100	2190	8		42	N.A.	N.A.	N.A.		
194		EP.1.05 CF.	3100	2190	8		6	N.A.	N.A.	N.A.		
195		EP.1.06 CF.	3100	2190	8		32	N.A.	N.A.	N.A.		
196		EP.1.07 CF.	3100	2190	8		39	N.A.	N.A.	N.A.		
197		B.1.01 Tab.	3100	2190	30		4	N.A.	N.A.	N.A.		
198		B.2.01 Tab.	3100	2190	30		0	N.A.	N.A.	N.A.		
199		B.1.05 Tab.	3100	2190	30		69	N.A.	N.A.	N.A.		
200		B.1.11a Tab.	3100	2190	30		11	N.A.	N.A.	N.A.		
201		B.1.11b Tab.	3100	2190	30		41	N.A.	N.A.	N.A.		
202		B.1.02 Tab.	3100	2190	30		5	N.A.	N.A.	N.A.		
203		B.2.02 Tab.	3100	2190	30		3	N.A.	N.A.	N.A.		
204		B.1.07b Tab.	3100	2190	30		76	N.A.	N.A.	N.A.		
205		B.2.07b Tab.	3100	2190	30		77	N.A.	N.A.	N.A.		
206		B.1.08 Tab.	3100	2190	30		21	N.A.	N.A.	N.A.		
207		B.1.09 Tab.	3100	2190	30		94	N.A.	N.A.	N.A.		
208		B.2.09 Tab.	3100	2190	30		10	N.A.	N.A.	N.A.		

Continued on Next Page...

Table E.1 – Continued

Ref #	Loc.	Plot	Precip. (mm)	Biomass (kg/m^2)	Evap. (mm/hr)	Type	Inf. Rate	% Sand	% Silt	% Clay	Source	Notes
209	Luq	B.2.10a Tab.	3100	2190	30	DR	83	N.A.	N.A.	N.A.	H&S	
210		B.1.13 Tab.	3100	2190	30		99	N.A.	N.A.	N.A.		
211		B.2.13 Tab.	3100	2190	30		74	N.A.	N.A.	N.A.		
212	Valle de la Joya	Upper Hill	240	2954	0.04	SR	59	N.A.	N.A.	N.A.	Bedford and Small [2008]	Biomass estimates from Huenneke [2001]
213		Middle Hill	240	2954	0.05		49	N.A.	N.A.	N.A.		
214		Lower Hill	240	2954	0.05		25	N.A.	N.A.	N.A.		
215		Upper Fan	240	2954	0.06		80	N.A.	N.A.	N.A.		
216		Middle Fan	240	2954	0.05		82	N.A.	N.A.	N.A.		
217		Lower Fan	240	2954	0.05		86	N.A.	N.A.	N.A.		
218	Sri Lanka	Reforested	2500	1270	60	DR	57	41	41	18	Mapa [1995]	Biomass estimates from [Cordero, 2002] [Freeman et al., 2007] Met data from [Wickramaarachchi, 2004]
219		Grassland	2500	1270	2.32		26	41	41	18		
220		Cultivated	2500	1270	0.32		26	41	41	18		
221	R.H. Spain	1	300	1584	0.1	RS	9	24	61	15	Nicolau 1996	Pan evaporation from [Alvarez et al., 2007]
222		2	300	1584	0.10		22	24	61	15		
223		3	300	1584	0.08		36	42	45	13		
224		4	300	1584	0.08		30	42	45	13		
225		5	300	1584	0.07		19	54	34	12		
226		6	300	1584	0.06		20	54	34	12		

Continued on Next Page...

Table E.1 – Continued

Ref #	Loc.	Plot	Precip. (mm)	Biomass (kg/m^2)	Evap. (mm/hr)	Type	Inf. Rate	% Sand	% Silt	% Clay	Source	Notes
227	Rambla Honda Spain	7	300	1584	0.05	RS	4	41	42	17	Nicolau et al. [1996]	
228		8	300	1584	0.05		11	41	42	17		
229		9	300	1584	0.05		0	34	46	21		
230		10	300	1584	0.06		7	34	46	21		
231		11	300	1584	0.04		0	38	43	19		
232		12	300	1584	0.04		3	38	43	19		
233		13	300	1584	0.01		12	30	47	23		
234		14	300	1584	0.02		11	30	47	23		
235		15	300	1584	0.00		2	27	50	24		
236		16	300	1584	0.01		2	27	50	24		
237		17	300	1584	0.01		11	37	45	18		
238		19	300	1584	0.01		9	37	45	18		
239	Nb Tx Ks Co Wy	–	N.A.	N.A.	0.12	RS	21	30	40	30	Spaeth et al. [1996]	Measurement locations not specified with enough precision to determine ppt or evap. Soil data from [USDA, 2009] Soil series include. Burchard, Olton Martin, Stoneham Kishona Parshall
240		–	N.A.	N.A.	0.39		26	30	40	30		
241		–	N.A.	N.A.	0.05		27	52.2	24.4	23.4		
242		–	N.A.	N.A.	0.18		10	13.5	50	36.5		
243		–	N.A.	N.A.	0.21		19	13.5	50	36.5		
244		–	N.A.	N.A.	0.05		26	13.5	50	36.5		
245		–	N.A.	N.A.	0.13		24	40	40	20		
246		–	N.A.	N.A.	0.09		34	40	40	20		
247		–	N.A.	N.A.	0.05		25	40	40	20		
248		–	N.A.	N.A.	0.67		40	20	65	15		
249		–	N.A.	N.A.	0.12		26	40	40	20		
250		–	N.A.	N.A.	0.12		41	70	20	10		
251		–	N.A.	N.A.	0.22		47	35	35	30		

Continued on Next Page...

Table E.1 – Continued

Ref #	Loc.	Plot	Precip. (mm)	Biomass (kg/m^2)	Evap. (mm/hr)	Type	Inf. Rate	% Sand	% Silt	% Clay	Source	Notes
252		–	N.A.	N.A.	0.09		11	70	20	10		Forkwood
253		–	N.A.	N.A.	0.09		56	60	30	10		Robin, Lonti
254	ND	–	N.A.	N.A.	0.16		33	70	20	10		Taylor's Flat
255		–	N.A.	N.A.	0.14		34	60	30	10		Rhoton et al. [2003]
256	Id	–	N.A.	N.A.	0.14	RS	49	20	65	15		
257		–	N.A.	N.A.	0.16		54	20	65	15		
258	Az	–	N.A.	N.A.	0.09		37	60	30	10		
259		–	N.A.	N.A.	0.23		32	60	30	10		
260	U	–	N.A.	N.A.	0.17		42	60	30	10		
261		–	N.A.	N.A.	0.08		39	60	30	10	Spaeth et al. [1996]	

Appendix F

Heterogeneity in soil properties induced by microtopographic variation

The supplementary material here addresses the effects of correlations between microtopographic variation and variation in soil properties, specifically hydraulic conductivity. It is not intended to provide a complete overview of the impacts of correlations between soil properties and microtopography, but instead provides an illustration of how topographic induced variations in the infiltration parameters may amplify or damped the effects of microtopography discussed in section 5.2. Again these effects are assessed primarily in terms of their impact on partitioning rainfall into overland flow and infiltration. The results are referenced to a background case where the soil properties are constant and microtopography is absent.

F.1 Case 1: variations in infiltration rate with depth

Before commencing with this derivation, a reference frame shown below is considered:

For simplicity, we assume that a deterministic relationship between infiltration capacity and depth can be prescribed in the form:

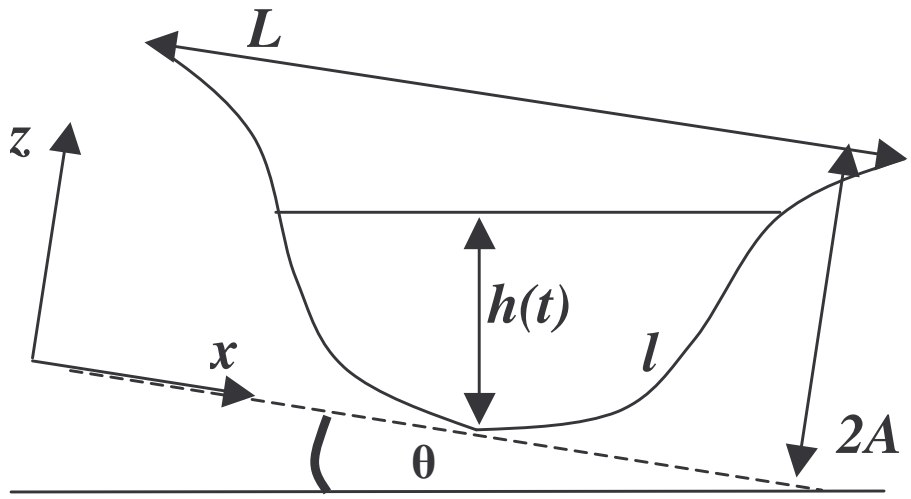

FIGURE F.1: Definition of the reference frame and parameters

$$f_c(t,z) = K_{sat}(z) + \frac{1}{2}\chi_{oM.T.}(t)^{-1/2}, \tag{F.1}$$

such that the infiltration rate after ponding may be approximated by

$$f(t,z) = K_{sat}(z) + \frac{1}{2}\chi_{oM.T.}(t - (t_p(z) - t_{ca}()))^{-1/2}, \tag{F.2}$$

where,

$$t_p(z) = \frac{\chi_o^2}{2IK_{sat}log\left(\frac{I}{I-K_{sat}(z)}\right)}, \tag{F.3}$$

and

$$t_c a\left(z\right) = t\left(\int_0^{t_{ca}(a)} f_c\left(t,z\right)dt = It_p\left(z\right)dz\right), \tag{F.4}$$

It was assumed that the sorptivity does not change with z, but it is a straightforward extension to allow the sorptivity to vary within a depression as well. Given ponding in a depression of arbitrary height h, there are three conditions that need to be considered:

1. Ponded conditions that are submerged by the standing water
2. Ponded conditions 'above' the standing water
3. Non-ponded conditions 'above' the standing water

For condition (1) the time to ponding is determined by the lesser of the time of inundation and the time to ponding computed based on soil properties. The defined condensation time / compression time is then computed based on this time to ponding. These two values are then used to estimate the instantaneous infiltration rate at a point. For condition (2) the time to ponding is determined by soil properties, and is again used to compute the local value of the t_{ca} and f. For condition (3) the time to ponding has not yet been reached and $f = I$.

The change in stored volume in the depression must then be calculated as a local property. At elevations greater than h, the storage volume cannot decline so that:

$$\frac{dV\left(x\right)}{dt} = max\left(0, 1 - f\left(x\right)\right) \tag{F.5}$$

However at elevations less than h the storage volume may be negative, provided it does not entirely drain the stored volume. The total change in volume can then be integrated across the regions and a total change in V computed. For any specified

geometry an expression for the volume in terms of the depth of inundation can be derived such that in general:

$$h = g_2\left(V, A, L, \theta\right) \tag{F.6}$$

$$\frac{dh}{dV} = \frac{dg_2\left(V, A, L, \theta\right)}{dV}$$

The change in ponded depth at any time can then be expressed as:

$$\frac{dh}{dt} = \frac{dV}{dt}\frac{dh}{dV} \tag{F.7}$$

If a peak storage height, hmax is identified then the time for runoff to leave each depression can be identified as tr, defined implicitly as:

$$h_{max} = \int_0^{t_r} \frac{dV}{dt}\frac{dh}{dV}dt \tag{F.8}$$

For the case of a non-tilted depression these expressions can be solve numerically to allow an estimation of the effects of the synchronization to be evaluated. We utilize the same parameters for the base case that were used in the main text, but considered shallower depressions ($A \approx$ 1cm, $\lambda \approx$ 40cm), and $I \approx 3.5 \times 10^{-6}$ m/s, $K_{sat} \approx 1 \times 10^{-6}$ m/s and $\chi_o \approx 3.7 \times 10^{-4}$ m/s$^{1/2}$.

As described in the text, we considered three possibilities:

1. K_{sat} varies around a fixed mean value (K_o), which is adopted at the elevation $z = A$, i.e. $K_{sat} = K_o + \alpha\left(z - A\right)$. In this case, there is limited change in the mean K_{sat} integrated over the depression, and only the distribution of K_{sat} is important.

2. K_{sat} declines from K_o at the peak of the mounds, i.e. where $z = 2A$ to a minimum at $z = 0$, i.e. $K_{sat} = K_o + \alpha\left(z - 2A\right)$. In this case, the mean value

of K_{sat} averaged over the depression is reduced as the minimum K_{sat} (at the base of the depression) is lowered.

3. K_{sat} increases from K_o at the peak of the mounds, i.e. where $z = 2A$ to a maximum at z = 0, i.e. $K_{sat} = K_o - \alpha\,(z - A)$. In this case, the mean value of K_{sat} averaged over the depression is increased as the minimum K_{sat} (at the base of the depression) is lowered.

The strength of the variation in K_{sat} can be measured as a parameter γ where $\gamma = K_{sat}(z = 2A)/K_{sat}(z = 0)$. The effect of γ can then be expressed in terms of the proportion of rainfall that infiltrates in the microtopographic case, normalized by the reference case.

F.2 Case 1. K_{sat} varies around a fixed mean value

In this case, the correlation between microtopography and hydraulic properties has no significant impact upon the partitioning of infiltration and runoff. Across all values of the mean saturated conductivity (K_o) and for cases that range from constant K_{sat} to a 50-fold increase in K_{sat} at the peaks compared to the troughs, the partitioning compared to the background flat case with uniform K_o infiltration rates was unchanged. This suggests that where the correlations of K_{sat} with microtopography preserve the average K_{sat} across the microtopographic depression there is no net affect on partitioning.

F.3 Case 2. K_{sat} declines from a fixed mean value

In this case, the correlation between microtopography and hydraulic properties decreases the proportion of rainfall that infiltrates relative to the case where K_{sat} is constant (i.e. $\gamma = 1$). The sensitivity of the response to changing γ declines with declining K_o. Consequently in regimes where microtopography induces only small

Table F.1: For the case where $K_{sat} = K_o + \alpha\,(z - A)$. Ratio of the proportion of rainfall that infiltrates infiltration in a microtopographic case to that in the flat background case for different levels of contrast of infiltration rate with ponded water depth (γ). No matter how great the contrast in K_{sat} is, the relative partitioning is unchanged.

		$K_o\,(m/s) \times 10^5$									
		6	5	4	3	2	1	0.75	0.5	0.25	0.1
γ	1	1	1	1	1.1	1.2	1.4	1.6	1.8	2.7	5.2
	2	1	1	1	1.1	1.2	1.4	1.6	1.8	2.7	5.2
	5	1	1	1	1.1	1.2	1.4	1.6	1.8	2.7	5.2
	10	1	1	1	1.1	1.2	1.4	1.6	1.8	2.7	5.2
	20	1	1	1	1.1	1.2	1.4	1.6	1.8	2.7	5.2
	50	1	1	1	1.1	1.2	1.4	1.6	1.8	2.7	5.2

Table F.2: For the case where $K_{sat} = K_o + \alpha\,(z - A)$. Effects of changing Γ and K_o on the time to runoff generation from the microtopographically varying surface

		$K_o\,(m/s) \times 10^5$									
		6	5	4	3	2	1	0.75	0.5	0.25	0.1
γ	1	> 1800	> 1800	> 1800	1232	374	218	197	179	164	156
	2	> 1800	> 1800	> 1800	936	375	218	197	179	164	156
	5	> 1800	> 1800	> 1800	630	373	218	197	179	164	156
	10	> 1800	> 1800	> 1800	547	363	218	197	179	164	156
	20	> 1800	> 1800	> 1800	509	354	218	197	179	164	156
	50	> 1800	> 1800	> 1800	488	348	217	196	179	164	156

relative increases in the percentage of rainfall that infiltrates, positive correlations between microtopography and depth may be sufficient to reverse this trend through inducing a decline in the effective (i.e. spatially averaged) K_{sat}. For sufficiently low Ko values, however the importance of the surface storage in delaying runoff increases relative to the importance of infiltration, and sensitivity to γ declines markedly.

F.4 Case 3. K_{sat} increases from a fixed mean value

Here the inverse correlation between microtopography and permeability leads to minimal change in the partitioning of infiltration and runoff in permeable soils, but

Table F.3: For the case where $K_{sat} = K_o + \alpha\,(z - 2A)$. Ratio of the proportion of rainfall that infiltrates infiltration in a microtopographic case to that in the flat background case for different levels of contrast of infiltration rate with ponded water depth (γ). The partitioning is sensitive to γ within the regime where microtopography produces relatively small increases in infiltration c.f. the background case. For highly permeable or impermeable soils, however, the sensitivity is damped.

		$K_o\,(m/s) \times 10^5$									
		6	5	4	3	2	1	0.75	0.5	0.25	0.1
γ	1	1	1	1	1.1	1.2	1.4	1.6	1.8	2.7	5.2
	2	1	1	0.94	0.88	0.95	1.2	1.3	1.6	2.5	5.0
	5	1	0.92	0.78	0.73	0.81	1.0	1.2	1.5	2.3	4.8
	10	0.98	0.86	0.73	0.68	0.76	0.97	1.12	1.4	2.3	4.8
	20	0.94	0.83	0.7	0.66	0.73	0.95	1.09	1.4	2.2	4.7
	50	0.92	0.81	0.69	0.65	0.72	0.93	1.08	1.4	2.2	4.7

Table F.4: For the case where $K_{sat} = K_o - \alpha\,(z - 2A)$. Ratio of the proportion of rainfall that infiltrates infiltration in a microtopographic case to that in the flat background case for different levels of contrast of infiltration rate with ponded water depth (γ). The partitioning is sensitive to γ in less permeable soils.

		$K_o\,(m/s) \times 10^5$									
		6	5	4	3	2	1	0.75	0.5	0.25	0.1
γ	1	1	1	1	1.1	1.2	1.4	1.6	1.8	2.7	5.2
	2	1	1	1	1.2	1.7	1.9	2.0	2.3	3.2	5.7
	5	1	1	1	1.2	1.7	3.3	3.5	3.8	4.7	7.2
	10	1	1	1	1.2	1.7	3.5	4.7	6.2	7.1	9.6
	20	1	1	1	1.2	1.7	3.5	4.7	7.0	11.8	14.5
	50	1	1	1	1.2	1.7	3.5	4.7	7.0	13.9	28.6

marked increases in the proportion of the rainfall that infiltrates in less permeable soils.

Bibliography

ABoM. Climate statistics Kingaroy. `http://www.bom.gov.au/climate/averages/tables/cw_040112.shtml`, 2009. Accessed 21 April 2009.

A. D. Abrahams and A. J. Parsons. Determining the mean depth of overland-flow in field studies of flow hydraulics. *Water Resources Research*, 26(3):501–503, 1990.

M. D. Abrams. Effects of burning regime on buried seed banks and canopy coverage in a Kansas tallgrass prairie. *Southwestern Naturalist*, 33(1):65–70, 1988.

R. Aerts, W. H. Maes, E. November, M. Behailu, J. Poesen, J. Deckers, M. Hermy, and B. Muys. Surface runoff and seed trapping efficiency of shrubs in a regenerating semiarid woodland in Northern Ethiopia. *Catena*, 65(1):61–70, 2006.

M.R. Aguiar and O.E. Sala. Patch structure, dynamics and implications for the functioning of arid ecosystems. *Trends in Ecology and Evolution*, 14(7):273–277, 1999.

H. Akaike. New look at statistical-model identification. *IEEE Transactions on Automatic Control*, 19(6):716–723, 1974.

G. B. Allison and M. W. Hughes. Use of environmental chloride and tritium to estimate total recharge to an unconfined aquifer. *Australian Journal of Soil Research*, 16(2):181–195, 1978.

G. B. Allison, G. W. Gee, and S. W. Tyler. Vadose-zone techniques for estimating groundwater recharge in arid and semiarid regions. *Soil Science Society of America Journal*, 58(1):6–14, 1994.

R.R. Allmaras, R.E. Burwell, W.E. Larson, R.F. Holt, and W.W. Nelson. Total porosity and random roughness of the interrow zone as influenced by tillage. *USDA-ARS Conservation Research Reports*, 7:1–22, 1966.

V. Martinez Alvarez, M. M. Gonzlez-Real, A. Baille, and J. M. Molina Martinez. A novel approach for estimating the pan coefficient of irrigation water reservoirs: application to South Eastern Spain. *Agricultural Water Management*, 92(1-2): 29–40, 2007.

V.J. Anderson and K.C. Hodgkinson. Grass-mediated capture of resource flows and the maintenance of banded mulga in a semi-arid woodland. *Australian Journal of Botany*, 45(2):331–342, 1997.

J. Aronson, J. Kigel, and A. Shmida. Reproductive allocation strategies in desert and mediterranean populations of annual plants grown with and without water-stress. *Oecologia*, 93(3):336–342, 1993.

S. Assouline and Y. Mualem. Modeling the dynamics of seal formation and its effect on infiltration as related to soil and rainfall characteristics. *Water Resources Research*, 33(7):1527–1536, 1997.

S. Assouline and Y. Mualem. Infiltration during soil sealing: The effect of areal heterogeneity of soil hydraulic properties. *Water Resources Research*, 38(12): doi:10.1029/2001wr001168, 2002.

B. Atwell, P. Kriedemann, and C. Turner. *Plants in action*, volume 1. McMillan Education Australia, South Yarra, 1999.

Australian BoM. Intensity - frequency - duration data for Karratha, Western Australia. http://www.bom.gov.au/hydro/has/cdirswebx/cdirsdoc.shtml, 2009. Accessed February 2009.

A. C. W. Baas and J. M. Nield. Modelling vegetated dune landscapes. *Geophysical Research Letters*, 34(6):doi:10.1029/2006GL029152, 2007.

V. Bagarello, M. Iovino, and G. Tusa. Factors affecting measurement of the near-saturated soil hydraulic conductivity. *Soil Science Society of America Journal*, 64 (4):1203–1210, July 1 2000.

R. A. Bagnold. Nature of saltation and of bed-load transport in water. *Proceedings of the Royal Society of London Series A-Mathematical Physical and Engineering Sciences*, 332(1591):473–504, 1973.

P. Bak, C. Tang, and K. Wiesenfeld. Self-organized criticality - an explanation of 1/f noise. *Physical Review Letters*, 59(4):381–384, 1987.

T. R. Baker, O. L. Phillips, Y. Malhi, S. Almeida, L. Arroyo, A. Di Fiore, T. Erwin, N. Higuchi, T. J. Killeen, S. G. Laurance, W. F. Laurance, S. L. Lewis, A. Monteagudo, D. A. Neill, P. N. Vargas, N. C. A. Pitman, J. N. M. Silva, and R. V. Martinez. Increasing biomass in Amazonian forest plots. *Philosophical Transactions of the Royal Society of London Series B - Biological Sciences*, 359(1443): 353–365, 2004.

P. Ball. *The self-made tapestry: pattern formation in nature*. Oxford University Press, Oxford, 2001.

N. Barbier, P. Couteron, J. Lejoly, V. Deblauwe, and O. Lejeune. Self organized vegetation patterning as a fingerpint of climate and human impact on semi-arid ecosystems. *Journal of Ecology*, 94:537–547, 2006.

N. Barbier, P. Couteron, R. Lefever, V. Deblauwe, and O. Lejeune. Spatial decoupling of facilitation and competition at the origin of gapped vegetation patterns. *Ecology*, 89(6):1521–1531, 2008.

G.K. Batchelor. *An Introduction to Fluid Dynamics*, volume 1. Cambridge University Press, New York, 3 edition, 1967.

C. Beck and E. G. D. Cohen. Superstatistics. *Physica A-Statistical Mechanics and Its Applications*, 322(1-4):267–275, 2003.

D. R. Bedford and E. E. Small. Spatial patterns of ecohydrologic properties on a hillslope-alluvial fan transect, central New Mexico. *Catena*, 73(1):34–48, 2008.

S. E. Belcher and J. C. R. Hunt. Turbulent shear flow over slowly moving waves. *Journal of Fluid Mechanics*, 251:109–148, 1993.

S. E. Belcher and J. C. R. Hunt. Turbulent flow over hills and waves. *Annual Review of Fluid Mechanics*, 30:507–538, 1998.

J. Belnap and O.L. Lange. Biological soil crusts: characteristics and distribution. In *Ecological Studies. Biological soil crusts: structure, function, and management*, volume 150 of *Ecological Studies*, pages 3–32. Springer-Verlag New York Inc, 2001.

S.S. Berg and D.L. Dunkerley. Patterned mulga near Alice Springs, central Australia and the potential threat of firewood collection on this vegetation community. *Journal of Arid Environments*, 59(2):313–350, 2004.

G. Bergkamp. A hierarchical view of the interactions of runoff and infiltration with vegetation and microtopography in semiarid shurblands. *Catena*, 33(3-4):201–220, 1998.

B. Berkowitz and R. P. Ewing. Percolation theory and network modeling applications in soil physics. *Surveys in Geophysics*, 19(1):23–72, 1998.

W. H. Blackburn, F. B. Pierson, C.L. Hanson, T.L. Thurow, and A.L. Hanson. The spatial and temporal influence of vegetation on surface soil factors in semiarid rangelands. *Transactions of the ASAE*, 35(2):479–486, 1992.

S.B. Boaler and C.A.H. Hodge. Observations on vegetation arcs in the northern region, Somali Republic. *Journal of Ecology*, 52(3):511–544, 1964.

E. Bochet, J. Poesen, and J.L. Rubio. Mound development as an interaction of individual plants with soil, water erosion and sedimentation processes on slopes. *Earth Surface Processes and Landforms*, 25(8):847–867, 2000.

G. Boedeltje, J. P. Bakker, A. Ten Brinke, J. M. Van Groenendael, and M. Soesbergen. Dispersal phenology of hydrochorous plants in relation to discharge, seed release time and buoyancy of seeds: the flood pulse concept supported. *Journal of Ecology*, 92(5):786–796, 2004.

J. Boone Kauffman, A.S. Thorpe, and E.N.J. Brookshire. Livestock exclusion and belowground ecosystem responses in riparian meadows of Eastern Oregon. *Ecological Applications*, 14(6):1671–1679, 2004.

BoR. Hydromet system for weather station at Seminoe Dam, WY. `www.usbr.gov/gp/hydromet/wswy.cfm`, 2009. Accessed 1 May 2009.

F. Borgogno, P. D'Odorico, F. Laio, and L. Ridolfi. Mathematical models of vegetation pattern formation in ecohydrology. *Reviews of Geophysics*, 47(RG1005):doi: 10.1029/2007RG00256, 2009.

J. M. Bosch and J. D. Hewlett. A review of catchment experiments to determine

the effect of vegetation changes on water yield and evapo-transpiration. *Journal of Hydrology*, 55(1-4):3–23, 1982.

C.K. Bowen, G.E. Shuman, R.A. Olson, and L.J. Ingram. Influence of topsoil depth on plant and soil attributes of 24-year old reclaimed mined lands. *Arid Land Research and Management*, 19:267–284, 2005.

L.J. Bracken and J. Croke. The concept of hydrological connectivity and its contributing to understanding runoff-dominated geomorphic systems. *Hydrological Processes*, 21(13):1749–1763, 2007.

L.J. Bracken and M.J. Kirkby. Differences in hillslope runoff and sediment transport rates within two semi-arid catchments in Southeast Spain. *Geomorphology*, 68 (3-4):183–200, 2005.

A. Branson, R.F. Miller, and I.S. McQueen. Effects of contour furrowing, grazing intensities and soils on infiltration rates, soil moisture and vegetation near Fort Peck, Montana. *Journal of Range Management*, 15(3):151–158, 1962.

A.D. Brede. *Turfgrass cultivars of Zoysia sinica*. U. S. Patent Office, July 1999. Jacklin Seed Company, Patent number 5,977,450.

G. E. Briggs and J. B. S. Haldane. A note on the kinetics of enzyme action. *Biochemical Journal*, 19(2):338–339, 1925.

J. Bromley, J. Brouwer, A. P. Barker, S. R. Gaze, and C. Valentin. The role of surface water redistribution in an area of patterned vegetation in a semi-arid environment, South-West Niger. *Journal of Hydrology*, 198(1-4):1–29, 1997.

Wilifred Brutsaert. *Hydrology, an Introduction*, volume 1. Cambridge University Press, New York, 2005.

B. Buchter, P.O. Aina, A.S. Azari, and D.R Nielsen. Soil spatial variability along transects. *Soil Technology*, 4:297–314, 1991.

U. Buczko, O. Bens, and R. F. Huttl. Water infiltration and hydrophobicity in forest soils of a pine-beech transformation chronosequence. *Journal of Hydrology*, 331 (3-4):383–395, 2006.

M. I. Budyko. *Climate and life*. International geophysics series, 18. Academic Press, New York, 1974.

J. M. Bullock, K. Shea, and O. Skarpaas. Measuring plant dispersal: an introduction to field methods and experimental design. *Plant Ecology*, 186(2):217–234, 2006.

Bureau of Land Management. Cedar mountain wilderness. `http://www.blm.gov/ut/st/en/fo/salt_lake/blm_special_areas/cedar_mountains_wilderness/photo_gallery.html`, 2008. Online resource, accessed April 21 2009.

P.A. Burrough. Multiscale sources of spatial variation in soil. 1. the application of fractal concepts to nested levels of soil variation. *Journal of Soil Science*, 34(3): 577–597, 1983.

J. M. Buttle and D. J. McDonald. Soil macroporosity and infiltration characteristics of a forest podzol. *Hydrological Processes*, 14(5):831–848, 2000.

M. L. Cain, B. G. Milligan, and A. E. Strand. Long-distance seed dispersal in plant populations. *American Journal of Botany*, 87(9):1217–1227, 2000.

M. M. Caldwell, T. E. Dawson, and J. H. Richards. Hydraulic lift: consequences of water efflux from the roots of plants. *Oecologia*, 113(2):151–161, 1998.

F. Canovaro, E. Paris, and L. Solari. Effects of macro-scale bed roughness geometry

on flow resistance. *Water Resources Research*, 43(10):doi:10.1029/2006WR005727, 2007.

D.H. Carlson, T.L. Thurow, R.W. Knight, and R.K. Heitschmidt. Effect of honey mesquite on the water balance of Texas Rolling Plains rangeland. *Journal of Range Management*, 43(6):491–497, 1990.

M. J. Castellano and T. J. Valone. Livestock, soil compaction and water infiltration rate: evaluating a potential desertification recovery mechanism. *Journal of Arid Environments*, 71(1):97–108, 2007.

K.K. Caylor, T.M. Scanlon, and I. Rodriguez-Iturbe. Feasbile optimality of vegetation patterns in river basins. *Geophysical Research Letters*, 31(13):doi: 10.1029/2004gl020260, 2004.

J. C. Chambers and J. A. MacMahon. A day in the life of a seed - movements and fates of seeds and their implications for natural and managed systems. *Annual Review of Ecology and Systematics*, 25:263–292, 1994.

C.L. Chen. Unified theory on power-laws for flow resistance. *Journal of Hydraulic Engineering*, 117:371–389, 1991.

T.S. Chirwa, P.L. Mafongoya, and R. Chintu. Mixed planted-fallows using coppicing and non-coppicing tree species for degraded acrisols in Eastern Zambia. *Agro-forestry Systems*, 59:243–251, 2003.

R. B. Clapp and G. M. Hornberger. Empirical equations for some soil hydraulic-properties. *Water Resources Research*, 14(4):601–604, 1978.

A. Clark, D. R. Phillips, and D. J. Frederick. Weight, volume, and physical-properties of major hardwood species in the Piedmont. *USDA Forest Service Southeastern Forest Experiment Station Research Paper*, SE-255:1–78, 1986.

J. S. Clark. Why trees migrate so fast: confronting theory with dispersal biology and the paleorecord. *American Naturalist*, 152(2):204–224, 1998.

J. S. Clark, C. Fastie, G. Hurtt, S. T. Jackson, C. Johnson, G. A. King, M. Lewis, J. Lynch, S. Pacala, C. Prentice, E. W. Schupp, T. Webb, and P. Wyckoff. Reid's paradox of rapid plant migration - dispersal theory and interpretation of paleoecological records. *BioScience*, 48(1):13–24, 1998.

J. S. Clark, M. Silman, R. Kern, E. Macklin, and J. HilleRisLambers. Seed dispersal near and far: patterns across temperate and tropical forests. *Ecology*, 80(5):1475–1494, 1999.

J. S. Clark, M. Lewis, and L. Horvath. Invasion by extremes: population spread with variation in dispersal and reproduction. *American Naturalist*, 157(5):537–554, 2001.

J. S. Clark, M. Lewis, J. McLachlan, and J. HilleRisLambers. Estimating population spread: what can we forecast and how well? *Ecology*, 84(8):1979–1988, 2003.

J.S. Clark, S. LaDeau, and I. Ibanez. Fecundity of trees and the colonization-competition hypothesis. *Ecological Monographs*, 74(3):415–442, 2004.

M. J. Clauss and D. L. Venable. Seed germination in desert annuals: an empirical test of adaptive bet hedging. *American Naturalist*, 155(2):168–186, 2000.

M. Clos-Arcedue. Étude sur photographices aeriennes d'une formation végétale sahelienne: la brousse tigrée. *Bulletin of the French African Institute*, 18:677–684, 1956.

B. Clothier. Infiltration. In K. Smith and C. Mullins, editors, *Soil and Environmental Analysis*, pages 273–274. Marcel Dekker, New York, 2001.

K. Conradsen, L. B. Nielsen, and L. P. Prahm. Review of Weibull statistics for estimation of wind-speed distributions. *Journal of Climate and Applied Meteorology*, 23(8):1173–1183, 1984.

J. R. Cooper, S. J. Tait, and K. V. Horoshenkov. Determining hydraulic resistance in gravel-bed rivers from the dynamics of their water surfaces. *Earth Surface Processes and Landforms*, 31(14):1839–1848, 2006.

L. D. P. Cordero. Wood specific gravity and aboveground biomass of *Bombacopsis quinata* plantations in Costa Rica. *Forest Ecology and Management*, 165(1-3):1–9, 2002.

A. Cornet, C. Montana, J-P. Delhoume, and J. Lopez-Portillo. *Landscape boundaries: consequences for biotic diversity and ecological flows*, volume 92 of *Ecological Studies*, pages 327–345. Springer, New York, 1 edition, 1992.

M. Cornick, B. Hunt, E. Ott, H. Kurtuldu, and M.F. Schatz. State and parameter estimation of spatiotemporally chaotic systems illustrated by an application to Rayleigh-Benard convection. *Chaos*, 19(1):doi:10.1063/1.3072780, 2009.

M. F. M. Costa. Application of image processing to the characterisation of nanostructures. *Reviews on Advanced Materials Science*, 6(1):12–20, 2004.

P. Coullet. Commensurate - incommensurate transition in nonequilibrium systems. *Physical Review Letters*, 56(7):724–727, 1986.

P. Couteron and K. Kokou. Woody vegetation spatial patterns in a semi-arid savanna of Burkina Faso, West Africa. *Plant Ecology*, 132(2):211–227, 1997.

P. Couteron and O. Lejeune. Periodic spotted patterns in semi arid vegetation explained by a propagation-inhibition model. *Journal of Ecology*, 89:12, 2001.

P. Couteron, A. Mahamane, P. Ouedraogo, and J. Seghieri. Differences between banded thickets (tiger bush) at two sites in West Africa. *Journal of Vegetation Science*, 11(3):321–328, 2000.

I.R. Cowan. *Stomatal behaviour and environment*, volume 4 of *Advances in Botanical Research*. Academic Press, New York, 1978.

I.R. Cowan. Economics of carbon fixation in higher plants. In TJ Givnish, editor, *On the economy of plant form and function*, pages 133–170. Cambridge University Press, Cambridge, 1986.

M. C. Cross and P. C. Hohenberg. Pattern formation out of equilibrium. *Reviews of Modern Physics*, 65:851–1112, 1993.

F. Darboux and C. H. Huang. Does soil surface roughness increase or decrease water and particle transfers? *Soil Science Society of America Journal*, 69(3):748–756, 2005.

F. Darboux, P. Davy, C. Gascuel-Odoux, and C. Huang. Evolution of soil surface roughness and flowpath connectivity in overland flow experiments. *Catena*, 46 (2-3):125–139, 2001.

J. T. Dauer, D. A. Mortensen, and M. J. Vangessel. Temporal and spatial dynamics of long-distance *Conyza canadensis* seed dispersal. *Journal of Applied Ecology*, 44 (1):105–114, 2007.

D. W. Davidson and S. R. Morton. Dispersal adaptations of some acacia species in the Australian arid zone. *Ecology*, 65(4):1038–1051, 1984.

T. E. Dawson. Hydraulic lift and water use by plants - implications for water balance, performance and plant-plant interactions. *Oecologia*, 95(4):565–574, 1993.

V. Deblauwe, N. Barbier, P. Couteron, O. Lejeune, and J. Bogaert. The global biogeography of semi-arid periodic vegetation patterns. *Global Ecology and Biogeography*, 17(6):715–723, 2008.

L.H. Dekker, C.J. Ritsema, K. Oostindie, and O.H. Boersma. Effect of drying temperature on the severity of soil water repellency. *Soil Science*, 163(10):780–796, 1998.

S.C. Dekker, M. Rietkerk, and M.F.P Bierkens. Coupling microscale vegetation-soil water and macroscale vegetation-precipitation feedbacks in semiarid ecosystems. *Global Change Biology*, 13:671–678, 2007.

P. A. Delcourt and H. R. Delcourt. Late-quaternary dynamics of temperate forests - applications of paleoecology to issues of global environmental-change. *Quaternary Science Reviews*, 6(2):129–146, 1987.

J. DeLima, L. Eppink, and W. H. Vandermolen. A kinematic overland-flow model to determine depression storage of tilled surfaces. *Soil and Tillage Research*, 15 (1-2):65–78, 1989.

M. Demlie, T. Ayenew, and S. Wohnlich. Comprehensive hydrological and hydrogeological study of topographically closed lakes in highland Ethiopia: the case of Hayq and Ardibo. *Journal of Hydrology*, 339(3-4):154–158, 2007.

L. Deschodt. Desert pavement. `http://commons.wikimedia.org/wiki/File:Desert_pavement_Myrdalssandur.JPG`, September 2003.

L. Descroix, D. Viramontes, J. Estrada, J. L. G. Barrios, and J. Asseline. Investigating the spatial and temporal boundaries of Hortonian and Hewlettian runoff in Northern Mexico. *Journal of Hydrology*, 346(3-4):144–158, 2007.

J.M. D'Herbes, C. Valentin, D.J. Tongway, and J.C. Leprun. *Banded vegetation patterning in arid and semiarid environments*, volume 149 of *Ecological Studies*, pages 1–19. Springer, New York, 1 edition, 2001.

P. D'Odorico, F. Laio, and L. Ridolfi. Vegetation patterns induced by random climate fluctuations. *Geophysical Research Letters*, 33(19), 2006a.

P. D'Odorico, F. Laio, and L. Ridolfi. Patterns as indicators of productivity enhancement by facilitation and competition in dryland vegetation. *Journal of Geophysical Research-Biogeosciences*, 111(G3), 2006b.

P. D'Odorico, F. Laio, A. Porporato, L. Ridolfi, and N. Barbier. Noise-induced vegetation patterns in fire-prone savannas. *Journal of Geophysical Research-Biogeosciences*, 112(G2), 2007.

S.H. Doerr, R.A. Shakesby, and R.P.D. Walsh. Soil water repellency: its causes, characteristics and hydro-geomorphological significance. *Earth Science Reviews*, 51, 2000.

Dryland Science for Development Consortium Working Group 1. Integrated methods for monitoring and assessing desertification / land degradation processes and drivers (land quality) - draft 1. *United Nations Convention on Combating Desertification*, pages 1–173, 2009.

D. Dunkerley. Hydrologic effects of dryland shrubs: defining the spatial extent of modified soil water uptake rates at an Australian desert site. *Journal of Arid Environments*, 45(2):159–172, 2000.

D. Dunkerley. Systematic variation of soil infiltration rates within and between the components of the vegetation mosaic in an Australian desert landscape. *Hydrological Processes*, 16(1):119–131, 2002a.

D. Dunkerley. Determining friction coefficients for inter-rill flows: the significance of flow filaments and backwater effects. *Earth Surface Processes and Landforms*, 28 (5):475–491, 2003.

D. Dunkerley. Flow threads in surface run-off: implications for the assessment of flow properties and friction coefficients in soil erosion and hydraulics investigations. *Earth Surface Processes and Landforms*, 29(8):1011–1026, 2004.

D.L. Dunkerley. Infiltration rates and soil moisture in a groved mulga community near Alice Springs, arid central Australia: evidence for complex internal rainwater redistribution in a runoff-runon landscape. *Journal of Arid Environments*, 51(2): 199–219, 2002b.

D.L. Dunkerley and K.J. Brown. Banded vegetation near Broken Hill, Australia: significance of surface roughness and soil physical properties. *Catena*, 37(1-2): 75–88, 1999.

T. Dunne, W. H. Zhang, and B. F. Aubry. Effects of rainfall, vegetation, and micro-topography on infiltration and runoff. *Water Resources Research*, 27(9):2271–2285, 1991.

S. Ellner and A. Shmida. Why are adaptations for long-range seed dispersal rare in desert plants? *Oecologia*, 51(1):133–144, 1981.

Kerry A. Emanuel. The dependence of hurricane intensity on climate. *Nature*, 326 (6112):483–485, 1987.

E.J. Ens, J.B. Bremmer, K. French, and J. Korth. Identification of volatile compounds released by roots of an invasive plant, bitou bush, *Chrysanthemoides monilifera* spp. *rotundata*), and their inhibition of native seedling growth. *Biological Invasions*, 11:275–287, 2009.

M. Esteves and J. M. Lapetite. A multi-scale approach of runoff generation in a Sahelian gully catchment: a case study in Niger. *Catena*, 50(2-4):255–271, 2003.

M. Esteves, X. Faucher, S. Galle, and M. Vauclin. Overland flow and infiltration modelling for small plots during unsteady rain: numerical results versus observed values. *Journal of Hydrology*, 228(3-4):265–282, 2000.

FAO. Aquastat: the Food and Agricultural Organization's information system on water and agriculture. Country profile: Cameroon. `http://www.fao.org/nr/water/aquastat/countries/cameroon/indexfra.stm`, 2009. Online source, accessed 21 April 2009.

R. Ferguson. Flow resistance equations for gravel- and boulder-bed streams. *Water Resources Research*, 43(5):doi:10.1029/2006WR005422, 2007.

V. Ferro. Flow resistance in gravel-bed channels with large-scale roughness. *Earth Surface Processes and Landforms*, 28(12):1325–1339, 2003.

F. R. Fiedler and J. A. Ramirez. A numerical method for simulating discontinuous shallow flow over an infiltrating surface. *International Journal for Numerical Methods in Fluids*, 32(2):219–240, 2000.

F.R. Fiedler, G. W. Frasier, J. A. Ramirez, and L. R. Ahuja. Hydrologic response of grasslands: effects of grazing, interactive infiltration, and scale. *Journal of Hydrologic Engineering*, 7(4):293–301, 2002.

J.J. Finnigan and S.E. Belcher. Flow over a hill covered with a plant canopy. *Quarterly Journal of the Royal Meteorological Society*, 130(596):1–29, 2004.

R. A. Fisher. The wave of advance of advantageous genes. *Annals of Eugenics*, 7: 355–369, 1937.

D.M. Fox, Y. Le Bissonais, and P. Quetin. The implications of spatial variability in surface seal hydraulic resistance for infiltration in a mound and depression microtopography. *Catena*, 32:101–114, 1998.

J. M. V. Fragoso. Tapir-generated seed shadows: scale-dependent patchiness in the Amazon rain forest. *Journal of Ecology*, 85(4):519–529, 1997.

J. M. V. Fragoso, K. M. Silvius, and J. A. Correa. Long-distance seed dispersal by tapirs increases seed survival and aggregates tropical trees. *Ecology*, 84(8): 1998–2006, 2003.

K.W. Freeman, K. Girma, D.B. Arnall, R.W. Mullen, K.L. Martin, R.K. Teal, and W.R. Raun. By-plant prediction of corn forage biomass and nitrogen uptake at various growth stages using remote sensing and plant height. *Agronomy Journal*, 99(2):530–536, 2007.

R.A. Freeze. Role of subsurface flow in generating storm runoff 2. upstream source areas. *Water Resources Research*, 8(5):1272 – 1283, 1972.

R.A. Freeze. Streamflow generation. *Reviews of Geophysics*, 12(4):627–647, 1974.

J. Friedman and Z. Stein. Influence of seed-dispersal mechanisms on the dispersion of *Anastatica hierochuntica* (Cruciferae) in the Negev Desert, Israel. *Journal of Ecology*, 68(1):43–50, 1980.

Sylvie Galle, Joost Brouwer, and Jean-Pierre Delhoume. Soil water balance. In *Ecological Studies. Banded vegetation patterning in arid and semiarid environments: ecological processes and consequences for management*, Ecological Studies : 149, pages 77–104. Springer-Verlag New York Inc., 2001.

A. Garcia, J. L. Torres, E. Prieto, and A. De Francisco. Fitting wind speed distributions: a case study. *Solar Energy*, 62(2):139–144, 1998.

G. A. Gayle and R. W. Skaggs. Surface storage on bedded cultivated lands. *Transactions of the ASAE*, 21(1):101–104, 1978.

G. W. Gee and D. Or. Particle size analysis. In J.H. Dane and G. Clarke Topp, editors, *Methods of Soil Analysis, Part 4 Physical Methods*, page 1692. Soil Science Society of America, Madison, WI, 2002.

C.J. Gerard, P. Sexton, and G. Shaw. Physical factors influencing soil strength and root growth. *Agronomy Journal*, 74(5):875–879, 1982.

D. Gerten, S. Schaphoff, U. Haberlandt, W. Lucht, and S. Sitch. Terrestrial vegetation and water balance–hydrological evaluation of a dynamic global vegetation model. *Journal of Hydrology*, 286(1-4):249–270, 2004.

J.D. Gibbons. *Nonparametric statistical inference*. Marcel Dekker, New York, 1985.

E. Gilad. Ecosystem engineers: from pattern formation to habitat creation. *Physical Review Letters*, 93(9):doi:0.1103/PhysRevLett.93.098105, 2004.

J. V. Giraldez and D. A. Woolhiser. Analytical integration of the kinematic equation for runoff on a plane under constant rainfall rate and Smith and Parlange infiltration. *Water Resources Research*, 32(11):3385–3389, 1996.

T Givnish. Optimal stomatal conductance, allocation of energy between leaves and roots and the marginal cost of transpiration. In *On the Economy of Plant Form and Function*, pages 171–207. Cambridge University Press, Cambridge, 1986.

J. A. Gomez, J. V. Giraldez, and E. Fereres. Analysis of infiltration and runoff in an olive orchard under no-till. *Soil Science Society of America Journal*, 65(2): 291–299, March 2001.

J. P. Goutorbe, T. Lebel, A. J. Dolman, J. H. C. Gash, P. Kabat, Y. H. Kerr, B. Monteny, S. D. Prince, J. N. M. Stricker, A. Tinga, and J. S. Wallace. An overview of HAPEX-Sahel: a study in climate and desertification. *Journal of Hydrology*, 189(1-4):4–17, 1997.

D. S. Green. The terminal velocity and dispersal of spinning samaras. *American Journal of Botany*, 67(8):1218–1224, 1980.

R.S.B. Greene and M. Valentin, C.and Esteves. Runoff and erosion processes. In *Ecological Studies. Banded vegetation patterning in arid and semiarid environments: ecological processes and consequences for management*, Ecological Studies : 149, pages 52–76. Springer-Verlag New York Inc., 2001.

A. C. Guglielmini. Shading effects on spatial growth and biomass partitioning of *Cynodon dactylon*. *Weed Research*, 42(2):123–134, 2002.

H.A. Gutierrez-Jurado, E. Vivoni, J.B.J. Harrison, and H. Guan. Ecohydrology of root zone water fluxes and soil development in complex semiarid rangelands. *Hydrological Processes*, 20(15):3289–3316, 2006.

V. Guttal and C. Jayaprakash. Self-organization and productivity in semi-arid ecosystems: implications of seasonality in rainfall. *Journal of Theoretical Biology*, 248(3):490–500, 2007.

M. S. Hale and J. G. Mitchell. Effects of particle size, flow velocity, and cell surface microtopography on the motion of submicrometer particles over diatoms. *Nano Letters*, 2(6):657–663, 2002.

G.W. Hamilton and D.V. Waddington. Infiltration rates on residential lawns in central Pennsylvania. *Journal of Soil and Water Conservation*, 54(3):564–568, 1999.

J. M. Hammersley. Percolation processes: lower bounds for the critical probability. *The Annals of Mathematical Statistics*, 28(3):790–795, 1957.

B. Hansen, P. Schjonning, and E. Sibbesen. Roughness indices for estimation of depression storage capacity of tilled soil surfaces. *Soil and Tillage Research*, 52 (1-2):103–111, 1999.

J. Happel. Viscous flow relative to arrays of cylinders. *American Institute of Chemical Engineering Journal*, 5(2):174–179, 1959.

C. P. Harden and P. D. Scruggs. Infiltration on mountain slopes: a comparison of three environments. *Geomorphology*, pages 5–24, 2003.

R. J. Hardy, S. N. Lane, R. I. Ferguson, and D. R. Parsons. Emergence of coherent flow structures over a gravel surface: a numerical experiment. *Water Resources Research*, 43(3):doi:10.1029/2006WR004936, 2007.

U. Hellden. A coupled human-environmental model for desertification simulation and impact studies. *Global and Planetary Change*, 64(3-4):158–168, 2007.

K. Helming, M.J.M. Romkens, and S.N. Prasad. Surface roughness related processes of runoff and soil loss: a flume study. *Soil Science Society of America Journal*, 62 (1):243–250, 1998.

S.M. Herrmann, A. Anyamba, and C.J. Tucker. Recent trends in vegetation dynamics in the African Sahel and their relationship to climate. *Global Environmental Change*, 15(4):394–404, 2005.

J. W. Hester, T. L. Thurow, and C. A. Taylor. Hydrologic characteristics of vegetation types as affected by prescribed burning. *Journal of Range Management*, 50 (2):199–204, 1997.

J.D. Hewlett and A.R. Hibbert. Unsaturated and saturated flow through a thin porous layer on a hillslope. *Journal of Geophysical Research*, 68:1081–1087, 1963.

R. D. Hey. Flow resistance in gravel-bed rivers. *Journal of the Hydraulics Division-ASCE*, 105(4):365–379, 1979.

S. I. Higgins, R. Nathan, and M. L. Cain. Are long-distance dispersal events in plants usually caused by nonstandard means of dispersal? *Ecology*, 84(8):1945–1956, 2003.

R. HilleRisLambers, M. Rietkerk, M. Rietkerk, H. H. T. Prins, F. Van Den Bosch, and H. De Kroon. Vegetation pattern formation in semi-arid grazing systems. *Ecology*, 82(1):50–61, 2001.

H. Hillewaert. Cathedral mopane forest. `http://commons.wikimedia.org/wiki/File:Cathedral_mopane_forest_-_South_Luangwa_Valley.jpg`, 2005. Online source, accessed April 21 2009.

J. Holden. Topographic controls upon soil macropore flow. *Earth Surface Processes and Landforms*, 34(3):345–351, 2009.

M. Hollander and D.A. Wolfe. *Nonparametric statistical methods*. John Wiley and Sons, Inc., Hoboken, NJ, 1999.

H. S. Horn, R. Nathan, and S. R. Kaplan. Long-distance dispersal of tree seeds by wind. *Ecological Research*, 16(5):877–885, 2001.

R.E. Horton. Erosional development of streams and their drainage basins - hydrophysical approach to quantitative morphology. *Geological Society of America Bulletin*, 56(3):275–370, 1945.

H. F. Howe and J. Smallwood. Ecology of seed dispersal. *Annual Review of Ecology and Systematics*, 13:201–228, 1982.

L. Howle, R. P. Behringer, and J. Georgiadis. Visualization of convective fluid-flow in a porous-medium. *Nature*, 362(6417):230–232, 1993.

C. Huang and J. M. Bradford. Depressional storage for Markov-Gaussian surfaces. *Water Resources Research*, 26(9):2235–2242, 1990.

L. F. Huenneke. Spatial heterogeneity in Chihuahuan Desert vegetation: implications for sampling methods in semi-arid ecosystems. *Journal of Arid Environments*, 47 (3):257–270, 2001.

N. R. Hulugalle and J. N. Ndi. Effects of no-tillage and alley cropping on soil properties and crop yields in a typic kandiudult of Southern Cameroon. *Agroforestry Systems*, 22(3):207–220, 1993.

T. Hwang, L. Band, and T.C. Hales. Ecosystem processes at the watershed scale: extending optimality theory from plot to catchment. *Water Resources Research*, 45:doi: 10.1029/2009wr007775, 2009.

M. B. Isichenko. Percolation, statistical topography, and transport in random-media. *Reviews of Modern Physics*, 64(4):961–1043, 1992.

P. S. Jackson and J. C. R. Hunt. Turbulent wind flow over a low hill. *Quarterly Journal of the Royal Meteorological Society*, 101(430):929–955, 1975.

R. B. Jackson, J. S. Sperry, and T. E. Dawson. Root water uptake and transport: using physiological processes in global predictions. *Trends in Plant Science*, 5(11): 482–488, 2000.

M. Jager, C. Zilkens, K. Zanger, and R. Krauspe. Significance of nano- and microtopography for cell-surface interactions in orthopaedic implants. *Journal of Biomedicine and Biotechnology*, page doi: 10.1155/2007/69036, 2007.

J. C. Jenkins, D. C. Chojnacky, L. S. Heath, and R. A. Birdsey. National-scale biomass estimators for United States tree species. *Forest Science*, 49:12–35, 2003.

A. Joel, I. Messing, O. Seguel, and M. Casanova. Measurement of surface water runoff from plots of two different sizes. *Hydrological Processes*, 16(7):1467–1478, 2002.

C.B. Johnson, J.V. Mannering, and W.C. Moldenhauer. Influence of surface-roughness and clod size and stability on soil and water losses. *Soil Science Society of America Journal*, 43(4):772–777, 1979.

D.W. Johnson. Nutrient export by leaching and whole-tree harvesting in a loblolly pine and mixed oak forest. *Plant and Soil*, 102:99–109, 1987.

A. Johnston. Effects of grazing intensity and cover on the water-intake rate of fescue grassland. *Journal of Range Management*, 15(2):79–82, 1962.

E. Kalnay, M. Kanamitsu, R. Kistler, W. Collins, D. Deaven, L. Gandin, M. Iredell, S. Saha, G. White, J. Woollen, Y. Zhu, M. Chelliah, W. Ebisuzaki, W. Higgins, J. Janowiak, K. C. Mo, C. Ropelewski, J. Wang, A. Leetmaa, R. Reynolds, R. Jenne, and D. Joseph. The NCEP/NCAR 40-year reanalysis project. *Bulletin of the American Meteorological Society*, 77(3):437–471, 1996.

E. C. Kamphorst, V. Jetten, J. Guerif, J. Pitkanen, B. V. Iversen, J. T. Douglas, and A. Paz. Predicting depressional storage from soil surface roughness. *Soil Science Society of America Journal*, 64(5):1749–1758, 2000.

G. Katul, P. Wiberg, J. Albertson, and G. Hornberger. A mixing layer theory for flow resistance in shallow streams. *Water Resources Research*, 38(11): doi:10.1029/2001WR000817, 2002.

G. G. Katul, C. D. Geron, C. I. Hsieh, B. Vidakovic, and A. B. Guenther. Active turbulence and scalar transport near the forest-atmosphere interface. *Journal of Applied Meteorology*, 37(12):1533–1546, 1998.

G. G. Katul, A. Porporato, R. Nathan, M. Siqueira, M. B. Soons, D. Poggi, H. S. Horn, and S. A. Levin. Mechanistic analytical models for long-distance seed dispersal by wind. *American Naturalist*, 166(3):368–381, 2005.

G.G. Katul, P. Todd, and D. Pataki. Soil water depletion by oak trees and the influence of root water uptake on the moisture content spatial statistics. *Water Resources Research*, 33:611–623, 1997.

K. Kawasaki, F. Takasu, H. Caswell, and N. Shigesada. How does stochasticity in colonization accelerate the speed of invasion in a cellular automaton model? *Ecological Research*, 21(3):334–345, 2006.

S. Kefi, M. Rietkerk, C.L. Alados, Y. Pueyo, V.P. Papanastasis, A. ElAich, and P.C. de Ruiter. Spatial vegetation patterns and imminent desertification in mediterranean arid ecosystems. *Nature*, 449(7159):213–218, 2007a.

S. Kefi, M. Rietkerk, M. van Baalen, and M. Loreau. Local facilitation, bistability and transitions in arid ecosystems. *Theoretical Population Biology*, 71(3):367–379, 2007b.

S. Kefi, M. Rietkerk, and G. G. Katul. Vegetation pattern shift as a result of rising atmospheric CO_2 in arid ecosystems. *Theoretical Population Biology*, 74(4):332–344, 2008.

B. Kell. Oglala national grassland. http://commons.wikimedia.org/wiki/File:Oglala_National_Grassland.jpg, 2005. Online source, accessed April 21 2009.

R.D. Kelly and B.H. Walker. The effects of different forms of land use on the ecology of a semi-arid region in South-eastern Rhodesia. *British Ecological Society*, 64(2): 553–576, 1976.

M. Kirkby. Modelling the interactions between soil surface properties and water erosion. *Catena*, 46(2-3):89–102, 2001.

M. Kirkby and R.J. Chorley. Throughflow, overland flow and erosion. *Bulletin of the International Association of Scientific Hydrology*, 12(3):5–21, 1967.

M. Kirkby, L. Bracken, and S. Reaney. The influence of land use, soils and topography on the delivery of hillslope runoff to channels in SE Spain. *Earth Surface Processes and Landforms*, 27(13):1459–1473, 2002.

C. A. Klausmeier. Regular and irregular patterns in semiarid vegetation. *Science*, 284(5421):1826–1828, 1999.

M.G. Kleinhans, M.F.P. Bierkens, and M. van der Perk. Hydrologists, bring out shovels and garden hoses and hit the dirt. *Hydrology and Earth Systems Science Discussions*, 6:6581–6610, 2009.

T.R. Knutson and R.E. Tuleya. Increased hurricane intensities with CO_2-induced warming as simulated using the GFDL hurricane prediction system. *Climate Dynamics*, 15:17, 1999.

A. Kolmogoroff, I. Petrovsky, and N. Piscounoff. Étude de l'equation de la diffusion avec croissance de la quantité de matiere et son application a un problem biologique. *The Moscow University Bulletin of Mathematics*, 1:25, 1937.

M. Kot, M. A. Lewis, and P. vandenDriessche. Dispersal data and the spread of invading organisms. *Ecology*, 77(7):2027–2042, 1996.

O. Kvernvold and P. A. Tyvand. Non-linear thermal-convection in anisotropic porous-media. *Journal of Fluid Mechanics*, 90(FEB):609–624, 1979.

R. W. J. Lacey and A. G. Roy. A comparative study of the turbulent flow field with and without a pebble cluster in a gravel bed river. *Water Resources Research*, 43 (5):doi:10.1029/2006WR005027, 2007.

E.R. Lapwood. Convection of a fluid in a porous medium. *Proceedings of the Royal Cambridge Philosophical Society*, 44:508–521, 1948.

D. S. L. Lawrence. Macroscale surface roughness and frictional resistance in overland flow. *Earth Surface Processes and Landforms*, 22(4):365–382, 1997.

D. S. L. Lawrence. Hydraulic resistance in overland flow during partial and marginal surface inundation: experimental observations and modeling. *Water Resources Research*, 36(8):2381–2393, 2000.

R. Lefever and O. Lejeune. On the origin of tiger bush. *Bulletin of Mathematical Biology*, 59:263–294, 1997.

R. Lefever, N. Barbier, P. Couteron, and O. Lejeune. Deeply gapped vegetation patterns: on crown/root allometry, criticality and desertification. *Journal of Theoretical Biology*, 261:194–209, 2009.

P. Lehmann, C. Hinz, G. McGrath, H. J. Tromp-van Meerveld, and J. J. McDonnell. Rainfall threshold for hillslope outflow: an emergent property of flow pathway connectivity. *Hydrology and Earth System Sciences*, 11(2):1047–1063, 2007.

O. Lejeune. Localized vegetation patches: a self-organized response to scarcity. *Physical Review E*, 66(1):doi: 010901, 2002.

L. B. Leopold and M. G. Wolman. River meanders. *Geological Society of America Bulletin*, 71(6):769–793, 1960.

J.C. Leprun. The influences of ecological factors on tiger bush and dotted bush patterns along a gradient from Mali to northern Burkina Faso. *Catena*, 37(1-2): 25–44, 1999.

M. A. Lewis and S. Pacala. Modeling and analysis of stochastic invasion processes. *Journal of Mathematical Biology*, 41(5):387–429, 2000.

D. R. Linden and D. M. Vandoren. Parameters for characterizing tillage-induced soil surface-roughness. *Soil Science Society of America Journal*, 50(6):1560–1565, 1986.

W. R. Lloyd. Microtopography for ductile fracture process characterization part 1: theory and methodology. *Engineering Fracture Mechanics*, 70(3-4):387–401, 2003.

R. J. Loch. Effects of vegetation cover on runoff and erosion under simulated rain and overland flow on a rehabilitated site on the Meandu Mine, Tarong, Queensland. *Australian Journal of Soil Research*, 38(2):299–312, 2000.

M. Lowe, J.P. Gollub, and T.C. Lubensky. Commensurate and incommensurate structures in a non-equilibrium system. *Physical Review Letters*, 51(9):786–789, 1983.

J. A. Ludwig, D.J. Tongway, and S.G. Marsden. A flow-filter model for simulating the conservation of limited resources in spatially heterogeneous semi-arid landscapes. *Pacific Conservation Biology*, 1:209–213, 1994.

J. A. Ludwig, D. J. Tongway, and S. G. Marsden. Stripes, strands or stipples: modelling the influence of three landscape banding patterns on resource capture and productivity in semi-arid woodlands, Australia. *Catena*, 37(1-2):257–273, 1999.

J. A. Ludwig, B. P. Wilcox, D. D. Breshears, D. J. Tongway, and A. C. Imeson. Vegetation patches and runoff erosion as interacting ecohydrological processes in semiarid landscapes. *Ecology*, 86(2):288–297, 2005.

I. Y. F. Lun and J. C. Lam. A study of Weibull parameters using long-term wind observations. *Renewable Energy*, 20(2):145–153, 2000.

W. M. Lush. Turf growth and performance evaluation based on turf biomass and tiller density. *Agronomy Journal*, 82(3):505–511, 1990.

F. P. Lyford and H. K. Qashu. Infiltration rates as affected by desert vegetation. *Water Resources Research*, 5(6):1373, 1969.

L. Lyles. Wind erosion effects on soil texture and organic matter. *Journal of Soil and Water Conservation*, 41(3):191–193, 1986.

J.A. Mabbutt and P.C. Fanning. Vegetation banding in arid Western Australia. *Journal of Arid Environments*, 12(1):41–59, 1987.

B. J. MacVicar and A. G. Roy. Hydrodynamics of a forced riffle pool in a gravel bed river: 2. scale and structure of coherent turbulent events. *Water Resources Research*, 43(12):doi:10.1029/2006WR005274, 2007.

A. Makela, F. Berninger, and P. Hari. Optimal control of gas exchange during drought: theoretical analysis. *Annals of Botany*, 77(5):461–467, 1996.

A. P. Mamolos. Temporal differentiation in maximum biomass and nutrient accumu-

lation rates in two coexisting annual plant species. *Journal of Arid Environments*, 64(3):377–389, 2006.

A. Manor and N. Shnerb. Facilitation, competition and vegetation patchiness: from scale free distribution to patterns. *Journal of Theoretical Biology*, 253:838–850, 2008.

R. B. Mapa. Effect of reforestation using *tectona grandis* on infiltration and soil-water retention. *Forest Ecology and Management*, 77(1-3):119–125, 1995.

G. A. Marquis and A. G. Roy. Effect of flow depth and velocity on the scales of macroturbulent structures in gravel-bed rivers. *Geophysical Research Letters*, 33 (24):doi:10.1029/2006GL028420, 2006.

P. Martre, G.B. North, E.G. Bobich, and P.S. Nobel. Root deployment and shoot growth for two desert species in repsonse to soil rockiness. *American Journal of Botany*, 80(12):1933–1939, 2002.

G. R. Matlack. Diaspore size, shape, and fall behavior in wind-dispersed plant-species. *American Journal of Botany*, 74(8):1150–1160, 1987.

G. R. Matlack. Influence of fruit size and weight on wind dispersal in *betula lenta*, a gap-colonizing tree species. *American Midland Naturalist*, 128(1):30–39, 1992.

A. Mauchamp, C. Montana, J. Lepart, and S. Rambal. Ecotone dependent recruitment of a desert shrub, *fluorensia cernua*, in vegetation stripes. *Oikos*, 68(1): 107–116, 1993.

A. Mauchamp, S. Rambal, and J. Lepart. Simulating the dynamics of a vegetation mosaic - a spatialized functional-model. *Ecological Modelling*, 71(1-3):107–130, 1994.

A. Mauchamp, S. Rambal, J.A. Ludwig, and D.J. Tongway. Multiscale modeling of vegetation bands. In *Ecological Studies. Banded vegetation patterning in arid and semiarid environments: ecological processes and consequences for management*, Ecological Studies : 149, pages 146–166. Springer-Verlag New York Inc., 2001.

A. G. Mayor, S. Bautista, E. E. Small, M. Dixon, and J. Bellot. Measurement of the connectivity of runoff source areas as determined by vegetation pattern and topography: a tool for assessing potential water and soil losses in drylands. *Water Resources Research*, 44(10):13, 2008.

M. C. McCarthy and B. J. Enquist. Consistency between an allometric approach and optimal partitioning theory in global patterns of plant biomass allocation. *Functional Ecology*, 21(4):713–720, 2007.

A.K. McDonald, R.J. Kinucan, and L.E. Loomis. Ecohydrological interactions within banded vegetation in the northeastern Chichuahuan Desert, USA. *Ecohydrology*, 2(1):66–71, 2009.

G.M. McDonald, editor. *Fossil Pollen Analysis and the Reconstruction of Plant Invasions*, volume 1 of *Advances in Ecological Research*. Academic Press Limited, San Diego, 1993.

J.S. McLachlan and J.S. Clark. Reconstructing historial ranges with fossil data at continental scales. *Forest Ecology and Management*, 197:139–147, 2004.

J.S. McLachlan, J.S. Clark, and P.S. Manos. Molecular indicators of tree migration capacity under rapid climate change. *Ecology*, 86(8):2088–2098, 2005.

E. Meron, E. Gilad, J. von Hardenberg, M. Shachak, and Y. Zarmi. Vegetation patterns along a rainfall gradient. *Chaos, Solitons and Fractals*, 19(2):367–376, 2004.

D.M. Merritt and E.E. Wohl. Processes governing hydrochory along rivers: hydraulics, hydrology and dispersal phenology. *Ecological Applications*, 12:1071–1087, 2002.

H. Millán, A. Kalauzi, G. Llerena, J. Sucoshaay, and D. Piedra. Climatic trends in the Amazonian area of Ecuador: classical and multifractal analyses. *Atmospheric Research*, 88(3-4):355–366, 2008.

J.K. Mitchell and A.J. Jones. Micro-relief surface depression storage: analysis of models to describe the depth-storage function. *Water Resources Bulletin*, 12(6): 1205–1223, 1976.

Y. M. Mohamoud, L. K. Ewing, and C. W. Boast. Small plot hydrology (1): rainfall infiltration and depression-storage determination. *Transactions of the ASAE*, 33 (4):1121–1131, 1990.

A. Molina, G. Govers, V. Vanacker, J. Poesen, E. Zeelmaekers, and F. Cisneros. Runoff generation in a degraded andean ecosystem: interaction of vegetation cover and land use. *Catena*, 71(2):357–370, 2007.

D. Mollison. Dependence of epidemic and population velocities on basic parameters. *Mathematical Biosciences*, 107(2):255–287, 1991.

C. Montana. The colonization of bare areas in 2-phase mosaics of an arid ecosystem. *Journal of Ecology*, 80(2):315–327, 1992.

C. Montana, J. Seghieri, and A. Cornet. Vegetation dynamics: recruitment and regeneration in two-phase mosaics. In *Ecological Studies. Banded vegetation patterning in arid and semiarid environments: ecological processes and consequences for management*, Ecological Studies : 149, pages 132–145. Springer-Verlag New York Inc., 2001.

P. R. Moorcroft, S. W. Pacala, and M. A. Lewis. Potential role of natural enemies during tree range expansions following climate change. *Journal of Theoretical Biology*, 241(3):601–616, 2006.

J. D. Murray. *Mathematical Biology*, volume 1 of *Interdisciplinary Applied Mathematics*. Springer, New York, 3^{rd} edition, 2003a.

J.D. Murray. *Mathematical Biology*, volume 2, chapter 2: Spatial pattern formation with reaction diffusion systems, pages 71–140. Springer-Verlag, Berlin, 3^{rd} edition, 2003b.

E. J. Mwendera and M. A. M. Saleem. Infiltration rates, surface runoff, and soil loss as influenced by grazing pressure in the Ethiopian highlands. *Soil Use and Management*, 13(1):29–35, 1997.

S. L. Naidu, E. H. DeLucia, and R. B. Thomas. Contrasting patterns of biomass allocation in dominant and suppressed loblolly pine. *Canadian Journal of Forest Research-Revue Canadienne De Recherche Forestiere*, 28(8):1116–1124, 1998.

O. Narayan and D. S. Fisher. Nonlinear fluid-flow in random-media - critical phenomena near threshold. *Physical Review B*, 49(14):9469–9502, 1994.

M. S. Nash, E. Jackson, and W. G. Whitford. Soil microtopography on grazing gradients in Chihuahuan Desert grasslands. *Journal of Arid Environments*, 55(1): 181–192, 2003.

R. Nathan and G. G. Katul. Foliage shedding in deciduous forests lifts up long-distance seed dispersal by wind. *Proceedings of the National Academy of Sciences of the United States of America*, 102:5, 2005.

R. Nathan, G. G. Katul, H. S. Horn, S. M. Thomas, R. Oren, R. Avissar, S. W.

Pacala, and S. A. Levin. Mechanisms of long-distance dispersal of seeds by wind. *Nature*, 418(6896):409–413, 2002.

R. P. Neilson, L. F. Pitelka, A. M. Solomon, R. Nathan, G. F. Midgley, J. M. V. Fragoso, H. Lischke, and K. Thompson. Forecasting regional to global plant migration in response to climate change. *BioScience*, 55(9):749–759, 2005.

M. G. Neubert, M. Kot, and M. A. Lewis. Dispersal and pattern-formation in a discrete-time predator-prey model. *Theoretical Population Biology*, 48(1):7–43, 1995.

C. Neuhauser. Mathematical challenges in spatial ecology. *Notices of the AMS*, 48 (11):11, 2001.

S.P. Neuman. On advective transport in fractal permeability and velocity fields. *Water Resources Research*, 31(6):1455–1460, 1995.

J. M. Nicolau, A. SoleBenet, J. Puigdefabregas, and L. Gutierrez. Effects of soil and vegetation on runoff along a catena in semi-arid Spain. *Geomorphology*, 14 (4):297–309, 1996.

J. M. Nield and A. C. W. Baas. Investigating parabolic and nebkha dune formation using a cellular automaton modelling approach. *Earth Surface Processes and Landforms*, 33(5):724–740, 2008.

NOAA. Climate data, Douglas weather station. `http://www4.ncdc.noaa.gov/cgi-win/wwcgi.dll?wwDI~StnSrch~StnID~10100044`, 2009a. Accessed 1 May 2009.

NOAA. Climate data, Union Exp weather station. `http://www4.ncdc.noaa.gov/cgi-win/wwcgi.dll?WWDI~StnSrch`, 2009b. Accessed 1 May 2009.

K. Novick, P. Stoy, G. G. Katul, D. S. Ellsworth, M. Siqueira, J. Juang, and R. Oren. Carbon dioxide and water vapour exchange in a warm temperate grassland. *Oecologia*, 138(2):259–274, 2005.

I. Noy-Meir. Structure and function of desert ecosystems. *Israel Journal of Botany*, 28(1):1–19, 1979.

North Carolina State Climate Office. NC climate retrieval and observations network of the southeast database. `http://www.nc-climate.ncsu.edu/cronos`, 19 January 2009 2008.

A. Okubo and P. Kareiva. Some examples of animal diffusion. In Akira Okubo and S. A. Levin, editors, *Diffusion and Ecological Problems*, volume 1 of *Interdisciplinary Applied Mathematics*, page 25. Springer-Verlag, New York, 2 edition, 1980.

A. Okubo and S.A. Levin, editors. *Diffusion and Ecological Problems*, volume 1 of *Interdisciplinary Applied Mathematics*. Springer-Verlag, New York, 2001.

C. A. Onstad. Depressional storage on tilled soil surfaces. *Transactions of the ASAE*, 27(3):729–732, 1984.

R. Oren, D. S. Ellsworth, K. H. Johnsen, N. Phillips, B. E. Ewers, C. Maier, K. V. R. Schafer, H. McCarthy, G. Hendrey, S. G. McNulty, and G. G. Katul. Soil fertility limits carbon sequestration by forest ecosystems in a CO_2-enriched atmosphere. *Nature*, 411(6836):469–472, 2001.

Y. A. Pachepsky and J. C. Ritchie. Seasonal changes in fractal landscape surface roughness estimated from airborne laser altimetry data. *International Journal of Remote Sensing*, 19(13):2509–2516, 1998.

Y. A. Pachepsky, J. C. Ritchie, and D. Gimenez. Fractal modeling of airborne laser altimetry data. *Remote Sensing of Environment*, 61(1):150–161, 1997.

F.M. Pallida, J.D. Miranda, M.J. Jorquera, and F.I. Pugnaire. Variability in amount and frequency of water supply affects roots but not growth of arid shrubs. *Plant Ecology*, 2:261–270, 2009.

S. Palmroth, C. A. Maier, H. R. McCarthy, A. C. Oishi, H. S. Kim, K. H. Johnsen, G. G. Katul, and R. Oren. Contrasting responses to drought of forest floor CO_2 efflux in a Loblolly pine plantation and a nearby Oak-Hickory forest. *Global Change Biology*, 11(3):421–434, 2005.

G. Pardini and F. Gallart. A combination of laser technology and fractals to analyse soil surface roughness. *European Journal of Soil Science*, 49(2):197–202, 1998.

J. Y. Parlange and R. E. Smith. Ponding time for variable infiltration rates. *Canadian Journal of Soil Science*, 56:121–123, 1976.

D. E. Pataki and R. Oren. Species differences in stomatal control of water loss at the canopy scale in a mature bottomland deciduous forest. *Advances in Water Resources*, 26(12):1267–1278, 2003.

E.G. Patton and G.G. Katul. Turbulent pressure and velocity perturbations induced by gentle hills covered with sparse and dense canopies. *Boundary Layer Meteorology*, 133(2):189–217, 2009.

E. Perfect and B. D. Kay. Applications of fractals in soil and tillage research: a review. *Soil and Tillage Research*, 36(1-2):1–20, 1995.

J. R. Philip. Numerical solution of equations of the diffusion type with diffusivity concentration-dependent. *Transactions of the Faraday Society*, 51(7):885–892, 1955.

J. R. Philip. The theory of infiltration: 1. The infiltration equation and its solution. *Soil Science*, 83:345–357, 1957.

J. R. Philip. Early stages of infiltration in two-dimensional and three-dimensional systems. *Australian Journal of Soil Research*, 7(3):213–221, 1969.

J. R. Philip. Infiltration and downslope unsaturated flows in concave and convex topographies. *Water Resources Research*, 27(6):1041–1048, 1991.

J. R. Phillips. Zunzun: interactive two dimensional and three dimensional data modelling. `http://www.zunzun.com`, 2007.

O. Planchon, M. Esteves, N. Silvera, and J. M. Lapetite. Microrelief induced by tillage: measurement and modelling of surface storage capacity. *Catena*, 46(2-3): 141–157, 2002.

D. Poggi, G. G. Katul, J. D. Albertson, and L. Ridolfi. An experimental investigation of turbulent flows over a hilly surface. *Physics of Fluids*, 19(3):doi: 10.1063/1.2565528, 2007.

D. Poggi, G. G. Katul, J.J. Finnigan, and S.E. Belcher. Analytical models for the mean flow inside dense canopies on gentle hilly terrain. *Quarterly Journal of the Royal Meteorological Society*, 134(634):1095–1112, 2008.

A. Porporato, F. Laio, L. Ridolfi, and I. Rodriguez-Iturbe. Plants in water-controlled ecosystems: active role in hydrologic processes and response to water stress - iii. vegetation water stress. *Advances in Water Resources*, 24(7):725–744, 2001.

A. Porporato, G. Vico, and P. A. Fay. Superstatistics of hydro-climatic fluctuations and interannual ecosystem productivity. *Geophysical Research Letters*, 33(15): doi:L15402, 2006.

C. A. Pott and I. C. De Maria. Comparison with field methods for assessing infiltration rates. *Revista Brasileira De Ciencia Do Solo*, 27(1):19–27, 2003.

R. Prasse and R. Bornkamm. Effect of microbiotic soil surface crusts on emergence of vascular plants. *Plant Ecology*, 150(1-2):65–75, 2000.

S. C. Pryor, J. T. Schoof, and R. J. Barthelmie. Winds of change? projections of near-surface winds under climate change scenarios. *Geophysical Research Letters*, 33(11):doi:L11702, 2006.

Y. Pueyo, S. Kefi, C. L. Alados, and M. Rietkerk. Dispersal strategies and spatial organization of vegetation in arid ecosystems. *Oikos*, 117(10):1522–1532, 2008.

J. Puigdefabregas. The role of vegetation patterns in structuring runoff and sediment fluxes in drylands. *Earth Surface Processes and Landforms*, 30(2):133–147, 2005.

J. Puigdefabregas, A. Sole, L. Gutierrez, G. del Barrio, and M. Boer. Scales and processes of water and sediment redistribution in drylands: results from the Rambla Honda field site in Southeast Spain. *Earth-Science Reviews*, 48(1-2):39–70, 1999.

M. R. Raupach, J. J. Finnigan, and Y. Brunet. Coherent eddies and turbulence in vegetation canopies: the mixing-layer analogy. *Boundary-Layer Meteorology*, 78 (3-4):351–382, 1996.

S. Ravi, P. D'Odorico, and G. S. Okin. Hydrologic and aeolian controls on vegetation patterns in arid landscapes. *Geophysical Research Letters*, 34(24), 2007.

S. M. Reaney, L. J. Bracken, and M. J. Kirkby. Use of the connectivity of runoff model (CRUM) to investigate the influence of storm characteristics on runoff generation and connectivity in semi-arid areas. *Hydrological Processes*, 21(7):894–906, 2007.

O. J. Reichman. Spatial and temporal variation of seed distributions in Sonoran Desert soils. *Journal of Biogeography*, 11(1):1–11, 1984.

W. D. Reynolds, B. T. Bowman, R. R. Brunke, C. F. Drury, and C. S. Tan. Comparison of tension infiltrometer, pressure infiltrometer, and soil core estimates of saturated hydraulic conductivity. *Soil Science Society of America Journal*, 64(2): 478–484, March 1 2000.

E.D. Rhoades, L.F. Locke, H.M. Taylor, and E.H. McIlvain. Water intake on a sandy range as affected by 20 years of differential cattle stocking rates. *Journal of Range Management*, 17(4):185–190, 1964.

F. E. Rhoton, M. J. M. Romkens, J. M. Bigham, T. M. Zobeck, and D. R. Upchurch. Ferrihydrite influence on infiltration, runoff, and soil loss. *Soil Science Society of America Journal*, 67(4):1220–1226, 2003.

P. M. Rich, K. Helenurm, D. Kearns, S. R. Morse, M. W. Palmer, and L. Short. Height and stem diameter relationships for dicotyledonous trees and arborescent palms of Costa Rican tropical wet forest. *Bulletin of the Torrey Botanical Club*, 113(3):241–246, 1986.

J. H. Richards and M. M. Caldwell. Hydraulic lift - substantial nocturnal water transport between soil layers by *artemisia tridentata* roots. *Oecologia*, 73(4):486–489, 1987.

H.G. Richter. Commercial timbers: descriptions, illustrations, identification and information retrieval. `http://delta-intkey.com/wood/en/index.htm`, 2006. Online resource, accessed 30 April 2009.

M. Rietkerk and J. van de Koppel. Regular pattern formation in real ecosystems. *Trends in Ecology and Evolution*, 23(3):169–175, 2008.

M. Rietkerk, P. Ketner, J. Burger, B. Hoorens, and H. Olff. Multiscale soil and vegetation patchiness along a gradient of herbivore impact in a semi-arid grazing system in West Africa. *Plant Ecology*, 148(2):207–224, 2000.

M. Rietkerk, M. C. Boerlijst, F. van Langevelde, R. HilleRisLambers, J. van de Koppel, L. Kumar, H. H. T. Prins, and A. M. de Roos. Self-organization of vegetation in arid ecosystems. *American Naturalist*, 160(4):524–530, 2002.

M. Rietkerk, S. C. Dekker, P. C. de Ruiter, and J. van de Koppel. Self-organized patchiness and catastrophic shifts in ecosystems. *Science*, 305(5692):1926–1929, 2004.

J. J. Robledo-Arnuncio and L. Gil. Patterns of pollen dispersal in a small population of *pinus sylvestris* l. revealed by total-exclusion paternity analysis. *Heredity*, 94 (1):13–22, 2005.

I. Rodriguez-Iturbe and A. Porporato. *Ecohydrology of water-controlled ecosystems*. Cambridge University Press, 2004.

L. Rosa. Conv2fft. `http://www.mathworks.com/matlabcentral/fileexchange/loadCategory.do`, 2004.

M. D. Rumberger. Changes in diversity and storage function of ectomycorrhiza and soil organoprofile dynamics after introduction of beech into scots pine forests. *Plant and Soil*, pages 111–126, 2004.

S. E. Russo, S. Portnoy, and C. K. Augspurger. Incorporating animal behavior into seed dispersal models: implications for seed shadows. *Ecology*, 87(12):3160–3174, 2006.

P.M. Saco, G.R. Willgoose, and G.R. Hancock. Ecogeomorphology of banded vegetation patterns. *Hydrology and Earth System Science*, 11:1717–1730, 2007.

U. Safriel and Z. Adeel. Dryland systems. In R. Hassan, R. Scholes, and N. Ash, editors, *Ecosystems and Human Well-Being: current State and Trends*, volume 1, pages 615–658. Island Press, Washington DC, 2003.

G. Sanchez and J. Puigdefabregas. Interactions of plant-growth and sediment movement on slopes in a semiarid environment. *Geomorphology*, 9(3):243–260, 1994.

B. R. Scanlon. Uncertainties in estimating water fluxes and residence times using environmental tracers in an arid unsaturated zone. *Water Resources Research*, 36 (2):395–409, 2000.

T.M. Scanlon, K.K. Caylor, S.A. Levin, and I. Rodriguez-Iturbe. Positive feedbacks promote power-law clustering of Kalahari vegetation. *Nature*, 449(7159):209–212, 2007.

F. N. Scatena, W. Silver, T. Siccama, A. Johnson, and M. J. Sanchez. Biomass and nutrient content of the bisley experimental watersheds, Luquillo Experimental Forest, Puerto Rico, before and after Hurricane Hugo, 1989. *Biotropica*, 25(1):15–27, 1993.

J. Schellekens. Evaporation from a tropical rain forest, Luquillo Experimental Forest, eastern Puerto Rico. *Water Resources Research*, 36(8):2183–2196, 2000.

P. Schippers. Biomass partitioning, architecture and turnover of six herbaceous species from habitats with different nutrient supply. *Plant Ecology*, 149(2):219–231, 2000.

B. E. Schlaegel. Boxelder *Acer negundo* L. Biomass component regression-analysis for the Mississippi Delta. *Forest Science*, 28(2):355–358, 1982.

W.H. Schlesinger, J.A. Raikes, A.E. Hartley, and A.E. Cross. On the spatial pattern of soil nutrients in desert ecosystems. *Ecology*, 77(2):364–374, 1996.

T. Schoch. Australia 2005. online source, available from http://www.retas.de/thomas/travel/australia2005/index.html, 2005.

R.J. Scholes and S.R. Archer. Tree-grass interactions in savannas. *Annual Review of Ecology and Systematics*, 28:517–544, 1997.

F.M. Schurr, W.J. Bond, G.F. Midgley, and S.I. Higgins. A mechanistic model for secondary dispersal by wind and its experimental validation. *Journal of Ecology*, 93(5):1017–1028, 2005.

S. Schwinning and J. R. Ehleringer. Water use trade-offs and optimal adaptations to pulse-driven arid ecosystems. *Journal of Ecology*, 89(3):464–480, 2001.

S. J. Schymanski, M. Sivapalan, M. L. Roderick, L. B. Hutley, and J. Beringer. An optimality-based model of the dynamic feedbacks between natural vegetation and the water balance. *Water Resources Research*, 45, 2009.

J. Seghieri and D.L. Dunkerley. Specific methods of study. In *Ecological Studies. Banded vegetation patterning in arid and semiarid environments: ecological processes and consequences for management*, Ecological Studies : 149, pages 32–51. Springer-Verlag New York Inc., 2001.

J. Seghieri, S. Galle, J. L. Rajot, and M. Ehrmann. Relationships between soil moisture and growth of herbaceous plants in a natural vegetation mosaic in Niger. *Journal of Arid Environments*, 36(1):87–102, 1997.

E. J. Semler, C. S. Ranucci, and P. V. Moghe. Tissue assembly guided via substrate biophysics: applications to hepatocellular engineering. *Tissue Engineering I: Scaffold Systems for Tissue Engineering*, 102:1–46, 2006.

M. D. Shattuck, R. P. Behringer, G. A. Johnson, and J. G. Georgiadis. Onset

and stability of convection in porous media - visualization by magnetic resonance imaging. *Physical Review Letters*, 75(10):1934–1937, 1995.

N. Shigesada, K. Kawasaki, and Y. Takeda. Modeling stratified diffusion in biological invasions. *American Naturalist*, 146(2):229–251, 1995.

V. P. Singh and D. A. Woolhiser. Mathematical modeling of watershed hydrology. *Journal of Hydrologic Engineering*, 7(4):270–292, 2002.

A Sitz, J. Kurths, and H.U. Voss. Identification of nonlinear spatiotemporal systems via partitioned filtering. *Physical Review E*, 68(1):doi:10.1103/016202, 2003.

M. Sivapalan and P. C. D. Milly. On the relationship between the time condensation approximation and the flux concentration relation. *Journal of Hydrology*, 105(3-4): 357–367, 1989.

K. Smettem and R. Smith. Field measurements of infiltration parameters. In *Infiltration Theory for Hydrologic Applications*, volume 1, pages 135–156. American Geophysical Union, Washington DC, 2002.

M.W. Smith, N.J. Cox, and L.J. Bracken. Applying flow resistance equations to overland flows. *Progress in Physical Geography*, 31(4):363–387, 2007.

P. Sollins. *Organic matter budget and model for a southern Appalachian Liriodendron forest.* PhD thesis, University of Tennessee, 1972.

M. B. Soons, G.W. Heil, R. Nathan, and G. G. Katul. Determinants of long-distance dispersal by wind in grasslands. *Ecology*, 85:3056–3078, 2004a.

M. B. Soons, R. Nathan, and G. G. Katul. Human effects on long-distance wind dispersal and colonization by grassland plants. *Ecology*, 85:3069–3079, 2004b.

K. E. Spaeth, F. B. Pierson, M. A. Weltz, and J. B. Awang. Gradient analysis of infiltration and environmental variables as related to rangeland vegetation. *Transactions of the ASAE*, 39(1):67–77, 1996.

J.S. Sperry. Hydraulic constraints on plant gas exchange. *Agricultural and Forest Meteorology*, 104(1):13–23, 2000.

J.M. Steichen. Infiltration and random roughness of a tilled and untilled claypan soil. *Soil and Tillage Research*, 4(3):251–262, 1984.

P. C. Stoy, G. G. Katul, M. B. S. Siqueira, J. Y. Juang, H. R. McCarthy, H. S. Kim, A. C. Oishi, and R. Oren. Variability in net ecosystem exchange from hourly to inter-annual time scales at adjacent pine and hardwood forests: a wavelet analysis. *Tree Physiology*, 25:887–902, 2005.

P. C. Stoy, G. G. Katul, M. B. S. Siqueira, J. Y. Juang, K. A. Novick, H. R. McCarthy, A. C. Oishi, J. M. Uebelherr, H. S. Kim, and R. Oren. Separating the effects of climate and vegetation on evapotranspiration along a successional chronosequence in the Southeastern US. *Global Change Biology*, 12(11):2115–2135, 2006.

P. C. Stoy, G. G. Katul, M. B. S. Siqueira, J. Y. Juang, K. A. Novick, H. R. McCarthy, A. C. Oishi, and R. Oren. Role of vegetation in determining carbon sequestration along ecological succession in the Southeastern United States. *Global Change Biology*, 14(6):1409–1427, 2008.

J. M. Straus. Large-amplitude convection in porous-media. *Journal of Fluid Mechanics*, 64(JUN3):51–63, 1974.

J. M. Straus and G. Schubert. Existence of 3-dimensional convection in a rectangular box containing fluid-saturated porous media. *Journal of Fluid Mechanics*, 87 (JUL):385–394, 1978.

O. Tackenberg. Modeling long-distance dispersal of plant diaspores by wind. *Ecological Monographs*, 73(2):173–189, 2003.

L. Taiz and E. Zeiger. *Plant physiology*. Sinauer Associates, New York, 2005.

E. S. Takle and J. M. Brown. Note on use of Weibull statistics to characterize wind-speed data. *Journal of Applied Meteorology*, 17(4):556–559, 1978.

M. Tal and C. Paola. Dynamic single thread channels maintained by the interaction of flow and vegetation. *Geology*, 35(4):347–350, 2007.

G. Tayfur, M. L. Kavvas, R. S. Govindaraju, and D. E. Storm. Applicability of st-venant equations for 2-dimensional overland flows over rough infiltrating surfaces. *Journal of Hydraulic Engineering-ASCE*, 119(1):51–63, 1993.

Temsabuita. Simpson Desert Australia. `http://commons.wikimedia.org/wiki/File:Desert_de_Simpson.jpg`, 2007.

Texas Department of Transport. Hydraulic design manual: The rational method. `http://onlinemanuals.txdot.gov/txdotmanuals/hyd/hyd_apxB.doc`, 2010.

J. M. Thiery, J. M. Dherbes, and C. Valentin. A model simulating the genesis of banded vegetation patterns in Niger. *Journal of ecology*, 83(3):497–507, 1995.

A. Thiombiano, R. Wittig, and S. Guinko. Conditions of sexual multiplication in some Combretaceae in Burkina Faso. *Revue D Ecologie-La Terre Et La Vie*, 58 (4):361–379, 2003.

D.J. Tongway and J.A. Ludwig. Theories on the origins, maintenance, dynamics, and functioning of banded landscapes. In *Ecological Studies. Banded vegetation patterning in arid and semiarid environments: ecological processes and consequences*

for management, Ecological Studies : 149, pages 20–31. Springer-Verlag New York Inc., 2001.

D.J. Tongway and J.A. Ludwig. Vegetation and soil patterning in semiarid mulga lands of eastern Australia. *Australian Journal of Ecology*, 15(1):23–34, 1990.

Troen and E.L. Peterson. *European Wind Atlas*, volume 1. Commission of the European Communities, Roskilde, 1989.

A. M. Turing. The chemical basis of morphogenesis. *Philosophical Transactions of the Royal Society of London. Series B, Biological Sciences*, 237(641):37–72, 1952.

TVA. Nolichucky reservoir flood remediation environmental review. Technical report, Tennessee Valley Authority, 2007.

R. Uchytil. *Pleuraphis mutica*, in: Fire effects information system. `http://www.fs.fed.us/database/feis/plants/graminoid/plemut/all.html`, 1988.

United States Department of Agriculture. *Silvics of Forest Trees of the United States*, volume 1. United States Department of Agriculture, Washington DC, 1990.

N. Ursino. Modeling banded vegetation patterns in semiarid regions: interdependence between biomass growth rate and relevant hydrological processes. *Water Resources Research*, 43(4), 2007.

N. Ursino and S. Contarini. Stability of banded vegetation patterns under seasonal rainfall and limited soil moisture storage capacity. *Advances in Water Resources*, 29(10):1556–1564, 2006.

Nadia Ursino. The influence of soil properties on the formation of unstable vegetation patterns on hillsides of semiarid catchments. *Advances in Water Resources*, 28(9): 956–963, 2005.

USDA. Official soil series descriptions. http://soils.usda.gov/technical/classification/osd/index.html, 2009. Online resource, accessed 24 May 2009.

C. Valentin and J. M. d'Herbes. Niger tiger bush as a natural water harvesting system. *Catena*, 37(1-2):231–256, 1999.

C. Valentin, J. M. d'Herbes, and J. Poesen. Soil and water components of banded vegetation patterns. *Catena*, 37(1-2):1–24, 1999.

N. C. van de Giesen, T. J. Stomph, and N. de Ridder. Scale effects of Hortonian overland flow and rainfall-runoff dynamics in a West African catena landscape. *Hydrological Processes*, 14(1):165–175, 2000.

I. Van der Hoven. Power spectrum of horizontal wind speed in the frequency range from 0.0007 to 900 cycles per hour. *Journal of Meteorology*, 14(2):160–164, 1957.

L. van der Pijl. *Principles of dispersal in higher plants*. Springer-Verlag, Berlin, 1972.

K. Van Oost, G. Govers, S. de Alba, and T. A. Quine. Tillage erosion: a review of controlling factors and implications for soil quality. *Progress in Physical Geography*, 30(4):443–466, 2006.

W.J.P. Vananckevort. Surface microtopography of aqueous-solution grown crystals. *Progress in Crystal Growth and Characterization of Materials*, 9(1-2):1–50, 1984.

E. V. Vazquez, J. G. V. Miranda, and A. P. Gonzalez. Characterizing anisotropy and heterogeneity of soil surface microtopography using fractal models. *Ecological Modelling*, 182(3-4):337–353, 2005.

J. von Hardenberg, E. Meron, M. Shachak, and Y. Zarmi. Diversity of vegetation patterns and desertification. *Physical Review Letters*, 8719(19), 2001.

J. Wainwright, A. J. Parsons, W. H. Schlesinger, and A. D. Abrahams. Hydrology-vegetation interactions in areas of discontinuous flow on a semi-arid bajada, Southern New Mexico. *Journal of Arid Environments*, 51(3):319–338, 2002.

K. Walsh. Tropical cyclones and climate change: unresolved issues. *Climate Research*, 27(1):77–83, 2004.

K. W. Watson and R. J. Luxmoore. Estimating macroporosity in a forest watershed by use of a tension infiltrometer. *Soil Science Society of America Journal*, 50(3): 578–582, 1986.

P. L. Weaver. Elfin woodland recovery 30 years after a plane wreck in Puerto Rico's Luquillo mountains. *Caribbean Journal of Science*, 36(1-2):1–9, 2000a.

P. L. Weaver. Environmental gradients affect forest structure in Puerto Rico's Luquillo mountains. *Interciencia*, 25(5):254–259, 2000b.

P. J. Webster, G. J. Holland, J. A. Curry, and H. R. Chang. Changes in tropical cyclone number, duration, and intensity in a warming environment. *Science*, 309 (5742):1844–1846, 2005.

R. Weisse. Reconstruction of potential evaporation for water balance studies. *Climate Research*, 16(2):123–131, 2001.

Wetlands Int. Ramsar sites information service: Zambia country profile. `http://ramsar.wetlands.org/Portals/15/ZAMBIA.pdf`, 2007. Online source, accessed 20 April 2009.

G.E. Wickens and F.W. Collier. Some vegetation patterns in Republic of Sudan. *Geoderma*, 6(1):43–59, 1971.

Wickramaarachchi. Preliminary assessment of surface water resources - a study from Deduru Oya Basin of Sri Lanka. http://www.wrrc.dpri.kyoto-u.ac.jp/~aphw/APHW2004/proceedings/OHS/56-OHS-A341/56-OHS-A341.pdf, 2004. Online resource, accessed 25 May 2009.

C. G. Williams, S. L. LaDeau, R. Oren, and G. G. Katul. Modeling seed dispersal distances: implications for transgenic *pinus taeda*. *Ecological Applications*, 16(1): 117–124, 2006.

E. F. Wood, M. Sivapalan, K. Beven, and L. Band. Effects of spatial variability and scale with implications to hydrologic modeling. *Journal of Hydrology*, 102(1-4): 29–47, 1988.

R. A. Wooding. Steady infiltration from a shallow circular pond. *Water Resources Research*, 4(6):1259, 1968.

J.M. Wooldridge. *Introductory econometrics: a modern approach*, volume 1. Cengage South-West Learning, Utah, 4 edition, 2009.

G.A. Worrall. The Butana grass patterns. *Journal of Soil Science*, 10(1):34–53, 1959.

M. Xu, C. P. Chang, C. B. Fu, Y. Qi, A. Robock, D. Robinson, and H. M. Zhang. Steady decline of east Asian monsoon winds, 1969-2000: evidence from direct ground measurements of wind speed. *Journal of Geophysical Research-Atmospheres*, 111(D24), 2006.

Z. Yan, S. Bate, R. E. Chandler, V. Isham, and H. Wheater. Changes in extreme wind speeds in NW Europe simulated by generalized linear models. *Theoretical and Applied Climatology*, 83(1-4):121–137, 2006.

H. Yizhaq, E. Gilad, and E. Meron. Banded vegetation: biological productivity and

resilience. *Physica A-Statistical Mechanics and Its Applications*, 356(1):139–144, 2005.

X.D. Zeng, S.S.P. Shen, X.B. Zeng, and R.E. Dickinson. Multiple equilibrium states and the abrupt transitions in a dynamical system of soil water interacting with vegetation. *Geophysical Research Letters*, 31(5):doi: 10.1029/2003gl018910, 2004.

X.D. Zeng, X.B. Zeng, S.S.P. Shen, R.E. Dickinson, and Q.C. Zeng. Vegetation-soil water interaction within a dynamical ecosystem model of grassland in semi-arid areas. *Tellus Series B - Chemical and Physical Meteorology*, 57(3):189–202, 2005.

T. M. Zobeck and C. A. Onstad. Tillage and rainfall effects on random roughness - a review. *Soil and Tillage Research*, 9(1):1–20, 1987.

Biography

Name: Sally Elizabeth Thompson

Date of Birth: 25 May 1981

Place of Birth: London, UK

Graduate Degrees:

1. **Doctor of Philosophy, Nicholas School of the Environment, Duke University**

Undergraduate Degrees:

1. **Bachelor of Science (*Hons, 1st class*), Environmental Chemistry, University of Western Australia, 2003**

2. **Bachelor of Engineering (*Hons, 1st class*), Environmental Engineering, University of Western Australia, 2003**